

~~SECRET~~  
N71-14227  
CR 114104

REPORT NO. GDC-DDB70-008  
CONTRACT NAS 8-21465

CAS FILE  
COPY

**LOW GRAVITY PROPELLANT CONTROL  
USING CAPILLARY DEVICES IN  
LARGE SCALE CRYOGENIC VEHICLES**

PHASE II FINAL REPORT

**GENERAL DYNAMICS**  
*Convair Division*



REPORT NO. GDC-DDB70-008

**LOW GRAVITY PROPELLANT CONTROL  
USING CAPILLARY DEVICES IN  
LARGE SCALE CRYOGENIC VEHICLES**

PHASE II FINAL REPORT

August 1970

Prepared Under  
Contract NAS8-21465  
CONVAIR DIVISION OF GENERAL DYNAMICS  
San Diego, California



## FOREWORD

This final report volume covers work performed under NASA/MSFC Contract NAS8-21465 during the second phase period extending from January 1969 to July 31, 1970. Contract Control Numbers are DCN-8-52-10174(IF) and S-1(IF). Personnel contributing to this report include M. H. Blatt, project manager, W. S. Betts Jr., K. R. Burton, F. Merino, C. K. Perkins, L. E. Siden, and J. A. Stark. The study was performed under the technical direction of Mr. Leon J. Hastings, NASA/MSFC, R-P&VE-PT.



# TABLE OF CONTENTS

	Page
1 INTRODUCTION . . . . .	1-1
2 FLUID ANALYSIS . . . . .	2-1
2.1 S-IVC LH <sub>2</sub> TANK START BASKET SURFACE AREA MINIMIZATION . . . . .	2-1
2.2 OUTFLOW ANALYSIS COMPUTER PROGRAMS . . . . .	2-1
2.2.1 S-IVC Residuals . . . . .	2-4
2.2.2 S-IVC Spilling and Vapor Ingestion (INGASP) . . . . .	2-5
2.2.3 Outflow Analysis of S-IVC Using DREGS2 and INGASP . . . . .	2-11
2.2.4 LO <sub>2</sub> Tanker Residuals . . . . .	2-19
2.3 SETTLING ANALYSIS . . . . .	2-20
2.4 WICKING ANALYSIS . . . . .	2-22
2.5 ULLAGE COLLAPSE . . . . .	2-25
2.6 SCREENED CAPILLARY LIQUID COLLECTOR TUBES . . . . .	2-27
2.7 PROPELLANT CONTROL SCREENS . . . . .	2-30
2.8 WICKING TO REDUCE STRATIFICATION . . . . .	2-31
2.9 VAPOR IMPINGEMENT . . . . .	2-33
3 SURFACE TENSION START BASKET AND COLLECTION SYSTEMS THERMAL ANALYSIS . . . . .	3-1
3.1 S-IVC THERMAL ANALYSIS . . . . .	3-1
3.1.1 Mixing Analysis . . . . .	3-6
3.1.2 Heat Transfer Coefficient . . . . .	3-10
3.1.3 Basket Surface Heat Transfer . . . . .	3-18
3.1.4 Two-Phase Pressure Drop Analysis . . . . .	3-19
3.1.5 Thermal Analysis of Start Basket Cooling Liquid Collector Channels . . . . .	3-22
3.1.6 Detail Analysis of LH <sub>2</sub> Start Basket Cooling Configuration . . . . .	3-24
3.1.7 Analysis of LH <sub>2</sub> Feedline Cooling . . . . .	3-27
3.1.8 LO <sub>2</sub> Start Basket Analysis . . . . .	3-29
3.1.9 LO <sub>2</sub> Feed Duct Cooling . . . . .	3-37
3.2 LO <sub>2</sub> TANKER THERMAL ANALYSIS . . . . .	3-38
4 EXPERIMENTAL PROGRAM . . . . .	4-1
4.1 SCALE MODEL OUTFLOW TESTS . . . . .	4-1
4.1.1 Introduction . . . . .	4-1
4.1.2 Summary . . . . .	4-4

## TABLE OF CONTENTS, Contd

	Page
4.1.3 Experiment Design . . . . .	.4-4
4.1.4 Test Procedures . . . . .	.4-13
4.1.5 Test Evaluation . . . . .	.4-13
4.1.6 Experiment Design . . . . .	.4-20
4.1.7 Test Procedure . . . . .	.4-21
4.1.8 Conclusions and Recommendations . . . . .	.4-21
4.2 WICKING TESTS . . . . .	.4-21
4.2.1 Introduction . . . . .	.4-21
4.2.2 Summary . . . . .	.4-22
4.2.3 Experimental Method . . . . .	.4-22
4.2.4 Evaluation of Data . . . . .	.4-28
4.2.5 Interpretation of Results . . . . .	.4-29
4.2.6 Conclusions . . . . .	.4-30
5 DETAILED DESIGNS . . . . .	.5-1
5.1 S-IVC FUEL START SYSTEM DESIGN . . . . .	.5-1
5.1.1 Reservoir Structure . . . . .	.5-6
5.1.2 Reservoir Support System . . . . .	.5-14
5.1.3 Collector System . . . . .	.5-14
5.1.4 Heat Exchanger Plumbing . . . . .	.5-14
5.1.5 Outlet Duct Accessories . . . . .	.5-20
5.1.6 Weight Analysis . . . . .	.5-24
5.1.7 Structural Analysis . . . . .	.5-32
5.2 S-IVC OXIDIZER START SYSTEM DESIGN . . . . .	.5-41
5.2.1 Reservoir Structure . . . . .	.5-41
5.2.2 Outlet Duct Accessories . . . . .	.5-45
5.2.3 Weight Estimates . . . . .	.5-50
5.2.4 Structural Analysis . . . . .	.5-50
5.3 OXIDIZER TANKER COLLECTOR SYSTEM DESIGN . . . . .	.5-62
5.3.1 Collector Structural Design . . . . .	.5-62
5.3.2 Reservoir Structural Design . . . . .	.5-70
5.3.3 Heat Exchanger Tubes . . . . .	.5-70
5.3.4 Weight Analysis . . . . .	.5-79
5.3.5 Structural Analysis . . . . .	.5-79
6 CONCLUSIONS AND RECOMMENDATIONS . . . . .	.6-1
7 REFERENCES . . . . .	.7-1

## ILLUSTRATIONS

Figure	Page
2-1	Minimum Start Basket Surface Area Vs Volume . . . . 2-2
2-2	S-IVC LH <sub>2</sub> Tank Start Basket - Minimum Area Configurations . . . . . 2-3
2-3	DREGS Model Terminology . . . . . 2-4
2-4	Fluid Configuration for Spilling and Vapor Analyses. . . 2-7
2-5	Initial Attempt at S-IVC LO <sub>2</sub> Tank Pullthrough Suppression. . . . . 2-9
2-6	Standpipe Area vs. Available Engine Flow . . . . . 2-10
2-7	S-IVC LO <sub>2</sub> Capillary Device . . . . . 2-11
2-8	S-IVC LO <sub>2</sub> Tank Residuals . . . . . 2-12
2-9	Residual Volume vs. Pullthrough Height. . . . . 2-13
2-10	S-IVC LO <sub>2</sub> Residuals . . . . . 2-14
2-11	S-IVC LH Tank . . . . . 2-15
2-12	S-IVC LH Residuals vs. Side Screen Area Pull- through at the Top of the Feedline. . . . . 2-16
2-13	S-IVC LH <sub>2</sub> Spilling and Refilling . . . . . 2-17
2-14	S-IVC LH <sub>2</sub> Capillary Device Configuration (Deflec- tor Screens Shown in Figure 2-21). . . . . 2-18
2-15	LO <sub>2</sub> Tanker Drawing . . . . . 2-19
2-16	Ullage Pressure After Engine Firing . . . . . 2-26
2-17	Screened Capillary Collector Tube Pressure Losses vs. Tube Diameter . . . . . 2-28
2-18	Surface Tension Pressure . . . . . 2-29
2-19	S-IVC LH <sub>2</sub> Tank Propellant Control Screen Placement . . . . . 2-31
2-20	Velocity Requirements for Penetration of Vapor or Liquid Through a Liquid Hydrogen Wetted Screen or Plate . . . . . 2-32
2-21	Schematic of Deflector Screen to Prevent Vapor Ingestion . . . . . 2-34

# ILLUSTRATIONS, Contd

Figure		Page
3-1	Schematic of S-IVC Wall Heat Exchanger Vent System . . .	3-3
3-2	H <sub>2</sub> Vent Flow Versus Energy Input ( $P_T = \text{Const @}$ 25 psia) . . . . .	3-4
3-3	Condensing Vapor Surrounding the Start Basket . . . .	3-5
3-4	Schematic of Series Start Basket/Bulk System . . . . .	3-6
3-5	Required Interface Mixing Velocities . . . . .	3-9
3-6	Required Interface Velocity Vs Accelerations . . . . .	3-9
3-7	Mixing Velocity as a Function of Pump Performance . . .	3-10
3-8	Total Mixing Time Versus Interface Velocity . . . . .	3-11
3-9	Mixing Time as a Function of Pump Performance . . . .	3-11
3-10	GH <sub>2</sub> Natural Convection Heat Transfer . . . . .	3-13
3-11	H <sub>2</sub> Laminar Flow Condensation Heat Transfer . . . . .	3-13
3-12	LH <sub>2</sub> Forced Convection Heat Transfer Coefficient . . .	3-14
3-13	GH <sub>2</sub> Forced Convection Heat Transfer Coefficient . . .	3-14
3-14	LO <sub>2</sub> Natural Convection Heat Transfer . . . . .	3-15
3-15	GO <sub>2</sub> Natural Convection Heat Transfer . . . . .	3-15
3-16	O <sub>2</sub> Laminar Flow Condensation Heat Transfer . . . . .	3-16
3-17	O <sub>2</sub> Forced Convection Heat Transfer . . . . .	3-16
3-18	Start Basket Heat Transfer to Cooling Tubes . . . . .	3-20
3-19	Maximum Start Basket Temperatures When Using Cooling Tubes . . . . .	3-20
3-20	LH <sub>2</sub> Two-Phase Pressure Drop . . . . .	3-21
3-21	Hydrogen Enthalpy Versus Quality . . . . .	3-22
3-22	S-IVC LH <sub>2</sub> Collection Tube Support Configuration . . .	3-23
3-23	S-IVC LH <sub>2</sub> Engine Feedline . . . . .	3-27
3-24	LH <sub>2</sub> Feed Duct Cooling Tube Spacing . . . . .	3-29
3-25	S-IVC LO <sub>2</sub> Start Basket . . . . .	3-30
3-26	LO <sub>2</sub> Start Bakset Nodes - S-IVC Half Section . . . .	3-31

# ILLUSTRATIONS, Contd

Figure	Page
3-27 S-IVC LO <sub>2</sub> Tank Cooling Load as a Function of Cooling Temperature . . . . .	3-35
3-28 LO <sub>2</sub> Tank Wall Temperature Distribution . . . . .	3-36
3-29 Equilibrium Wall Temperature as a Function of External Heat Transfer . . . . .	3-37
3-30 LO <sub>2</sub> Tank Feed Duct Cooling Tube Spacing . . . . .	3-38
3-31 LO <sub>2</sub> Tanker Configuration . . . . .	3-39
3-32 O <sub>2</sub> Tanker Vent Flow Rate Required for Constant Tank Pressure . . . . .	3-40
3-33 LOX Tanker Cooling With Cooling Channels Inside the Collector Channels . . . . .	3-41
3-34 LO <sub>2</sub> Tanker External Cooling Tube Attachment . . . . .	3-44
4-1 Scale Model Centaur Tank - Existing Housing . . . . .	4-2
4-2 Annulus Type Capillary Reservoir Model - General Assembly . . . . .	4-3
4-3 Annulus Type Capillary Reservoir Model - Detail "A" . . . . .	4-5
4-4 Annulus Type Capillary Reservoir Model - Capillary Reservoir Assembly . . . . .	4-6
4-5 Annulus Type Capillary Reservoir Model - Construction Details . . . . .	4-7
4-6 Annulus Type Capillary Reservoir Model - Construction Details . . . . .	4-8
4-7 Annulus Type Capillary Reservoir Model - Construction Details . . . . .	4-9
4-8 Annulus Type Capillary Reservoir Model - Construction Details . . . . .	4-10
4-9 Outflow Test Schematic . . . . .	4-11
4-10 Outflow Test Set-up . . . . .	4-12
4-11 Vapor Pullthrough Correlations . . . . .	4-15
4-12 S-IVC Scale Model Spilling Tests . . . . .	4-17
4-13 Transient Flow Rates - Pentane Spilling and Vapor Ingestion Tests . . . . .	4-18

# ILLUSTRATIONS, Contd

Figure		Page
4-14	S-IVC Scale Model Residual Test Correlation . . . . .	4-19
4-15	Cylindrical Outflow Test Schematic . . . . .	4-20
4-16	Wicking Test Setup . . . . .	4-23
4-17	Wicking Test Calorimeter Assembly . . . . .	4-24
4-18	Wicking Test Heater Detail . . . . .	4-25
4-19	Electrical Schematic - Wicking Test . . . . .	4-26
4-20	Wicking Test Apparatus . . . . .	4-27
4-21	Typical Wicking Data With Predictive Models . . . . .	4-30
5-1	Fuel Start Basket General Assembly and Design Ground Rules . . . . .	5-2
5-2	Heat Exchanger System Schematic . . . . .	5-3
5-3	Start Reservoir Exchanger System Schematic (Parallel Arrangement) . . . . .	5-4
5-3A	Start Reservoir Heat Exchanger System Schematic (Series Arrangement) . . . . .	5-5
5-4	Structural Arrangement . . . . .	5-7
5-4A	Heat Exchanger Tube Arrangement for Series Circuit . . . . .	5-8
5-5	Outboard Panel and Outlet Zone Details . . . . .	5-9
5-6	Detail for Structural Arrangement . . . . .	5-10
5-7	End Panel Details . . . . .	5-11
5-8	Deflector Screen Details . . . . .	5-12
5-9	Reservoir Support System . . . . .	5-15
5-10	Reservoir Support System . . . . .	5-16
5-11	Collector Tube Details . . . . .	5-17
5-12	Alternate Collector Tube Support . . . . .	5-18
5-13	Plumbing Arrangement for Forward Outboard and Inboard Heat Exchanger Parallel Circuits . . . . .	5-19
5-14	Plumbing Arrangement for End Panel Heat Exchangers . . . . .	5-21
5-15	Plumbing Arrangement From Reservoir to Outlet Duct Heat Exchangers . . . . .	5-22

# ILLUSTRATIONS, Contd

Figure		Page
5-16	Feed Duct Accessories . . . . .	5-23
5-17	Feed Duct Accessories/Alternate Screen Location . .	5-25
5-18	Weight Estimate/Fuel Start Basket . . . . .	5-26
5-19	Fuel Start Basket Weight Estimate (Continued) . . .	5-27
5-20	Fuel Start Basket Weight Estimate (Continued) . . .	5-28
5-21	Fuel Start Basket Weight Estimate (Continued) . . .	5-29
5-22	Weight Estimate Fuel Collector Tubew . . . . .	5-30
5-23	Fuel Duct Accessories Weight Estimate . . . . .	5-31
5-24	Forward Panel Circumferential Stiffener Estimate . .	5-33
5-25	Forward Panel Estimate . . . . .	5-34
5-26	Outboard Cylindrical Section Stiffeners . . . . .	5-35
5-27	Shear Panel Estimate . . . . .	5-36
5-28	Shear Panel Estimate (Continued) . . . . .	5-37
5-29	Shear Panel Estimate (Continued) . . . . .	5-38
5-30	Forward Panel Radial Stiffener Estimate . . . . .	5-39
5-31	Screen Deflector Stiffener Estimate . . . . .	5-40
5-32	Oxidizer Tank Reservoir General Arrangement and Design Ground Rules . . . . .	5-42
5-33	Oxidizer Reservoir Structural Arrangement . . . . .	5-43
5-34	Oxidizer Reservoir Structural Details . . . . .	5-44
5-35	Oxidizer Reservoir Structural Details . . . . .	5-46
5-36	Oxidizer Tank Reservoir Structural Details . . . . .	5-47
5-37	Oxidizer Tank Inlet Screen Details . . . . .	5-48
5-38	Oxidizer Feed Duct Accessories . . . . .	5-49
5-39	Oxidizer Reservoir Weight Estimate . . . . .	5-51
5-40	Oxidizer Reservoir Weight Estimate (Continued) . . .	5-52
5-41	Oxidizer Accessories Weight Estimate . . . . .	5-53
5-42	Oxidizer Reservoir Base Ring Estimate for Conical Section . . . . .	5-54

# ILLUSTRATIONS, Contd

Figure	Page
5-43	Oxidizer Reservoir Stiffener Estimate for Conical Section. . . . . 5-55
5-44	Oxidizer Reservoir Conical Section Stiffener Ring Estimate . . . . . 5-57
5-45	Oxidizer Reservoir Apex Ring Estimate for Conical Section . . . . . 5-58
5-46	Oxidizer Reservoir Support Skin Estimate for Forward Screen at Cone Apex . . . . . 5-60
5-47	Oxidizer Outlet Screen Support . . . . . 5-61
5-48	Oxidizer Tanker General Arrangement and Design Ground Rules . . . . . 5-63
5-49	Oxidizer Tanker Heat Exchanger Schematic . . . . . 5-64
5-50	Oxidizer Tanker Collector Structural Arrangement . . . . . 5-65
5-51	Oxidizer Tanker Collector Alternate Structural Arrangement . . . . . 5-66
5-52	Oxidizer Tanker Collector Support Fitting Arrangement . . . . . 5-68
5-52A	Oxidizer Tanker Collector Support Fitting Arrangement (Alternate) . . . . . 5-69
5-53	Oxidizer Tanker Collector Arrangement at Equator Junction . . . . . 5-71
5-54	Oxidizer Tanker Reservoir Structural Arrangement. . . . . 5-72
5-55	Oxidizer Tanker Reservoir Structural Details . . . . . 5-73
5-56	Oxidizer Tanker Reservoir Structural Details . . . . . 5-74
5-57	Oxidizer Tanker Reservoir Structure (Alternate Ring Details) . . . . . 5-75
5-58	Location of Heat Exchanger Coils Relative to Collector Supports (External Systems) . . . . . 5-76
5-59	Oxidizer Tanker Heat Exchanger Coils (Typical Attachment Methods) . . . . . 5-77
5-60	Oxidizer Tanker Heat Exchanger Coils (Alternate Support Method) . . . . . 5-78

# ILLUSTRATIONS, Contd

Figure		Page
5-60A	Heat Exchanger System Located Inside of Tank . . .	5-80
5-60B	Collector Support Heat Exchanger Details . . . . .	5-81
5-60C	Collector Support Heat Exchanger Details . . . . .	5-82
5-61	Oxidizer Tanker Collector Channels Weight Estimate . . . . .	5-83
5-62	Oxidizer Tanker Collector Channels Weight Estimate . . . . .	5-84
5-63	Oxidizer Tanker Reservoir Weight Estimate . . . .	5-85
5-64	Oxidizer Tanker Reservoir Weight Estimate (Contd)• . .	5-86
5-65	Oxidizer Tanker Collector Channel Panel Estimate . .	5-87
5-66	Oxidizer Tank Collector Channel Panel Estimate . . .	5-89
5-67	Oxidizer Tanker Cylindrical Reservoir Forward Panel and Ring Estimate . . . . .	5-90
5-68	Oxidizer Tanker Reservoir Cylindrical Shell Estimate . . . . .	5-92



## SUMMARY

This report covers work performed at Convair during the second phase of the study "Low Gravity Propellant Control Using Capillary Devices in Large Cryogenic Vehicles." The second phase was an extension of first phase analytical experimental and design effort. This report contains a discussion of the fluid, thermal, experimental and design information developed for the two missions which were considered.

The missions considered were an S-IVC  $\text{LH}_2$  and  $\text{LO}_2$  tank restart in orbit and a propellant transfer mission using a LOX tanker to fill an S-IIB.

Fluid analysis of the missions included capillary device outflow, liquid settling, wicking, vapor impingement, and refilling. This information, coupled with Convair screen flow testing IRAD results, was utilized to refine the preliminary capillary device designs developed in Phase I. Information on wicking and outflow was formulated into computer programs to predict these phenomena for experimental correlation.

Thermal analysis was devoted mainly to detailed sizing of capillary device cooling configurations and consideration of destratification and mixing effects on cooling system operation. Systems designed for both missions used the cooling capacity of a thermodynamic vent system to prevent capillary device vapor formation. System sizing was based on maintaining slightly subcooled liquid in the capillary device with the cooling capacity made available by normal boiloff requirements.

The experimental effort consisted of normal gravity bench tests designed to complement the fluid and thermal analysis of the two missions considered. Outflow tests were conducted with a transparent scale model S-IVC tank and capillary device to evaluate capillary device draining, spilling and vapor ingestion. Results were successfully correlated with DREGS2 and INGASP computer models. Pullthrough suppression tests in a simple cylindrical container verified the analytical procedures used for sizing pullthrough suppression screens. Wicking tests were run to obtain wicking rates in screens subjected to heating, most applicable to the LOX tanker mission, and results were compared with several analytical and semiempirical models. Results were correlated semiempirically with a viscous capillary flow model.

The structural design effort refined Phase I designs based on thermal and fluid analysis performed in the second phase. The detailed designs developed for the two applications are presented with weight estimates, support, attachment and cooling configuration details along with load analysis and assembly drawings.

Conclusions of the study are that capillary devices are effective means of controlling propellant in large scale cryogenic vehicles. Additional work is recommended including prototype testing and analytical prediction of reorientation and refilling.

# 1

## INTRODUCTION

In orbiting spacecraft containing subcritical storage vessels, periods of orbital drag and disturbing accelerations may position liquid away from the tank outlet. Prior to engine restart or propellant transfer it is necessary to have liquid positioned over the outlet in order to effectively accomplish fluid transfer.

Acquisition devices for controlling propellants prior to transfer come under two categories; partial orientation devices that control only a small percentage of the tank contents and total orientation devices that attempt to control all the propellant in the tank. For the present study partial acquisition devices are required for the S-IVC restart mission and total acquisition is required for the  $\text{LO}_2$  tanker mission.

Spacecraft low gravity restarts have primarily been accomplished in the past through the use of linear acceleration to provide settling thrust with which to collect fluid over the outlet. This well proven technique introduces weight penalties and operational constraints compared to more advanced methods of acquisition. These methods include positive displacement devices such as bladders, bellows and diaphragms, dielectrophoretic devices and capillary devices.

Capillary devices are particularly attractive because they are lightweight, passive and introduce minimal operational constraints. These devices, while successfully applied to non-cryogenic propellant acquisition, have not been adequately studied for cryogenic fluid applications. Using cryogenic fluids introduces thermodynamic and heat transfer problems which greatly affect capillary control system design.

The purpose of this contract is to ascertain the feasibility of using capillary devices such as screens and/or perforated plates, for propellant control in large scale cryogenic vehicles.

The first phase of the two-phase program defined the thermodynamic and heat transfer problems associated with the use of capillary devices, derived methods for solving these problems and selected promising propellant control schemes. This was predominately an analytical study with some low cost bench testing required to verify basic concepts. Based on the general results of the initial analytical and experimental effort, designs were developed for an S-IVC  $\text{LH}_2$  and  $\text{LO}_2$  tank restart mission and

an S-IIB LOX tanker propellant transfer mission. Promising capillary control designs were compared with other means of propellant control in order to ascertain the feasibility of using capillary devices for propellant control in large-scale cryogenic vehicles.

During the second phase of the study, Phase I results were used as a base for an experimental/analytical program which examined the various problems in detail and developed design solutions. Techniques developed in Phase I were refined and expanded. A series of bench tests were run with noncryogenic fluids to provide information with which to correlate analytical models and develop empirical relationships where analytical models were not applicable. Second phase results have been presented in the form of a design handbook containing useful fluid, thermal and structural information, and a report covering analytical, experimental and design studies performed for the missions of interest.

This report is one of four volumes to the final report. The other volumes are the Design Handbook, Phase I Final Report and Related IRAD Studies.

# 2

## FLUID ANALYSIS

The fluid analysis performed in the second phase was devoted primarily to more detailed consideration of problems uncovered in Phase I. Areas investigated were capillary device residual, spilling, vapor ingestion, refilling and wicking predictions and analysis of settling, pullthrough and pullthrough suppression, vapor impingement, propellant control screens and wicks for temperature control.

### 2.1 S-IVC $\text{LH}_2$ TANK START BASKET SURFACE AREA MINIMIZATION

In the course of the thermal analysis it became obvious that the surface area of the S-IVC  $\text{LH}_2$  tank start basket would be a critical factor for effective start basket cooling. It was, therefore, deemed necessary to minimize the surface area of the  $\text{LH}_2$  start basket. Calculations indicated that the minimum surface area configuration should follow the contour of the aft bulkhead. The results of the parametric analysis of the start basket configuration are presented in Figure 2-1.

For the anticipated volume of  $200 \text{ ft}^3$ , the minimum surface area as illustrated in Figure 2-1, is  $275 \text{ ft}^2$ . This area was within the allowable limits determined by the thermal analysis of Chapter 3. The surface area for the start basket of Figure 6, Reference 2, is  $375 \text{ ft}^2$  which exceeded cooling capacity allowable limits. Based on the thermal requirements, the  $\text{LH}_2$  start basket configuration was therefore revised to that shown in Figure 2-2.

### 2.2 OUTFLOW ANALYSIS COMPUTER PROGRAMS

A major portion of the second phase fluid analysis was devoted to consideration of capillary device outflow during restart and during tank draining. Two computer programs were written to predict those two outflow phenomena. The INGASP program predicts spilling, vapor ingestion, pullthrough and refilling of a capillary propellant control device during restart. The DREGS2 program predicts liquid levels and volumes in a draining tank containing a capillary device. Both programs were written with screen flow and vapor pullthrough equations obtained from Convair test data correlations. Correlation of DREGS2 and INGASP predictions with S-IVC scale model tests was successfully accomplished, as discussed in Section 4.

120° ANNULAR BASKETS WITH INSIDE RADIUS CONFORMING TO  
INTERMEDIATE BULKHEAD WITH 1.5" SPACING AND OUTSIDE  
RADIUS OF 128.5"

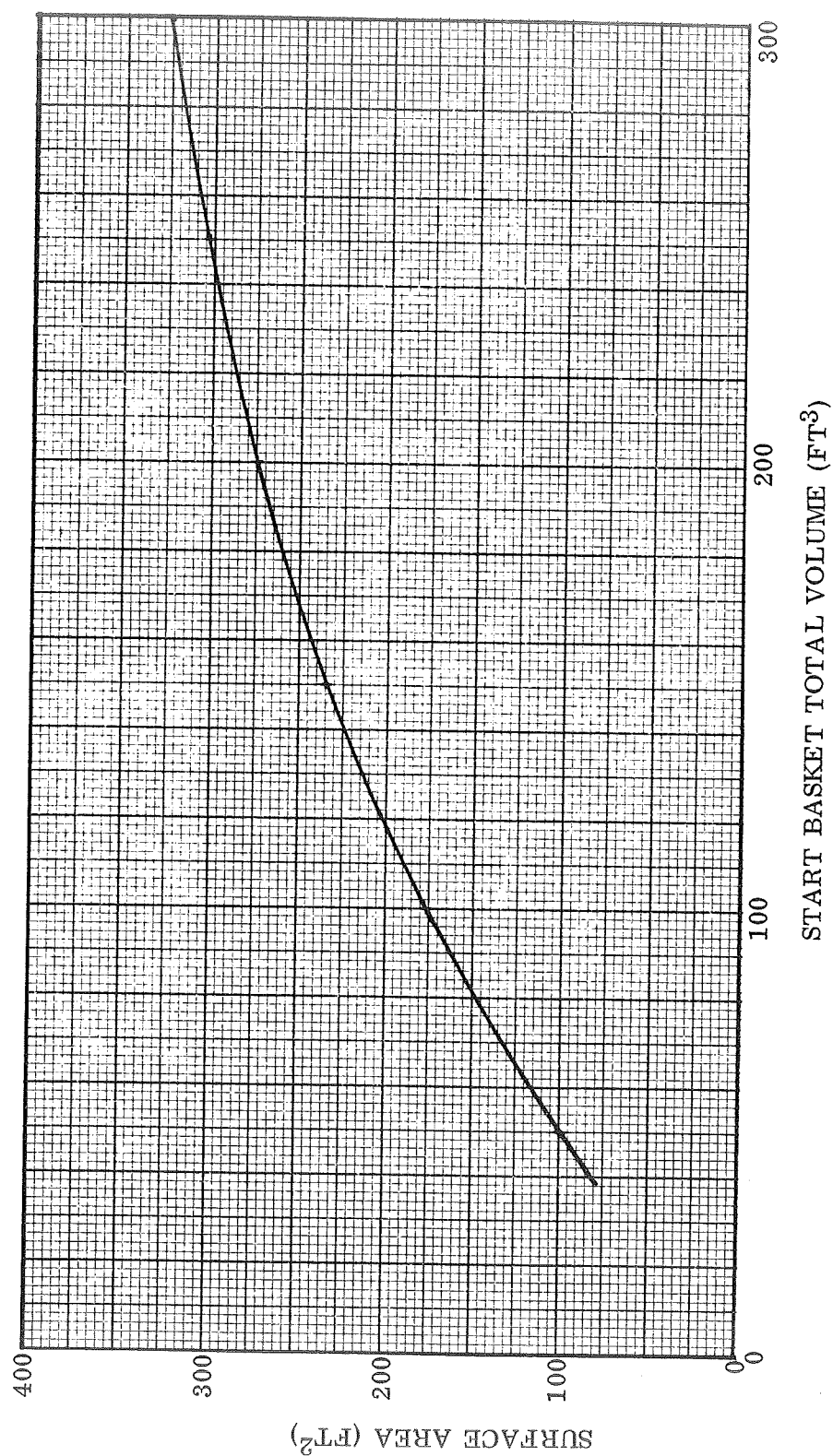
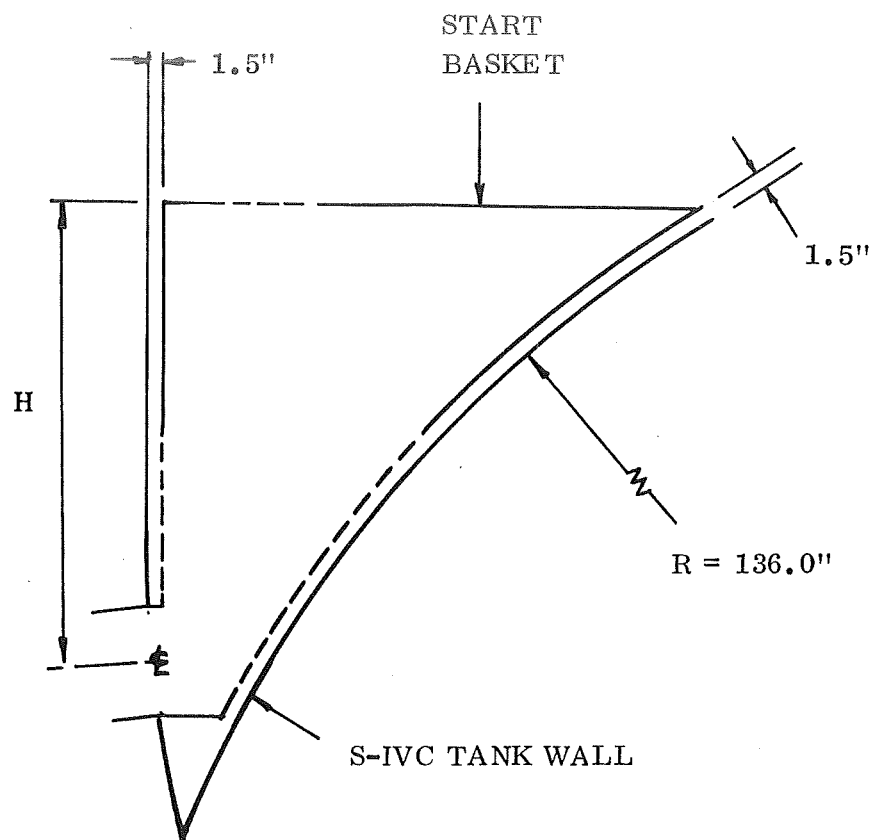


Figure 2 -1. Minimum Start Basket Surface Area Versus Volume



VOLUME (FT <sup>3</sup> )	H (IN.)	AREA (FT <sup>2</sup> )
50	20.0	100
100	32.0	177
150	41.5	235
175	45.5	256
200	49.0	275
250	55.5	303
300	61.3	325

Figure 2-2. S-IVC LH<sub>2</sub> Tank Start Basket - Minimum Area Configurations

The following paragraphs will discuss the development of the outflow computer programs and indicate their application in obtaining parametric data for optimizing S-IVC LH<sub>2</sub> and LO<sub>2</sub> designs.

**2.2.1 S-IVC RESIDUALS.** Residuals were determined for the S-IVC case by analyzing the flow in the capillary device region during draining using the DREGS2 computer program. A brief discussion of the program presented in the design handbook is repeated here for convenience. A complete listing of the DREGS2 coding may be found in Appendix B, design handbook.

The problem is trivial until the liquid level recedes to the top of the capillary device. At this point the liquid pressure drop through the side screen is evaluated to see if the surface tension pressure of the top screen is exceeded. If it is, vapor flow through the top screen is computed by equating pressure drop across the top screen to pressure drop across the side screen. A criteria which also must be satisfied is  $QGA + QL1 = QLO$ . These two equations are solved to obtain the flow rates and pressure drop.

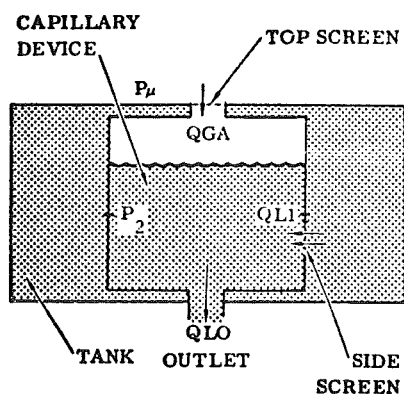
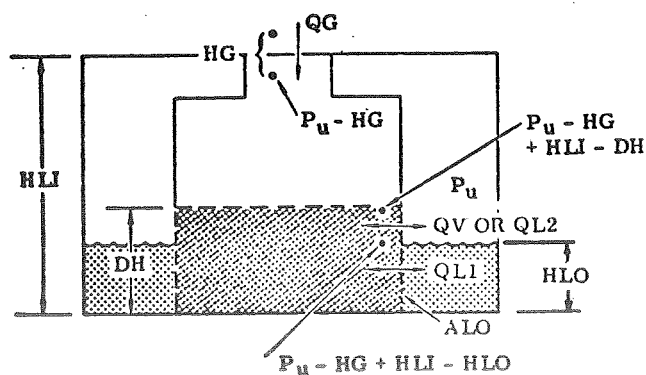


Figure 2-3 . DREGS Model Terminology



The other initial possibility is that the surface tension pressure of the top screen is not exceeded by the flow pressure drop. Liquid volume outside the capillary device is then reduced until either the side or top screen pressure drop is exceeded. The calculation at this point relates the pressure drops and flow rates as indicated below.

The program calculates the flow rates and pressure drops in the system. This is done by iteration. The pressure drop across the top screen is calculated to determine the direction of the flow, i.e., if  $HG > HLI - HLO$  liquid would flow from the capillary device to the tank and if  $HG < HLI - HLO$  flow would occur into the capillary device. Flows are computed using the pressure drops referenced against the common ullage pressure. For example if  $HG > HLI - HLO$ , flow across the top portion of the side screen would be from liquid to vapor, designated by  $QL2$  and would be found by integrating the expression

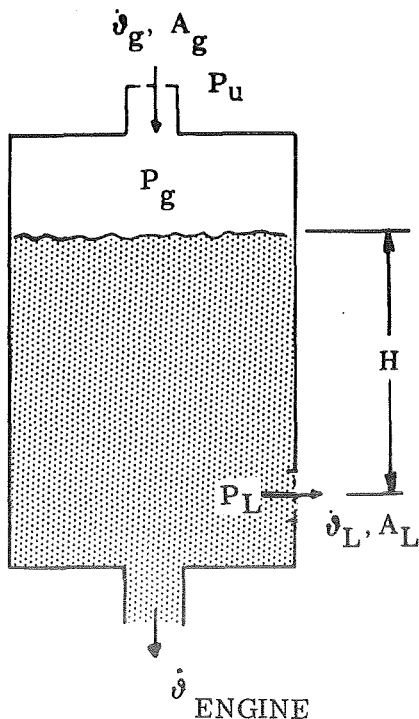
$$QL2 = \frac{x}{2BL} \int_{HLO}^{DH} \left[ -AL + (AL^2 + 4BL [HLI - HG])^{1/2} \right] dH$$

which is obtained by inverting the screen flow pressure drop equation. BL and AL are screen flow pressure drop constants, X is the width of the screen, and DH, HLI, HLO, and HG are head terms shown in the figure above.

Proceeding from these two initial states; for each time step the flow rates and relative volume changes are computed. New liquid levels are computed for the new time steps and calculations of flow rates are repeated. The general procedure is iteration to satisfy both pressure drop and volume conservation considerations. Computations are considered for all possible variations in liquid level. Pullthrough terminates each case when the liquid level inside the capillary device falls below the pullthrough height as computed by using the flow from the free surface inside the start basket or QLO-QL1-QL2.

A complete listing of the program in Appendix B of the design handbook indicates the equations used to evaluate the liquid level cases not discussed in detail here.

2.2.2 S-IVC SPILLING AND VAPOR INGESTION (INGASP) — The phase I final report and the design handbook discuss how liquid can be retained within a screened reservoir during the S-IVC restart sequence. The third quarterly progress report identified the method of analysis which was used to develop the initial capillary device configurations for minimizing vapor ingestion and spilling in the S-IVC LO<sub>2</sub> and LH<sub>2</sub> capillary devices. The basic analytical approach is summarized below for liquid spillage and vapor penetration calculations.



For Liquid Spillage:  $P_L > P_u$

$$P_L = P_g + \rho(g/g_c) H$$

$$P_g = P_u - \Delta P_g \text{ where } P_g = f(A_g, \dot{V}_g)$$

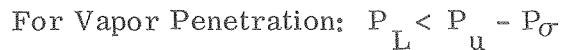
$$\therefore P_L - P_u = \rho(g/g_c) H - \Delta P_g$$

$$\text{when } P_L - P_u = 0, H = \Delta P_g / \rho(g/g_c)$$

$$\text{where } \dot{V}_L = 0 \text{ and } \Delta P_g = \Delta P_{g_0}$$

$$\dot{V}_g = \dot{V}_{ENGINE} + \dot{V}_L$$

$$\text{where } \dot{V}_g \propto A_g \sqrt{\frac{\Delta P_g}{\rho_g}} \text{ and } \dot{V}_L \propto A_L \sqrt{\frac{(P_L - P_u)}{\rho_L}}$$



$$P_{\sigma} = 4\sigma/D_{BP}$$

where  $\dot{V}_g \propto A_g \sqrt{\frac{\Delta P}{\rho_g}}$  and  $\dot{V}_v \propto A_v \sqrt{\frac{(P_u - P_L)}{\rho_v}}$

$$\Delta P_{\sigma} > \Delta P_g - \rho(g/g_c) H \quad \text{where } \Delta P_g > \rho \left( \frac{g}{g_c} \right) H$$
$$\Delta P = \frac{A_1 \mu V L}{D_a^2 g_c} + \frac{A_2 \rho V^2 L}{D_a g_c}$$

Several simple cases considered by the program are illustrated in the following equations. This first case is where no liquid has been collected outside the start basket and vapor is being ingested into the capillary device.

Vapor will break through the top screen initially when a restart occurs. The magnitude of the pressure drop is critical in determining the flow across the screen surfaces on the side of the capillary device. Looking at one case, the pressure drop  $\Delta P_L = P_u - P_L$  at the top of the side screen, with no liquid collected outside the basket is,

$$\Delta P_L = HG - HT$$

if  $\Delta P_L < 0$ , liquid will spill from  
from the capillary device

if  $\Delta P_L > 0$ , and  $> HS$  (surface tension  
pressure head) vapor will  
be ingested into the cap-  
illary device

if  $\Delta P_L > 0$ , and  $< HS$  no flow will occur  
at this point.

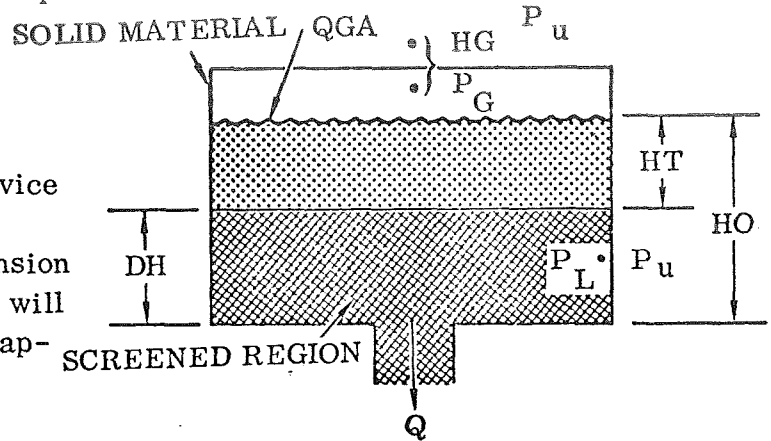


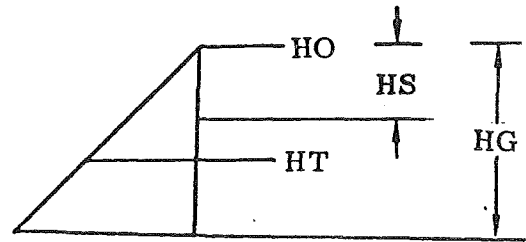
Figure 2-4. Fluid Configuration for  
Spilling and Vapor  
Analyses.

At the bottom of the screen  $\Delta P_L = HG - HO$  and the same inspection of  $\Delta P_L$  is made to determine the direction of the flow. For illustration, assume  $\Delta P_L > 0$  and  $> HS$  at the top of the screen and  $\Delta P_L < 0$  at the bottom of the screen. The vapor will be ingested over the top portion of the screen at a volume flow rate

$$\dot{Q}_v = \int_0^{HG-HS-HT} dQ_v$$

which yields

$$\dot{Q}_v = \frac{2}{3} \times \sqrt{\frac{2g \rho_L}{CSV \rho_g}} (HG-HS-HT)^{3/2}$$



No flow will occur over a region  $HS$  wide. Liquid flow will be

$$\dot{Q}_L = \frac{2}{3} \times \sqrt{2g/(CSL)} (HO-HG)^{3/2}$$

where  $CSL$  and  $CSV$  are flow constants defined in the appendix in the INGASP listing.

Using triangle diagrams, such as shown above, the pressure drops and flow equations for all possible cases were considered and coded into the INGASP program. These cases included liquid level in the capillary device below the screened area and liquid present outside the capillary device due to collection, with consequent refilling calculations. Initially the program made calculations to determine motion of ingested bubbles based on drag between liquid and vapor flowing in the capillary device. This calculation is not present in the current listing because the change in velocity due to drag was found to be negligible for all cases run with that option included. The problem case is terminated when the liquid level in the start basket falls below the pullthrough height.

A listing of the complete program showing all the cases handled is given in Appendix A of the design handbook.

The program was first applied to optimizing the S-IVC LO<sub>2</sub> tank capillary device volume. The initial configuration considered was a 96-inch diameter cylinder, 18.2 inches high, having a 17.5-inch high conical section. This configuration was a preliminary design developed for the weight comparisons of Phase I and did not consider the use of screen pressure drop to minimize spillage. An analysis described in the third quarterly progress report was thus performed to enable a smaller LO<sub>2</sub> tank capillary device to be designed. Calculations indicated that the capillary device cylindrical section height could be reduced because the tank shape allowed spilled liquid to readily reentry the capillary device. The height was thus reduced to 6.1 inches in the cylindrical section. After the INGASP program was developed it was convenient to optimize the configuration still further by reducing spillage. Initially, the start basket with 6.1 inch cylindrical height was inputted on the INGASP program. The configuration proved to have too much spilling due to the low standpipe pressure drop. The area for standpipe flow was reduced to minimize spilling so premature pullthrough would not occur. Initial runs before the scale model S-IVC LH<sub>2</sub> testing was performed indicated that pullthrough still occurred at a relatively high start basket volume. Examination of the pullthrough correlations indicated that the correlation used was good for  $h_c \gg r$  which was not the case. Using a correlation where  $h_c \ll r$  reduced pullthrough height from .87 to .65 feet. Later a more accurate correlation where  $h_c \sim r$  was used.

In order to reduce the pullthrough height below .65 ft, a screen was placed over the outlet of the tank. The placement of the screen was determined graphically by superimposing a template of the interface shape during pullthrough on the locus of minimum liquid flow areas allowable, as shown in Figure 2-5. This locus was obtained by equating the flow pressure drop to the surface tension pressure for a 200 × 600 screen. The point at which the interface intersects the locus of minimum area is the optimum point to place the screen. Placing the screen lower will not reduce residuals from the unscreened case because the flow pressure drop will exceed the surface tension pressure as soon as vapor encroaches on the screen. Placing the screen higher than the .37 ft selected, results in higher residuals due to the relatively flat interface shape. For a highly curved low-g draining case it may be optimum to place the screen above the minimum height position as was selected here.

With a pullthrough height of .37 ft, several top screen flow areas were run to find the optimum area. Based on these runs, depicted in Figure 2-6, an area of .50 ft<sup>2</sup> was chosen for the top screen. Pullthrough suppression, using a correlation for interface shape, where  $h_c \sim r$ , obtained from scale model tests was used in a similar manner to obtain screen placement at .20 inches above the outlet. This allowed a volume reduction of 6 ft<sup>3</sup> by reducing spilling. This is accomplished by reducing midsection height from .508 to .390 feet. Additional optimizations using Phase II test results and iterations between INGASP and DREGS are illustrated at the end of this section.

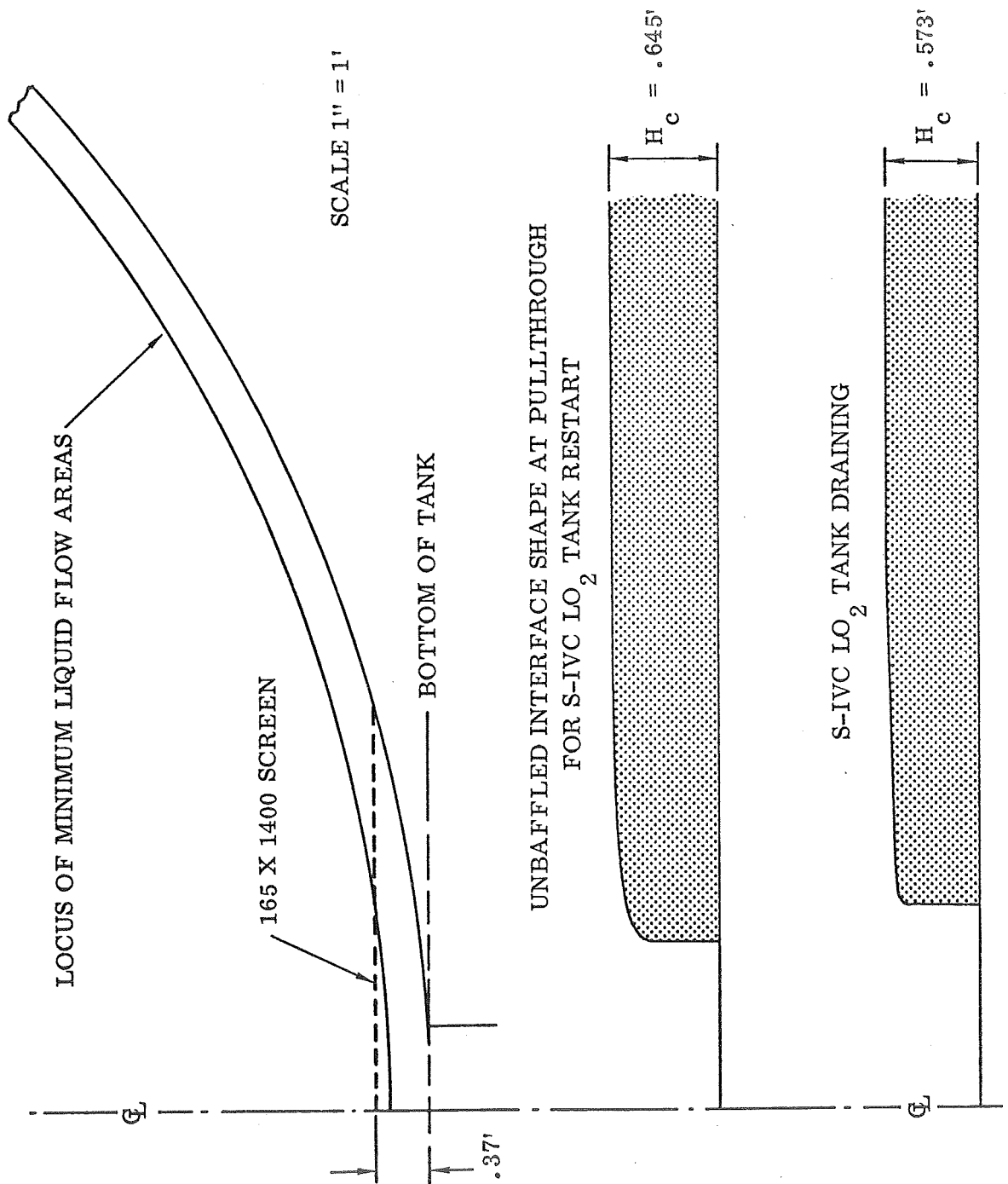


Figure 2-5. Initial Attempt at S-IVC LO<sub>2</sub> Tank Pullthrough Suppression

S-IVC, 64 FT<sup>3</sup> LOX TANK START BASKET

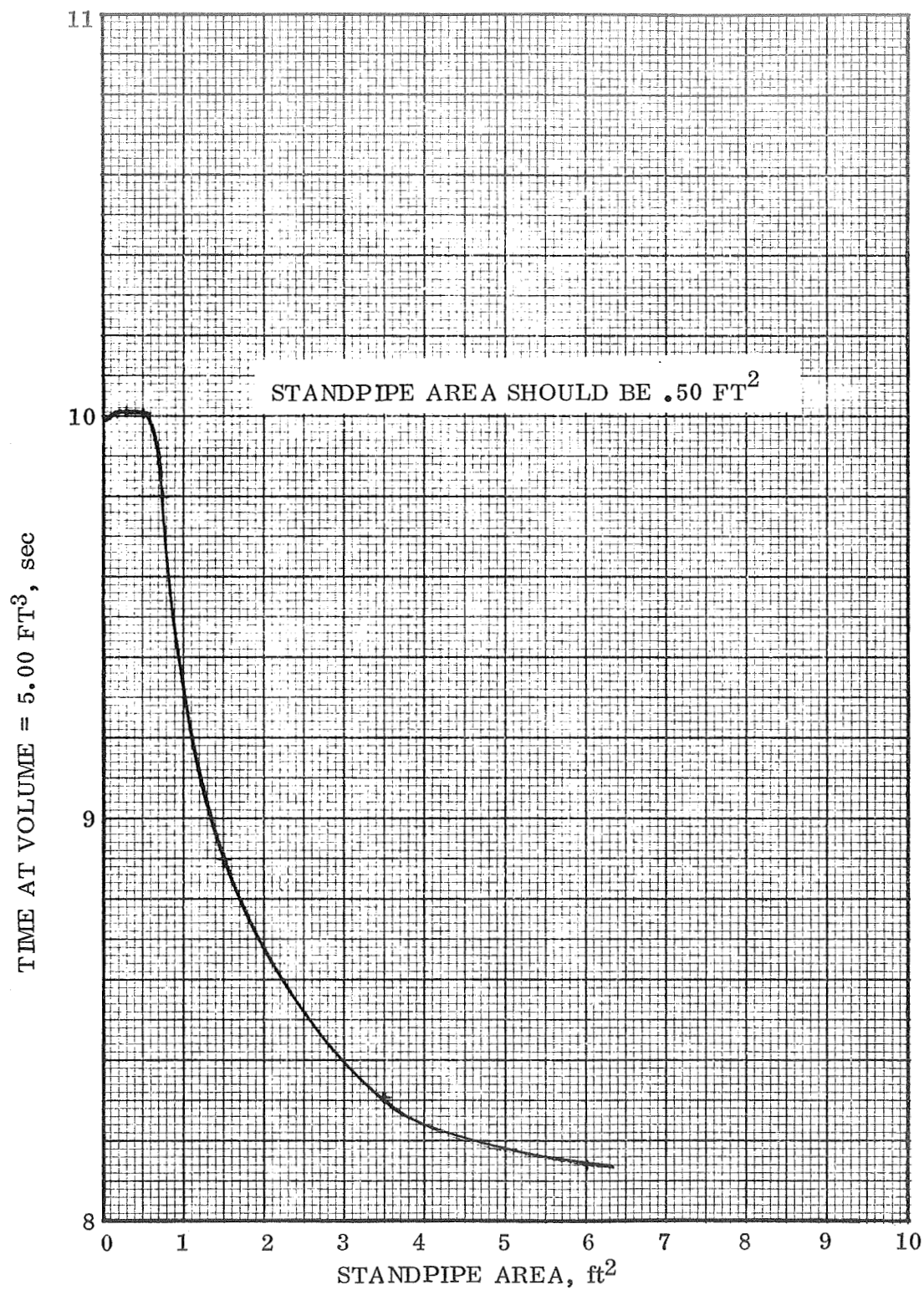


Figure 2-6. Standpipe Area Vs Available Engine Flow

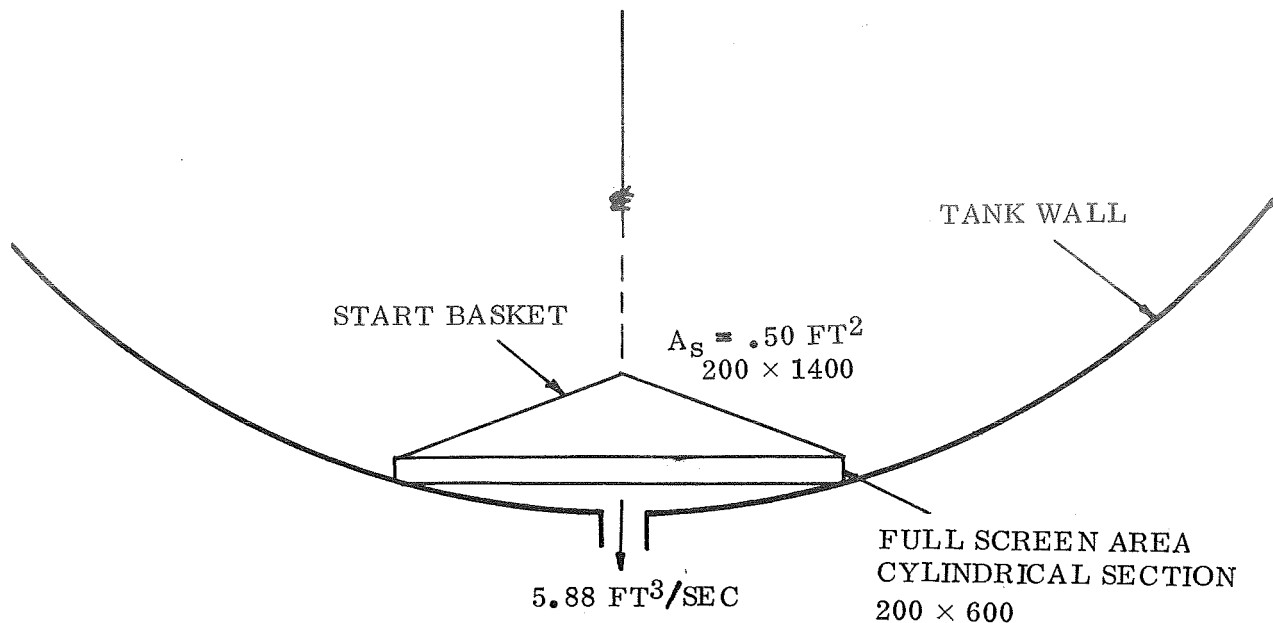


Figure 2-7. S-IVC LO<sub>2</sub> Capillary Device

**2.2.3 OUTFLOW ANALYSIS OF S-IVC USING DREGS2 AND INGASP.** After determining initial volume constraints for the S-IVC LH<sub>2</sub> and LO<sub>2</sub> start baskets, the INGASP and DREGS2 programs were used to arrive at a configuration which optimally satisfied spilling, vapor ingestion, refilling and residual considerations.

For the S-IVC LO<sub>2</sub> case, initial runs were made to determine optimum top screen area to provide maximum volume availability for restart purposes. This INGASP evaluation, presented in Figure 2-6, indicated that the top screen area should be 0.50 ft<sup>2</sup>. Dregs evaluation of residuals presented in Figure 2-8 illustrates that a top screen area of 0.50 ft<sup>2</sup> also gives minimum total residual volume. If top screen area is increased, spilling and residuals outside the capillary device will increase due to the decrease in top screen pressure drop. The lower pressure drop allows liquid to drain or spill from the capillary device at a faster rate. For the draining case, more liquid will thus remain in the tank when pullthrough occurs in the capillary device. For restart the liquid head in the capillary device will exceed the gas pressure drop and spilling will occur. If the area is reduced, the screen pressure drop increases and during restart vapor ingestion could occur in the capillary device which might be entrained into the outlet. Reducing the top screen area increases residuals by tending to make pull through occur at a higher liquid level. This is because the flow from the tank becomes reduced as the level drops well below the capillary device level. The increased flow from inside the capillary device causes higher residuals to remain in the capillary device, offsetting residual reductions outside the capillary device.

Additional runs were made with DREGS2 to evaluate the effect of pullthrough height and side screen area on LO<sub>2</sub> tank residuals and are shown in Figures 2-9 and 2-10. The configuration initially selected is confirmed by the low residual volume for ALO = 9.85 ft<sup>2</sup>. The increase in residuals when the side screen is increased beyond this area is due to the reduced gas pressure drop when liquid falls below the top of the side screen. Figure 2-9 may be used to predict residuals for given pullthrough

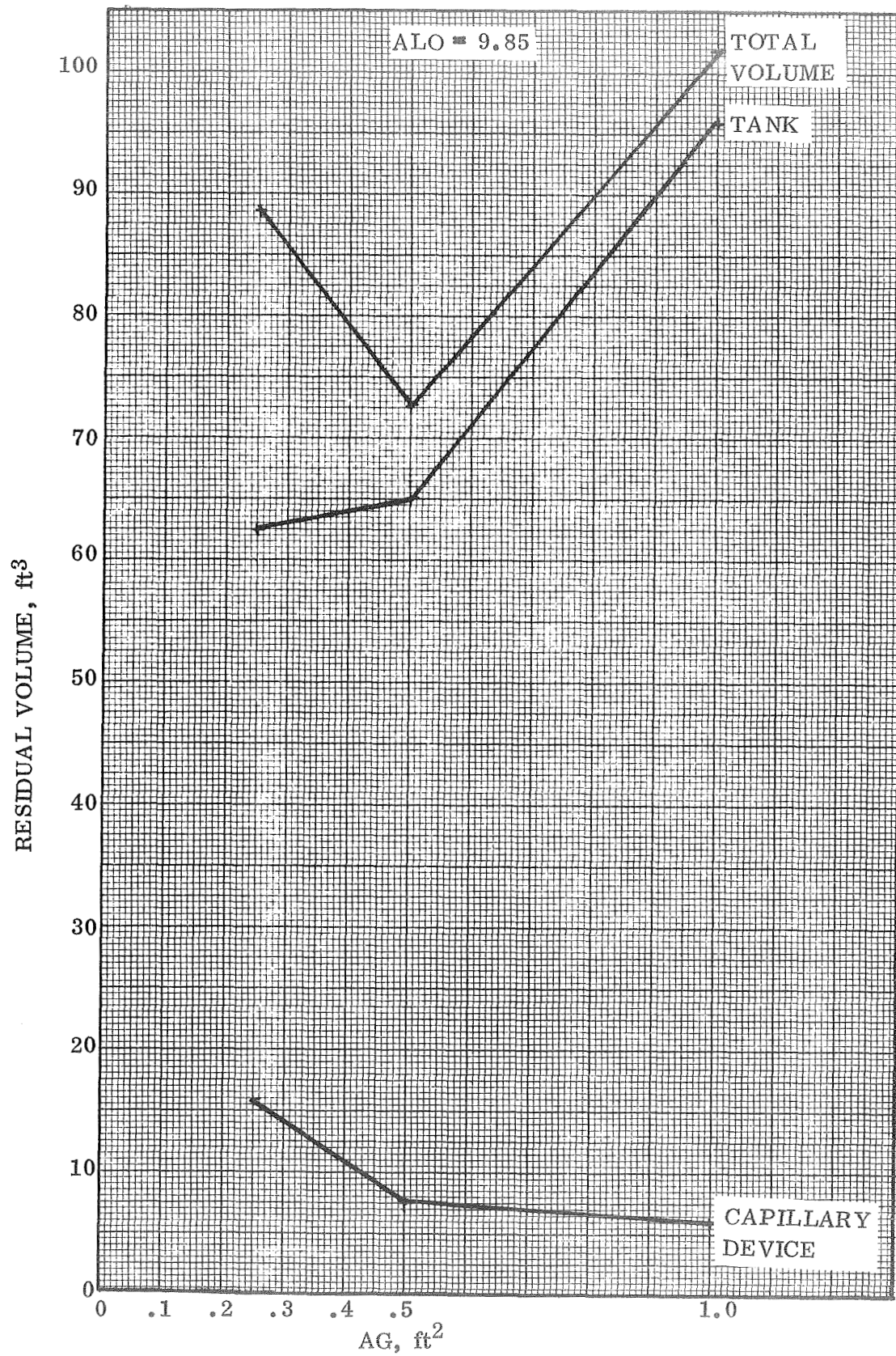


Figure 2-8. S-IVC LO<sub>2</sub> Tank Residuals

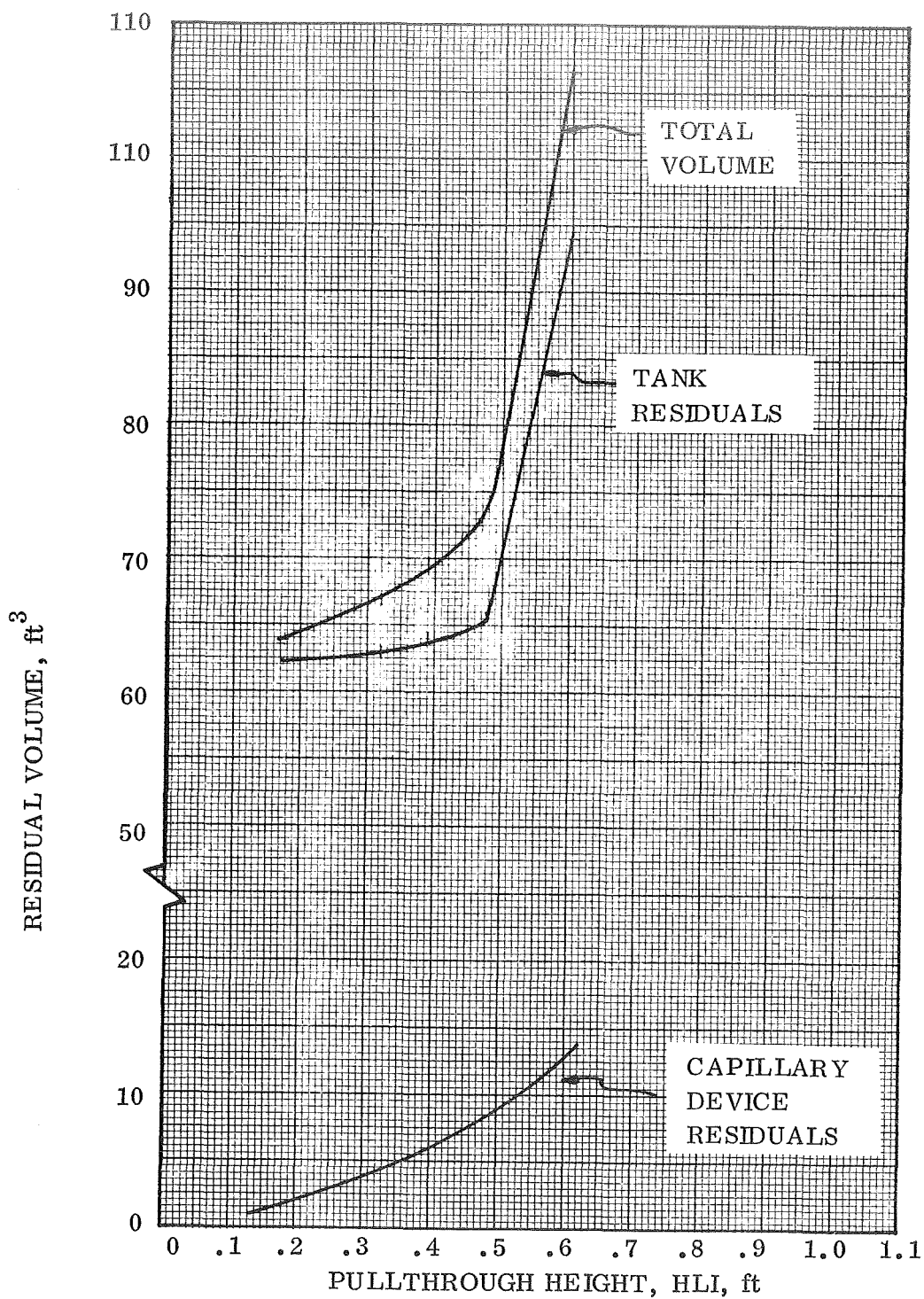


Figure 2-9. Residual Volume Vs Pullthrough Height

AG = 0.5  
HLI = 0.25

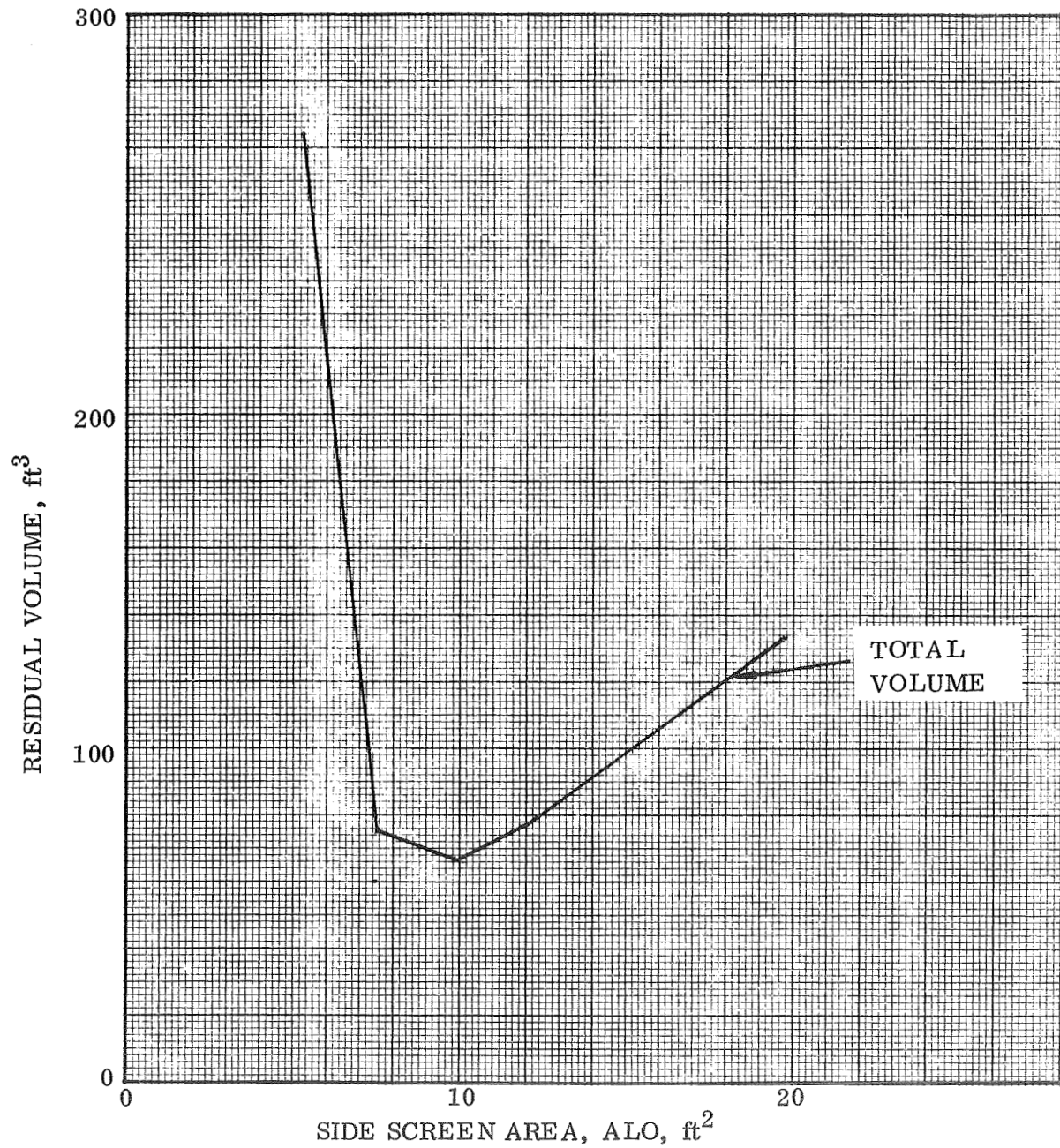


Figure 2-10. S-IVC LO<sub>2</sub> Residuals

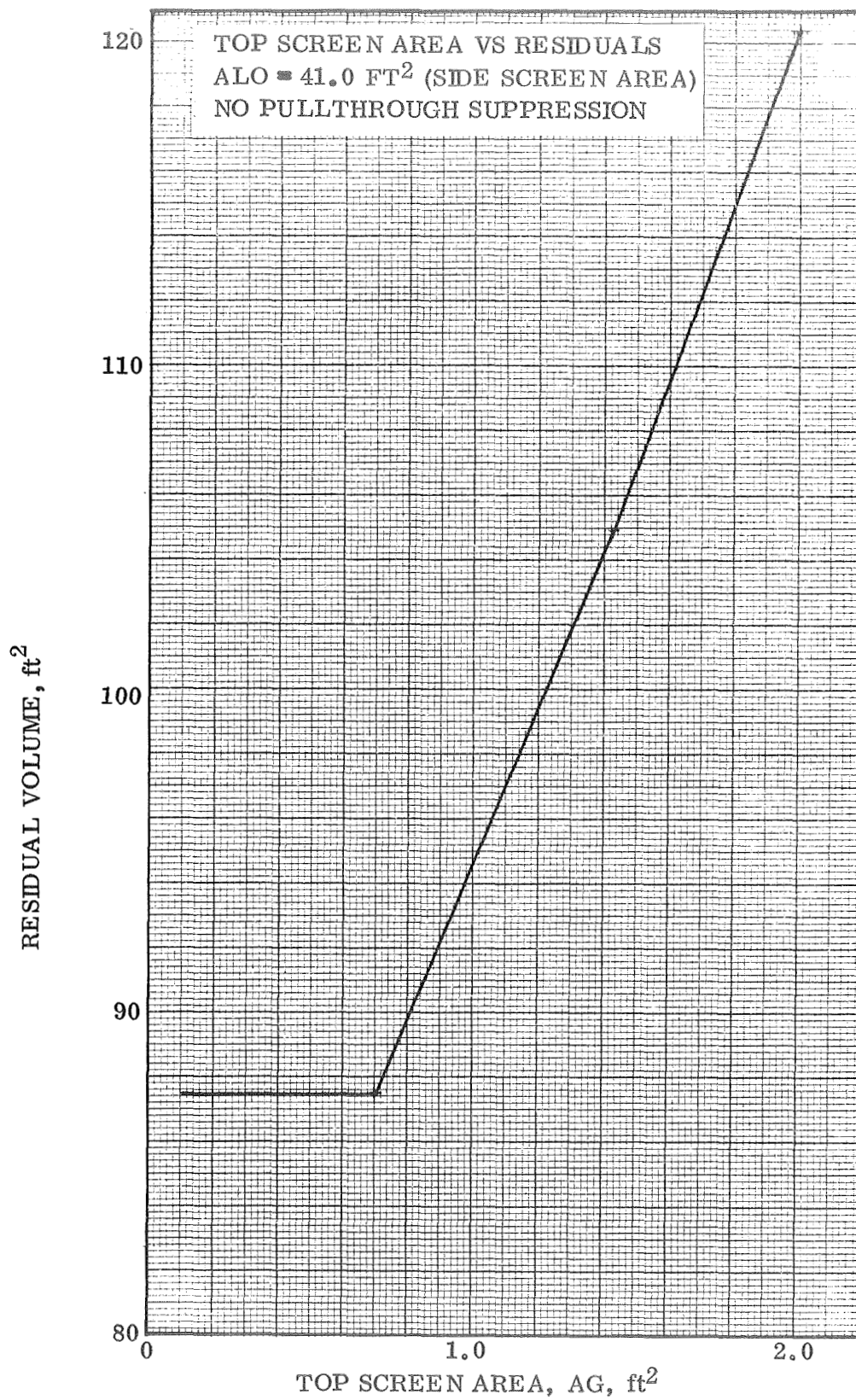


Figure 2-11. S-IVC LH<sub>2</sub> Tank

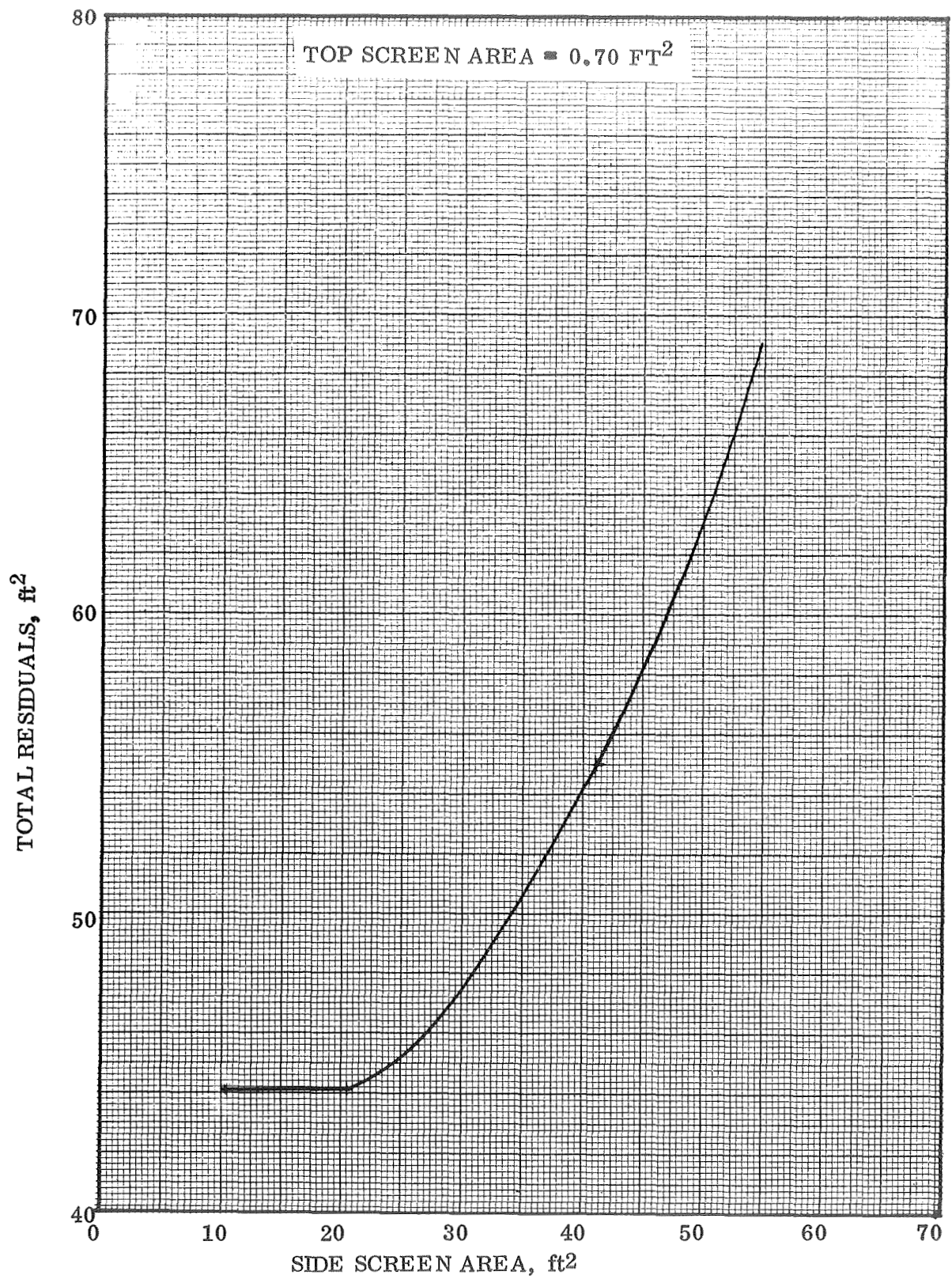


Figure 2-12. S-IVC LH<sub>2</sub> Residuals Vs Side Screen Area Pullthrough at the Top of the Feedline

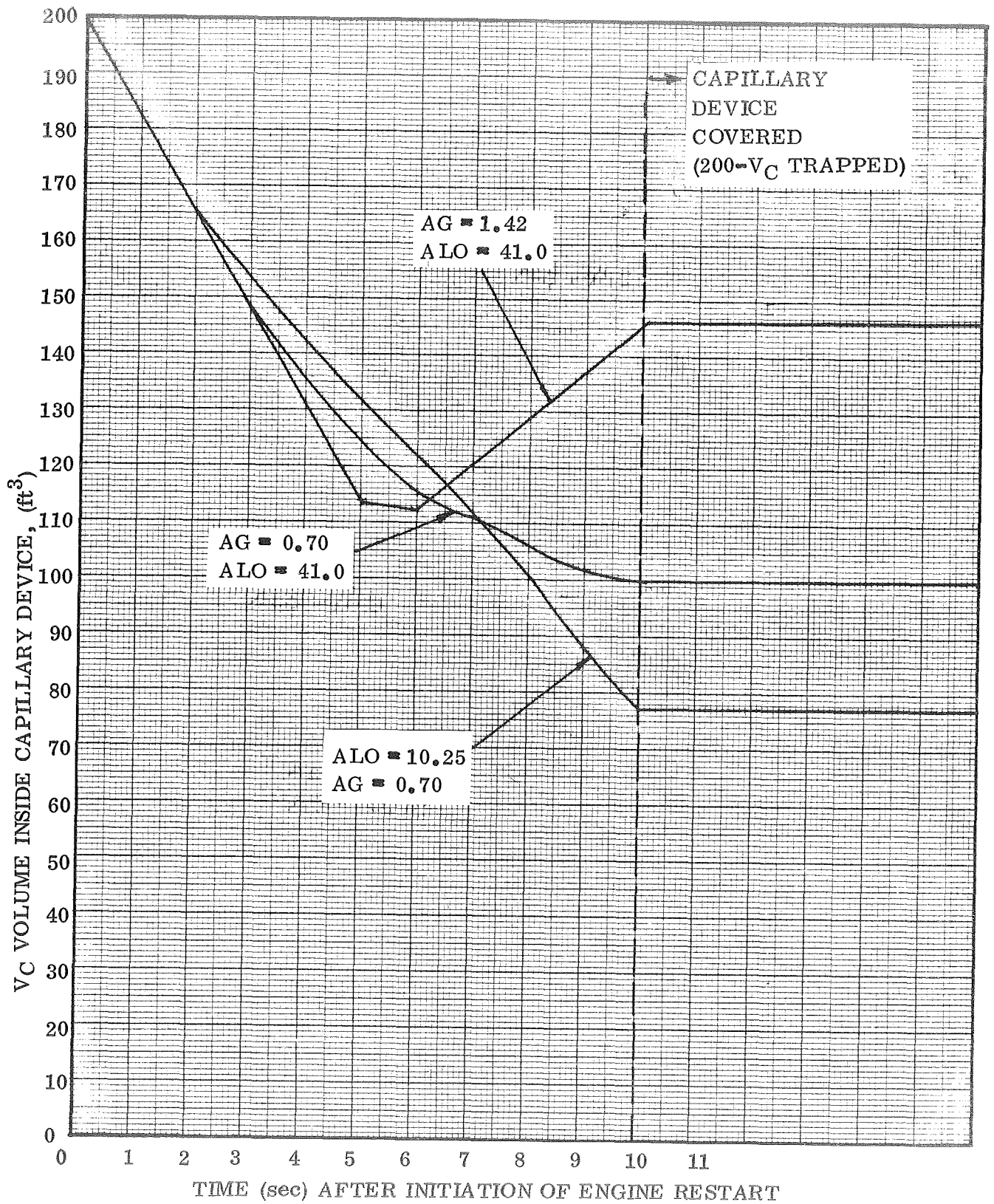


Figure 2-13. S-IVC LH<sub>2</sub> Spilling and Refilling

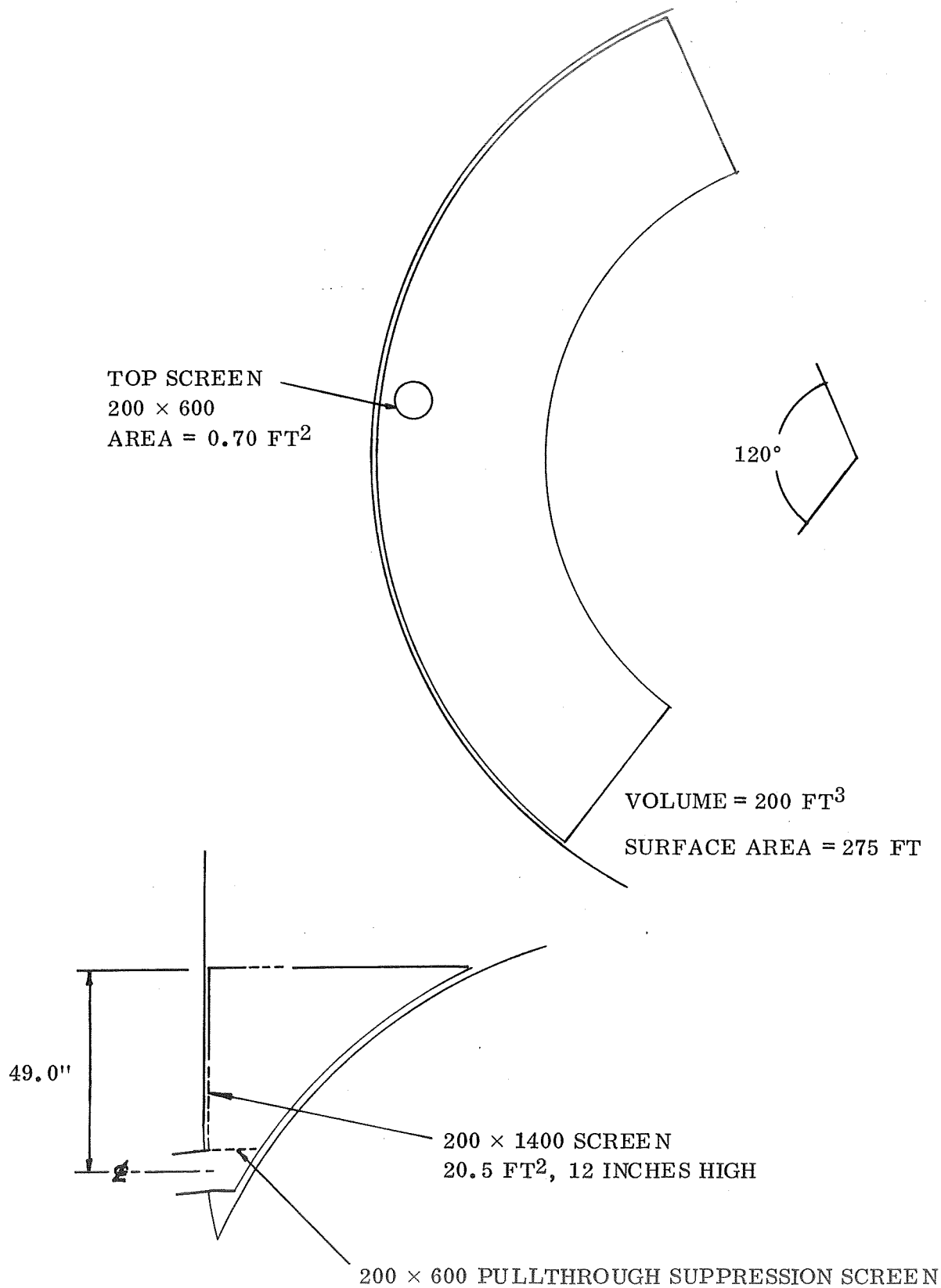


Figure 2-14. S-IVC LH<sub>2</sub> Capillary Device Configuration (Deflector Screens Shown in Figure 2-21)

suppression. For the screen placement suggested in Reference 2-2, residuals will be approximately  $68.5 \text{ ft}^3$ . This is based on interface shape generated from the pull-through expression when  $h_c \ll r$ . Pullthrough suppression to below this level is discussed in Section below.

For the S-IVC  $\text{LH}_2$  tank, the configuration initially selected had the top screen area  $AG = 1.42$  and the side screen area  $AL\phi = 41 \text{ ft}^2$ . This configuration was selected mainly from INGASP evaluation. Using DREGS2, this configuration was found not to be optimum in terms of residuals. The top screen was found to be .70 for minimum residuals, as shown in Figure 2-11. With this top screen area, the side screen area, as shown in Figure 2-12, for minimum residuals is  $20.5$  or  $10.25 \text{ ft}^2$ . Inputting configurations with  $AG = .70$  and  $ALO = 10.25 \text{ ft}^2$ , and  $AL\phi = 41 \text{ ft}^2$ , results of restart and refilling runs from INGASP are shown in Figure 2-13. This figure illustrates that, for the refilling profile which is based on extrapolated MAC model settling, the refilling is more difficult with the new configurations than with the initial standpipe and side screen dimensions. The vapor in the capillary device at the time liquid outside the capillary device reaches a level above the top screen will be trapped within the capillary device. This time is estimated to be 10 seconds, as shown in Figure 2-13. Based on these settling assumptions, it appears feasible to safely use the configuration which yields minimum residuals even though the initial configuration performs better from a refilling standpoint. If the mission were a multiple restart mission, a configuration such as initially selected might be selected because of the higher relative importance of the refilling process.

The configurations selected based on this analysis are shown in Figures 2-6 and 2-15. Pullthrough suppression screens were placed, using S-IVC scale model interface shape data, at .20 inches above the outlet for the  $\text{LO}_2$  case and right at the top of the outlet for the  $\text{LH}_2$  case. Residuals will thus be  $64.5 \text{ ft}^3$  for the  $\text{LO}_2$  tank and  $44.2$  for the  $\text{LH}_2$  tank.

**2.2.4  $\text{LO}_2$  TANKER RESIDUALS.** For gravity fields of  $6.5 \times 10^{-4}$  to  $3.0 \times 10^{-5} \text{ g's}$  experienced by the  $\text{LO}_2$  tanker during draining, the capillary device shown in Figure 5-48 will be able to hold liquid within the channels until the pressure drop across the screen exceeds the surface tension retention pressure drop of the screen. At this point, vapor will begin to flow across the screen, causing a loss of capillary device retention capillary with subsequent liquid spillage from the channels.

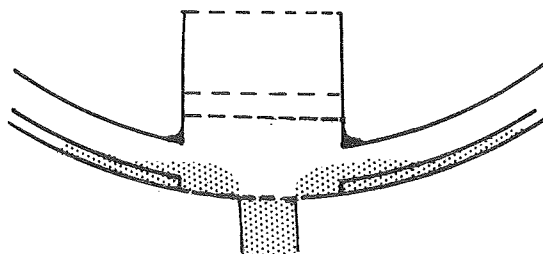


Figure 2-15.  $\text{LO}_2$  Tanker Drawing.

Draining will occur as discussed in Section 2.8 of the design handbook. If no precautions are taken it is likely that vapor will be ingested into the capillary device near the outlet and would probably be transferred into the outlet before the spilled liquid would cover the outlet. Spilling should thus be forced to occur well before this time by causing the top screens to dry out during scavenging, well before vapor is ingested into the capillary device near the outlet. Eventually a configuration will occur as shown in Figure 2-15 with vapor pullthrough just about to occur.

The residuals in the tank can be estimated if the interface shape at pullthrough is known. An attempt was made to use the Convair SURF model to predict pullthrough and resultant interface shape during draining. Several runs were made at  $6.5 \times 10^{-4}$  g's with a simulated  $\text{LO}_2$  tanker configuration. Numerical instabilities resulted due to the cell mesh being too coarse near the outlet. Refining the cell mesh prevented instabilities however unfortunately, time steps were forced to be so small as to make running of the problem to pullthrough financially infeasible. The prediction of pullthrough in the  $\text{LO}_2$  tanker was thus estimated from semiempirical correlations suggested in Reference 2-3. Using the method outlined for the S-IVC  $\text{LO}_2$  tank, the pullthrough suppression screen was placed .30 feet above the outlet. This is for a configuration without a sump. For a configuration with a sump, it should be possible to drain the tank completely with the exception of some small fillets between the channels and tank and channels and reservoir. A residual estimate of 33 lbs was made for this case in the systems comparison of Phase I.

### 2.3 SETTLING ANALYSIS

Based on the MAC model runs made in Phase I, additional analysis was conducted to determine S-IVC  $\text{LH}_2$  tank liquid settling and reorientation times. Two techniques were employed; the SLØSH program and the summing of the fluid dynamic sequential processes.

Several settling cases were run using SLØSH, a simplified MAC code, with relatively coarse mesh ( $6 \times 6$  cells) in cylindrical coordinates. The un baffled tank, containing  $\text{LH}_2$  in a simulated zero-g configuration, is 10.8 feet in radius and 28.8 feet tall. Settling acceleration is 0.337 g.

Because of the low kinematic viscosity of liquid hydrogen and the large distance to the aft end of the tank, violent splashing occurred as the two descending fluid columns met. As time progressed, the violent splashing resulted in a situation where almost all of the cells contained fluid marker particles. Since the MAC method considers such cells as full, this point marked the limit of usefulness of this problem.

The obvious solution is to increase resolution by decreasing the cell size to approximate the size of the splashing blobs of fluid. This would, of course, materially increase the problem running time. For the above problem, three seconds output were produced in three minutes of computer time. To decrease the cell size to the size of the fluid particles would make the problem unfeasible to run due to the large amount

of computer time required. It thus appears that the settling results presented in Reference 2-1 for the S-IVC application are as accurate as can be expected with the MAC method.

The other method used divided settling phenomena into these separate categories:

1. liquid descent
2. splashing up and free fall descent
3. high amplitude sloshing
4. turbulence decay
5. rise of entrained vapor

#### Liquid Descent

SURF analysis, Reference 2-1, shows that at about four seconds after the 0.337 g acceleration is applied, enough liquid has left the top of the tank so that sufficient liquid has reached the aft bulkhead to initially submerge the start basket.

#### Splashing

SURF analysis indicates that local tank bottom velocities probably do not exceed 20 ft/sec. The splashing time was estimated by computing the trajectory of a splashing stream of propellant. For the velocities anticipated, the fluid will take approximately four seconds to redescend to the tank bottom after splashing.

#### Slosh Decay

Precise slosh decay times are difficult to obtain without extensive quantitative analysis. Estimates indicate that several seconds would be required to permit continuous submergence of the start basket. The slosh decay relationships for viscous damping of linear motion, Ref. 2-4, cannot be used because it is obvious that the high amplitude waves are highly non-linear.

#### Turbulence Decay to Release Bubbles

Bubble size and rise is governed by the scale and intensity of the fluid turbulence. Assuming that the Kolmogorov scale, Ref. 2-5, is of the order of the bubble size, bubble rise can be estimated by comparing the inertia (turbulence) forces with the buoyancy forces. Using References 2-5 and 2-6 we find that in order to obtain indication of good bubble rise  $t \ll 17$  seconds.

## Bubble Rise

Bubble speed can be estimated by balancing drag and buoyancy forces. Using the turbulent drag law, we find that the bubble rise velocity will be approximately 0.3 ft/sec. Thus, for a three foot liquid depth we must allow 10 seconds.

The settling times can individually be listed as:

- |   |           |
|---|-----------|
| 1. Liquid descent to cover start basket | 4 sec.    |
| 2. Splashing                            | 4 sec.    |
| 3. Slosh Decay                          | 2-10 sec. |
| 4. Turbulence Decay                     | 17 sec.   |
| 5. Bubble Rise                          | 10 sec.   |

This summary is not entirely satisfactory because, even if the times are assumed additive (the processes mutually exclusive), production of slosh energy and turbulence will continue until all liquid descent and splashing has ceased.

A practical solution is to assume:

1. Complete liquid descent takes 10 seconds.
2. Splashing and high amplitude sloshing will occur, but the start basket will not be uncovered.
3. Turbulence decay cannot start until 10 seconds after thrust application.

## Conclusions

Ten seconds is required to start turbulence decay. At that time the basket will be continuously covered and refilling will proceed continuously. Turbulence decay will take perhaps 20-30 seconds (maybe more). Bubble rise will occur in about 10 seconds.

## 2.4 WICKING ANALYSIS

Wicking along screens and between perforated plates may be used to prevent drying out of screens and vapor formation in a capillary device caused by heating. A discussion in Reference 2-3 summarizes the equations to be used to predict wicking. Wicking data was compared to analytical models which are described in this section. On this basis a semiempirical correlation was chosen for predicting screen wicking.

Four models were examined to predict screen wicking: a capillary flow model including momentum and end drag terms, a simplified capillary flow model, a semi-

empirical model based on screen flow data developed under a Convair IRAD program, and a semi-empirical model developed by Armour and Cannon, Reference 2-7.

The capillary flow model for a vertical capillary is given by

$$\begin{aligned} \frac{d}{dt} \left\{ \pi R^2 \left[ \rho h + \rho_a (\ell - h) \right] \right\} \frac{dh}{dt} &= 2 \pi R \sigma \cos \psi - 8 \pi \frac{dh}{dt} \left[ \mu h + \mu_a (\ell - h) \right] \\ &\quad - \pi R^2 g h (\rho - \rho_a) - \frac{1}{4} \pi R^2 \rho \left( \frac{dh}{dt} \right)^2 \end{aligned} \quad 2-1$$

rate of change of momentum                      surface tension                      viscous resistance                      gravity                      end drag

where

- R is the average capillary radius
- $\rho$  the liquid density
- $\rho_a$  the vapor density
- $h_\infty$  the final wicking height =  $(2\sigma \cos \psi) / (\rho g R)$
- h the height at time (t)
- $\ell$  the height of the screen
- $\sigma$  the surface tension
- $\psi$  the contact angle
- $\mu$  is the liquid viscosity
- $\mu_a$  is the vapor viscosity

This equation is generally simplified by assuming the rate of rise is slow enough to permit the rate of change of momentum and end drag terms to be neglected. This results in an expression,

$$t = \frac{8}{R^2 \rho g} \left\{ \left[ (\mu - \mu_a) h_\infty + \mu_a \ell \right] \ln \left( \frac{h_\infty}{h_\infty - h} \right) - (\mu - \mu_a) h \right\} \quad 2-2$$

and for a horizontal screen with  $\psi = 0$ , and  $\mu \gg \mu_a$ ,

$$t = \frac{2\mu h^2}{\sigma R}$$

Equation 2-2 has been correlated with test results at normal gravity using heptane, butyl alcohol and other similar organic fluids. Results show good agreement and indicate that the simplifying assumptions are reasonable. Where wicking velocities are high such as in low gravity applications of interest, the rate of change of momentum and end drag terms will be larger relative to the other terms of equation 2-1.

Thus, an attempt was made to solve equation 2-1 in order to correctly model low gravity wicking. Equation 2-1 was manipulated to the form:

$$\left[ \rho h - \rho_a (h_\infty - h) \right] \frac{d^2 h}{dt^2} + \left[ \frac{5\rho}{4} - \rho_a \right] \left( \frac{dh}{dt} \right)^2 + \frac{8}{R^2} \left[ \mu h + \mu_a (\ell - h) \right] \frac{dh}{dt} + (\rho - \rho_a) gh - \rho g h_\infty = 0$$

which simplifies to

$$\frac{d^2 h}{dt^2} = - \frac{5}{4h} \left( \frac{dh}{dt} \right)^2 - \frac{8\mu dh}{R^2 \rho dt} - g + \frac{gh_\infty}{h} \quad \text{where } h_\infty = \frac{2\sigma \cos \psi}{\rho g R} \text{ and } \rho \gg \rho_a, \mu \gg \mu_a$$

This equation has been numerically evaluated using a Runge-Kutta method computer program solution.

Another model which was examined to evaluate screen wicking was the screen flow pressure drop model of Armour and Cannon given by the equation

$$\frac{\Delta P g_c \epsilon^2 D}{Q B \rho \mu^2} = \frac{8.61}{Re} + 0.52$$

where  $D = D_{BP}$ ,  $\epsilon = \phi$ , the porosity,  $Q$  is the tortuosity and  $B$  is the screen thickness. Setting  $\Delta P$  to the surface tension driving pressure  $\frac{4\sigma}{D_{BP}}$ , and  $B$  equal to  $h$  the distance wicked along the screen we can solve the velocity in a wicking screen

$$\frac{dh}{dt} = - \frac{8.25 \mu a^2 D}{\rho} + \sqrt{\left( \frac{8.25 a^2 D}{\rho} \right)^2 + \frac{1.92 \epsilon^2 D (h_\infty - h) g_c \sin \theta}{h}}$$

for the non-horizontal case where

$a$  = surface to volume ratio

$\theta$  = angle between the screen and the horizontal plane

$$h_\infty = 4\sigma / \rho g D_{BP}$$

and for the horizontal case

$$\frac{dh}{dt} = \frac{-8.25 \mu a^2 D}{\rho} + \sqrt{\left(\frac{8.25 a^2 D}{\rho}\right)^2 + \frac{15.35 \epsilon^2 \sigma g_c}{h \rho}} \quad 2-3$$

Both the horizontal and non-horizontal case were solved using the Runge-Kutta numerical technique.

The other approach to predicting screen wicking was to use screen flow data, represented by an equation of the form

$$\Delta P = \frac{4\sigma}{D_{BP}} = \frac{A_1 \mu V L}{D_a^2 g_c} + \frac{A_2 L \rho V^2}{D_a g_c} \quad \text{for the horizontal wicking.} \quad 2-4$$

Solutions were obtained for wicking tests discussed in Section 4.0 . Wicking predictions made using the equations discussed were used to simulate test conditions for the screens tested. Typical results are shown in Figure 4-1 along with the recommended correlation equation obtained from the test data. Since the equations presented did not successfully predict wicking, the numerical solution computer programs will not be presented here, but may be found in the third quarterly progress report, Appendices A and B.

## 2.5 ULLAGE COLLAPSE

Pressurization with hot gas during engine firing may lead to severe ullage pressure decay after engine shutdown due to liquid mixing with the ullage. If decay proceeds to below liquid vapor pressure, boiling may occur within the start basket.

An analysis was performed for the S-IVC LH<sub>2</sub> tank, based on AS-203 and Centaur data to determine acceptable GH<sub>2</sub> pressurant inlet temperature to assure that bulk boiling would not occur. The PRISM program was used to determine ullage pressure collapse from a tank pressure of 40 psia following an engine firing. A liquid vapor pressure of 25.0 psia, and 70% propellants were assumed. Ullage temperature (which was assumed equal to the unwetted tank skin temperature) was the variable in this analysis. Two cases of fluid mixing to equilibrium were considered: (1) liquid quenching of the tank walls, whose energy release would result in liquid evaporation, followed by liquid/vapor mixing to equilibrium, and (2) fluid mixing with no tank wall quenching. Figure 2-16 shows the influence of initial ullage temperature upon final ullage pressure. The quenching and mixing curve indicates that boiling will not occur at any initial ullage temperature. A minimum final pressure of 25.0 psia will occur for a 100°R ullage, which indicates that the boiling threshold will be attained for that ullage condition. The mixing-only curve indicates that LH<sub>2</sub> boiling will occur for initial ullage temperatures greater than 80°R. A 0.55 psi vapor pressure reduction will occur for a 200°R ullage. This pressure decay will cause sufficient boiling in the start basket to generate 7% vapor by volume. This quantity of vapor generation does not

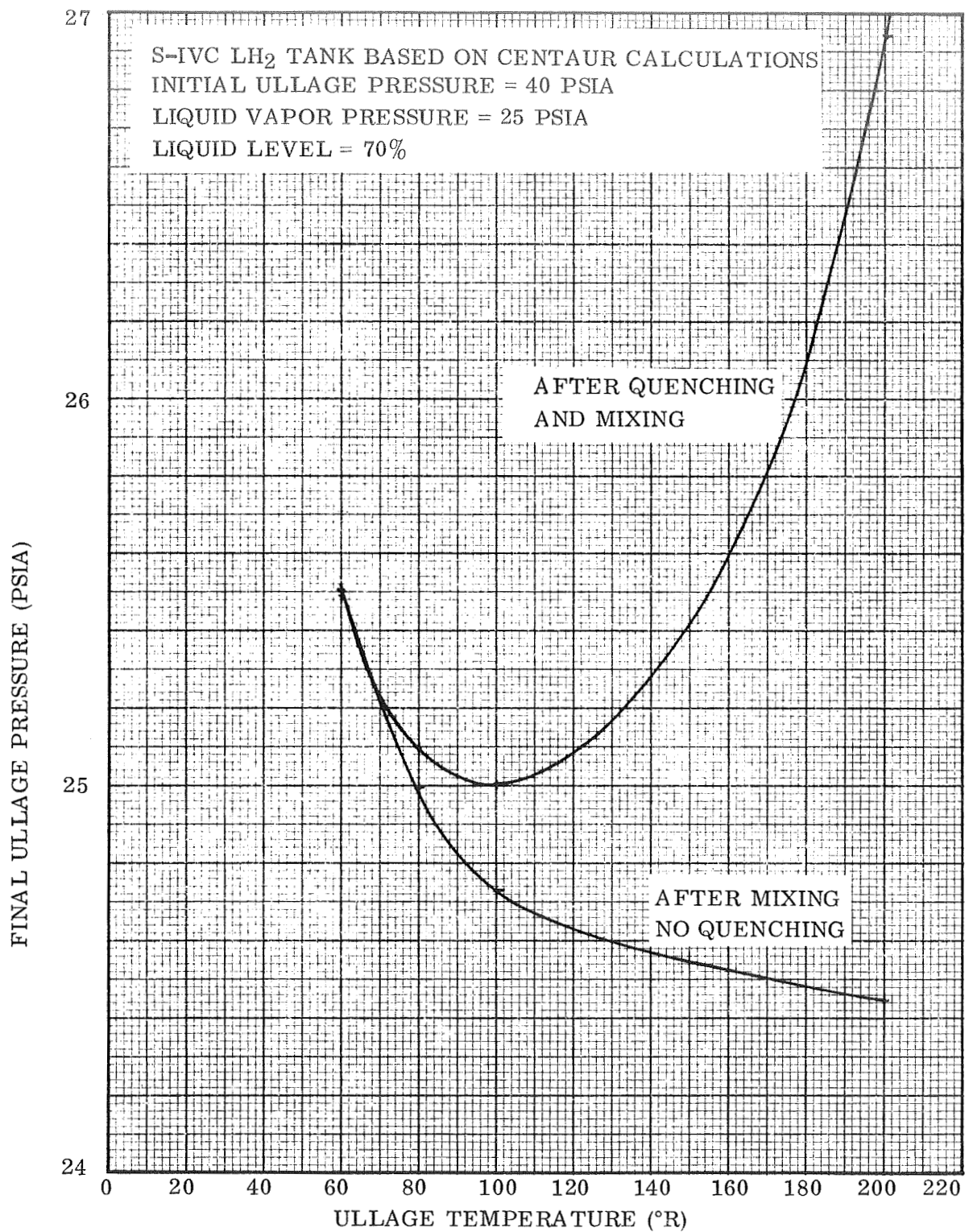


Figure 2-16. Ullage Pressure After Engine Firing

appear to be excessive. Furthermore, it is unrealistic to assume that complete liquid and vapor mixing will occur while tank skin quenching does not exist. It would be more accurate to assume the converse is true.

It is expected that the real tank condition could lie above the quenching plus mixing curve. A conservative estimate, however, would place the fluid conditions between the two curves of Figure 2-16. Thus, one would conclude that the minimum tank pressure would occur for an initial ullage temperature between 100°R and 120°R. Assuming a final tank pressure midway between the curves results in a minimum of 24.86 psia, or a vapor pressure collapse of 0.14 psia. Bulk boiling would result in about 2% vapor by volume generated within the start basket, which should prove to be no hazard for engine start purposes. Cooling of the basket by vent fluid can further minimize this effect.

## 2.6 SCREENED CAPILLARY LIQUID COLLECTOR TUBES

The LH<sub>2</sub> tank heat exchanger vent system will require a continuous liquid supply for operation during an extended coast duration. It has been decided to employ screened capillary tubes as liquid collectors to achieve this end. The choice of a small tube diameter in the order of 1-2 inches will guarantee liquid containment under aerodynamic drag conditions and attitude control motor operations. The use of a 200 × 600 dutch twill screen material for tube fabrication will assure a liquid film throughout and permit flow losses of approximately 7 psf without vapor breakthrough. An evaluation has been conducted to consider the effects of collector tube placement and system losses on the design of such a liquid collection device.

The placement of collector tubes within the fuel tank is not critical. Because of the approximate 60% full tank condition to exist in orbit, any number of collector tube configurations should suffice. The selected configuration shown in Figure 5-11 will assure that a sufficient percentage of the tube surface area will be covered with liquid to prevent liquid pressure drop across the screen from exceeding the surface tension pressure retention capability of the screen.

An analysis was made to compute collector tube line pressure losses as well as screen flow losses during operation. An LH<sub>2</sub> vent rate of 10.8 lb/hr was assumed which is required to remove 2100 Btu/hr of energy from the tank. Friction factors were determined for 1/2 inch diameter tube on the basis of rough internal surface. The pressure loss per unit length is plotted in Figure 2-17. Pressure losses due to flow through the wetted area of 200 × 600 dutch twill screened collector tubes were computed for 1.0, 2.0 and 10.0 ft of wetted length. These flow losses were based on empirical data given in Figure 50 of the Second Quarterly Progress Report, and is presented in Figure 2-17.

It is clear that the total collector tube pressure loss will be in the order of 0.1 psf. A wetted 200 × 600 dutch twill material can withstand approximately 7 psf differential pressure, as shown on Figure 2-18 for a 19μ bubble point, before the surface tension pressure is exceeded. It is evident, therefore, that system pressure losses will

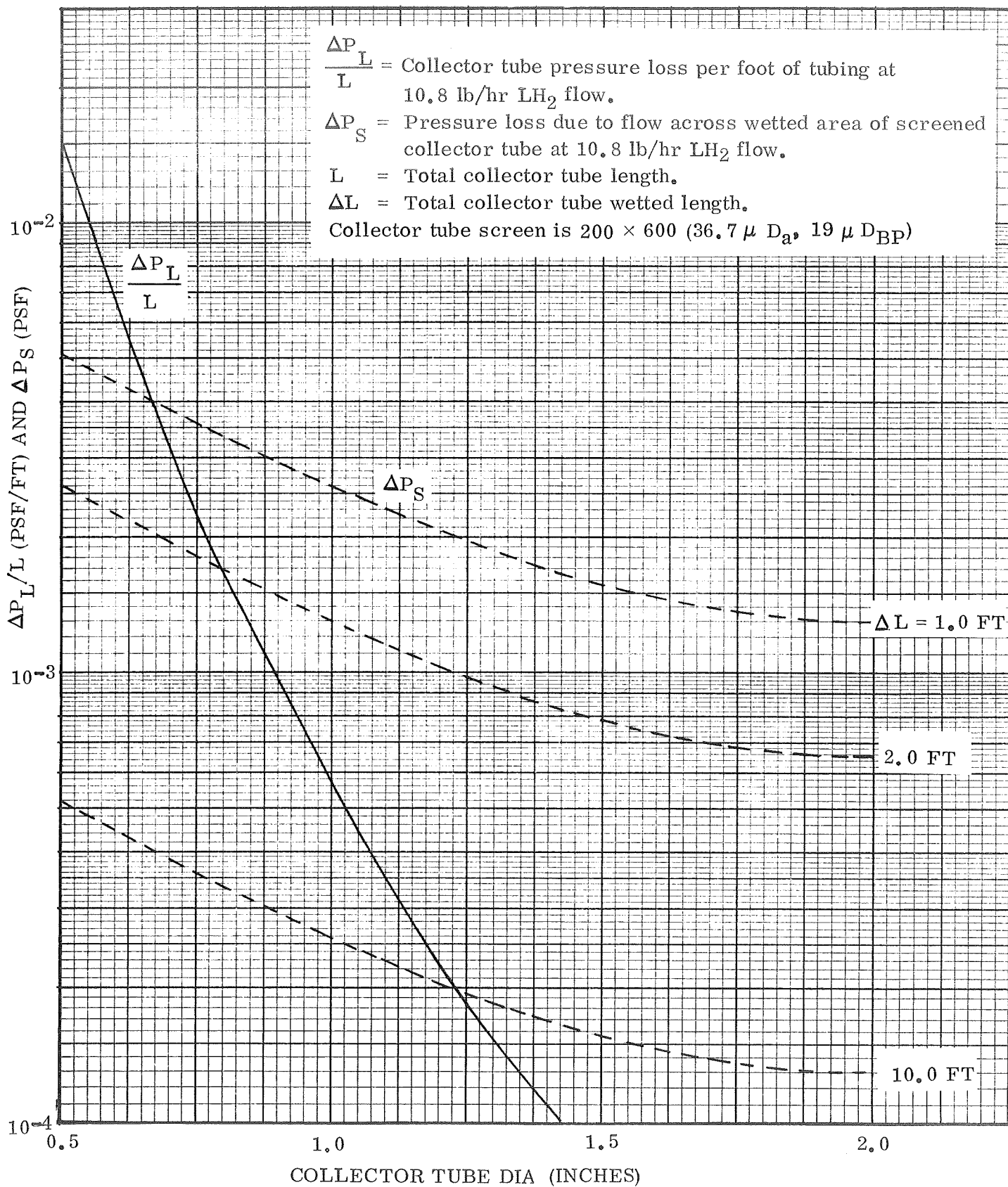


Figure 2-17. Screened Capillary Collector Tube Pressure Losses Versus Tube Diameter

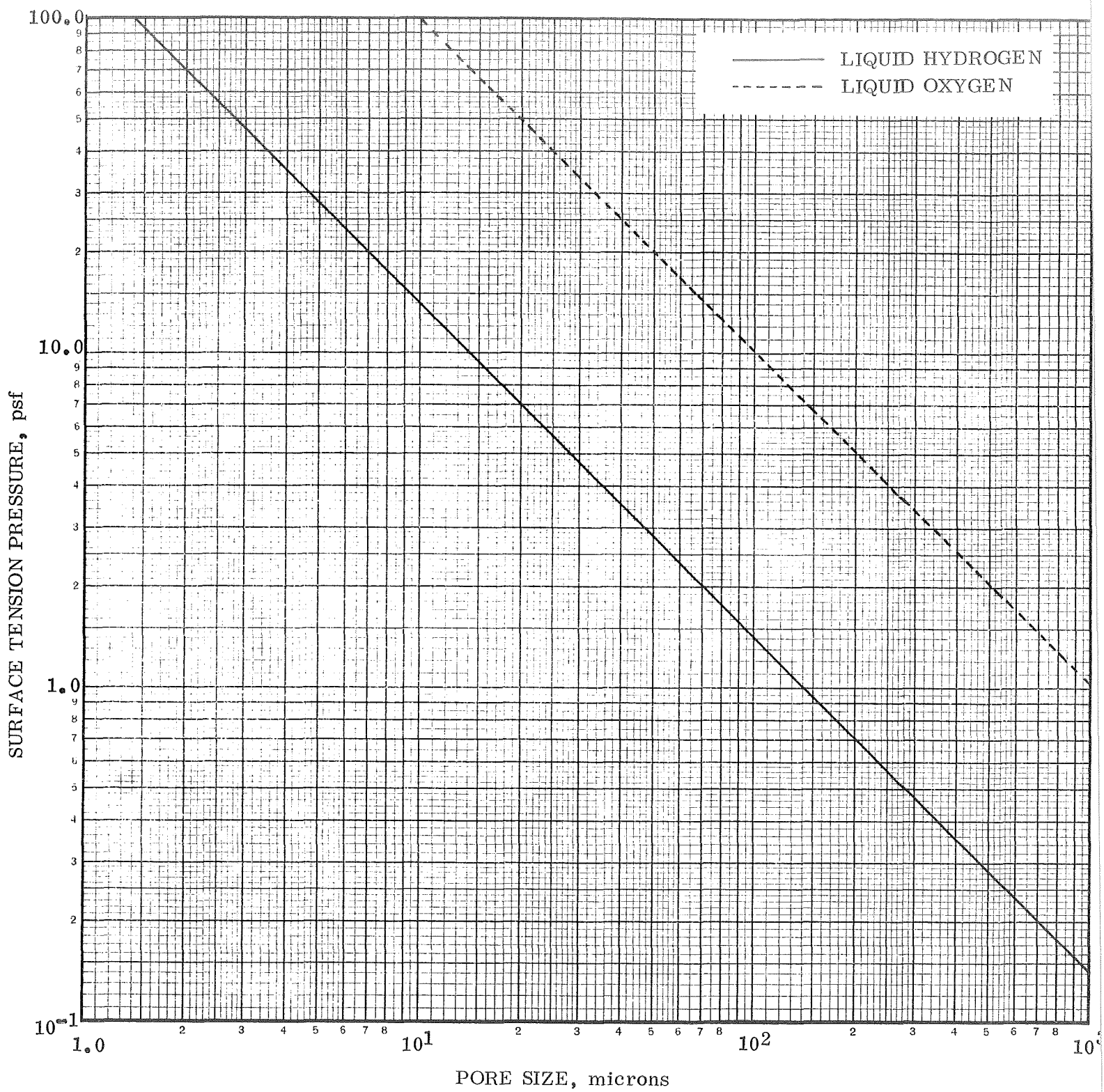


Figure 2-18. Surface Tension Pressure

be sufficiently small that liquid collector tube design will not be compromised by requirements to minimize flow losses.

Collector tube sizing calculations were also made for supplying pure liquid inlet to the vent device for the LOX tanker configuration. The channels are individually thermal controlled by collection  $\text{LO}_2$  from each  $14" \times 1.4"$  channel, throttling the fluid through separate "viscojets" for each channel and then flowing the vent fluid through individual heat exchanger tubing attached to the channels.

An analysis was conducted to evaluate system flow losses both upstream and downstream of the throttling device. It was determined that the combined flow losses, excluding the throttling device, would be considered negligible. These flow losses were based on a channel cross-section of  $1.4 \times 14.0$  inches,  $1/8$  inch I. D. tubing, and a 2.0 lb/hr vent flow rate split into eight separate paths.

## 2.7 PROPELLANT CONTROL SCREENS

Positioning propellants near the aft bulkhead of a propellant tank will reduce the time required to refill a capillary device located at the tank outlet. An analysis was performed to see if the additional weight of a system using propellant screens to reduce settling time would be offset by the reduction in capillary device weight.

The propellant control screen placement chosen for the S-IVC  $\text{LH}_2$  tank is shown in Figure 2-19. Initial calculations were made to determine how much boiling would occur in the aft end of the tank. The boiloff, based on the heating rates given in Reference 2-1, Table 2-1, was expressed as  $(1546 + 8.8h) \text{ft}^3$  where  $h$  is the distance between the screen and the highest point on the intermediate bulkhead. The volume of the liquid contained within the screen is given by  $h = 3.22 + (V_s/361.2)$ , where  $V_s$  is the volume available for settling. For a volume of  $400 \text{ft}^3$  available for settling,  $h = 4.32 \text{ft}$ . For this volume and height settling time will be reduced approximately in half, thus allowing reduction in capillary device volume.

In order for the propellant control screen to contain propellant during the low gravity coast period prior to restart, the screen must remain completely wetted. This requires the screen surface to be cooled by the thermodynamic vent system cooling coils. The reduced start basket volume allows some of the cooling coils for the start basket to be used to cool the propellant control screen. Screen hole sizes are governed by the Bond number criteria at  $10^{-6} \text{g's}$ . These large holes should not interfere significantly with the settling of the main propellant mass.

Based on weight calculations of Reference 2-1, the propellant control screen would weigh 291 lbs including supports and cooling coils. Total start basket weight reduction is 101 lbs. Since the original start basket weighed 313 lbs, it is obvious that the propellant control screen concept is not attractive even if the settling time could be reduced to a very small value.

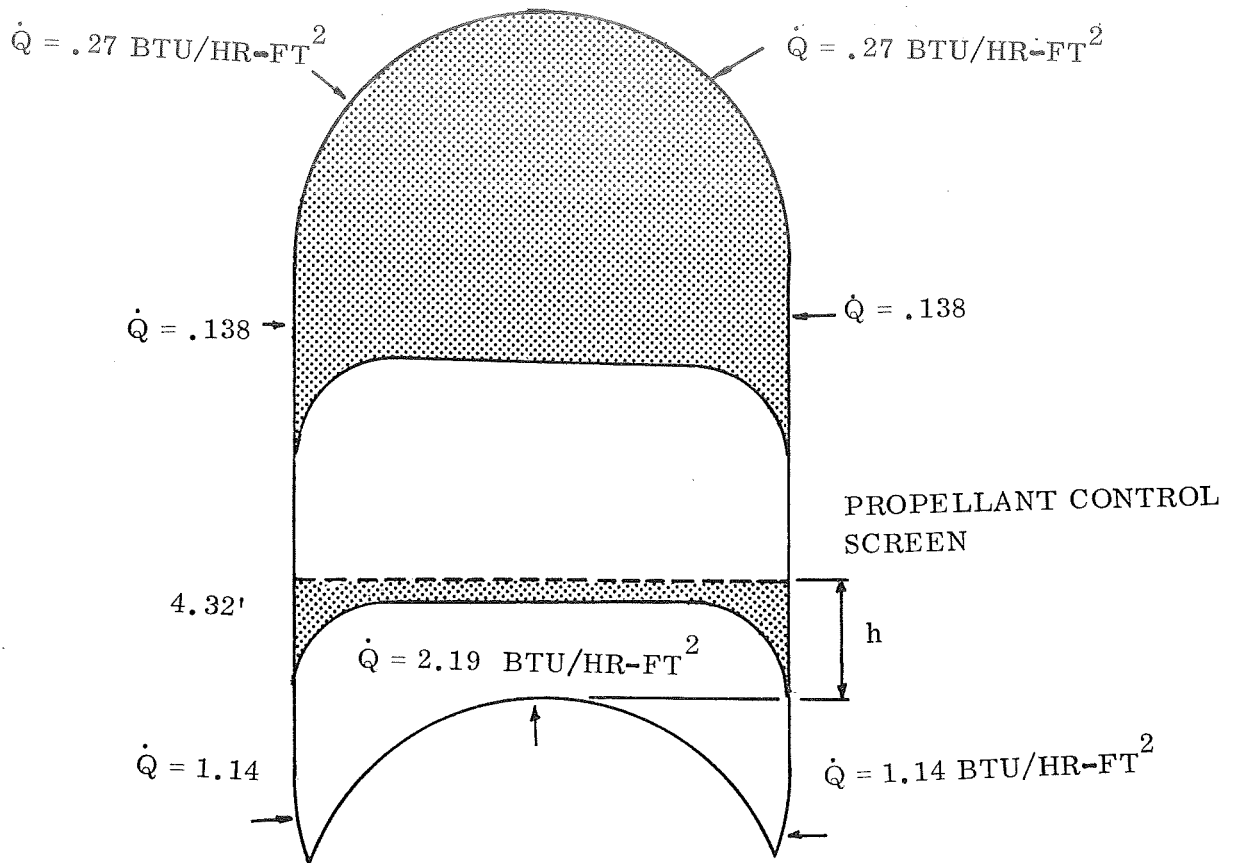


Figure 2-19 . S-IVC LH<sub>2</sub> Tank Propellant Control Screen Placement

Propellant control screens would prove more attractive if the heating rates to the aft bulkhead were lower. This would allow propellant to be positioned closer to the aft bulkhead and settling time could be reduced more substantially. Also, if a smaller amount of propellant was present in the tank, settling time without control screens would be longer. This would necessitate a large start basket which would not be needed if the propellant control screens were used. Propellant control screens could be useful if these mission conditions are present.

## 2.8 WICKING TO REDUCE STRATIFICATION

It is possible to use wicking materials as in a heat pipe to provide uniform temperature within a closed vessel. Calculations were made to determine the usefulness of wicks in reducing temperature stratification. Wicks were sized for the S-IVC LH<sub>2</sub> tank to handle the maximum heating rate which occurs at the intermediate bulkhead. For a screen liner to cover the inside of the tank, the total weight including supports will be approximately 315 lbs. This wick saves an equivalent hardware weight of 90 lbs due to mixer weight and added boiloff. The wicks will thus not be useful for the S-IVC mission.

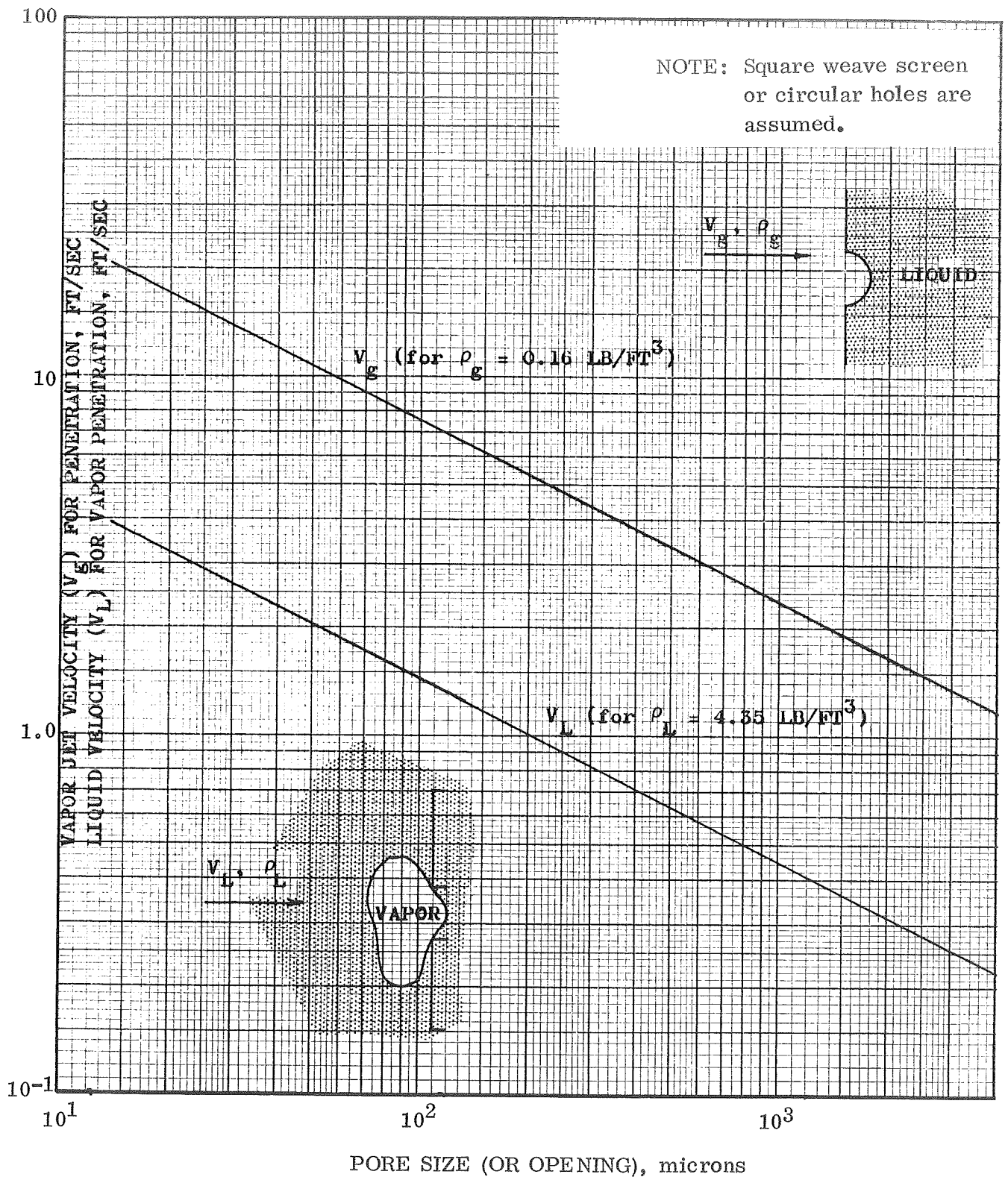


Figure 2-20. Velocity Requirements for Penetration of Vapor or Liquid Through a Liquid Hydrogen Wetted Screen or Plate

If the lateral accelerations are held to a minimum it will be possible to use a single wick along one side of the tank to reduce stratification. This configuration would, roughly, weigh 90 lbs. This makes the mixer system slightly better than the wick because some mixer power is used to provide high heat transfer coefficient to the hot side of the thermodynamic vent system, thus reducing the weight of this system.

For a mission such as the LOX tanker propellant transfer mission the capillary device covers a substantial portion of the tank surface area. This screen material can be utilized to reduce or eliminate temperature stratification in the propellant. However, based on Reference 2-8, heat pipe information and wicking rates for the screens to be used on the LO<sub>2</sub> tanker, insufficient volume flow will be pumped to effectively reduce stratification unless a wick is fabricated specifically for this purpose. Another problem with attempting to use the heat pipe principle is the degradation in performance due to a noncondensable pressurant gas.

## 2.9 VAPOR IMPINGEMENT

During the reorientation of fluid from its low gravity position to a settled orientation, the fluid experiences extreme turbulence for the S-IVC case. This turbulence could cause vapor to be entrained in the liquid which is flowing into the capillary device. Vapor alone will not have sufficient momentum to overcome the surface tension pressure and enter the capillary device.

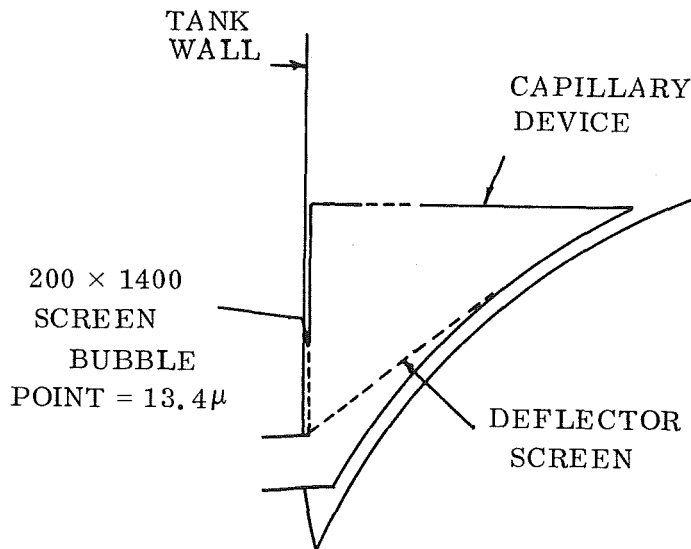
The vapor which has entered the capillary device since it has been slowed by passing through the screen, can be intercepted by placing a screen over the outlet to deflect any vapor which would otherwise enter the outlet.

Figure 2-20 shows that for a 15 micron bubble point screen, the impingement velocity must exceed 20 feet/sec for vapor to break through the screen. Results of MAC model runs for the S-IVC LH<sub>2</sub> tank indicate that the fluid velocities will reach a maximum of 55 ft/sec in the vicinity of the aft bulkhead. Thus, vapor impinging on the screen will be carried through and into the start basket.

Velocity reduction across the outer screen was found by using equations from Hoerner, Fluid Dynamic Drag, page 3-24. The outer screen lowered the velocity to below 4 ft/sec. Bubbles can thus be eliminated from entering the outlet by using a screen deflector. The deflector, a 200 × 1400 screen shown in Figure 2-21, operates by utilizing the surface tension pressure retention of the screen to resist the passage of vapor impinging upon it. A deflector configuration for the LO<sub>2</sub> tank would appear as a spheroid mounted over the outlet within the capillary device.

The tangential component of the velocity of the bubble, coupled with the hydrophilic tendencies of the screen in  $\text{LH}_2$  and  $\text{LO}_2$  will cause the vapor to be rejected into the top of the capillary device away from the outlet.

Vapor entering the basket due to impingement should not force liquid to spill from the start basket. The effect of vapor entering the side screen will be to reduce the vapor flow through the standpipe.



DEFLECTOR SCREEN IS ATTACHED ACROSS  
ENTIRE CAPILLARY DEVICE

Figure 2-21. Schematic of Deflector Screen to Prevent Vapor Ingestion.

# 3

## SURFACE TENSION START BASKET AND COLLECTION SYSTEMS THERMAL ANALYSIS

Of major importance in the design of capillary control devices for cryogenic fluids is the prevention of liquid evaporation due to heating and/or tank pressure changes. A concern with propellant heating is not only that internal evaporation will force liquid out the device, but that the capillary liquid retentive capability may be impaired.

This section describes the thermal analysis performed on the S-IVC start baskets and LO<sub>2</sub> tanker collection systems. Basic mission data applicable to this analysis are presented in Table 3-1.

The basic purpose of the thermal control systems is to prevent vapor formation within the containment systems and associated feed lines. The design approach taken was to eliminate all vapor formation, even though in actual operation a small amount may be permitted.

In the case of a perfectly mixed tank fluid (no superheated gas) at constant pressure with no direct contact of the basket fluid with warm tank walls, no vaporization would occur in the basket. However, under actual conditions basket supports are required, tank mixing is not complete, and the tank pressure does change. The effect of these real conditions are taken into account in the analyses presented in the following paragraphs.

### 3.1 S-IVC THERMAL ANALYSIS

The basic system proposed utilizes heat exchangers to cool the start baskets, engine feed line and to maintain constant pressure in the LH<sub>2</sub> and LOX tanks. Heat transfer to the cooling channels must be predicted in order to properly size the system. However, even with the best heat transfer predictions, fluid conditions may vary sufficiently so additional heat exchanger length must be provided for insurance.

One possible configuration is illustrated in Figure 3-1. The cold side fluid is liquid, collected by screened tubes designed to provide the necessary cooling flow. The detail design of this collection system is described in Section 5.1. Liquid inlet to the cooling system is required to assure sufficient cooling capacity. Heat exchanger coils are wrapped around the start basket to assure that no vapor is formed within it.

Table 3-1. Basic Mission Data Used in Thermal Analysis

---

S-IVC Mission

$10^{-6}$  g's Acceleration

LH<sub>2</sub> Tank

Total Heating = 2140 Btu/hr

Forward Dome and Joints = 200

Cylinder Wall = 170

Aft Dome and Joint Area = 470

Common Bulkhead = 1300

P<sub>T</sub> = 25 psia; 30 Day Mission

60% LH<sub>2</sub> During Coast

Thermodynamic Separator Assumed with 1-2 psi Band

LO<sub>2</sub> Tank

Total Heat Input = 2500 Btu/hr

Net Heating = 1200 Btu/hr

P<sub>T</sub> = 25 psia

LO<sub>2</sub> Tanker

163 Day Mission

95% Initial LO<sub>2</sub>

$10^{-6}$  Orbital Drag

LMSC Tank (218" Dia Sphere)

Total Orbital Heating = 8050 lb<sub>B.O.</sub> in 163 Days (188 Btu/hr)

P<sub>T</sub> = 15 psia

---

The engine feed line is then coiled with tubing to keep vapor from forming there. For the system shown in Figure 3-1, tubing is then wrapped around the tank to provide maximum cooling efficiency of the vented hydrogen. The LO<sub>2</sub> tank is then coiled with the GH<sub>2</sub> heat exchanger tubing around the start basket and feed line area to eliminate formation of oxygen vapor. Local overcooling of the tank wall is a possibility however. Thoroughly mixing the S-IVC LOX tank contents should prevent solid oxygen from forming. This condition is analyzed further in Section 3.1.6.

Initially the possibility of eliminating vaporization within the start baskets was investigated with the idea of reducing  $\Delta T$  for normal spacecraft surfaces. The conclusion, based on this finding, was that in order to assure no vapor formation, the start baskets

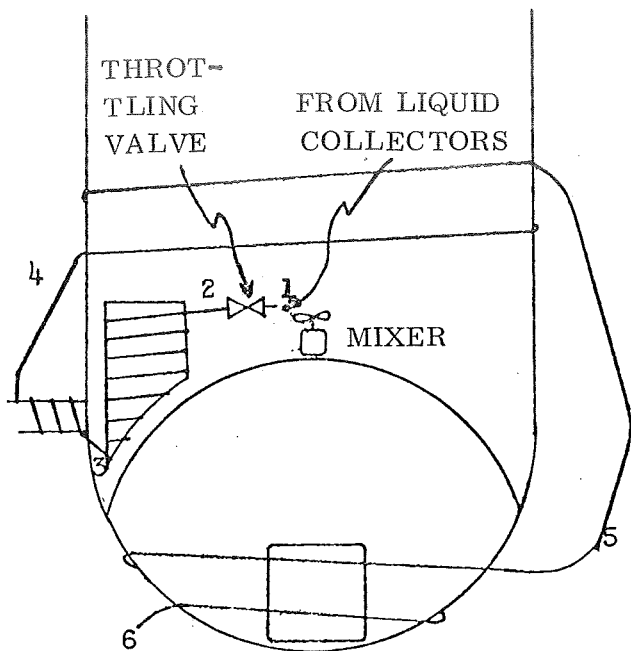


Figure 3-1. Schematic of S-IVC Wall Heat Exchanger Vent System

must be protected with vent system cooling coils and the basket surface areas maintained at or below the tank saturation temperature.

Heat exchanger sizing for start basket cooling and tank pressure venting is based on the first law relationship of Reference 3-2, as presented below.

$$\dot{m}_v = \frac{\dot{Q} + \dot{P}}{h_2 + e\lambda/(1-e) - h_L} \quad (3-1)$$

$P_T = \text{Const.}$

where

$\dot{m}_v$  is the vent flow rate

$h_2$  is the exit enthalpy

$h_L$  is the tank liquid enthalpy

$e$  is the vapor density/liquid density ratio

$\lambda$  is the heat of vaporization

$\dot{Q}$  is the heat input rate

$\dot{P}$  is any power input

Using Equation 3-1, values of vent flow rate as a function of total energy input are presented in Figure 3-2.

The basic sizing problem is to assure that for a given flow rate, the desired exit enthalpy of Equation 3-1 is attained. This equation must be satisfied in addition to  $\dot{m}_v = \dot{Q}_e / (h_o - h_2)$  where  $\dot{Q}_e$  is the engine feed line heating and  $h_o$  is the exit enthalpy of the vent fluid after cooling the feed line.

For the cold side of the cooling tube, heat transfer to the flowing fluid is computed by considering the process to consist of three phases (x indicates quality - % vapor):

1. nucleate boiling,  $0 \leq x \leq 0.90$ .
2. fully developed turbulent flow at constant temperature (saturation)  $0.90 < x \leq 1.0$ .

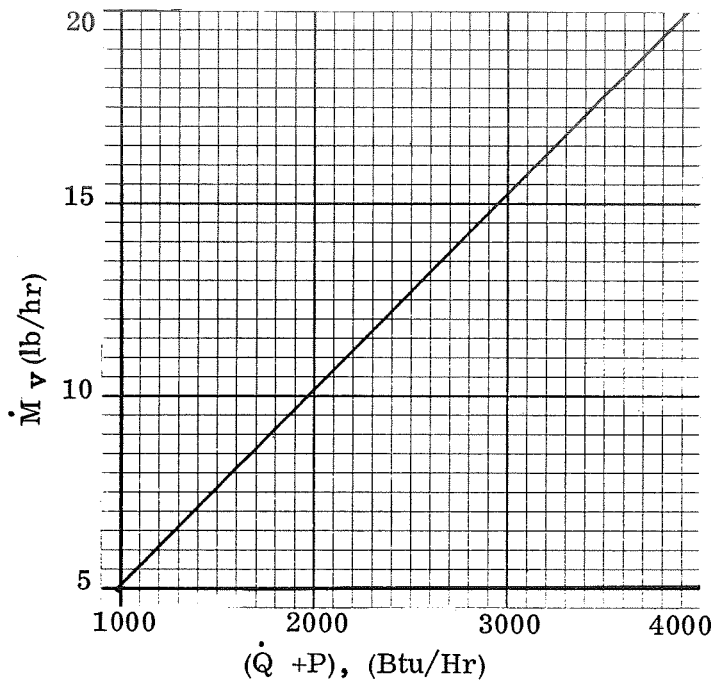


Figure 3-2.  $H_2$  Vent Flow Versus Energy Input  
( $P_T = \text{Const @ 25 psia}$ )

3. fully developed turbulent gas flow with increasing temperature  $T > T_{SAT}$

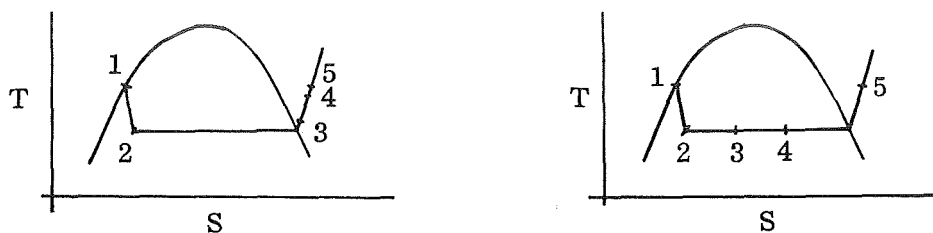
Heat transfer coefficients on the outside of the tube can take on a wide range of values depending on the external fluid conditions. Because the inside coefficients are so high the tube design is controlled by the exterior coefficients. Some of the possible fluid conditions and resulting external heat transfer coefficient ranges for the S-IVC application are

1. liquid free convection,  
 $0.1 < h < 1.0 \text{ Btu/hr ft}^2 \text{ } ^\circ\text{F}$
2. gas free convection,  
 $.02 < h < .2 \text{ Btu/hr ft}^2 \text{ } ^\circ\text{F}$
3. liquid forced convection,  $1.0 < h < 10 \text{ Btu/hr ft}^2 \text{ } ^\circ\text{F}$
4. gas forced convection,  $.1 < h < 1 \text{ Btu/hr ft}^2 \text{ } ^\circ\text{F}$
5. film condensation with free vapor convection,  $4 < h < 10 \text{ Btu/hr ft}^2 \text{ } ^\circ\text{F}$

Specific heat transfer coefficients are presented in section 3.1.2.

From the above data it is seen that for different fluid conditions existing at the start basket the total heat transfer can be significantly different and thus the outlet enthalpy or fluid condition can vary. This is illustrated in Figure 3-3 where typical coolant fluid state conditions are shown for different start basket external fluid conditions. The numbers shown on Figure 3-3 correspond to those of Figure 3-1 and illustrate typical state conditions throughout the vent path.

The system must be designed to assure that cooling temperatures below saturation exist throughout the length of the cooling coils without requiring cooling flow in excess of the normal hydrogen tank boiloff rate. The maximum total vent flow is determined from Figure 3-2 where  $\dot{Q} + \dot{P}$  is the total hydrogen tank energy input. The basket and feed line exchanger sizing is thus based on providing essentially a saturated  $GH_2$  vent fluid at the feed duct cooling outlet (state 4, Figure 3-1) under the maximum heat transfer conditions which can exist at the basket and feed line. Based on this sizing restriction,



a) Condensing Vapor Surrounding the Start Basket.

b) Low Velocity Liquid Surrounding the Start Basket.

Figure 3-3. Typical Thermodynamic Performance of Start Basket Cooling System

tube lengths at the tank wall required to provide the desired exit enthalpy for the low range of start basket heat transfer coefficients are very long.

In order to provide forced convection heat transfer coefficients, rather than free convection at low-g, mixing can be utilized. Small flow velocities can produce a considerable increase in the minimum external heat transfer coefficients. In a complicated tank configuration the strength and direction of circulation currents are very difficult to predict.

Three objectives must be met by a circulation system: the induced heat transfer coefficients must be high enough, they must be reasonably uniform over the start basket surface, and the fluid motion must be effective in reducing temperature stratification. Location, quantity and size of fans or pumps to accomplish the above objectives must be determined. Obtaining this type of information is discussed in Section 3.1.1

In order to take full advantage of the high heat transfer coefficients which can be provided by a mixer the coils leaving the feed line can be routed directly to a bulk exchanger integrated directly with a mixer. Two such systems are shown in Figure 3-4 and Figure 5-2.

The system shown in Figure 3-4 has the bulk heat exchanger in series with the start basket and line cooling coils. With this type of system, in order to provide a continuous vent flow, a continuous flow tank pressure regulator would be required at the vent outlet of the bulk exchanger as well as a throttling regulator at the inlet to the start basket cooling coils.

The system shown in Figure 5-2 utilizes a bulk exchanger operating independent of the start basket cooling system to provide final tank pressure control through on-off flow



$$A_Z = \pi \delta^2 \quad (3-4)$$

$$\dot{V}_Z = A_Z (V_e)_Z \quad (3-5)$$

$$\delta = bZ \quad (3-6)$$

$$\theta_m = \frac{N_p D_t^2}{.456 V_o D_o} \quad (3-7)$$

where

$V_o$	= velocity at mixer exit
$D_o$	= diameter of mixer exit
$(V_o D_o)_b$	= velocity-diameter product required to penetrate warm liquid layer at vapor/liquid interface
$\beta$	= coefficient of volumetric expansion for the liquid
$\Delta T_{max}$	= maximum temperature difference between bulk liquid and liquid/vapor interface usually assumed to be 1°F
$Z$	= distance from mixer to liquid/vapor interface
$a$	= local acceleration
$P$	= exponential constant usually taken as 1.0
$V_{max}$	= maximum centerline velocity with a temperature gradient
$V'_{max}$	= maximum centerline velocity without a temperature gradient
$V_{max}/V'_{max}$	is taken to be 0.9
$\dot{V}_Z$	= volume flow rate at the distance $Z$ from the mixer. Includes entrained flow.
$\dot{V}_o$	= volume flow at mixer exit
$A_Z$	= total flow area at the distance $Z$ from the mixer
$(V_e)_Z$	= mixer exit velocity at distance $Z$ from the mixer
$\delta$	= radius of flow at distance $Z$ from the mixer

b	= proportionality factor determining the spreading rate of flow from the mixer, taken to be 0.25 for the present case
$\theta_m$	= bulk mixing time
$N_p$	= dimensionless mixing time constant approximating 6.0 for present conditions
$D_t$	= tank diameter

In order to determine required velocities at the liquid/vapor interface to destroy stratification Equations 3-2 through 3-6 were solved for  $(V_i)_Z$ , the required mixing interface velocity. The resulting equation is presented below.

$$(V_i)_Z = \frac{.057}{b^2} \left[ \frac{\beta \Delta T_{\max} P}{[1 - (V_{\max}/V'_{\max})^2] (P + 1) (P + 3)} \right]^{1/2} a^{1/2} Z^{1/2} \quad (3-8)$$

Based on the general definitions of the above terms, required interface velocities are plotted in Figure 3-5 as a function of the distance of the interface from the mixer for various acceleration levels. For the particular case where  $Z_i$  is a maximum, for the S-IVC hydrogen tank, of 33 feet the data are plotted in Figure 3-6 as a function of acceleration.

These velocities are taken as a minimum for determination of heat transfer coefficients at the start basket. The velocities so determined apply to both gas and liquid surrounding the start basket since the mixer is essentially a constant volume flow device.

In order to specify pump sizing requirements the pump outlet flow and diameter necessary to provide a specific velocity at a certain distance from the mixer is desired. Rearrangement of Equations 3-3 through 3-6 result in the following relation.

$$V_Z, \text{ fps} = .465 \frac{(\dot{V}_o / D_o, \text{ cfm/in.})}{(Z, \text{ ft})} \quad (3-9)$$

Solutions to this equation are plotted in Figure 3-7 for easy reference.

A further criteria which is important in establishing mixing requirements is the time to mix. A reasonably short mixing time allows intermittent operation of the mixers thus minimizing total power requirements. Also at initiation of the coast phase it would not be desirable to wait too long for mixing to occur during which time a significant amount of stratification could build up and allow vaporization in the start basket. Using Equations 3-3 through 3-7, mixing time as a function of interface velocity and pump outlet conditions is plotted in Figures 3-8 and 3-9 respectively.

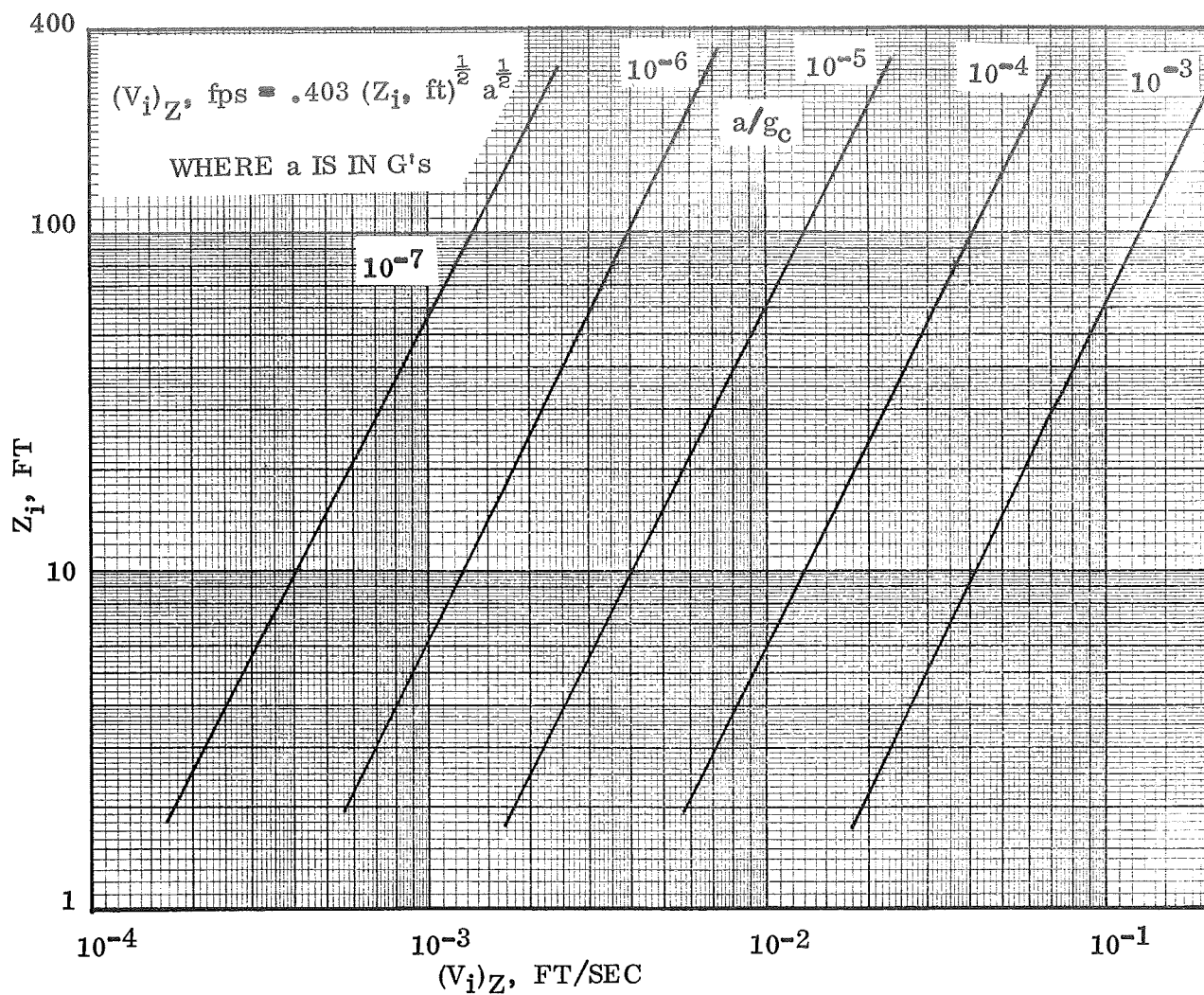


Figure 3-5. Required Interface Mixing Velocities

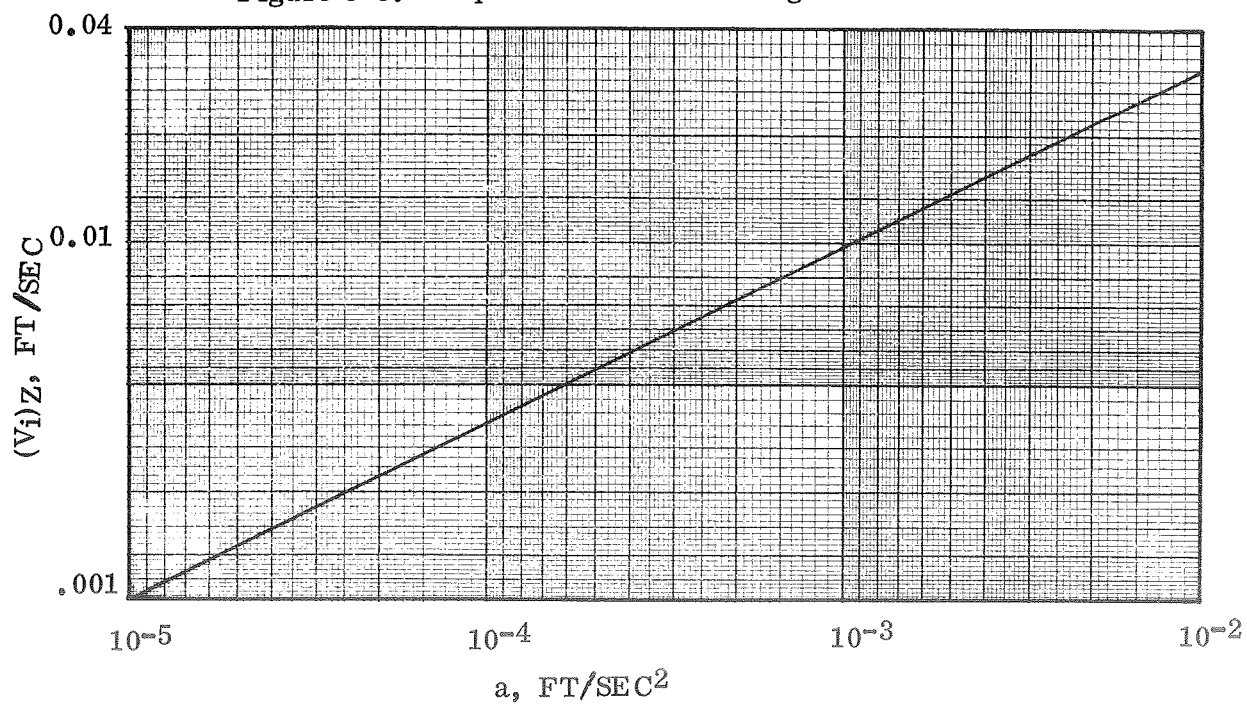


Figure 3-6. Required Interface Velocity Vs Accelerations

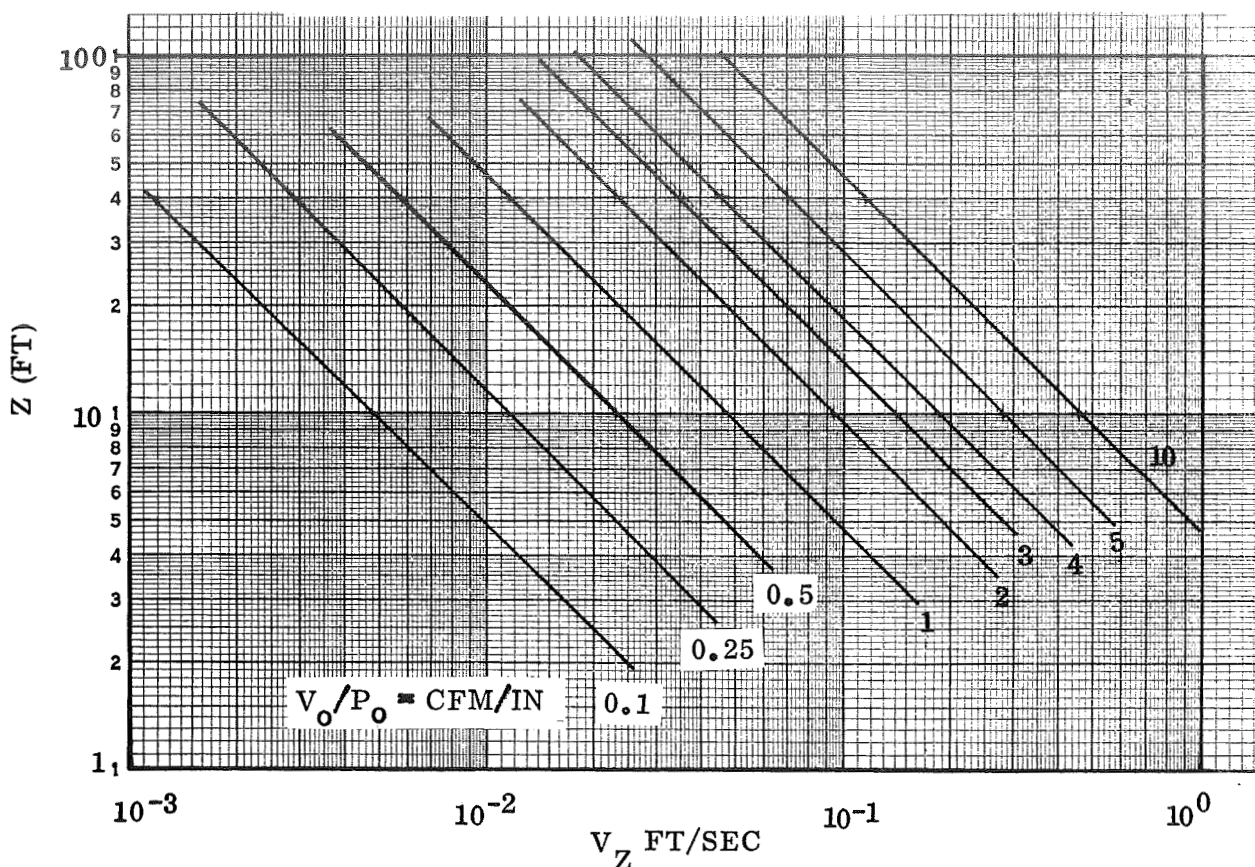


Figure 3-7. Mixing Velocity as a Function of Pump Performance

In order to fully evaluate the effect of mixing and non-mixing on system performance heat transfer coefficients over the full range of possible tank conditions are required. These data are presented in the following paragraph.

**3.1.2 HEAT TRANSFER COEFFICIENT.** Applicable heat transfer coefficients to be used throughout the detailed thermal analysis are presented in this section. Conditions of forced flow and natural convection for both liquid and gas are analyzed. Condensation heat transfer was also considered for the gas case. The following equations from Reference 3-4 were used.

Forced Convection, Laminar Flow  $Re_x \leq 5 \times 10^5$

$$\bar{h}_f = .664 (Pr)^{1/3} (Re_x)^{1/2} \left( \frac{K}{X} \right) \quad (3-10)$$

Natural Convection, Laminar Flow  $Gr_x < 10^9$

$$\bar{h}_f = \frac{.677 Pr^{1/2} (Gr_x)^{1/4}}{(.952 + Pr)^{1/4}} \left( \frac{K}{X} \right) \quad (3-11)$$

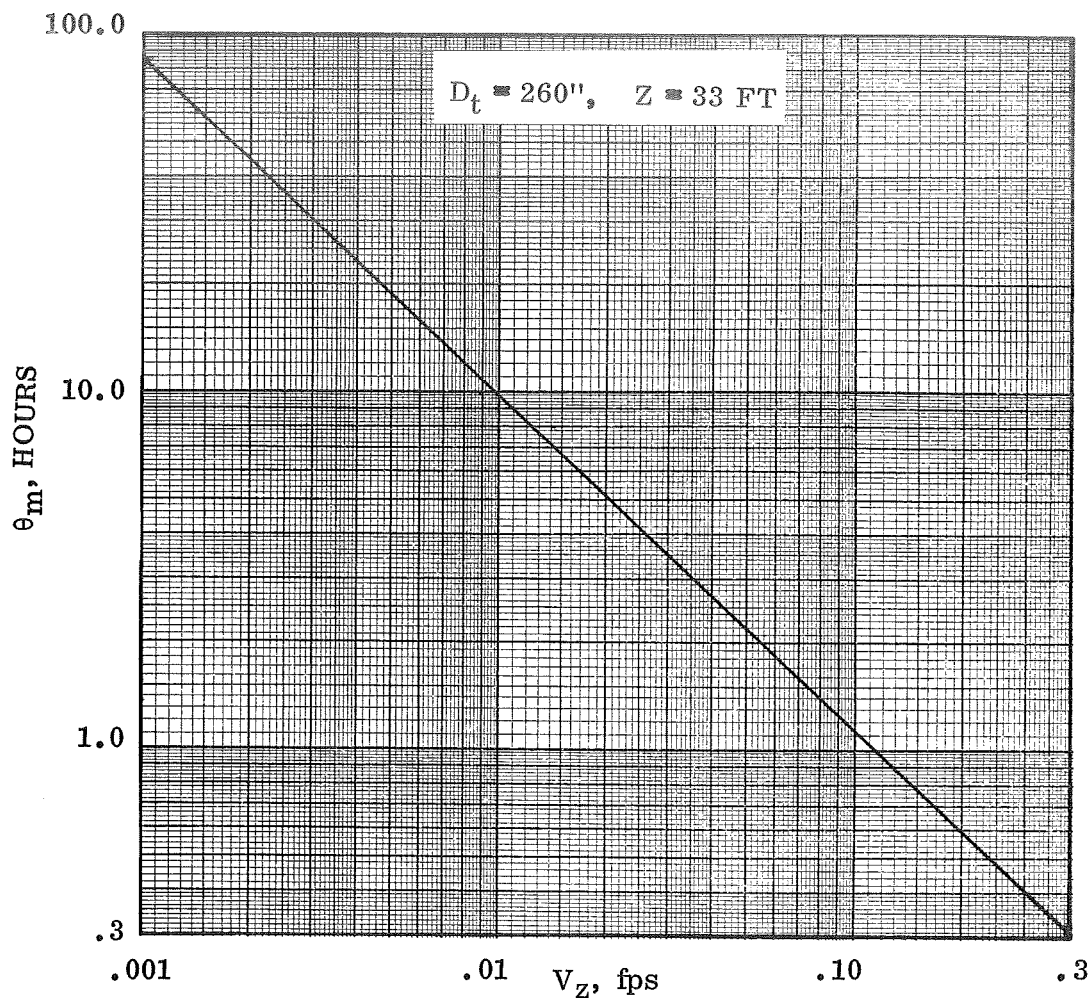


Figure 3-8. Total Mixing Time Versus Interface Velocity

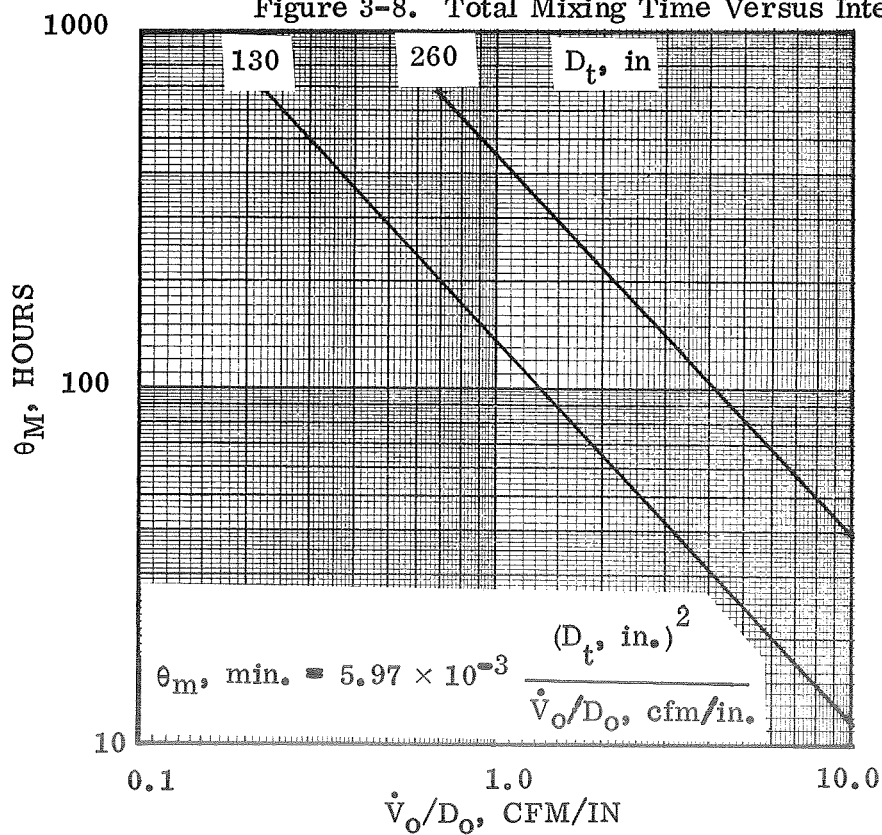


Figure 3-9. Mixing Time as a Function of Pump Performance

# Condensation, Laminar Flow

$$\bar{h}_f = \frac{4}{3} (N_{SH})^{1/4} \left( \frac{K}{X} \right) \quad (3-12)$$

where:

$\bar{h}_f$  = average film heat transfer coefficient

X = length from start of temperature boundary layer at a flat plate

$$Re_x = \frac{\rho V x}{\mu}$$

$$Gr_x = \frac{g \beta \Delta T X^3 \rho^2}{\mu^2}$$

$$Pr = \frac{C_p \mu}{K}$$

$$N_{SH} = \frac{g \rho_L^2 \lambda X^3}{4 \mu_L K_L (T_s - T_w)}$$

$\Delta T$  = temperature difference between bulk fluid and heated or heating surface

$T_s$  = saturation temperature

$T_w$  = wall temperature

Data were generated over the expected range of  $\Delta T$ , acceleration and flow velocity for both hydrogen and oxygen. Results are presented in Figures 3-10 through 3-17. Fluid properties used in developing the data are presented in Table 3-2.

It is seen from the above heat transfer data that for temperature differences expected and in the absence of forced flow, condensation heat transfer will be the limiting factor in maintaining a subcooled liquid in the start basket. Comparing with forced flow heat transfer for the case where  $T_s - T_w = 1^\circ F$  and  $a = 32 \times 10^{-6} \text{ ft/sec}^2$ , from Figure 3-11,  $\bar{h}_f = 7.19 \text{ Btu/hr-ft}^2\text{-}^\circ F$  and from Figure 3-12 it is seen that the velocity at the  $LH_2$  start basket can be as high as 0.205 fps without increasing the heat transfer over that of the condensation case. Also from Figure 3-8 this velocity is seen to provide a mixing time of only 0.46 hours. In the final design, in order to minimize mixer power, the actual velocity would likely be somewhat less. From Figure 3-5 at  $10^{-6} g$ 's, the velocity required to mix the liquid/vapor interface is only 0.0023 fps at  $Z_i = 33 \text{ ft}$ .

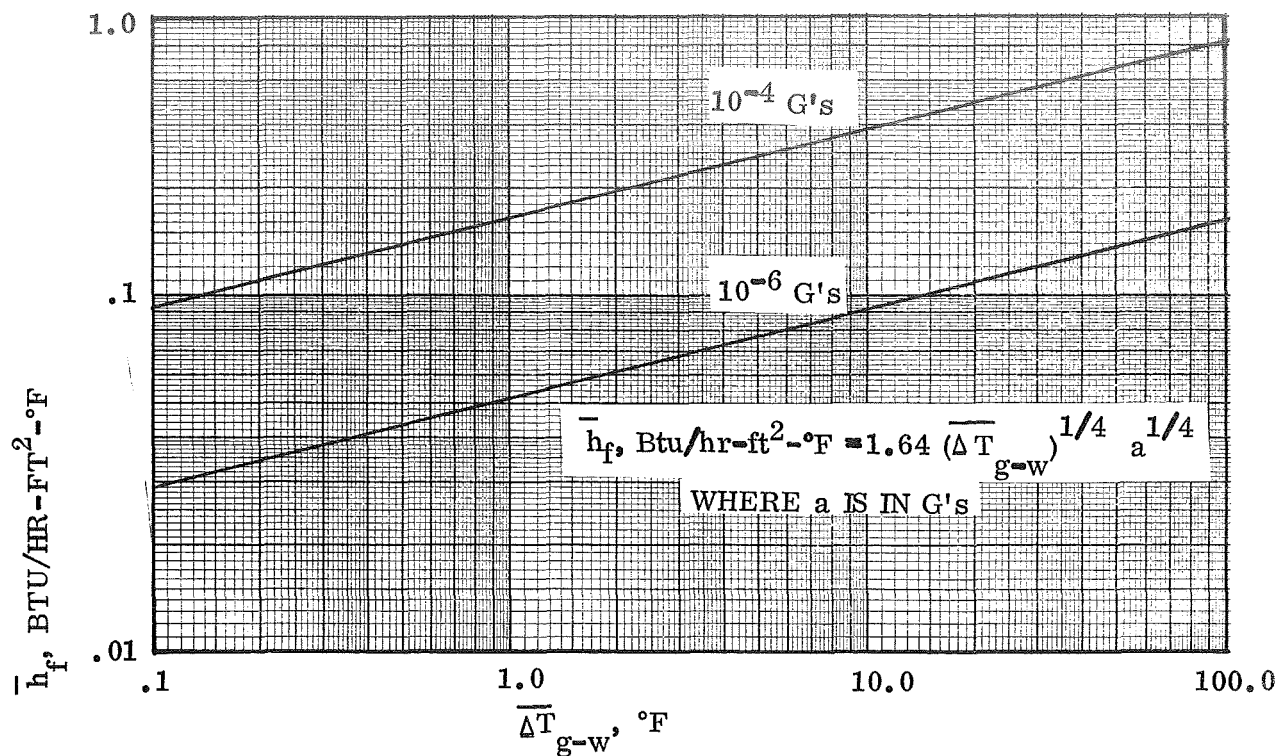


Figure 3-10. GH<sub>2</sub> Natural Convection Heat Transfer

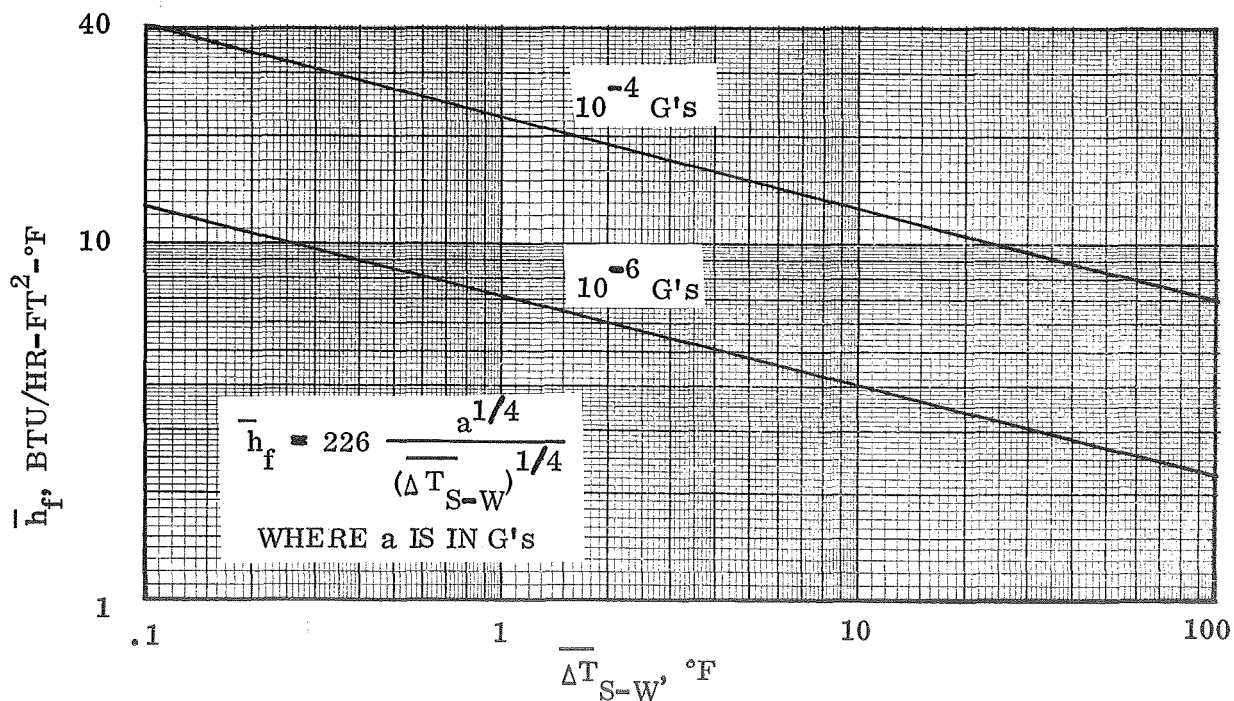


Figure 3-11. H<sub>2</sub> Laminar Flow Condensation Heat Transfer

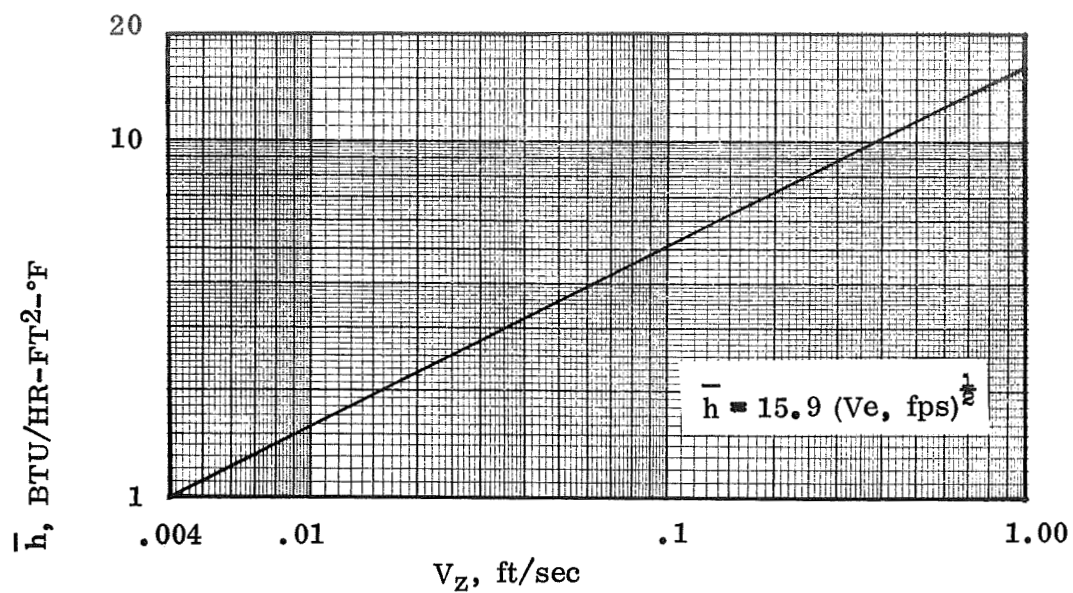


Figure 3-12. LH<sub>2</sub> Forced Convection Heat Transfer Coefficient

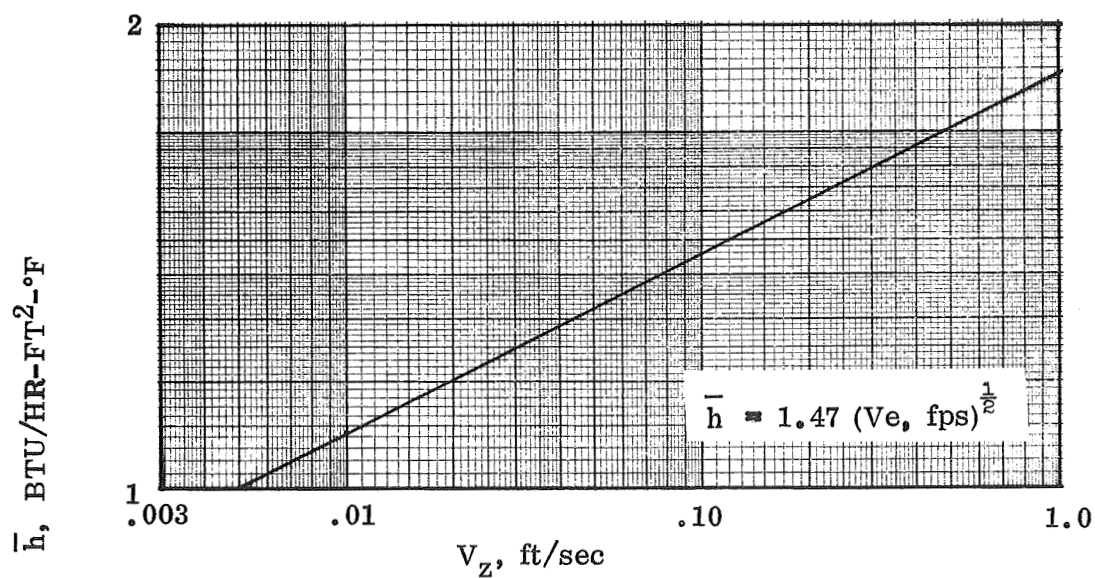


Figure 3-13. GH<sub>2</sub> Forced Convection Heat Transfer Coefficient

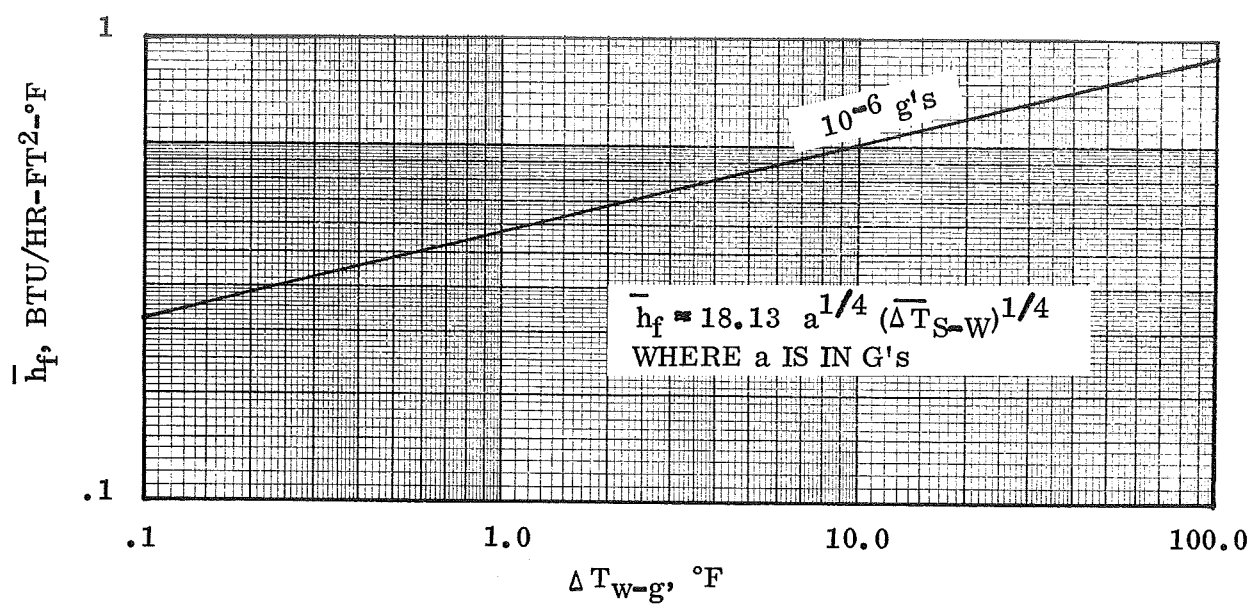


Figure 3-14. LO<sub>2</sub> Natural Convection Heat Transfer

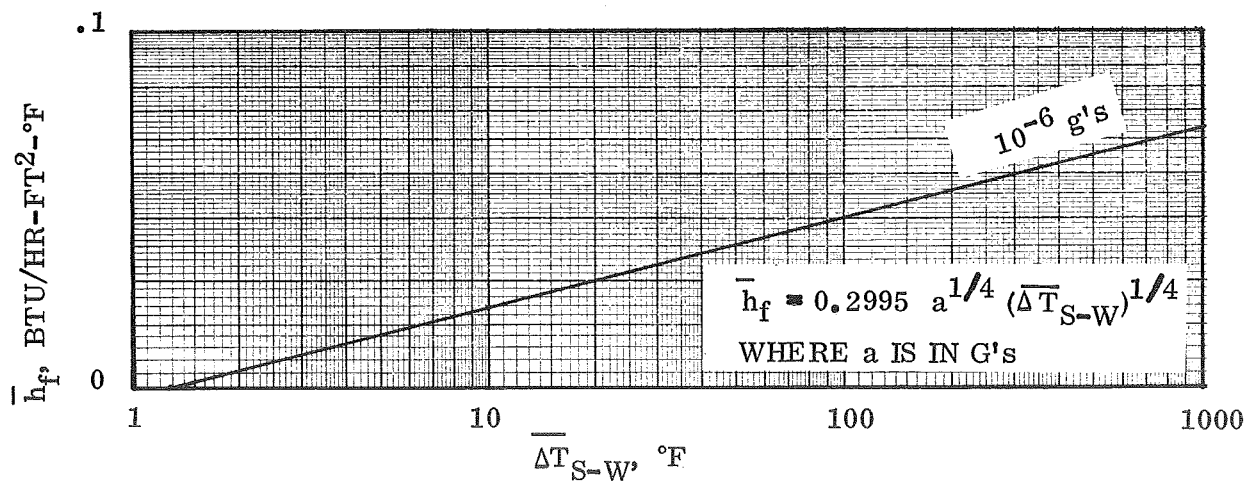


Figure 3-15. GO<sub>2</sub> Natural Convection Heat Transfer

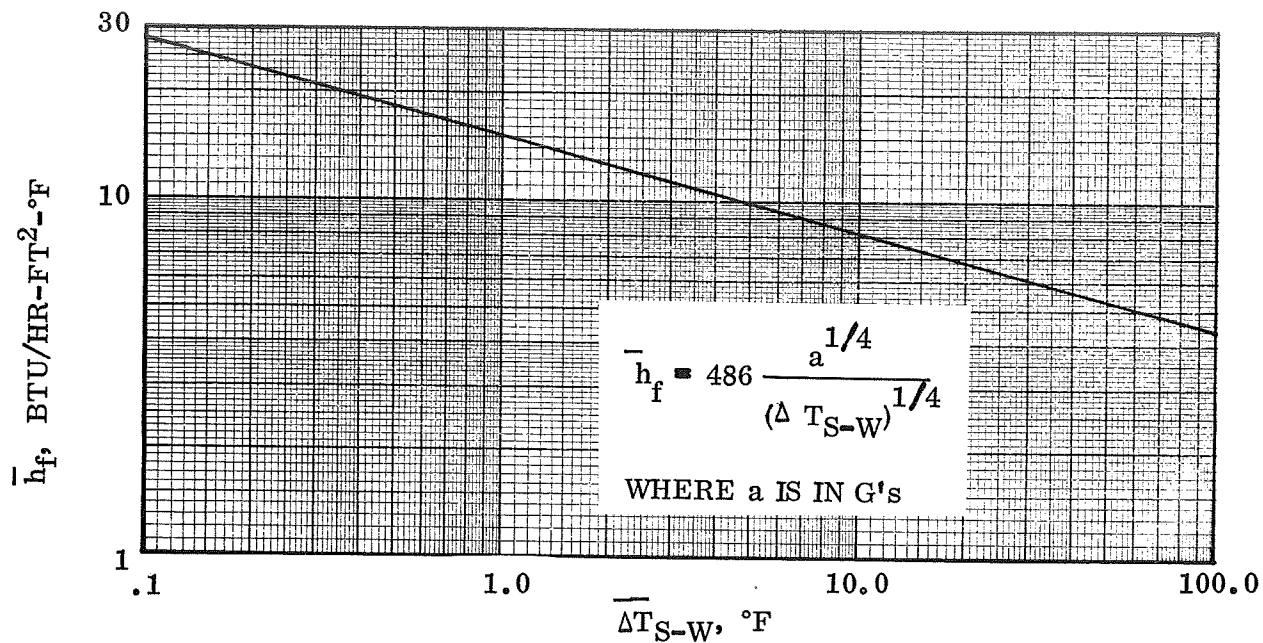


Figure 3-16. O<sub>2</sub> Laminar Flow Condensation Heat Transfer

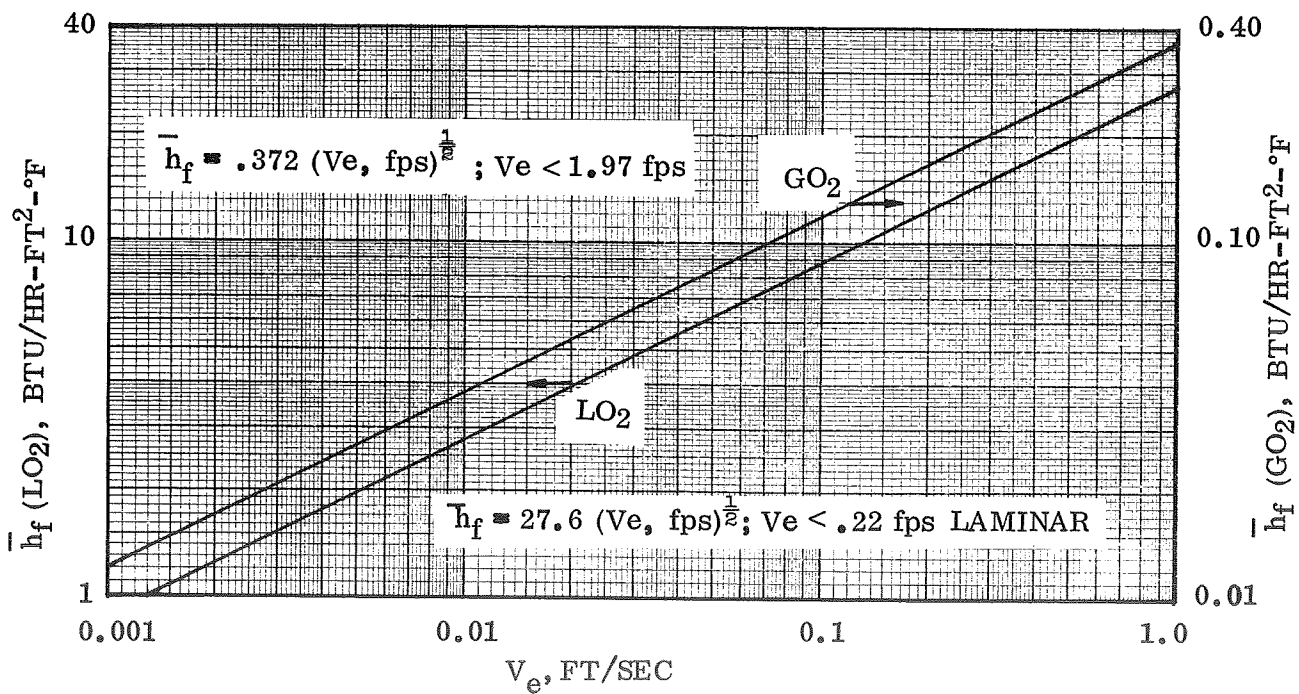


Figure 3-17. O<sub>2</sub> Forced Convection Heat Transfer

Table 3-2. Properties Data Used in Heat Transfer Calculations

---

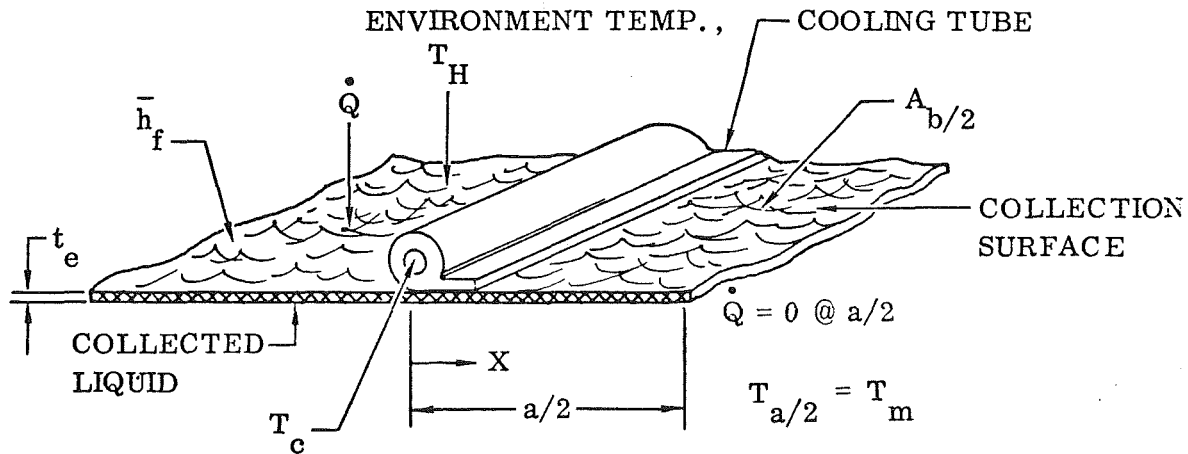
LH <sub>2</sub> :	$\beta$	= .00916/°R
	$\mu$	= $9.25 \times 10^{-6}$ lb/ft-sec
	$\rho$	= 4.26 lb/ft <sup>3</sup>
	k	= .0679 Btu/ft-hr-°F; P <sub>r</sub> = 1.13
	c <sub>p</sub>	= 2.3 Btu/lb-°F
	$\lambda$	= 188 Btu/lb for condensation heat transfer calculation
GH <sub>2</sub> :	$\rho$	= .14 lb/ft <sup>3</sup> ; $\beta = 1/T = 1/40^\circ\text{R}$
	$\mu$	= $0.77 \times 10^{-6}$ lb/ft-sec
	k	= .0106 Btu/hr-ft-°R
	Pr	= .87
LO <sub>2</sub> :	$\beta$	= .0024/°R; K = .0865 Btu/hr-ft-°F
	$\mu$	= $12.4 \times 10^{-5}$ lb/ft-sec, $\rho = 71.08$ lb/ft <sup>3</sup>
	c <sub>p</sub>	= .4054 Btu/lb-°F
	Pr	= 2.11
	$\lambda$	= 91.4 Btu/lb; N <sub>SH</sub> = $3.2 \times 10^{11}/\Delta T$ @ (a, = $10^{-6}$ g's)
	Gr	= $1.605 \times 10^6 \Delta T$ @ (a = $10^{-6}$ g's)
GO <sub>2</sub> :	$\rho$	= .285 lb/ft <sup>3</sup> ; $\beta = 1/162.75$
	K	= .005 Btu/hr-ft-°F; c <sub>p</sub> = .219 Btu/lb-°F
	$\mu$	= $.45 \times 10^{-5}$ lb/ft-sec
	Gr <sub>x</sub>	= $5.085 \times 10^4 \Delta T$ @ a = $10^{-6}$ g's; Pr = .71

---

Thus, in designing the start basket cooling system, condensing heat transfer is taken to be the maximum heat transfer case.

As mentioned previously, two major design requirements are imposed on the system; (1) the maximum temperature at any point on the start basket ( $T_m$ ) must be no greater than the tank fluid saturation temperature and (2) the total heat transferred to the basket and thus the cooling system ( $\dot{Q}_b$ ) must be less than the total external heating. Along with this there must be sufficient heat capacity in the vent exiting from the basket to cool the hydrogen feed line. Data for determining values of  $T_m$  and  $\dot{Q}_b$  as a function of cooling configuration are developed in the following section.

**3.1.3 BASKET SURFACE HEAT TRANSFER.** The configuration analyzed is shown below, along with applicable equations from Reference 3-5.



$$\frac{T_x - T_H}{T_c - T_H} = \frac{\cosh \left[ N (a/2) \left( 1 - \frac{x}{a/2} \right) \right]}{\cosh N \frac{a}{2}} \quad (3-13)$$

$$T_{(a/2)} = T_H - \frac{(T_H - T_c)}{\cosh N \frac{a}{2}} \quad (3-14)$$

$$\frac{\dot{Q}}{A_b (T_H - T_c)} = \frac{K_w t_e N \tanh N \frac{a}{2}}{a/2} \quad (3-15)$$

$$\frac{T_H - T_c}{T_H - T_M} = \cosh N \frac{a}{2} \quad (3-16)$$

where

$$N = \sqrt{\frac{h_f}{K_w t_e}}$$

$K_w t_e$  = effective conductivity - conduction thickness of the structure to which the cooling coils are attached. Estimated to be nominally .03415 Btu/hr-°F for the LH<sub>2</sub> start basket case.

$A_b$  = total surface area of basket

$T_c$  = coolant temperature

$a/2$  = half the distance between the coils

Data obtained from the solutions to Equations 3-15 and 3-16 are presented in Figure 3-18 and 3-19 respectively.

3.1.4 TWO-PHASE PRESSURE DROP ANALYSIS. Two phase flow pressure drop calculations are made using the methods and data presented in Reference 3-2. In all cases the tank pressure upstream of the throttling device was assumed to be 25 psia. From Reference 3-2 the two phase flow pressure drop ( $\Delta P_{TPF}$ ) is taken as

$$\Delta P_{TPF} = \Delta P_v (\Phi_{vtt})^2 \quad (3-17)$$

where

$\Delta P_v$  = single component frictional pressure drop assuming only the vapor fraction is flowing.

$\Phi_{vtt}$  = function obtained experimentally

Substituting for  $\Delta P_v$  where

$$\Delta P_v = \frac{fL}{D} \rho_v \frac{V_e^2}{2g} \quad (3-18)$$

and since  $\dot{m}_v = \rho_v A V_e$  and  $\dot{m}_v = X_{avg} \dot{m}_T$

$$\Delta P_{TPF} = \frac{fL}{D} \frac{\rho_v X_{avg}^2 \dot{m}_T^2}{2g_c \rho_v A^2} (\Phi_{vtt})^2 \quad (3-19)$$

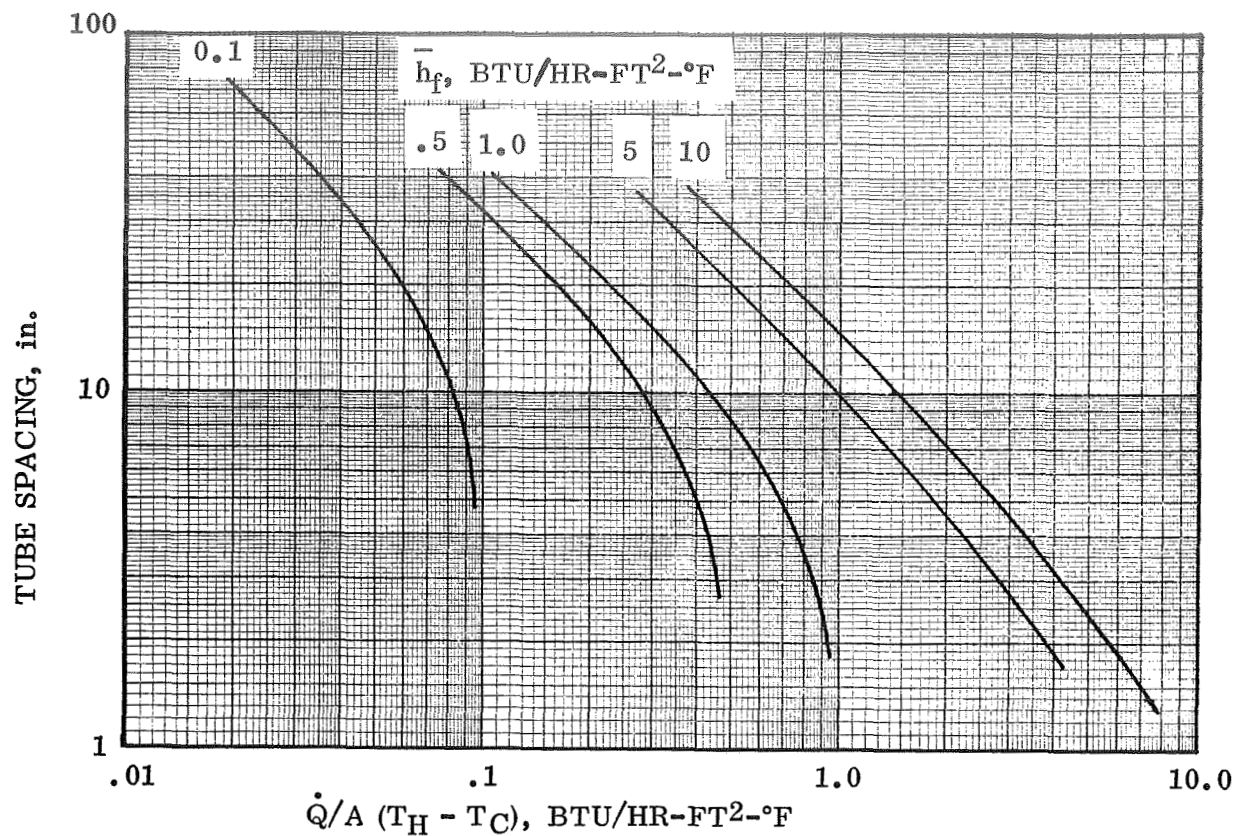


Figure 3-18. Start Basket Heat Transfer to Cooling Tubes

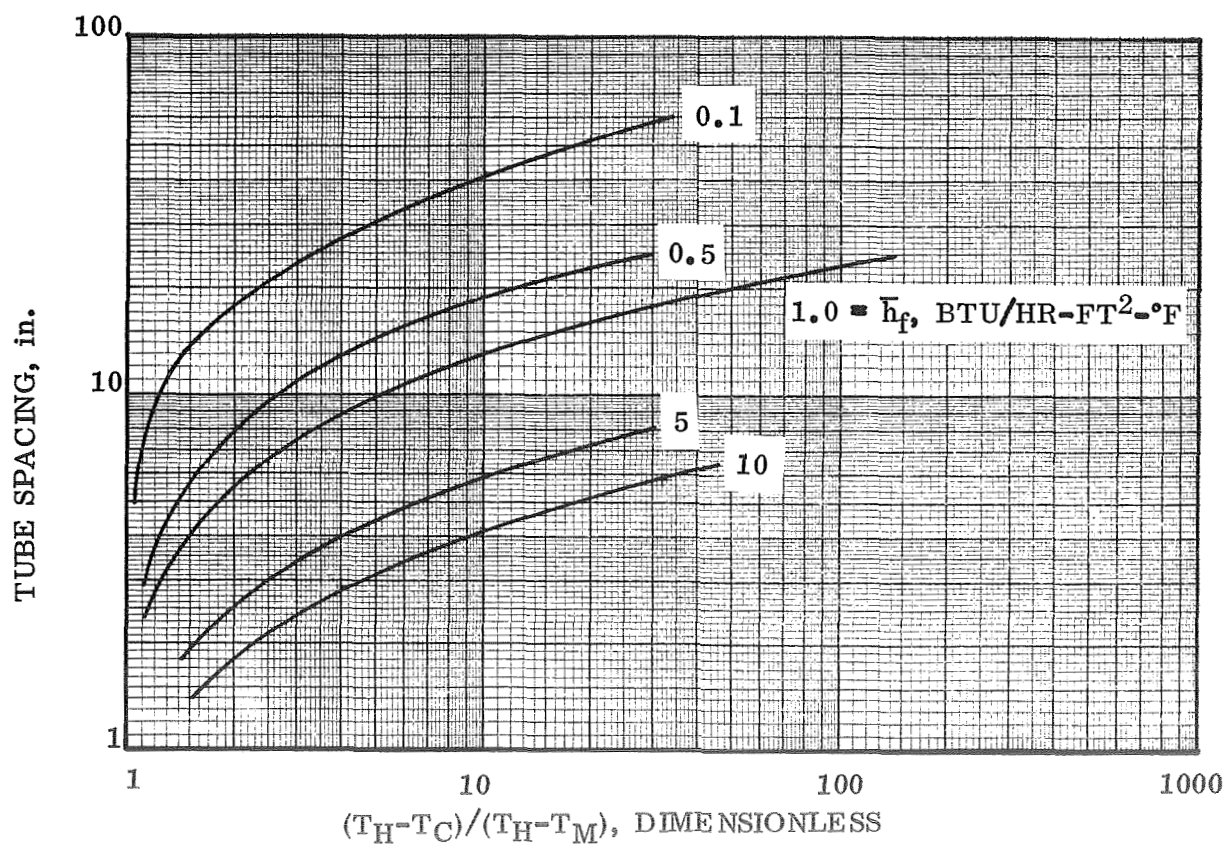


Figure 3-19. Maximum Start Basket Temperatures When Using Cooling Tubes

Substituting  $A = \pi D^2/4$  into Equation 3-19 and simplifying

$$\Delta P_{TPF} = \frac{fL}{D^5} \frac{16}{\pi^2 2 g_c} \frac{1}{\rho_v} X_{avg}^2 \dot{m}_T^2 (\phi_{vtt})^2 \quad (3-20)$$

Putting Equation 3-20 in a convenient parametric form results in

$$\frac{\Delta P_{TPF}, \text{ PSI}}{[L, \text{ in.}/(D, \text{ in.})^5] [\dot{m}_T, \text{ lb/hr}]^2} = \frac{4.2 \times 10^{-9}}{(\rho_v, \text{ lb/ft}^3)} (X_{avg})^2 (\phi_{vtt})^2 \quad (3-21)$$

where  $f$  is based on vapor only flowing in a relatively smooth pipe.

Data obtained from the above equation for hydrogen are plotted in Figure 3-20 as a function of vent pressure for several exit qualities. The average quality is an arithmetic average of inlet and outlet quality. The inlet quality is based on throttling from 25 psia to the vent pressure at constant enthalpy with a 100% liquid inlet to the throttling device. Values of  $\phi_{vtt}$  are found from data presented in Reference 3-2.

In order to determine the quality at various points in the cooling system as a function of energy absorbed enthalpy values are presented in Figure 3-21 for various vent pressures.

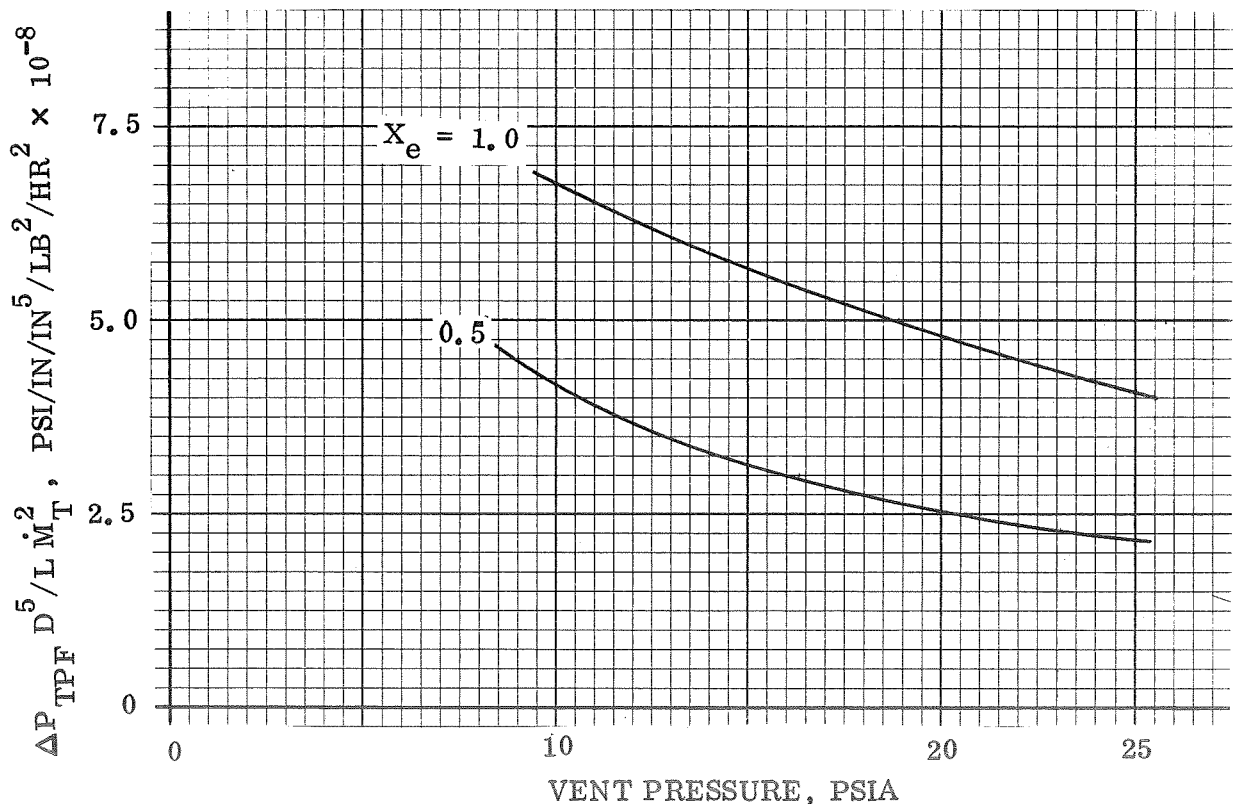


Figure 3-20.  $LH_2$  Two-Phase Pressure Drop

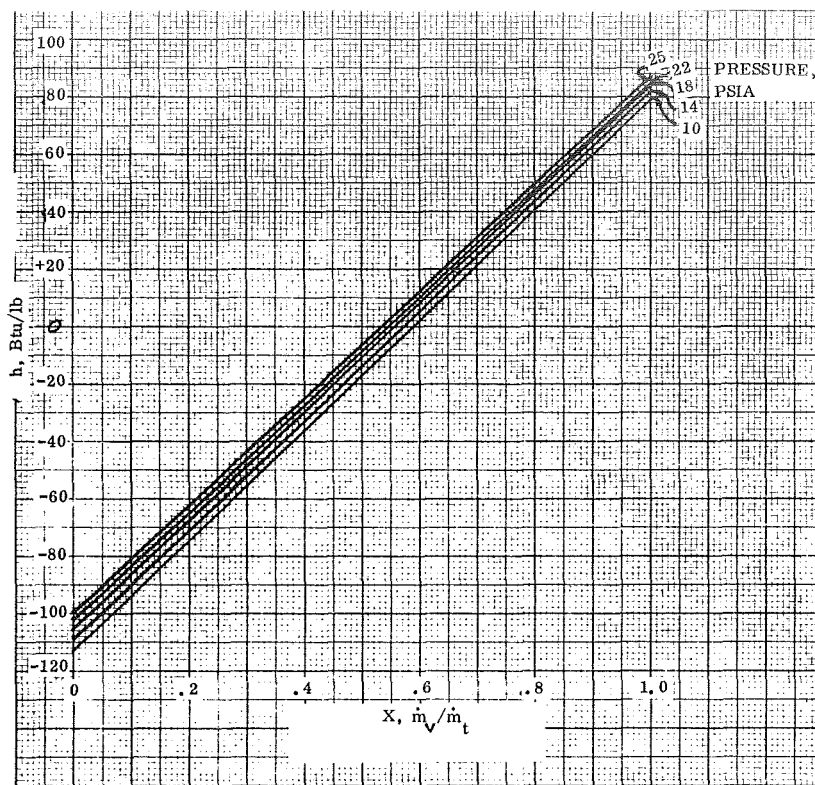


Figure 3-21. Hydrogen Enthalpy Versus Quality

**3.1.5 THERMAL ANALYSIS OF START BASKET COOLING LIQUID COLLECTOR CHANNELS.** A liquid inlet to the start basket cooling system is necessary to provide a sufficient amount of cooling. A system was sized on the basis of collection and flow requirements as discussed in Section 3.1. The basic system is illustrated in Figure 3-22. The following thermal analysis was performed in order to determine the criticality of supports and the total amount of energy which may be transferred to the cooling fluid prior to entry into the basket cooling tubes. A knowledge of this energy transfer is important in that the available cooling in the vent fluid is thus reduced by an equivalent amount.

Two sources of heat transfer to the collection channel fluid are present;

1. Heat from the bulk tank fluid due to the temperature difference between bulk and collection fluid due to pressure drop through the collection screens.
2. Heat transfer through the supports which are intercepted from going into the tank bulk fluid due to conduction in the tank walls.

In the case of item 1. the maximum  $\Delta P$  across the screens was estimated to be 10 psf which corresponds to a temperature change of  $0.0201^{\circ}\text{R}$  at a tank saturation pressure of 25 psia.

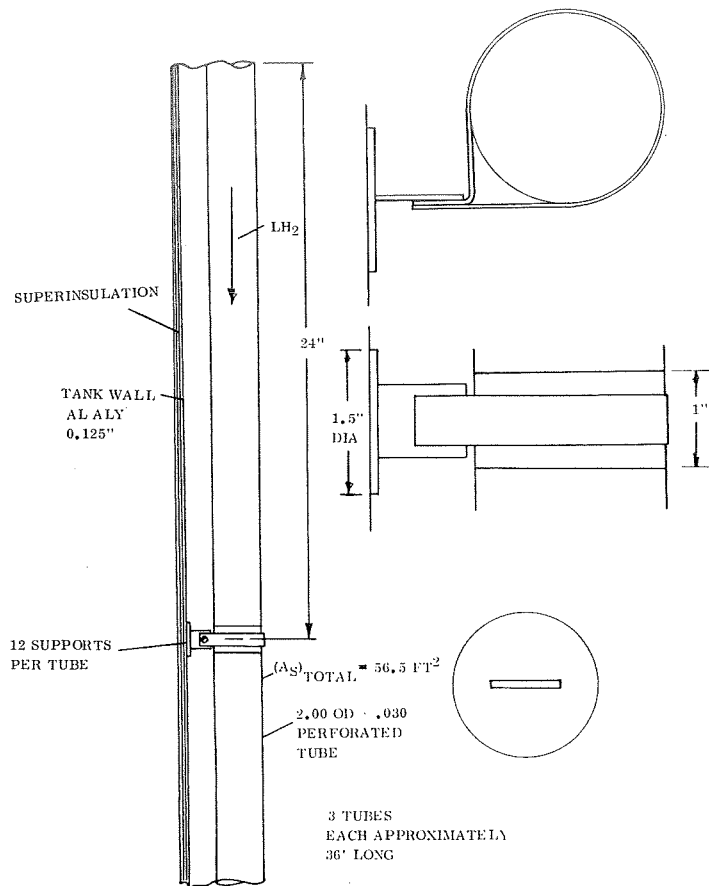


Figure 3-22. S-IVC LH<sub>2</sub> Collection Tube Support Configuration

Assuming condensing heat transfer as the worst case then from the equation presented with Figure 3-11 and the data illustrated in Figure 3-22,  $\dot{Q}_{TOTAL}$  is calculated to be 21.8 Btu/hr. This represents only 1% of the total tank heat leak.

In the case of heat transfer through the supports the applicable equation is taken from Reference 3-5 and is presented below.

$$\dot{Q}_o = (T_n - \zeta) 2\pi k_w \delta \epsilon r_s \frac{K_1(\epsilon r_s)}{K_0(\epsilon r_s)} \quad (3-22)$$

where

$\dot{Q}_o$  = heat transfer at each support assuming the support path between the wall and channel does not restrict the heat flow.

$\delta$  = tank wall thickness, in this case taken to be 0.125 in.

$$\epsilon = \sqrt{(h_{f1} + h_{f2}) / k_w \delta}$$

$h_{f1}$  = heat transfer coefficient external to the tank wall. Taken to be  $3.82 \times 10^{-4}$  Btu/hr-ft<sup>2</sup>-°F in this case for the superinsulated tank where the total heat leak through the cylindrical portion of the tank was 170 Btu/hr from Reference 3-6 over an area of 1238 ft<sup>2</sup>. The total temperature difference across the insulation was taken as 360°R (400-40°R).

$h_{f2}$  = heat transfer coefficient between the wall and tank fluid.

$r_s$  = the radius of the channel support at the tank wall.

$\zeta$  = wall temperature at an infinite distance from the support =

$$\frac{h_{f1} T_{g1} + h_{f2} T_{g2}}{h_{f1} + h_{f2}}$$

$T_{g1}$  = temperature external to the insulation.

$T_{g2}$  = tank fluid temperature

$T_n$  = temperature at the support, taken to be 40°R in this case

$k_w$  = wall thermal conductivity taken to be 40 Btu/hr-ft-°F at -420°F. This is representative of material likely to be used in practice.

$K_1$  = first order modified Bessel function

$K_0$  = zero order modified Bessel function

Assuming a worst case condition of gas at the tank wall and acceleration of  $10^{-6}$  g's and a  $\Delta T$  of 1°F then from Figure 3-10  $h_{f2} = .052$  Btu/hr-ft<sup>2</sup>-°F. Taking  $r_s = 0.75$  in. then  $\dot{Q}_0 = 1.73$  Btu/hr from Equation 3-22 and for 36 supports the total heat leak is 62.3 Btu/hr. This gives a grand total of 84.1 Btu/hr possible, including that due to pressure drop.

**3.1.6 DETAIL ANALYSIS OF LH<sub>2</sub> START BASKET COOLING CONFIGURATION.** Based on the mixing and heat transfer data developed in the previous paragraphs a recommended cooling configuration for the S-IVC hydrogen tank conditions can be determined. The design conditions to be defined are coolant temperature, flow rate and tube spacing. The basic start basket configuration is shown in Figure 2-2. From Figure 2-1 the total surface area is 275 ft<sup>2</sup>. An examination of the overall heating data presented in Table 3-1 and the location of the basket shows that the most critical cooling area is where the basket is close to the intermediate bulkhead. Heating through this bulkhead is relatively high and stagnant gas can exist in the area between the basket and wall and become significantly superheated. This represents a potential area of vaporization at the start basket surface if sufficient cooling is not provided. The step by step analysis proceeds as follows.

1. Determine the maximum heat transfer which can exist between any superheated gas and the basket surface. This is a combination of the maximum heat transfer coefficient and superheated gas temperature which can be expected. In the present case this will occur in the common bulkhead area. Assuming the 1300 Btu/hr heating at the bulkhead is distributed evenly over the 591 ft<sup>2</sup> surface and further that the temperature of the hydrogen and oxygen are 40°R and 170°R respectively (under normal conditions) then an equivalent heat transfer coefficient across the bulkhead [ $\bar{h}_f = Q/(A\Delta T)$ ] is 0.017 Btu/hr-ft<sup>2</sup>-°F.

Then for the 1.5 inch gap between start basket and bulkhead with a GH<sub>2</sub> conductivity of .0106 Btu/hr-ft an equivalent heat transfer coefficient between wall and basket is determined to be .085 Btu/hr-ft<sup>2</sup>-°F. The wall temperature is then calculated by an equilibrium heat balance as

$$T_w = \frac{.017 (170) + .085 (40)}{.102} = 61.5^\circ\text{R}$$

2. Assume a value for cooling temperature or throttling pressure and calculate a value for  $(T_H - T_c)/(T_H - T_m)$  where  $T_m$  is the maximum allowable temperature at the start basket. This is taken as the saturation temperature at the minimum tank pressure, assumed to be 25 psia ( $39.9^\circ\text{R}$ ). In this case  $T_H = T_w$  and for a throttling pressure of 15 psia ( $T_c = 36.8^\circ\text{R}$ ) and

$$\frac{T_H - T_c}{T_H - T_m} = \frac{61.5 - 36.8}{61.5 - 39.9} = 1.145$$

3. From Figure 3-19 find an allowable value for the tube spacing to meet the above conditions. A value of 10 inches is found to be reasonable.
4. The above analysis can then be repeated for the other basket surfaces and an overall tube spacing determined. As a conservative first cut analysis the 10 inch spacing is assumed to be distributed over the entire basket.
5. For the spacing determined above calculate the total heat transfer which may occur between the tank fluid and cooling coils under maximum heat transfer conditions. In the present case, from an examination of the mixing and heat transfer data, condensing heat transfer was found to be limiting. Then from Figures 3-11 and 3-18 a total heat transfer can be determined. In the present case  $\Delta T_{\text{avg}} = 1.55^\circ\text{F}$ ,  $\bar{h}_f = 6.45 \text{ Btu/hr-ft-}^\circ\text{F}$  and  $\dot{Q}/[A_b (T_H - T_c)] = 1.15$ . Then since  $A_b = 275 \text{ ft}^2$  and  $T_H - T_c = 3.1^\circ\text{F}$ ,  $\dot{Q}_{\text{TOTAL}} = 1.15 (275) 3.1 = 980 \text{ Btu/hr}$ , which is within the allowable limits. Including the potential heat pickup in the collector channels of  $84.1 \text{ Btu/hr}$  the total maximum energy absorbed up to the basket outlet is  $1,064 \text{ Btu/hr}$ .
6. Determine a cooling flow rate from a fluid energy balance. From Figure 3-2, assuming it is desirable to remove a total maximum heat energy of  $1800 \text{ Btu/hr}$  through the circuit up to state 5 as shown in Figure 3-4, then a reasonable flow rate would be  $9 \text{ lb/hr}$ . This allows for a reasonable variation in heat transfer from nominal values presented in Table 3-1. The maximum energy or enthalpy change of the cooling fluid between the tank and basket exit is thus determined to be  $\dot{Q}_T/\dot{m}_v = 1064/9 = 118.5 \text{ Btu/lb}$ .

Referring to Figure 3-21 the basket cooling exit quality is thus  $0.665$ . Considering the energy required to be removed in the feed duct of approximately  $100 \text{ Btu/hr}$  (Reference Section 3.1.7) the exit quality from the feed duct would be on the order of  $.725$ . The overall cooling requirements and energy balances have been thus satisfied and a sufficient margin of safety provided.

7. The tube size must now be determined and the overall pressure drop calculated. The total tubing length for a uniform 10 inch spacing is determined to be 4,297 in., including the required manifolding. From Figure 3-20

$$\Delta P_{TPF} = \frac{L \dot{m}_T^2}{D_i^5} (4.4 \times 10^{-8})$$

at  $x_e = 0.725$  and a vent pressure of 15 psia. Assuming a tube diameter of  $3/8" \times .030$  or  $D_i = 0.315$  inches then for  $\dot{m}_T = 9$  lb/hr.

$$\Delta P_{TPF} = \frac{4,297 (9)^2 4.4 \times 10^{-8}}{(.315)^5} = 4.94 \text{ psi}$$

which is considered to be excessive. Next, assuming a  $1/2" \times .030$  tube with  $D_i = .440$  in.

$$\Delta P_{TPF} = 0.925 \text{ psi}$$

which is considered to be reasonable.

In order to minimize the pressure drop a parallel flow arrangement using  $3/8$  inch tubing was investigated and is illustrated in Figure 5-4.

The main disadvantage of this type of system is that proper flow distribution of the liquid and vapor among the various passages can become a problem. Assuming only gas flows in some of the tube passages then hot spots can develop due to insufficient cooling in these areas and vapor thus formed within the start basket.

In order to estimate the relative magnitude of the problem the volumes of vapor and liquid entering the basket coils under typical flow conditions were calculated.

For throttling from 25 psia ( $39.9^\circ\text{R}$ ) to 16 psia ( $37.1^\circ\text{R}$ ) the amount of vapor formed on a volume basis was determined to be close to twice that of the liquid even though the quality on a mass basis was only .039. This indicates that prevention of vapor from flowing in some passages at the exclusion of liquid would be very difficult. The calculation is presented below.

$$X = \frac{h_2 - h_L}{h_v - h_L}$$

$$\dot{m}_g = X \dot{m}_T$$

$$\dot{m}_L = (1 - X) \dot{m}_T$$

For  $\rho_g = .0935 \text{ lb/ft}^3$ ;  $\rho_L = 4.38$

$$\frac{\dot{V}_g}{\dot{V}_L} = \frac{X}{\rho_g} \left[ \frac{\rho_L}{1 - X} \right] = \frac{3.75}{1.98} = 1.892$$

The magnitude of this vapor fraction would seem to dictate the use of a series flow arrangement with 1/2" cooling tubes.

One further refinement was made to the cooling tube configuration to reduce the total tubing length. Since reasonably good mixing is anticipated in the regions near the top and ends of the basket a greater tube spacing than 10 inches can be used in these area.

Assuming a tube spacing of 16 inches and performing an iteration between the data of Figures 3-10 and 3-19 where  $T_m = 39.9^\circ\text{R}$ ,  $T_c = 36.8^\circ\text{R}$  and the acceleration level is  $10^{-6} \text{ g's}$ , then an allowable gas temperature ( $T_H$ ) of  $47^\circ\text{R}$  is obtained. This represents a  $7^\circ$  superheat which can be tolerated in this area and is considered to be a reasonable design assumption where complete tank mixing is accomplished. This system design is presented in Figure 5-4A. For this configuration the total tubing length is still approximately 4,000 in. and a final estimate of the pressure drop results in a value of .86 psi.

**3.1.7 ANALYSIS OF LH<sub>2</sub> FEEDLINE COOLING.** The basic feedline configuration analyzed is illustrated below.

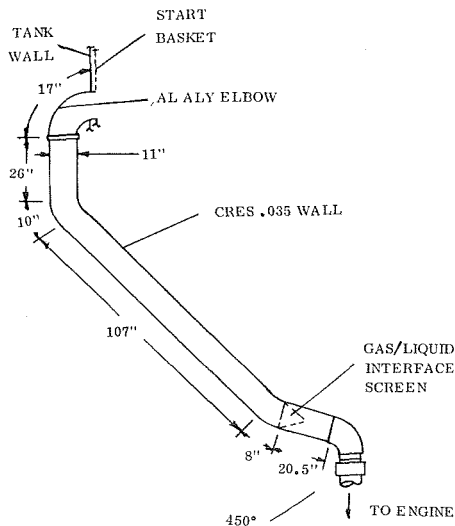


Figure 3-23. S-IVC LH<sub>2</sub> Engine Feedline

This line, whether liquid filled or dry, is connected to a heat source from which it cannot be effectively insulated. The central problems are how to best remove the heat introduced into the tank from the feedline and how to ensure that the propellant feed system will function properly when called upon.

Initially, the feedline will be wet, and any subsequent evaporation of the contained liquid may cause expulsion of a volume of liquid from the start basket equal to approximately 30 times the volume of liquid evaporated. It is thus essential to either eliminate evaporation completely or to provide a vent for the evaporated fluid. Elimination of vaporization entirely

requires removal of all incident heat, part of which is radiation from the warm end of the tube. Radiation, unlike convection and conduction cannot be taken out at the warm end because it can penetrate the liquid. A cooled optical baffle could be used at the warm end of the pipe but since heat is continuously entering the liquid through the insulation on the pipe some cooling over the entire surface will be necessary anyway.

Heat to be removed from the propellant feedline is tabulated below, assuming that a four inch GH<sub>2</sub> gap exists between the heat source and the liquid/vapor interface.

Radiation	24.5 Btu/hr
Gas Conduction	25.7 Btu/hr
Metal Conduction	45.2 Btu/hr
Insulation Heat Leak	<u>5.3 Btu/hr</u>
Total	100.7 Btu/hr

Heat from gas conduction and metal conduction can be removed at the warm end of the pipe by heat exchanger coils wrapped on the outside of the pipe under the insulation. The remaining 30 Btu/hr can be removed over the entire pipe surface by heat exchanger tubes, coiled on the outside surface of the pipe, under the insulation.

In order to estimate the cooling tube spacing required along the duct wall, Equation 3-6 is used. The duct is assumed to be superinsulated with the same effectiveness as the main tank such that  $\dot{Q}/A = .113 \text{ Btu/hr-ft}^2$  with an external insulation temperature of 450°R. The equivalent  $h_f$  for use in Equation 3-16 is thus  $2.76 \times 10^{-4} \text{ Btu/hr-ft}^2\text{-}^\circ\text{F}$ . For the following duct parameters, values of  $(T_H - T_C)/(T_H - T_m)$  are plotted as a function of tube spacing in Figure 3-24.

$$t_e = .035''; N = .2745/\text{ft}$$

$$k_w = 1.25 \text{ Btu}/(\text{hr-ft-}^\circ\text{F}) \text{ of CRES @ } -420^\circ\text{F}$$

Additional cooling coils are, of course, placed at insulation penetration areas such as at the entrance to the tank and near the end where conduction from the engine is high.

It was further determined from solutions to Equation 3-15 that the presence of the cooling tubes had negligible effect on the total heat transfer to the feed duct which must be intercepted by cooling.

Calculations were made to thermally control the feedline interface screen configuration in order to prevent vapor formation within the liquid on the upstream side of the screen.

Heating to the screen from gaseous conduction and radiation due to the hot engine and feedline was conservatively computed to be 9.86 and 3.21 Btu/hr respectively. Metal conduction along the duct was 18.8 Btu/hr and heat flux thru the insulation was 4.61 Btu/hr.

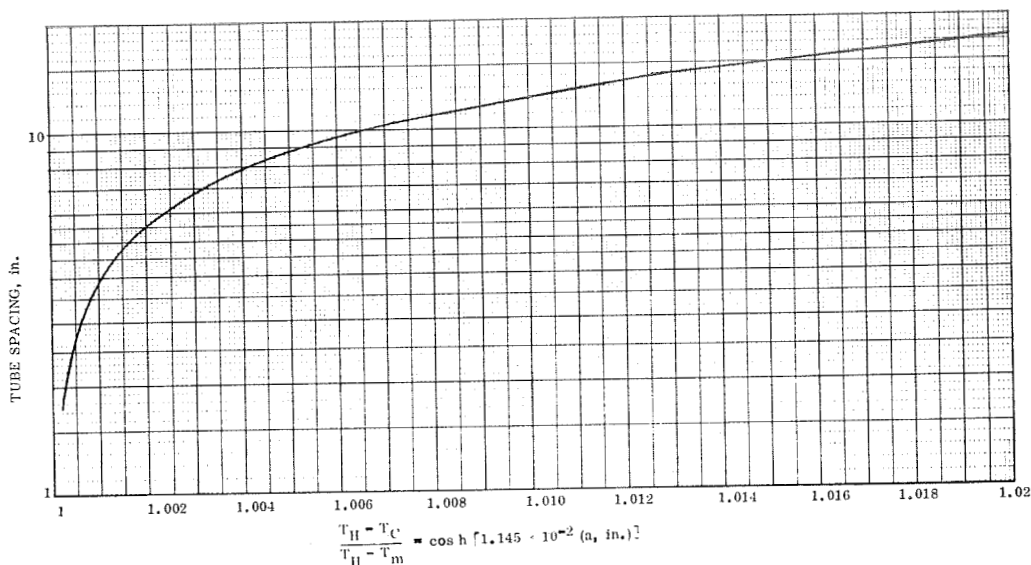


Figure 3-24. LH<sub>2</sub> Feed Duct Cooling Tube Spacing

Using a stainless steel screen and backup support in the stainless duct proved to be unsatisfactory because of the low thermal conductivity of stainless steel. Copper radial strips on the screen were looked at but proved to be unsatisfactory due to high temperatures between the strips. Copper screens with a relatively large cross section (30 × 250) were analyzed and proved to have sufficient conductance to keep fluid temperatures well below saturation conditions. A configuration using a conical copper screen attached to a stainless steel perforated cone which is in turn welded to the inside of the duct will be thermally and fluid dynamically satisfactory. Cooling capacity and heat transfer coefficients of the vented fluid are sufficient to use a single coil of heat exchanger tubing at the circumferential screen-duct attachment locus.

**3.1.8 LO<sub>2</sub> START BASKET ANALYSIS.** Thermal analysis was accomplished on the S-IVC LO<sub>2</sub> tank start basket configuration using external cooling, illustrated in Figures 3-1 and 3-4. In this configuration cooling coils containing hydrogen vent gas are wrapped around the outside of the LO<sub>2</sub> tank. Basket characteristics used in the analysis are presented in Figure 3-25.

An initial analysis was performed to determine whether or not it would be practical to prevent evaporation from occurring at the basket during transient tank pressure decay with an external cooling configuration. In order to prevent vaporization of any of the

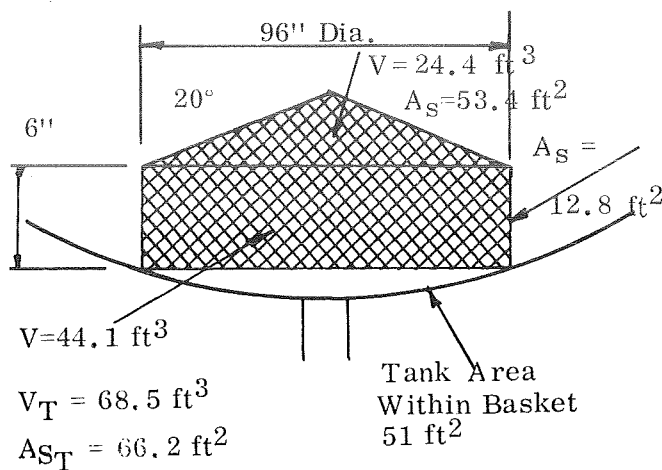


Figure 3-25. S-IVC LO<sub>2</sub> Start Basket

designed to remove 1440 Btu/hr and assuming a 10% tolerance on this system a maximum heat removal of approximately 1600 Btu/hr could occur. This results in a maximum net heat removal from the tank of  $1600 - 960 = 640 \text{ Btu/hr}$ .

3. The total mass of oxygen is 108,000 lb.
4. Using the stratified pressure change model from Reference 3-7, where the percent ullage is taken as 30%.
5. Then from Equation 3 of Reference 3-7 the rate of pressure change,  $\Delta P/\Delta t = 1450 (.00593)^{1.14} = .087 \text{ psi/hr}$

In order to be reasonably conservative a value of 0.1 psi/hr was used in the subsequent analysis.

A thermal network was constructed and inputted to the Convair Thermal Analyzer Computer program (Ref. 3-8). The tank and basket section nodal set-up is shown in Figure 3-26. The basket section was divided into 9 nodes with equal lengths between node centers and the tank wall was divided into 8 equal length nodes. The section considered is taken to be 1/10 of the total tank circumference. During the pressure decay cycle the warmest temperature of the start basket would be  $T_{12}$  as shown in Figure 3-26 and prevention of fluid vaporization at this point would be dependent on the relative rates of tank pressure decay and hydrogen cooling effect.

Computer calculations were made to determine complete temperature histories under the following conditions.

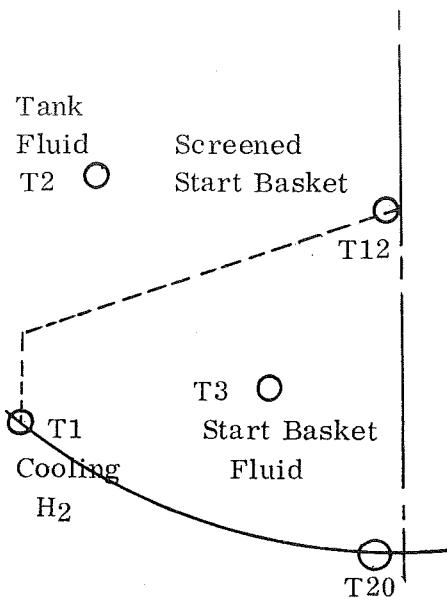
1. The tank fluid at the basket was taken to be a gas and condensing heat transfer (Figure 3-16) was assumed to occur between  $T_2$  and all start basket nodes. Based on previous analysis (Section 3.1.2) condensing was determined to

start basket fluid it is assumed that this fluid and also the surrounding surfaces must be maintained below the fluid saturation temperature.

A maximum tank pressure decay rate was determined on the following basis.

1. LO<sub>2</sub> tank net heating = 1200  $\pm$  240 Btu/hr.
2. At the upper LO<sub>2</sub> tank pressure limit the H<sub>2</sub> cooling system is

produce the highest heat transfer.



2. Heat transfer between the start basket fluid ( $T_3$ ) and start basket and wall is by natural convection (Figure 3-14) with an assumed acceleration of  $10^{-6}$  g's.
3. Heat transfer between adjacent wall nodes and basket nodes is by conduction.
4. The maximum saturation temperature drop was calculated to be  $0.12^\circ\text{R/hr}$  based on a  $0.1$  psi/hr pressure decay.
5. A steady state temperature solution was obtained prior to initiation of the transient calculations. This was based on  $T_1 = 100^\circ\text{R}$  and an initial saturation temperature ( $T_2$ ) of  $163^\circ\text{R}$ .

Figure 3-26.  $\text{LO}_2$  Start Basket Nodes - S-IVC Half Section

The computer calculations show that the tank wall exchanger cooling system is capable of preventing vapor formation in the  $\text{LO}_2$  start basket under the conditions analyzed. At initiation of pressure decay  $T_3$ ,  $T_{12}$ , and  $T_{20}$  were calculated to be  $149.22^\circ\text{R}$ ,  $162.14^\circ\text{R}$  and  $147.43^\circ\text{R}$  respectively. This results in a minimum subcooling at any point of  $0.86^\circ\text{R}$ . During a subsequent 10 hour pressure decay period the minimum subcooling ( $T_2 - T_{12}$ ) was found to be not less than  $0.76^\circ\text{R}$ , thus preventing basket fluid vaporization. The data showed that for this temperature or pressure decay rate the temperatures at all nodes corresponded to essentially steady state values throughout the cycle.

From the above analysis it is seen that the anticipated pressure decay rate would not cause vaporization to occur in the basket with any reasonable amount of basket cooling. The next step in the analysis is to determine cooling system details as to tube sizing and attachment configuration. From the computer analysis it is noted that the heat transfer to the cooling fluid (Node 1) was  $131.25$  Btu/hr for the  $1/10$  section. The total cooling for such a continuous tube attachment configuration would thus be a minimum of  $1,312$  Btu/hr. The actual cooling for a continuous tube attachment would be even more, since conduction to the cooling node from the tank area outside the start basket was not pertinent to the transient response analysis and therefore not included. Such conduction would, however, add to the total heat absorbed by the cooling fluid.

The actual heat transfer will depend on the temperature range in the cooling tube and internal heat transfer coefficients. Attachment of the cooling tube at discrete points rather than continuously to control the total cooling load is analyzed below.

A heat balance was made on the cooling fluid to determine the applicable temperature range.

Letting the  $\text{GH}_2$  flow = 9 lb/hr, then for the maximum heat transfer removal of 1440 Btu/hr ( $1200 \pm 20\%$ ) the change in cooling fluid enthalpy is 160 Btu/lb. This corresponds to a temperature rise of  $62^\circ\text{F}$  from an assumed inlet temperature to the oxygen exchanger of  $50^\circ\text{R}$ . Since the nominal oxygen tank temperature is  $172^\circ\text{F}$  (sat. temperature at 25 psia) the exchanger effectiveness  $[(T_{\text{CD}} - T_{\text{Ci}})/(T_{\text{H}} - T_{\text{Ci}})]$  need only be  $62/122 = 0.51$ . Thus the basic exchanger design is to control the amount of heat transfer rather than maximize it.

Calculations were made to define an actual exchanger configuration. The basic attachment is assumed to correspond to that shown in Figure 5-36. Applicable equations taken from Reference 3-5 are presented below.

$$\dot{Q}_n = (\zeta - T_n) 2 \pi k_w \delta_w \epsilon r_s \frac{K_1(\epsilon r_s)}{K_0(\epsilon r_s)} \quad (3-23)$$

$$\dot{Q}_i = 2L (T_n - T_v) \sqrt{k_{t_w} \delta_{t_w} h_{fi}} + h_{fi} A_i \quad (3-24)$$

where

$\dot{Q}_n$  = heat transfer rate to the attachment point from the tank fluid taking account of conduction in the tank wall.

$$\zeta = \frac{h_{f1} T_{g1} + h_{f2} T_{g2}}{h_{f1} + h_{f2}}$$

$$\epsilon = \sqrt{(h_{f1} + h_{f2})/k_w \delta_w}$$

This was determined to be a valid assumption for the tank temperature far from the support since the resistance to heat flow is high (low  $h_2$ ) through the superinsulation as compared to that between the tank wall and the fluid.

$\dot{Q}_i$  = heat transfer rate from the attachment to the cooling fluid.

$L$  = tube circumference.

$A_i$  = tube area in intimate contact with the tube support.

$T_v$  = cooling vapor temperature.

$h_{f_i}$  = cooling tube internal heat transfer coefficient.

Otherwise the terms are defined the same as for Equation 3-22 with the subscript t here referring to the cooling tube.

Assuming that  $\dot{Q}_i = \dot{Q}_n$  and solving for  $T_n$  in Equation 3-24 results in

$$T_n = T_v + \frac{\dot{Q}_n}{2L \sqrt{k_{t_w} \delta_{t_w} h_{f_i}} + h_{f_i} A_i} \quad (3-25)$$

Substituting into Equation 3-23 and solving for  $\dot{Q}_n$ ,

$$\dot{Q}_n = \frac{\zeta - T_v}{\frac{K_o (\epsilon r_s)}{2\pi k_w \delta_w \epsilon r_s K_1 (\epsilon r_s)} + \frac{1}{2L \sqrt{k_{t_w} \delta_{t_w} h_{f_i}} + h_{f_i} A_i}} \quad (3-26)$$

Assuming a 1/2 inch aluminum cooling tube, and

$$\delta_{t_w} = .032 \text{ in.}$$

$$L = 1.57 \text{ in.}$$

$$k_{t_w} = 55 \text{ Btu/hr-ft-}^\circ\text{F @ } 120^\circ\text{R avg. temp.}$$

$$T_B = 172^\circ\text{R} = \text{tank fluid bulk temperature.}$$

$$r_s = 0.5 \text{ in.}$$

$$\delta_w = .125 \text{ in.}$$

$$(T_v)_{\text{avg}} = 50 + 62/2 = 81^\circ\text{R}$$

$$h_{f_1} = 7.25 \text{ Btu/hr-ft}^2\text{-}^\circ\text{F from Figure 3-16 @ } \Delta T_{\text{avg}} = 20^\circ\text{F condensing heat transfer}$$

$$h_{f_2} \approx 0, \text{ which assumes a superinsulated tank wall with low heat transfer coefficient with respect to that internal to the tank.}$$

The tube internal heat transfer coefficient is calculated using Reynolds Analogy (Reference 3-9) where

$$\bar{h}_{f_i} = \frac{f}{2} \rho V_e C_{pf} = \frac{f}{2} \frac{\dot{m}}{A} C_{pf} \quad (3-27)$$

For a flow rate of 9 lb/hr,  $C_{pf} = 2.5 \text{ Btu/lb-}^\circ\text{F}$ , and  $f = .015$  for turbulent flow in smooth tubes;  $h_{f_i} = 31 \text{ Btu/hr-ft}^2\text{-}^\circ\text{F}$ .

Substituting values into Equation 3-26 results in a heating or cooling of 53.5 Btu/hr per attachment.

From Equation 3-25 the support temperature,  $T_n$  is  $140.8^\circ\text{R}$ . This results in an average temperature difference between bulk and wall of  $(172-140.8)/2 = 15.6^\circ\text{F}$ . The above calculations must then be repeated with a new condensing heat transfer coefficient based on an average  $\Delta T$  of  $15^\circ\text{F}$ . From Figure 3-16  $h_f = 7.75 \text{ Btu/lb-}^\circ\text{F-ft}^2$  and the new heating or cooling value is 53.8 Btu/hr with  $T_n = 141^\circ\text{R}$ . This shows that the cooling per attachment is not sensitive to changes in heat transfer coefficients in the range considered. Assuming a minimum total  $\text{LO}_2$  tank cooling of 960 Btu/hr then the number of attachments would be 17.85. For this case the use of 17 attachments at the start basket as shown in Figure 5-36 would be satisfactory. An additional coil is continuously attached to the tank in an area up from the start basket to provide any additional tank cooling which might be necessary. The circulation of fluid through this additional loop would be controlled by a pressure switch sensing oxygen tank pressure. The flow configuration and attachment areas are shown in Figures 5-32 and 5-38. Flow would be continuous through the start basket and feedline cooling coils. Mixing would be accomplished in the tank to minimize temperature gradients.

A further concern which was analyzed was the possibility of freezing of oxygen in the tank. To check this possibility an analysis was made of the first attachment point where the hydrogen is coldest and the cooling thus greatest. The hydrogen temperature is assumed to be  $50^\circ\text{R}$  at this point and the tank fluid in contact with the wall is taken to be liquid. This condition will result in the lowest temperature at the wall support ( $T_n$ ). Analytical results are presented below.

Assuming  $(\Delta T_{B-N})_{\text{avg}}$  to be  $30^\circ\text{F}$  then from Figure 3-14,  $\bar{h}_{f_1} = 1.335 \text{ Btu/hr-ft}^2\text{-}^\circ\text{F}$ . Then from Equations 3-26  $\dot{Q}_n = 63.4 \text{ Btu/hr}$  and from Equation 3-25  $T_n = 121^\circ\text{R}$  which is significantly above the freezing point of oxygen of approximately  $100^\circ\text{R}$ . Therefore, freezing for the present system configuration should not be a problem.

Compressible flow pressure drop calculations were made for the 1/2 inch tubing assuming a total length of 1200 inches including both tank coils and feedline cooling coils. The ratio of outlet to inlet pressure ( $P_2/P_1$ ) was found to be 0.885 or  $\Delta P \cong 1.7 \text{ psi}$  which is reasonable

The above thermal analysis assumes that the heat transfer resistance through the external insulation is large compared to that internal to the tank. Therefore, wall temperatures are low and vaporization not a problem as long as sufficient overall heat is being removed from the start basket area by the cooling tubes. Consideration

of the overall heat leak on a uniform basis shows a fairly high wall heat flux. As an example the total heating is 2500 Btu/hr (Reference 3-6, page 80) for the net of 1200 Btu/hr listed in Table 3-1.

This results in an average  $Q/A$  of  $2500/591 = 4.23$  Btu/hr-ft<sup>2</sup> and assuming an outer surface temperature of 450°R and a LO<sub>2</sub> temperature of 170°R an equivalent heat transfer coefficient for the entire surface is calculated to be 0.0151 Btu/hr-ft<sup>2</sup>-°F. This can result in a fairly high equilibrium wall temperature. Therefore, cooling system design is critical in preventing wall temperatures above saturation in the start basket area. Analysis for this high external heating case is presented below. For this condition proper temperature control must be obtained by locating the cooling attachments on the tank wall within the basket area.

The maximum allowable heat removal from the tank by this exchanger is assumed to be 960 Btu/hr. From Figure 3-25, the basket area exposed to the tank fluid has an area of 66.2 ft<sup>2</sup>. Assuming a worst case heat transfer of condensing gas on the basket surface then from  $Q = \bar{h}_f A \Delta T$  and Figure 3-16 the maximum subcooling ( $\Delta T$ ) of the basket fluid is found to be 0.934°F. Since the placement of tube attachments are at the tank wall within the circumference of the basket only heat from within the basket and that intercepted at the wall is transferred to the cooling fluid. The tank internal heat transfer, as effecting attachment cooling, is then by LO<sub>2</sub> natural convection at the wall. Equations 3-25 and 3-26 are still applicable, and now  $h_{f2} = .0151$  Btu/hr-ft<sup>2</sup>-°F and  $h_{f1}$  is obtained from Figure 3-14. In order to determine the allowable cooling tube

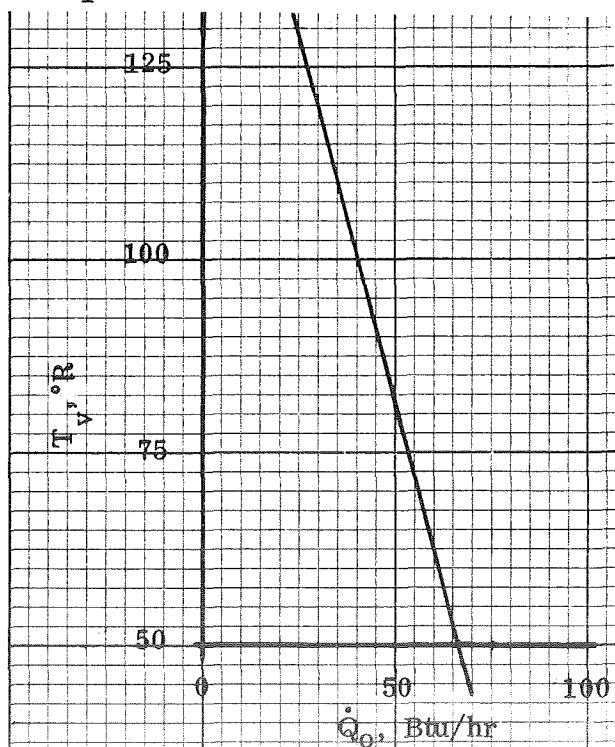


Figure 3-27. SIV C LO<sub>2</sub> Tank Cooling Load as a Function of Cooling Temperature

placements, values of heat transfer as a function of cooling temperature are determined from Equation 3-26 and plotted in Figure 3-27.

For the present conditions:

$$\frac{1}{2L \sqrt{K_t} \delta_t h_{t_i}} = 1.118/\text{Btu/hr-°F}$$

$$\frac{K_o (\epsilon r_s)}{2\pi K_w \delta_w \epsilon r_s K_1 (\epsilon r_s)} = \frac{.278 K (\epsilon r_s)}{\epsilon r_s K_1 (\epsilon r_s)}$$

A required spacing necessary to prevent the tank wall temperature from rising above the tank saturation temperature at any point is determined from the following equation.

$$T_w = \zeta - \frac{\dot{Q}_n K_o (\epsilon r)}{2 K_w \zeta r_s K_1 (\epsilon r_s)} \quad (3-28)$$

where  $\dot{Q}_n$  is taken from Figure 3-27.

The value,  $\zeta$ , represents the equilibrium wall temperature at  $r = \infty$  and is very important in determining the area which a single cooling attachment can maintain below saturation. From the definition of  $\zeta$  it is seen that the lower the external heat transfer coefficient  $h_{f1}$  and the higher the internal value  $h_{f2}$  the closer this equilibrium wall temperature will be to the basket fluid temperature. With high enough values of  $h_{f2}$  in relation to  $h_{f1}$  the value of  $\zeta$  will be below the saturation temperature and the total heat removed from the basket would be the sole criteria for attachment spacing.

For the present conditions where  $h_{f1} = .0151$  Btu/hr-ft  $^{\circ}$ F and  $h_{f2}$  is found from Figure 3-14,  $\zeta$  was found to be  $176.9^{\circ}$ R. Equation 3-28 is then solved for temperature distribution in the tank wall. An average temperature difference was used in determining  $h_{f2}$  and an iterative solution accomplished between Figure 3-14 and Equation 3-28.

This data is presented in Figure 3-28.

From this figure it is seen that temperatures below tank saturation are maintained out to a radius of approximately 10 inches. This represents a satisfactorily cooled area of  $314 \text{ in}^2$ . From Figure 3-27 the average heat transfer per attachment is  $49.75 \text{ Btu/hr}$  (taken at  $81^{\circ}$ R cooling temperature). This results in an allowable number of attachments of,  $960/49.75 = 19$ . The total area being maintained below saturation is thus  $314 (19) = 5,960 \text{ in}^2$ . From Figure 3-25, the tank wall area within the start basket is  $7,350 \text{ in}^2$  and thus the above configuration would not be satisfactory for assuring that no vapor formation occur within the basket.

It is noted that for the actual vehicle system most of the  $2500 \text{ Btu/hr}$  heat transfer into the oxygen tank is through the thrust structure support by conduction. The above analysis should, therefore, be conservative since the thrust structure attachment is located somewhat outside the basket area.

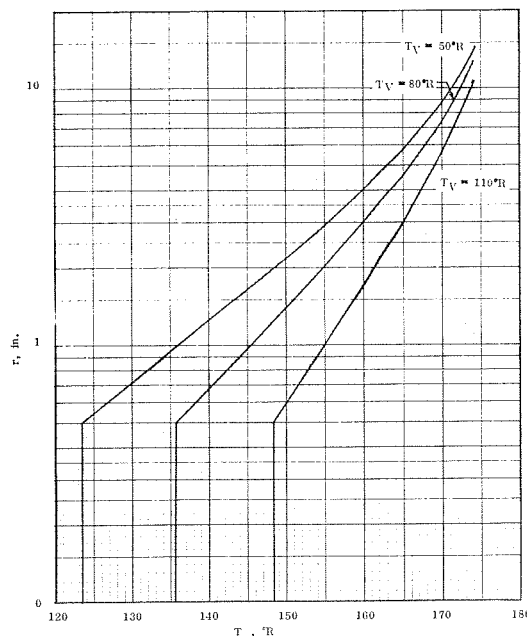


Figure 3-28. LO<sub>2</sub> Tank Wall Temperature Distribution

Figure 3-28. LO<sub>2</sub> Tank Wall Temperature Distribution.

It would thus be reasonable to apply high performance insulation to the tank area within the thrust structure in conjunction with the start basket. Values of the equilibrium wall temperature ( $T_w$ ) are plotted in Figure 3-29 as a function of insulation effectiveness.  $\text{LH}_2$ , with heat transfer coefficients from Figure 3-14, is assumed to exist on the fluid side of the wall.

Assuming 19 supports, the minimum required area per support would be  $\frac{7,350}{19} = 386 \text{ in}^2$  or an effective radius of 11.1 in. Taking account of overlap and tolerances an effective radius requirement of 15 inches would seem reasonable. An inspection of Figure 3-28 indicates that this could be accomplished if the equilibrium wall temperature ( $\zeta$ ) were on the order of  $173^\circ\text{R}$  or  $[(\zeta - T_R) = 1^\circ\text{F}]$ . For this to occur, from Figure 3-29, an effective external heat transfer coefficient in the start basket area would need to be on the order of  $2 \times 10^{-3} \text{ Btu/hr-ft}^2\text{-}^\circ\text{F}$ . This would appear to be a reasonable value assuming the use of superinsulation in this area. As an example, the effective heat transfer coefficient for the  $\text{LO}_2$  tanker vehicle (see Section 3.2) is estimated to be  $3.38 \times 10^{-4}$ .

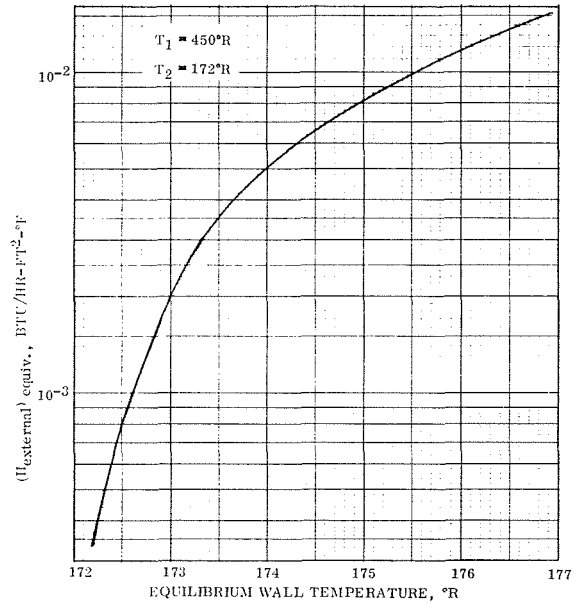
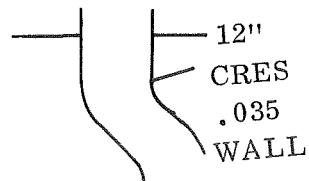


Figure 3-29. Equilibrium Wall Temperature as a Function of External Heat Transfer.

**3.1.9  $\text{LO}_2$  FEED DUCT COOLING** — An estimate of required cooling tube spacing for the  $\text{LO}_2$  feed duct was made in a similar manner to that as discussed in Section 3.1.7 for the hydrogen tank. Equation 3-16 is applicable. The basic duct conditions are illustrated below. The duct material was assumed to be the same as for the hydrogen case.

Then for  $K_w = 5 \text{ Btu/hr-ft-}^\circ\text{F}$  and  $h_{fe} = .0151 \text{ Ftu/hr-ft}^2\text{-}^\circ\text{F}$  from Equation 3-16,

$$\frac{T_H - T_C}{T_H - T_M} = \cosh [(.0424) (a, \text{in.})]$$


The solution is presented in Figure 3-30 as a function of tube spacing. For the present conditions where  $T_M = 450^\circ\text{R}$ ,  $T_C = 100$  or the  $T_M = 172^\circ\text{R}$  the tube spacing would need to be on the order of 16 inches. For  $T_{C_{\max}} = 120^\circ\text{R}$  the required spacing is approximately 14 inches.

### 3.2 $\text{LO}_2$ TANKER THERMAL ANALYSIS

The basic configuration analyzed is presented in Figure 3-31 along with pertinent data. As discussed with respect to the SIVC thermal analysis the following possibilities exist for the generation of vapor within the collector channels.

- a) Heat transfer directly to the channels and/or reservoir from the environment through conduction in the support members.
- b) Heat transfer from superheated gas in contact with the channel fluid. If the heat transfer from such gas is greater than the rate of dissipation to the cooling medium or subcooled liquid then vapor can be formed. One advantage of the collector channels over the SIVC start basket system is that some part of the channels are always in contact with liquid and thus the screen tends to remain wetted at all times. Any evaporation occurring at the screen surface should thus be immediately replaced with liquid, thus preventing vapor formation within the channels. Also, this wicking action tends to minimize stratification in a similar manner as a heat pipe.
- c) Bulk boiling due to a drop in tank pressure caused by gas venting or heat removal not at the screen surface. In the SIVC oxygen tank analysis presented in Section 3.1.8 it was shown that such pressure decay is generally slow enough such that a cooling system employed to prevent excessive external heating will also be able to prevent evaporation during the pressure decay transient.

From the above discussion it is seen that heat leak into the channels or reservoir from supports and areas not completely covered with screen is the most critical. The main problem is in uniformly distributing the relatively low vent cooling capacity to the many potential channel hot spots.

The basic system proposed utilizes a thermodynamic vent system designed to operate with liquid at the inlet to the heat exchanger. The liquid collectors will be tapped to provide this liquid. The oxygen ventage will chill critical areas of the collection,

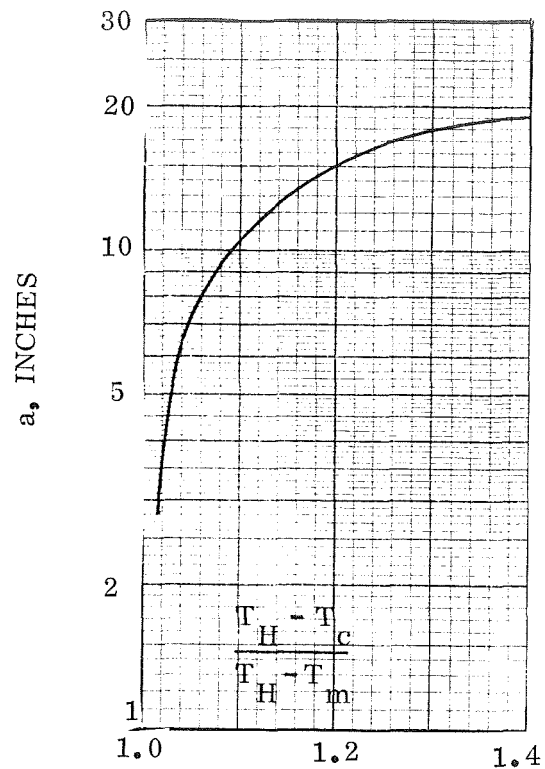


Figure 3-30.  $\text{LO}_2$  Tank Feed Duct Cooling Tube Spacing.

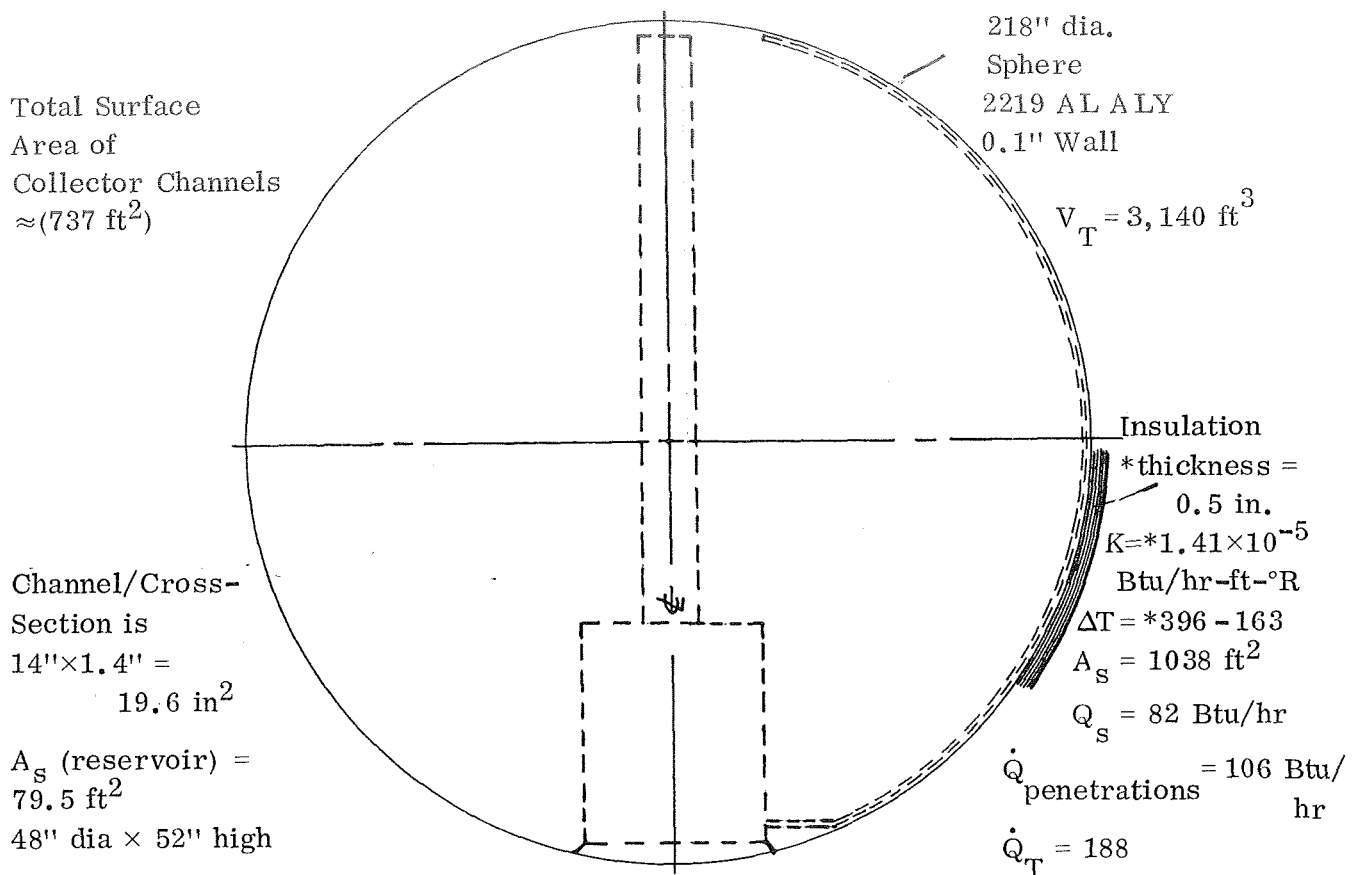


Figure 3-31.  $\text{LO}_2$  Tanker Configuration

reservoir and feed line to intercept heat leaks and assure a vapor free condition at the tank outlet and within the liquid reservoir. The cooling fluid will then be vented to a bulk heat exchanger and mixer within the tank to assure that essentially all the available energy is extracted from the vent for tank pressure control. This system could also employ a separate bulk exchanger for on-off pressure control in order to allow a constant vent cooling system. The basic considerations between the two systems is essentially the same as discussed for the SIVC vehicle in Section 3.1

The cooling fluid is initially throttled to a lower temperature and pressure. The resulting loss is the  $\Delta T$  available for heat transfer. In order to minimize the flow distribution problem it is assumed that each cooling circuit has a separate throttling device and liquid is taken directly from each channel or reservoir to be cooled. The total available flow rate is determined by requiring that the tank pressure remain constant. If all of the heat added to the venting fluid comes either directly or indirectly from the tank liquid then Equation 3-1 can be used to relate the flow rate to the exit enthalpy for constant pressure venting.

Either liquid or vapor can be introduced into the vent system, but after consulting a T-S diagram for oxygen one sees that the heat capacity of vented vapor is insufficient to remove a significant fraction of the incident heat rate. Liquid, therefore, is drawn from the tank and circulated through the heat exchanger tubing where

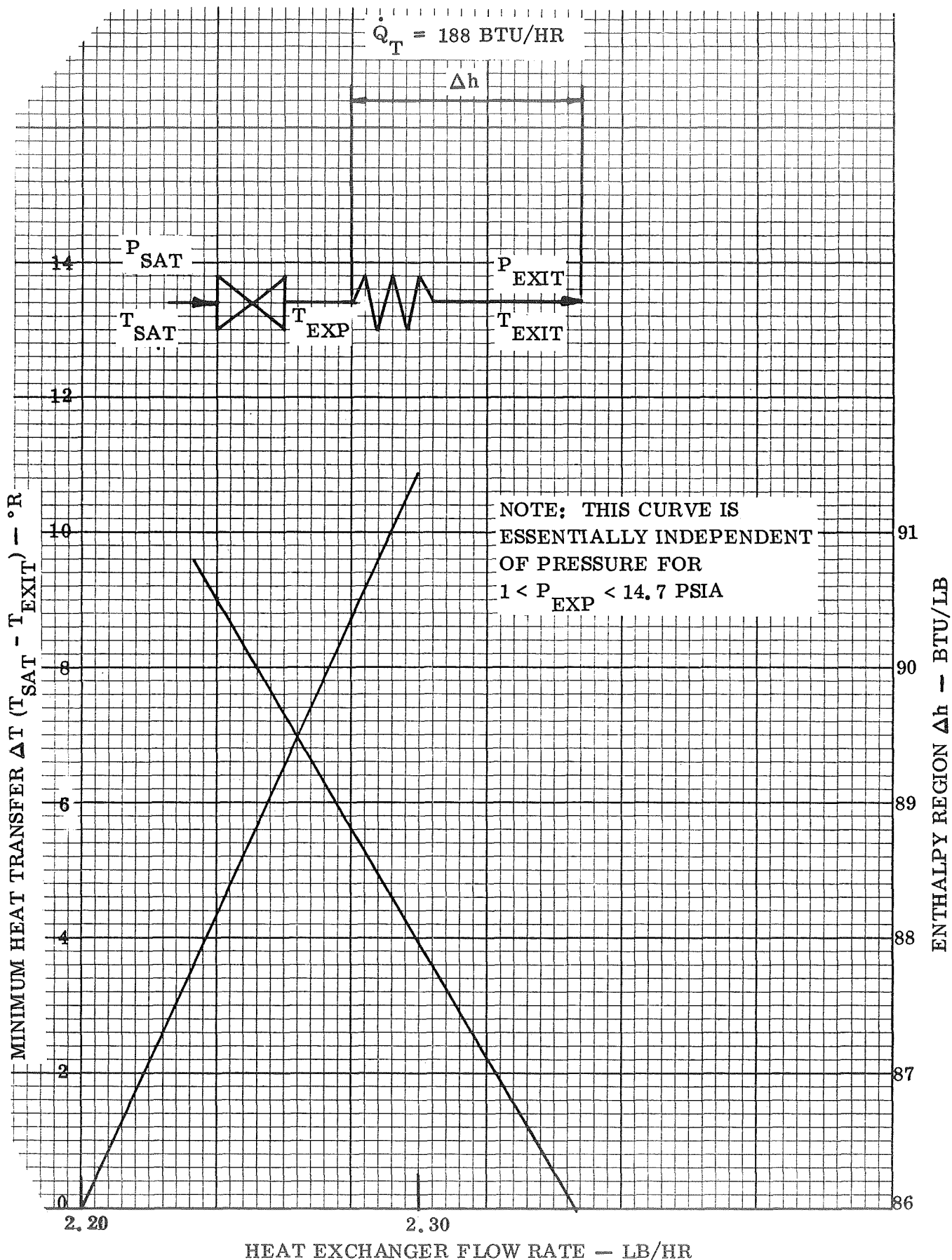


Figure 3-32.  $O_2$  Tanker Vent Flow Rate Required for Constant Tank Pressure

it rises in enthalpy to  $h_{\text{exit}}$ . Values of  $\dot{m}_v$  computed from Equation 3-1 are presented in Figure 3-32.

Expanding the vent liquid to low pressures provides a small  $\Delta P$  for flow through the tubes, the results in a large  $\Delta T$  (in the boiling region) for heat transfer from the saturated tank fluid. By expanding to pressures only slightly less than tank pressure the  $\Delta P$  for flow in the tubes is increased and the  $\Delta T$  for heat transfer is reduced. The  $\Delta h$  available for energy absorption is only slightly decreased however, because the sensible heat of the vapor at these temperatures is only a small fraction of the heat of vaporization. Also the enthalpy of saturated vapor is insensitive to pressure in the range considered.

A balance in energy exchange rates is sought whereby the expanded vent fluid absorbs enough energy to prevent vaporization in the collector channels and can be exhausted from the  $O_2$  tanker at the flow rate and exit enthalpy which results in constant tank pressure.

A mixer is required within the tank to assure a homogeneous thermodynamic condition within the tank.

Any heat incident on the tank skin must be removed if a possibility exists that it will enter the collector channel. After the initial chilldown period all of the collected liquid will have reached steady state at temperatures at or below saturation. A cooled channel thus becomes a heat sink and the heat exchanger must remove heat incident on the tank skin and heat transferred to the collector channel by the propellant.

Two basic cooling methods are analyzed below. In both cases individual cooling tubes and throttling devices are used for each collector channel and also for the reservoir basket.

The two configurations analyzed are shown in Figure 3-33 and Figure 3-34.

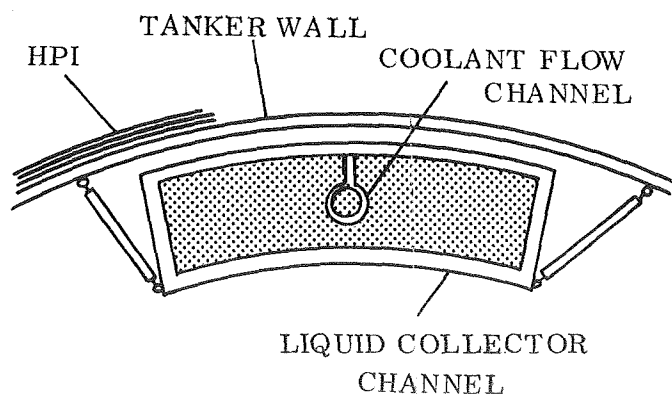


Figure 3-33. LOX Tanker Cooling With Cooling Channels Inside the Collector Channels

In both cases the reservoir is cooled at the external tank surface as described in Section 3.1.8 for the S-IVC oxygen tank.

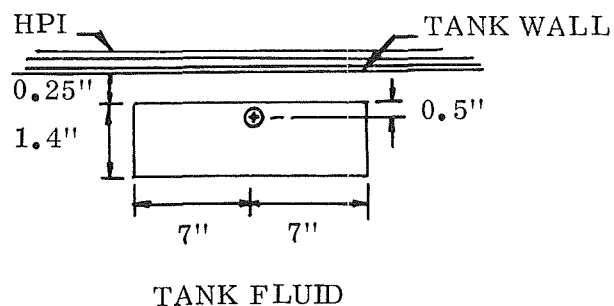
The first system considered utilizes a small channel or tube running inside of each collector channel, which slightly subcools the liquid within the collector channels.

Based on the thin profile geometry as presented in Figure 3-31, heat transfer between the screen surface and the cooling tube is by conduction. The worst case for maintaining a subcooled condition is when condensing heat transfer can occur at the screen surface. The surface is thus raised to essentially the tank saturation temperature and any small amount of additional heating such as at a support would cause vapor to form.

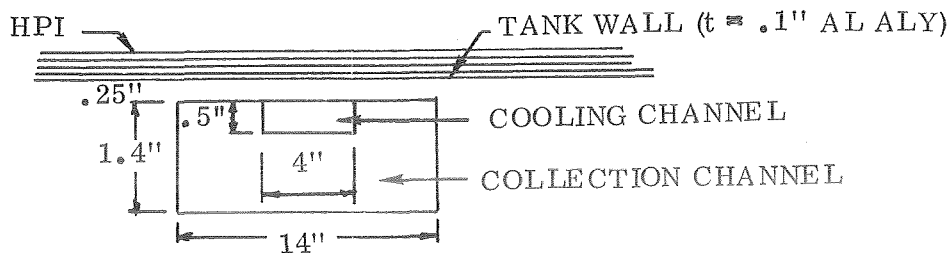
For the case where cooling flow was within the collector channels a thermal analysis was performed using the Convair thermal analyzer program (Reference 3-8). Boiling heat transfer was assumed to occur internal to the cooling tube. From Reference 3-10, for oxygen at 1 atmosphere

$$Q/A, \frac{\text{Btu}}{\text{hr-ft}^2} = 20.3 [(T_{c_w} - T_c)]^{2.5} \quad (3.29)$$

For heat transfer from the tank fluid to the start basket, condensation and forced convection  $\text{LO}_2$  heat transfer were assumed. The initial configuration analyzed is shown below.



Heat transfer from the collection channel surface to the cooling channel and from the wall to the collection channel is by conduction through the  $\text{LO}_2$ . For a coolant temperature of  $155^\circ\text{R}$  and a bulk tank fluid temperature of  $163^\circ\text{R}$  the heat transfer to the coolant was 12.48 Btu/hr per foot of length and for 288 foot of channel the total heating was 3,600 Btu/hr. This is much too high and therefore a configuration with the cooling tube located within the channel, as shown below, was considered in an attempt to reduce the total required cooling load.



The cross-sectional area of the tube was assumed to be negligible with respect to that of the collection channel.

Cases were run with cooling temperatures of 155 and 160°R resulting in cooling loads of 7.06 and 1.79 Btu/Hr-ft respectively. These correspond to total loads of 2,030 Btu/hr and 515 Btu/hr, both of which are still too high. 188 Btu/hr is the desired maximum over the total length. In all cases the main resistance to heat transfer was found to be between the collector surface and the internal tubing, therefore, further analysis was performed assuming a collection channel surface temperature of 163°R and pure conduction between this surface and the cooling tube.

Looking first at a 1/2 inch tube and taking into account the actual diameter of the tube in calculating the tube distance from the collector channel wall, cooling for a 160°R cooling temperature was found to be 2.36 Btu/hr-ft (680 Btu/hr).

The following iterations were then accomplished in an attempt to reduce the cooling load to acceptable levels.

- a) Reduced cooling tube size to 1/4" resulting in  $\dot{Q}_T = 1.18$  Btu/hr-ft (340 Btu/hr).
- b) Moved 1/4" tube to channel center with  $\dot{Q}_T = .95$  Btu/hr-ft (274 Btu/hr) resulting.
- c) Reduced cooling tube to 1/8" dia. resulting in  $\dot{Q}_T = .678$  Btu/hr-ft (195 Btu/hr).

The above analysis indicates the problem with a cooling tube inside the channels; since even with the 1/8" diameter tube located in the channel center with low conductive supports, the total heating load could be greater than the maximum desired value of 188 Btu/hr. It is also noted that additional heat capacity within the 188 Btu/hr must be allowed for cooling of the reservoir and feed line.

A further reduction in maximum cooling load could be accomplished by increasing the cooling temperature. However there are certain tolerances on the exit pressure control and in order to be assured of some throttling a maximum pressure differential between tank and cooling of approximately 2 psi is considered reasonable. This corresponds to a cooling temperature of 160°R, for a tank condition of 15 psia (163°R) which has been used in the above analyses.

A further possibility for balancing the cooling with external heating is to provide a number of short lengths of cooling tube only in the areas of the supports where cooling is most critical. In order to do this effectively a large number of throttling devices would be required. This would tend to reduce the overall system reliability since such throttling devices are subject to plugging due to contamination. This is especially true for the small passage sizes which would be required in the present case. Also, the number of throttling locations is limited by the minimum flow which

can be handled by each device, since the total vent flow is essentially constant for a given total tank heating. Use of a viscojet throttling restriction, as described in Reference 3-11, is considered most applicable for the present system. Calculations were made on the basis of a total vent of 2 lb/hr, a 3 psi pressure drop and the minimum size device available. From this a maximum of 30 cooling points were determined to be feasible. Since there are a total of 50 supports and because of the reliability problem the internal cooling configuration does not look promising.

A more promising solution to the  $\text{LO}_2$  tanker cooling problem appears to be location of the cooling tubes external to the tank wall with direct attachment only at critical collector and reservoir support points. Analyses were made of such a system using the basic Equations of Section 3.1.8. A typical attachment is shown in Figure 3-34.

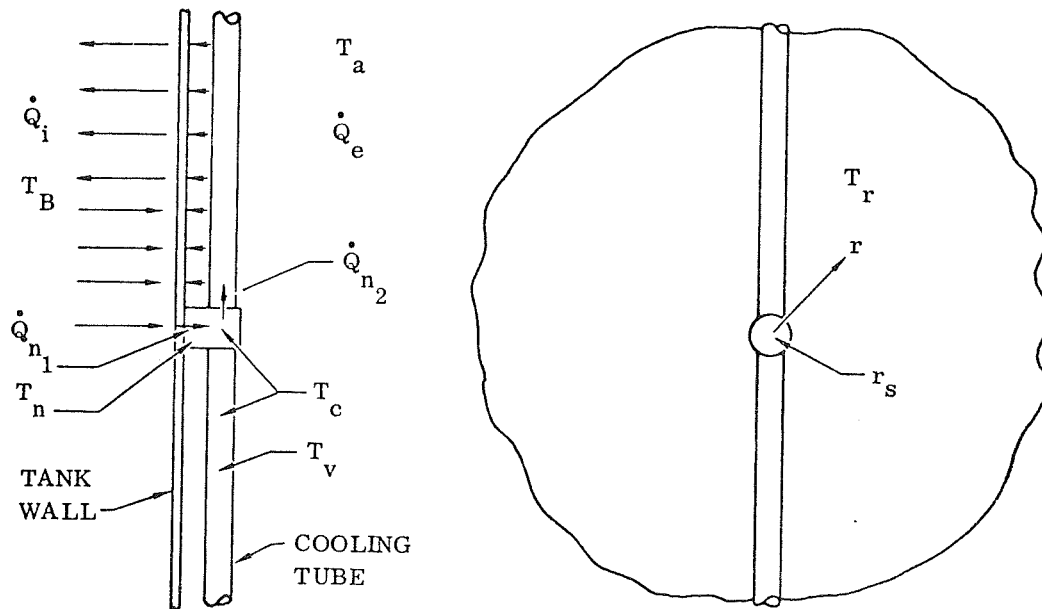


Figure 3-34  $\text{LO}_2$  Tanker External Cooling Tube Attachment.

The following data apply to the configuration analyzed.

$$\begin{aligned}
 k_w &= 55 \text{ Btu/hr-ft}^2\text{F} \\
 \delta_w &= 0.1 \text{ in.} \\
 T_a &= 396^\circ\text{R} \\
 T_c &= 159^\circ\text{R} \quad (P_e = 12 \text{ psia}) \\
 T_B &= 163^\circ\text{R} \\
 \delta_{tw} &= .024 \text{ in.} \\
 K_{tw} &= 55 \text{ Btu/hr-ft}^2\text{F} \\
 D_t &= .125 \text{ in.} \\
 h_f &= 57.5 \text{ Btu/hr-ft}^2\text{F} \quad (\text{LO}_2 \text{ Boiling at } T = 2^\circ\text{R from Eq. 3-29}) \\
 h_e &= 3.38 \times 10^{-4} \text{ Btu/hr-ft}^2\text{F} \\
 A_s &= (.125)/.392 \text{ in.}^2 \\
 L &= (.125) = .392 \text{ in.} \\
 D_t &= 1/8" \\
 r_s &= 0.5"
 \end{aligned}$$

$$\frac{1}{2L \sqrt{\frac{K_t}{K_w} \frac{\delta_t}{\delta_w} \frac{h_f}{h_i} + h_f \frac{A_i}{A_s}}} = 3.1/\text{Btu/hr-}^\circ\text{F}$$

$$\frac{K_o (\epsilon r_s)}{2\pi K_w \delta_w \epsilon r_s K_l (\epsilon r_s)} = \frac{.347 K_o (\epsilon r_s)}{\epsilon r_s K_l (\epsilon r_s)}$$

It is assumed that mixing is accomplished in the tank in order to minimize temperature stratification. This mixing is especially important for the present system since direct cooling of the channel fluid is not accomplished and superheated vapor, if present, might cause vaporization in areas not completely covered with screen. Screened areas are assumed to remain wet at all times due to wicking.

Assuming a maximum internal heat transfer coefficient of  $10 \text{ Btu/hr-ft}^2\text{F}$ ,  $\zeta = 163^\circ\text{R}$ ;  $\epsilon = 4.66/\text{ft}$  and from Equations 3-25 and 3-26  $\dot{Q}_n = 1.067 \text{ Btu/hr}$  per attachment and  $T_n = 162.3^\circ\text{R}$ .

For the 80 attachments,  $\dot{Q}_T = 85.4$  Btu/hr which leaves approximately 103 Btu/hr for reservoir and feed line cooling. Referring to Figure 3-16 and 3-17 it is seen that a heat transfer coefficient of 10 corresponds to condensing heat transfer at  $\Delta T = 5.6^\circ\text{R}$  and a  $\text{LH}_2$  forced convection flow of .13 ft/sec. For other fluid conditions the coefficient will be somewhat less. The minimum case would be for  $\text{LO}_2$  forced flow, and per Figure 3-17 a reasonable value would be on the order of 0.1 Btu/hr-ft<sup>2</sup>°F. For this condition  $\rho \cong 164^\circ\text{R}$ ,  $\epsilon = .466/\text{ft}$ ,  $\epsilon_r = .01945$  and from Equations 3-25 and 3-26  $\dot{Q}_n = 1.11$  Btu/hr per attachment and  $T_n = 162.4^\circ\text{R}$ .

For the 80 attachments,  $\dot{Q}_T \cong 88.8$  Btu/hr which leaves approximately 99.2 Btu/hr for cooling the other areas. This shows that the above system is good over the full range of heat transfer to be expected and that the cooling load is rather insensitive to internal heat transfer over this range. This is primarily due to the very low heat leak through the external tank insulation. It is noted that it is important in a final design that insulation penetrations do not occur at the collection channel support points. The above analysis is applied to the short load supports shown in Figure 5-58. The drag struts are long and have sufficient thermal resistance that by proper tank mixing the temperature at the end on the channel will not be above saturation.

In order to verify the use of 1/8" tubing, pressure drop calculations were made in the same manner as described for two-phase hydrogen in Section 3.1.4. Assuming a total flow of 216/hr split into 10 equal flow passages, an exit flow pressure of 12 psia, and a length per flow passage of 30 feet, the total pressure drop was calculated to be only 0.08 psi.

# 4

## EXPERIMENTAL PROGRAM

During the second phase, experiments were run to determine wicking rates in screens, vapor ingestion and draining of capillary devices and pullthrough suppression using screen baffles. The experimental program consisting of scale model non-cryogenic bench tests was successful in providing correlations and verification of computer models and design techniques.

Wicking tests were conducted using horizontal screens with pentane and silicone oil as the working fluid. Results are presented in the form of semiempirical correlations since tests did not agree with any of the three wicking models proposed. Spilling, vapor ingestion and draining tests were conducted using water and pentane using a scale model S-IVC transparent tank and capillary device. Results for capillary device spilling and vapor ingestion were successfully correlated with the INGASP computer model while results of draining tests with a capillary device were correlated with the DREGS2 model. Pullthrough suppression tests, run in a cylindrical plexiglass container indicated the usefulness of screens in reducing vapor pullthrough.

Testing conducted under a Convair IRAD program yielded screen flow data for dutch twill and square weave screens. Screen meshes used were  $20 \times 20$ ,  $200 \times 1400$ ,  $165 \times 1400$ ,  $200 \times 600$ ,  $165 \times 800$ ,  $150 \times 700$ ,  $180 \times 700$ ,  $50 \times 250$ ,  $30 \times 250$  and  $20 \times 250$ . Test fluids were water, liquid hydrogen, liquid nitrogen, gaseous nitrogen, gaseous hydrogen and gaseous helium. Results are presented in the form of semi-empirical equations in Reference 4-1, Section 2.2 and Reference 4-2, since the capillary and packed sphere models proposed could not be accurately correlated with the test data.

The objective of Phase II testing was to verify analytical models — DREGS2 and INGASP, substantiate design principles — screen pullthrough suppression and empirically evaluate problems which could not be evaluated analytically — screen flow and wicking. Test data correlations have been incorporated into Reference 4-1 in a form useful to the capillary device designer.

### 4.1 SCALE MODEL OUTFLOW TESTS

**4.1.1 INTRODUCTION.** Minimization of residuals and control of vapor ingestion and spilling are important considerations in design of a capillary device. The analytical models formulated into the INGASP and DREGS2 computer programs were developed to handle these problems. To assure the accurate predictive capability of the computer models a transparent scale model S-IVC tank and capillary device were designed,

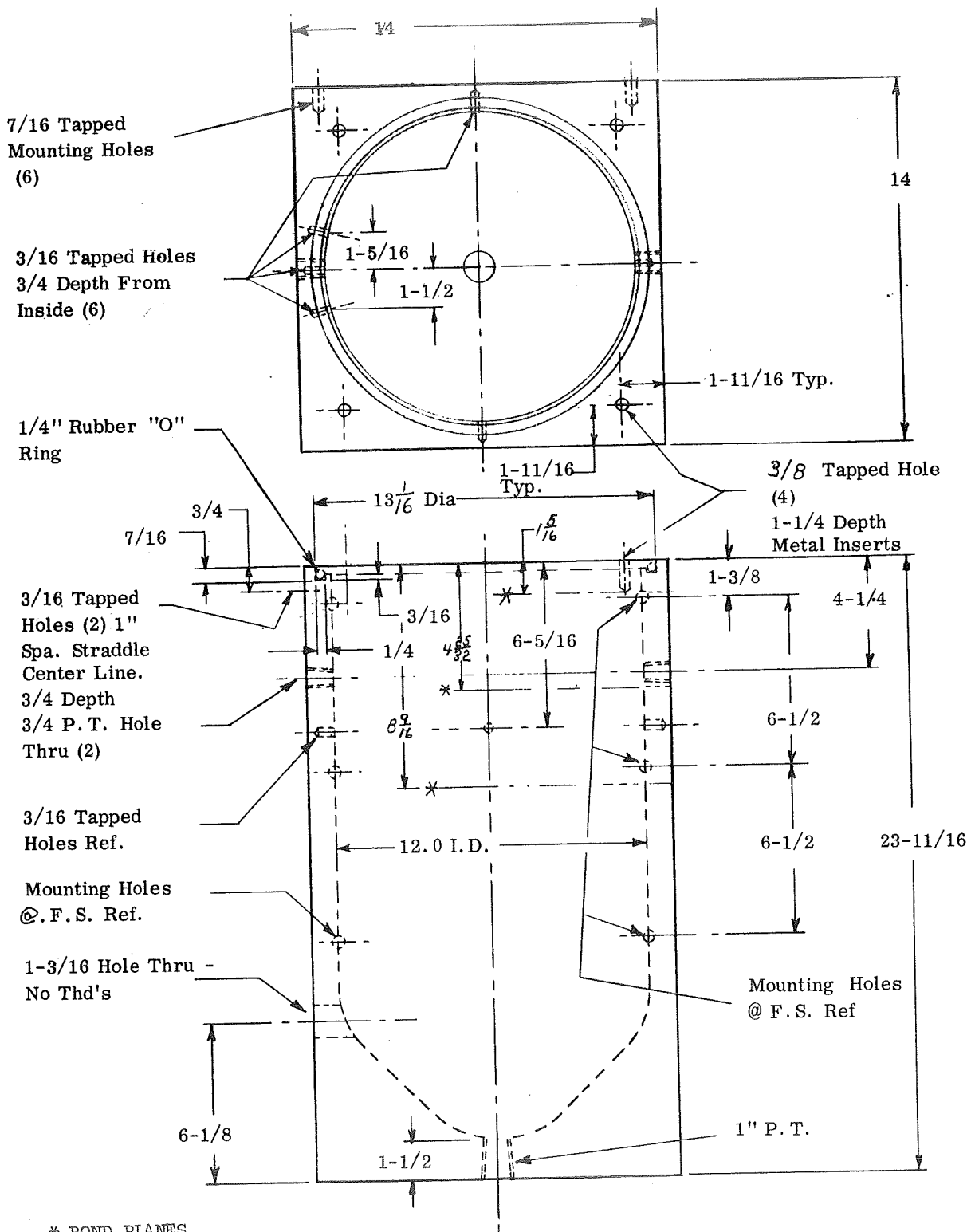


Figure 4-1. Scale Model Centaur Tank — Existing Housing

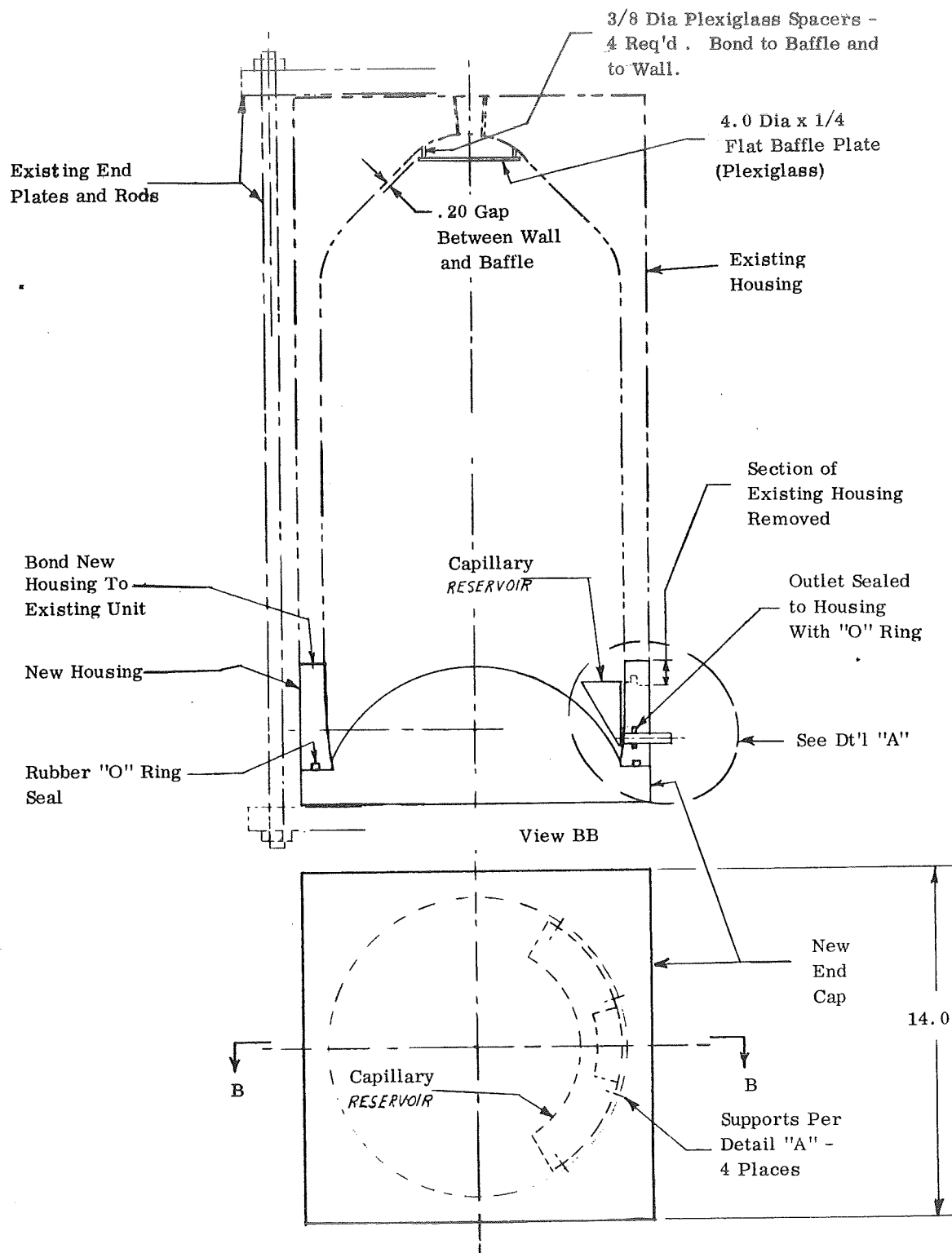


Figure 4-2. Annulus Type Capillary Reservoir Model - General Assembly

fabricated and tested to obtain data which was successfully correlated with the analyses.

4.1.2 SUMMARY. The test article was designed to provide visual data on liquid levels, vapor and liquid flow and to assure that correlations obtained would be applicable to the S-IVC  $\text{LH}_2$  full scale tank and capillary device. Screens, fluids and capillary device geometry were scaled from the  $\text{LH}_2$  case, while the test tank was a Centaur scale model tank modified with a pressurant baffle, capillary device supports and scale model S-IVC aft bulkhead and engine feedline. Tests conducted with pentane and water were visually recorded for a range of outflow rates using a high-speed motion picture camera. For each of the tests the film was observed on a Vanguard motion analyzer and data was compared to computer runs which modelled the tests. The agreement between the test data and analytical predictions corroborated the use of the DREGS2 model for predicting residuals and the INGASP model for predicting spilling and vapor ingestion in tanks containing capillary devices.

#### 4.1.3 EXPERIMENT DESIGN

4.1.3.1 Test Article Design. The test article was designed to simulate the geometry of an S-IVC tank and capillary device. A scale model Centaur tank, shown in Figure 4-1, was modified as shown in Figure 4-2. The dimensions of the capillary device and aft bulkhead were scaled linearly in ratio to the tank radius,  $\frac{130''}{6''}$ . The capillary device assembly and construction details are shown in Figures 4-3 through 4-8. The capillary device was a 120" annulus section with a triangular cross section, consisting of clear plexiglass sheets with cutouts in the ends and the inboard side which are equipped with capillary screens. The outlet tube is engaged with an "O" ring seal in the test housing and the reservoir was attached to the housing using four angle clips and screws.

##### Fluid Section

Pentane was selected as the working fluid by comparing pressure drop with nine different dutch twill screen meshes and all feasible working fluids, with the pressure drop of  $\text{LH}_2$  using  $200 \times 1400$  screen. The mesh used in the model was  $200 \times 600$  screen. (Pentane is an excellent wetting fluid and was also selected for the wicking tests due to its fluid and thermal properties.) Also taken into account was the surface tension retention capability of the screen mesh.

##### Apparatus Design

The test article plumbing design is as shown in Figure 4-9 with a regulator controlling tank pressure within .1 psi during outflow. The actual test configuration is shown photographically in Figure 4-10.



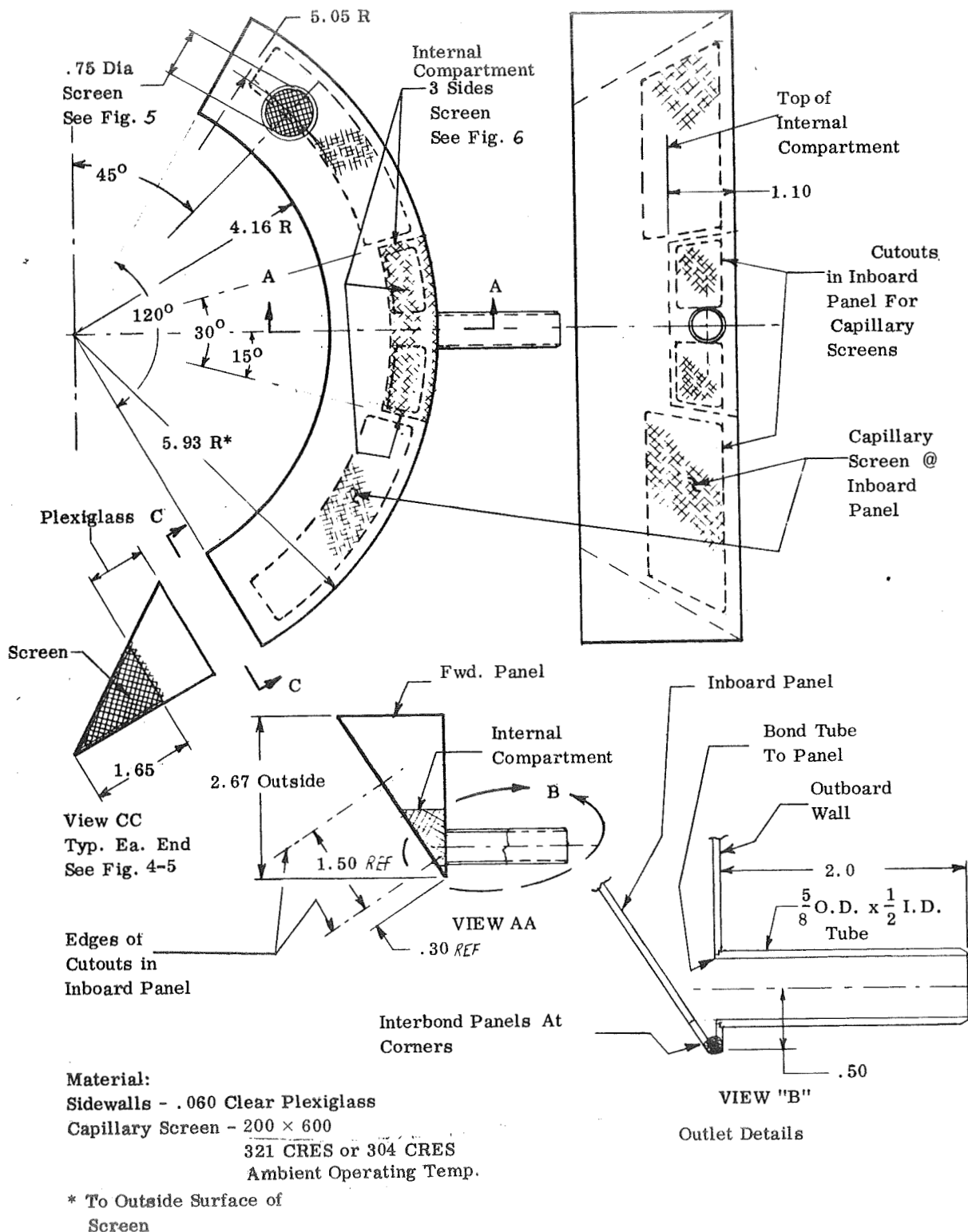
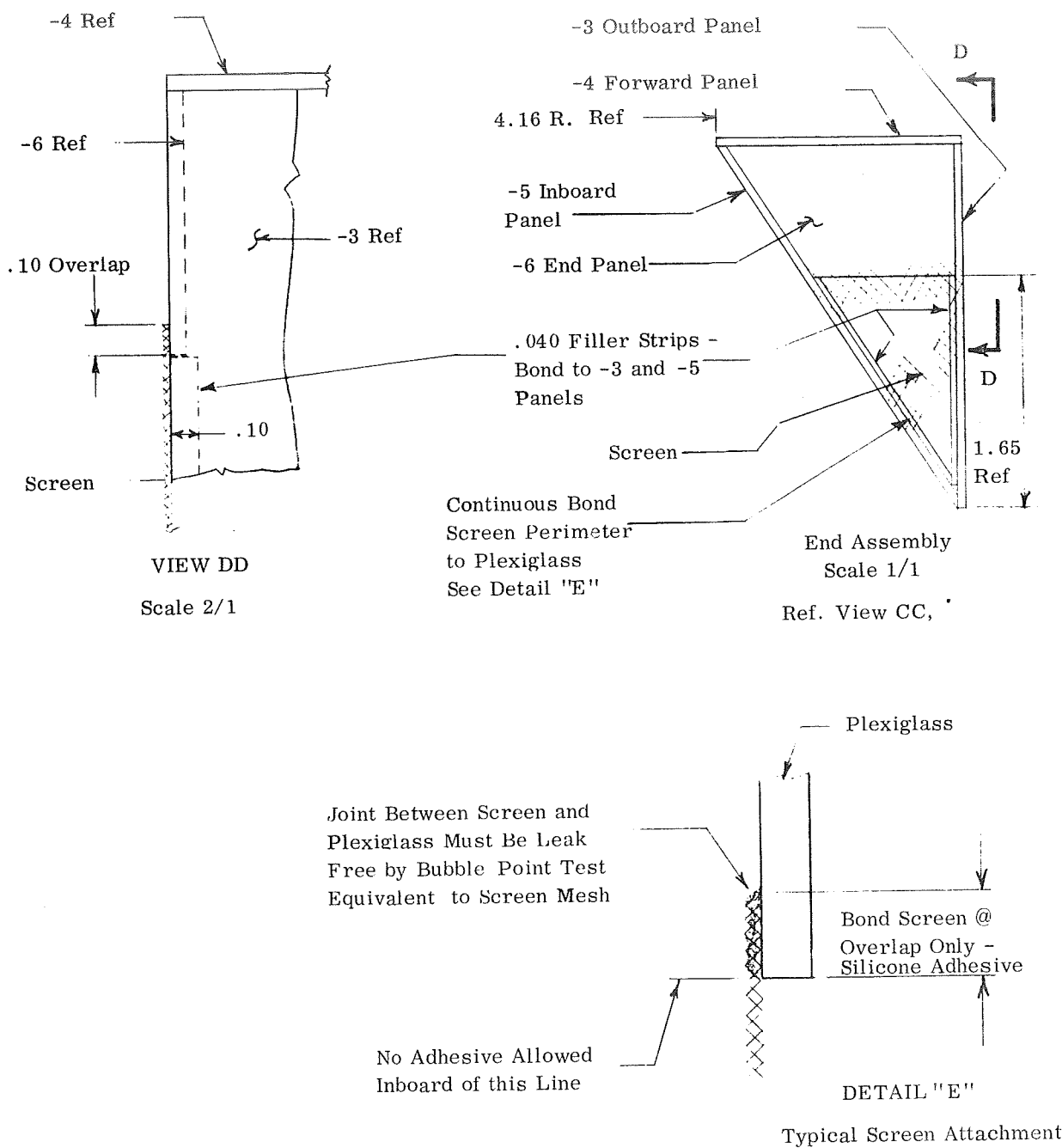


Figure 4-4. Annulus Type Capillary Reservoir Model - Capillary Reservoir Assembly



Join Plexiglass Components  
With Acrylic Cement

Figure 4-5. Annulus Type Capillary Reservoir Model — Construction Details

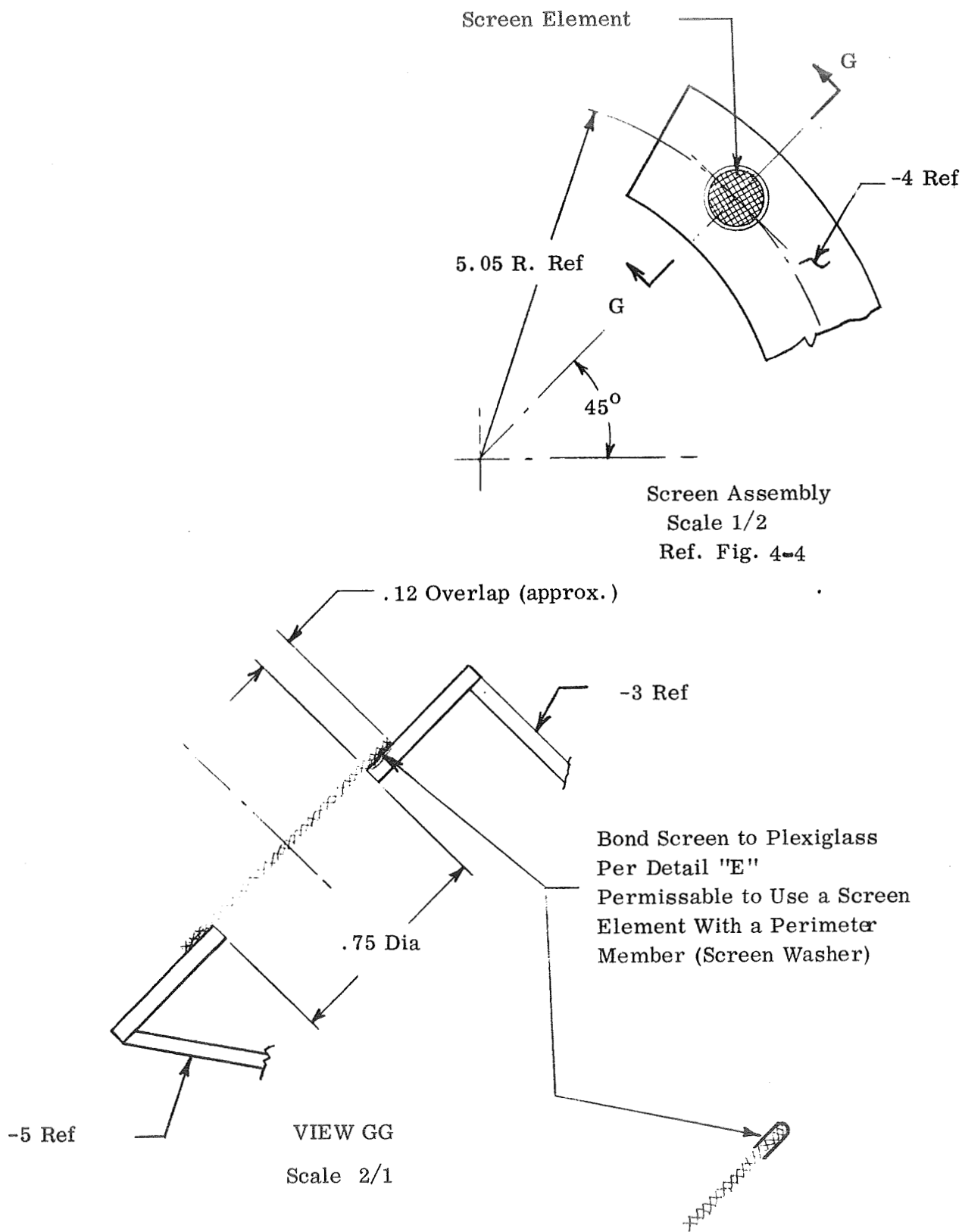


Figure 4-6. Annulus Type Capillary Reservoir Model  
Construction Details

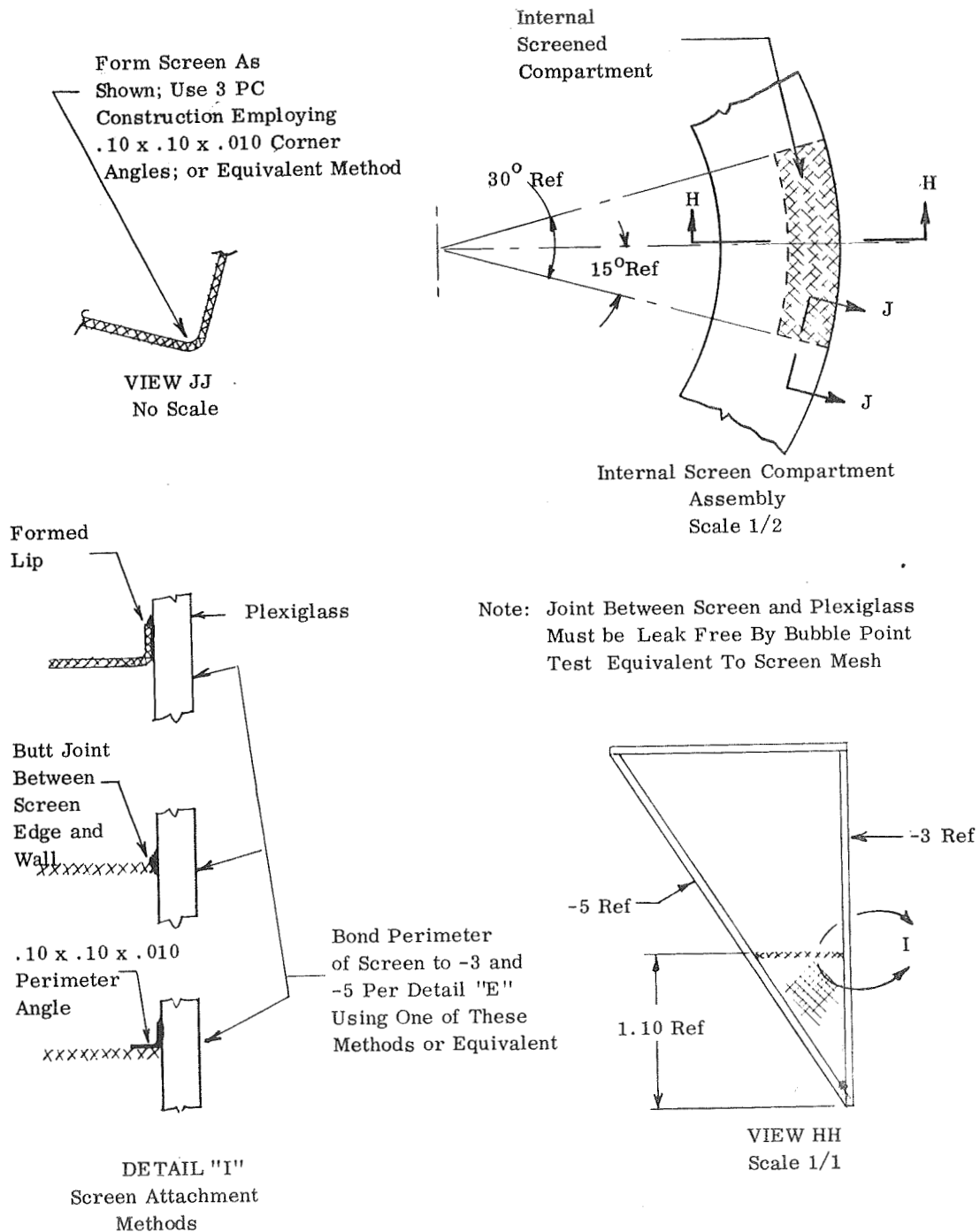
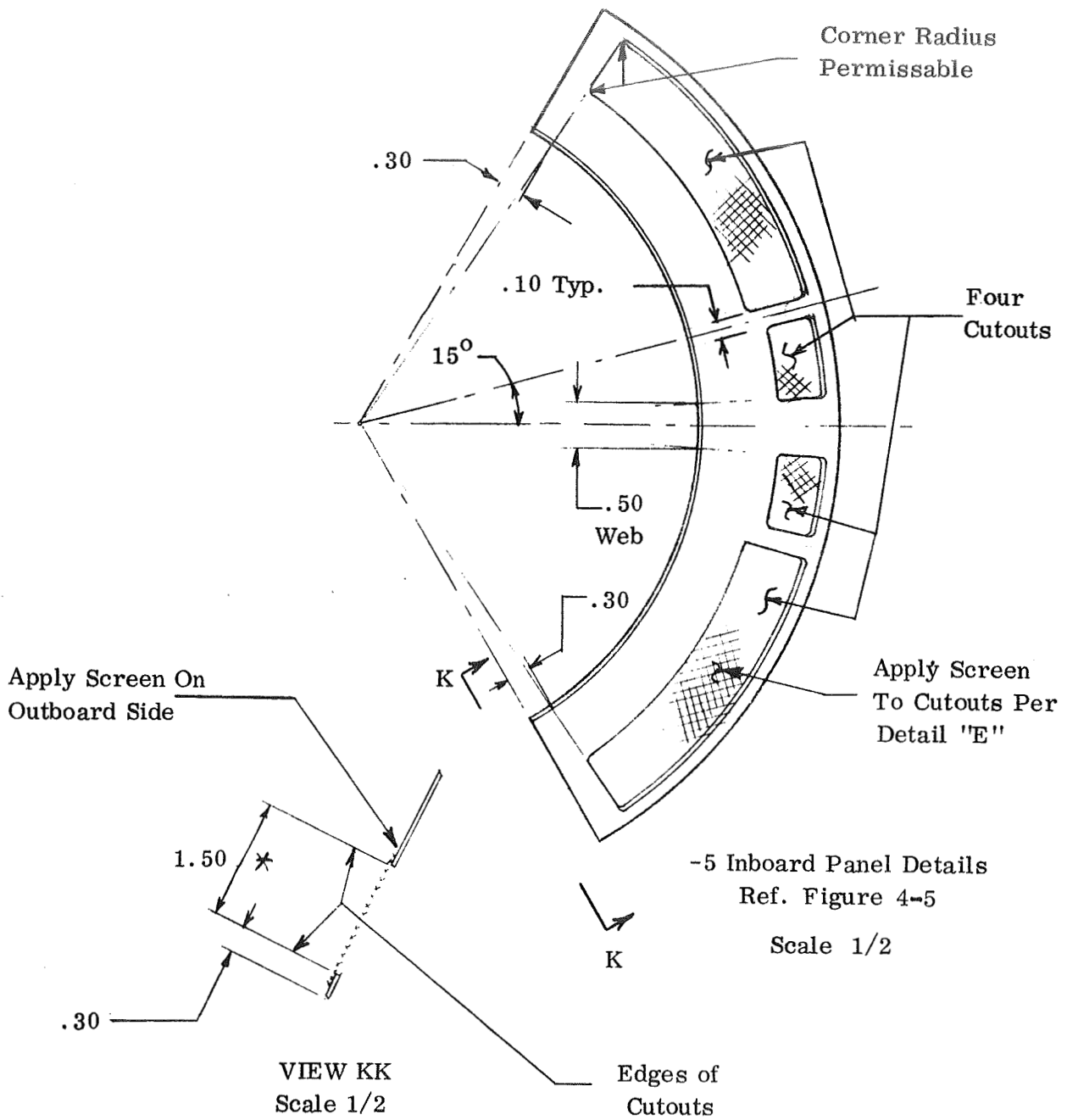


Figure 4-7. Annulus Type Capillary Reservoir Model — Construction Details



\* Reduce to .90 For The Two Small Cutouts

Figure 4-8. Annulus Type Capillary Reservoir Model — Construction Details

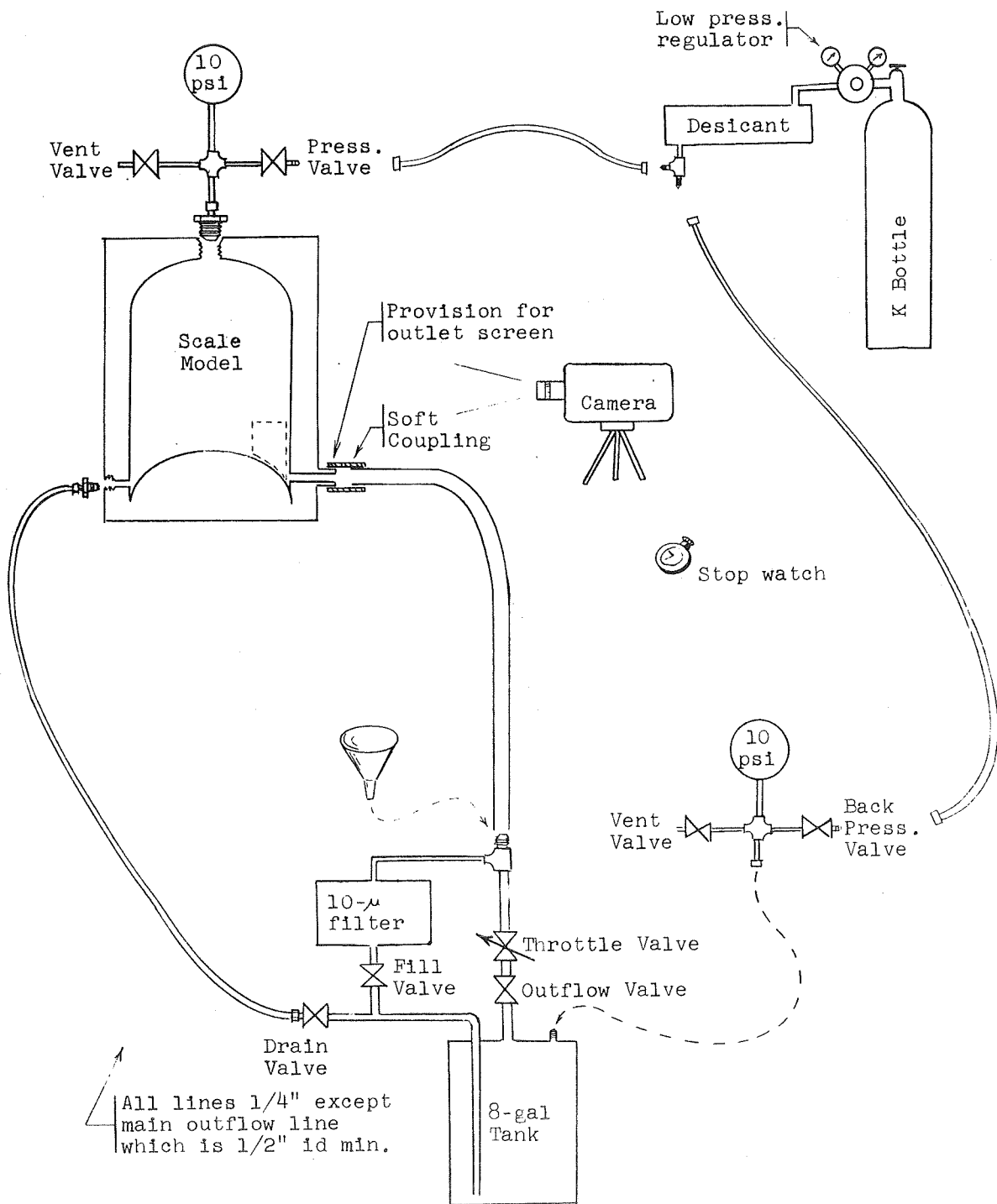


Figure 4-9. Outflow Test Schematic

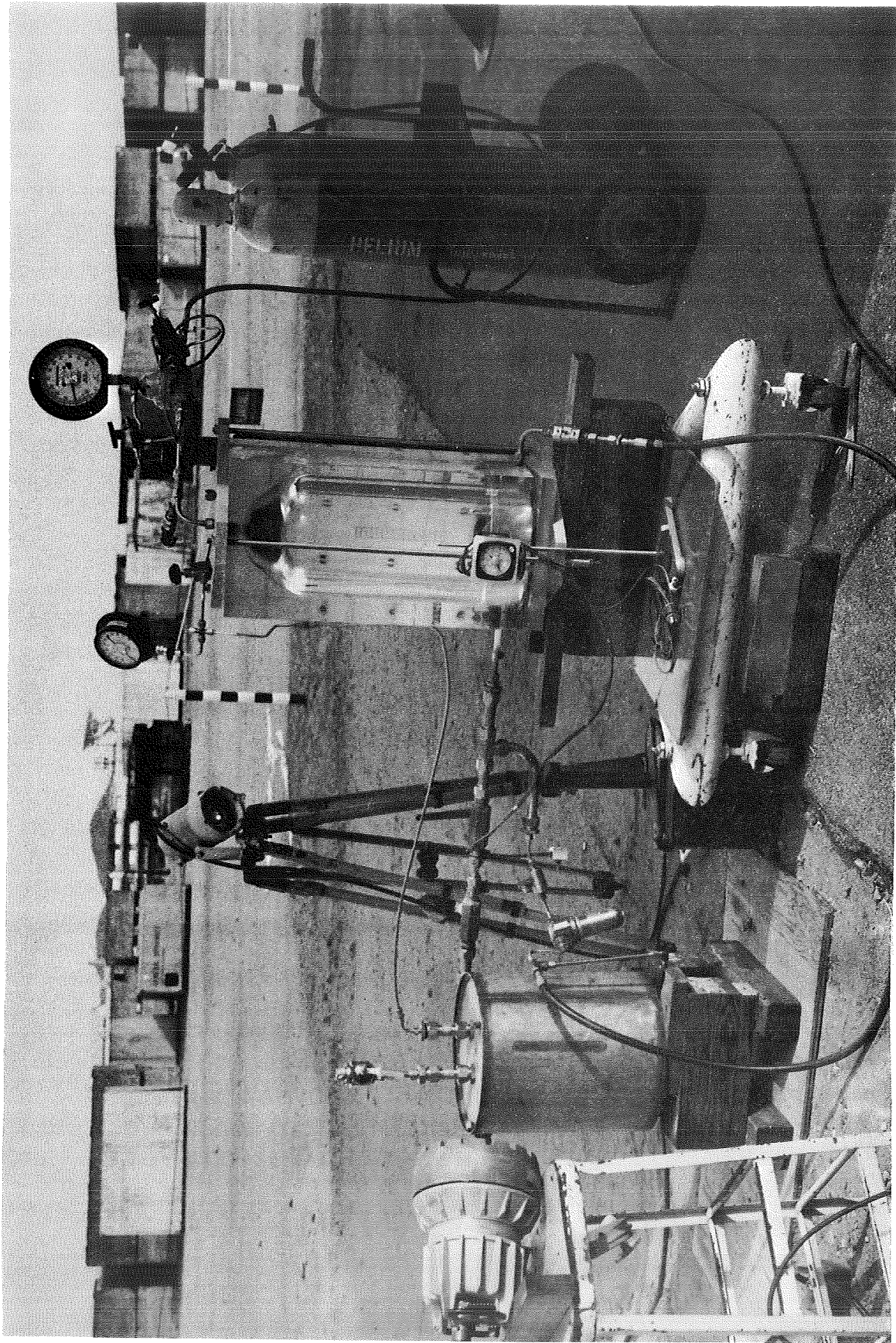


Figure 4-10. Outflow Test Set-up

4.1.4 TEST PROCEDURES. After calibrating the test tank and capillary device by adding measured amounts of water and measuring the height vs. volume, the test tank was hydrostatically tested with water above 75 psig.

All outflow testing was initially run with water and then repeated with pentane. This was done mainly to check out the apparatus and test procedures prior to running with pentane. The runs for both fluids were recorded on film and correlated with INGASP and DREGS2. Runs were repeated for all capillary device tests with the camera viewing the side and front of the tank. Outflow tests without the capillary device installed were run in order to obtain pullthrough correlations for use in the computer models.

For the residual tests the S-IVC scale model tank was filled to approximately the middle of the tank through the capillary device. The filling process was carried out by flowing incrementally, allowing the liquid level inside and outside the devices to equalize before adding additional fluid. When the level went above the capillary device the filling rate was increased and carried out in a continuous manner. This procedure prevented vapor from being trapped in the capillary device during filling. When the tank was filled to the required level, the test tank vent valve was closed, the fill line valves were closed, and the catch tank vent valve was opened. The pressure regulator and flow throttle valve were set to desired levels and the motion picture camera and timer were prepared for start-up. The head of liquid was small compared to the relatively uniform gauge pressures used for each run; thus, the flow rate was constant once the initial start transient period was past. Flow rates were measured visually using the volume calibration. The initial start transient was measured at each gauge pressure setting used in order to determine the flow rate transient during the spilling and vapor ingestion tests. For the residual tests the tank was drained until vapor pullthrough occurred.

For the spilling tests the tank was filled above the capillary device and then the tank fluid was drained from a drain line in the bottom of the tank, leaving the tank empty and the capillary device full. Because of the smaller volume flowing during these tests, the camera speed was increased substantially over the residual tests. The outflow procedure was then similar to the residual tests.

#### 4.1.5 TEST EVALUATION

##### Pullthrough Correlations

Outflow tests for the S-IVC model with no capillary device were evaluated. The objective of the tests, run with water and pentane, were to evaluate vapor pullthrough during the draining under realistic outflow conditions.

One equation for predicting pullthrough is

$$\frac{Q^2}{gh_c^5} = 6.5 \quad (4-1)$$

where  $Q$  is the outflow rate,  $h_c$  is the height of the interface at the tank wall when vapor enters the tank outlet, and  $g$  is the gravity. This equation applies when  $h_c \gg r$ , where  $r$  is the outlet radius.

The other equation for determining  $h_c$ , when  $r \gg h_c$  is

$$\frac{Q^2}{r^2 gh_c^3} = 11.8 \quad (4-2)$$

Neither of these equations is valid when  $h_c \sim r$ , as anticipated in many vehicle draining applications. For example, for the S-IVC mission LH<sub>2</sub> draining, equation 4-1 predicts  $h_c/r = 2.3$  while equation 4-2 predicts  $h_c/r = 2.9$ . Since  $h_c \gg r$  usually implies  $h_c > 10r$ , neither equation applies to this case. More significant differences in  $h_c$  can be obtained than indicated by this example, as illustrated by the graphical representation of the two equations in Figure 4-11. Data points obtained for the S-IVC scale model tests indicate that the case of  $h_c \sim r$  falls between the two equations. The trend of the data, at high  $h_c$  is to approach equation 4-1 while at low  $h_c$  the data should approach equation 4-2. This is, in fact, the case, indicating the data can be used to predict pullthrough when  $h_c \sim r$ , in the low surface force regime.

Empirical correlations were developed from S-IVC data for surface height at pullthrough and interface shape at pullthrough. Data from Figure 4-11 yielded a correlation for pullthrough height for both water and pentane data. This equation is  $Q^2/gh_c \alpha r_o^\beta = C$ , where  $Q$  is the volume flow rate,  $g$  the gravity level,  $h_c$  is the height of the surface at the tank wall at inception of pullthrough, and  $r_o$  is the outlet radius.  $\alpha$ ,  $\beta$  and  $C$  are empirical factors defined by,  $\alpha = 3 + (h_c/r)^{1/10}$ ,  $\alpha \leq 5$ ,  $\beta = 2 - (h_c/r_o)^{1/10}$ ,  $\beta \geq 0$ , and  $C = 11.8 - 2.65 (h_c/r)^{1/10}$ . This correlation is designed for  $h_c \sim r$  and to also agree with equation 4-1 for  $h_c \gg r$  and equation 4-2 for  $h_c \ll r$ . Interestingly, there is divergence between water and pentane data which is proportional to the fluid density. Since this is not predicted by theory, the equation shown here represents a fit of both sets of data without including the density correction. This equation was then used to correlate spilling and residual tests.

Interface shape was plotted for each of the S-IVC outflow test runs in the form of  $y/h_c$  vs.  $r/r_o$  where  $h_c$  and  $r_o$  are as previously defined and  $y$  and  $r$  are the coordinates of the interface. An empirical equation which provided a good fit of the data is given by:  $y/h_c = (r/r_o)^{1.37} - 0.56$  for both water and pentane tests. This information is useful in retarding pullthrough with screens and baffles.

- (1) LINE IS BASED ON  $Q^2/(gh_c^5) = 6.5$ , for  $r = .25'' \therefore Q = 1.51 (h_c/r)^{5/2}$   
 (2) LINE IS BASED ON  $Q^2/(r^2 gh^3) = 11.8$ , for  $r = .25'' \therefore Q = 2.11 (h_c/r)^{3/2}$   
 ▲ SIVC MODEL PENTANE TEST (NO CAPILLARY DEVICE)  
 □ SIVC MODEL WATER TEST (NO CAPILLARY DEVICE)

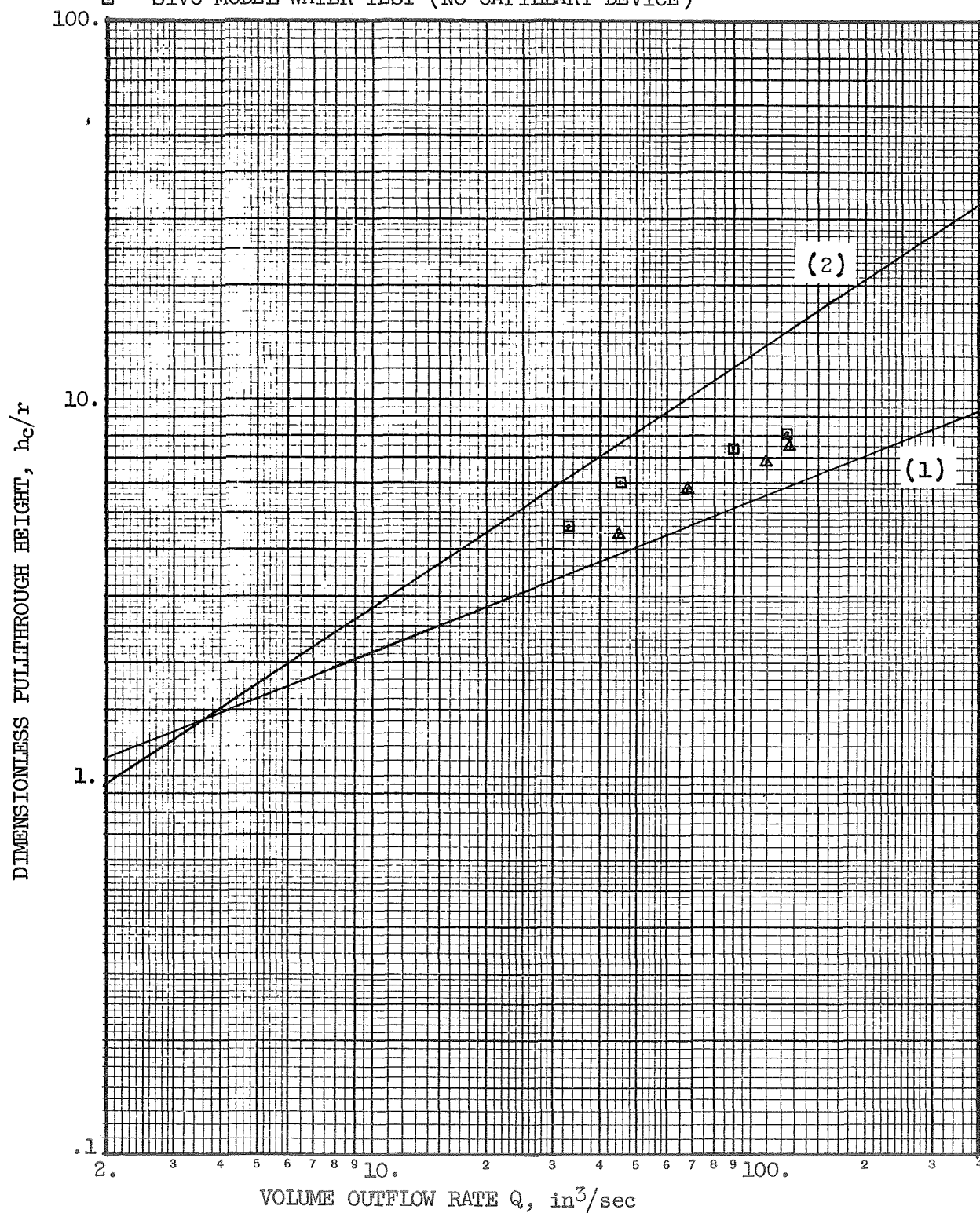


Figure 4-11. Vapor Pullthrough Correlations

## Spilling and Vapor Ingestion Tests

Some difficulties were initially encountered in evaluating these tests because the bubble point of the side screen exceeded that of the top screen. This was not expected because Western Filter, the capillary device fabricator, had been instructed to make the top standpipe screen have a lower bubble point than the side screen. This would have caused vapor to initially break through the top screen rather than the side screen as evidenced in the water checkout tests. The screens were replaced prior to pentane testing which apparently alleviated this bubble point problem as evidenced by the visual data from the pentane tests. This replacement of screens was made after the silicone adhesive used for the water tests was attacked by the pentane test fluid during initial spilling runs. A more compatible adhesive was used with the new  $200 \times 600$  screens for the remainder of the pentane tests. Realizing the difference between the relative bubble points of the top and side screen for the water and pentane tests run, allowed the test results to be more clearly understood. Using flow rates from the initial start transients of the residual tests, empirical pullthrough correlations previously cited, and test model geometry and fluid properties, the computer model was run and correlated with the test data. The computer model predicted the time from start of outflow to vapor pullthrough within 10% of test results for the three pentane test runs. These runs are correlated in Figure 4-12. Flow rate profiles are shown in Figure 4-13. The low rate runs were modelled as initially having spilling from the capillary device with vapor ingestion occurring when the liquid level dropped below the side screen. Increased top screen pressure drop in the highest flow case prevented the initial spilling. This was substantially corroborated with visual observation.

The preliminary checkout runs with water were adversely affected by the bubble point problem. Vapor entered the capillary device at the point of highest bubble point which was apparently directly opposite the outlet. This allowed vapor to directly enter the tank outlet causing liquid to be drained slowly from the start basket.

## Residual Tests

The DREG2 program was used to correlate the scale model S-IVC residual tests. Results of both water and pentane tests were compared with the program predictions on the basis of the time between the liquid level inside and outside the tank being at the top of the capillary device and the occurrence of vapor pullthrough at the outlet. The agreement was within 10% for the pentane test runs. Agreement was slightly worse for the water tests. This correlation is shown graphically in Figure 4-14. The differences between the test data and model were believed to be due to visual inaccuracies in reading the test films rather than any problem with the computer model. With the water tests the additional bubble point problem, mentioned in the previous paragraphs, accounts for the increased divergence between test and theory. On the basis of this test data correlation, the DREGS2 program was used to analyze S-IVC  $LO_2$  and  $LH_2$  capillary device draining presented in Section 2.2.

TIME FROM START OF OUTFLOW TO VAPOR PULLTHROUGH, seconds

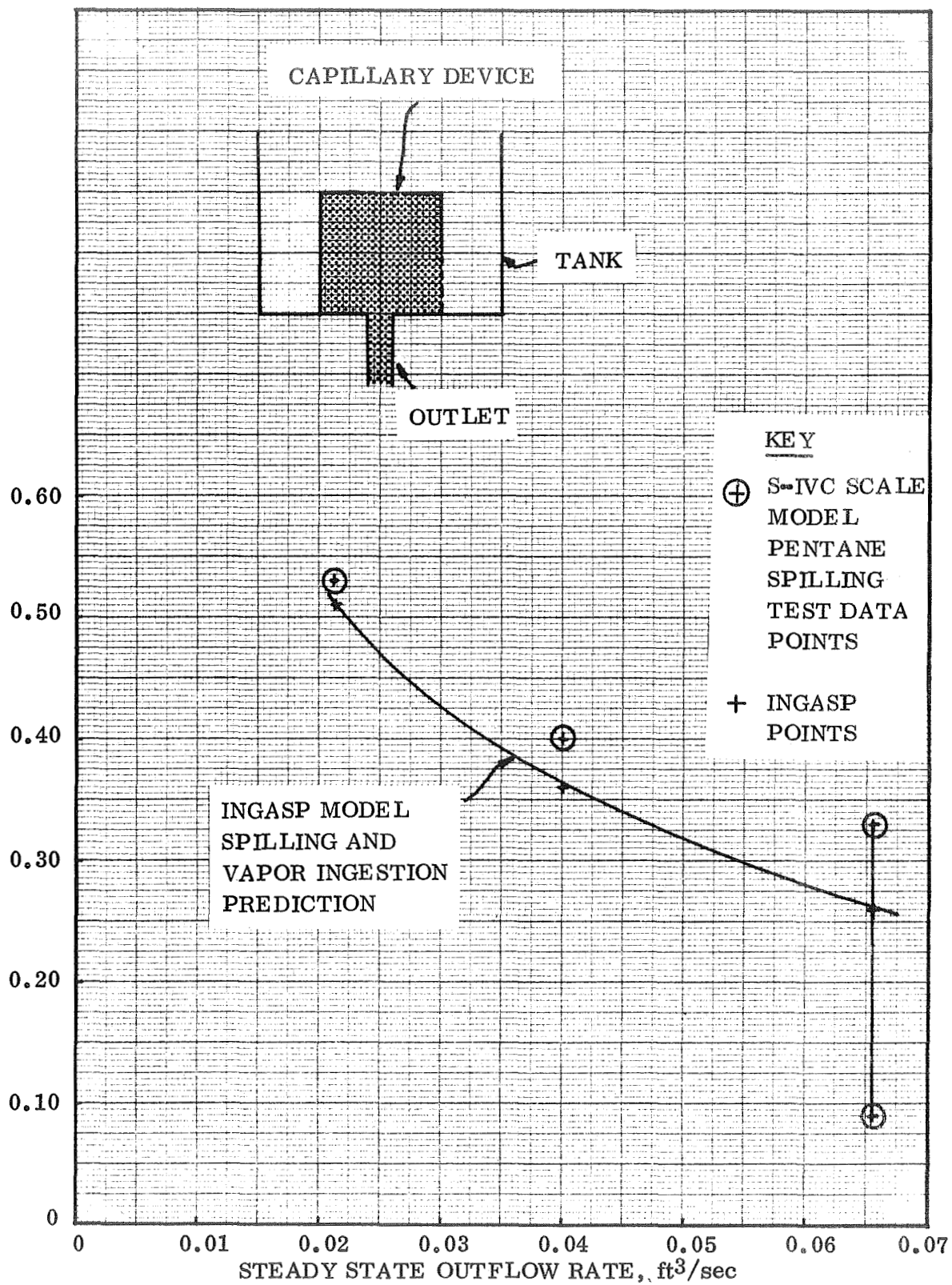


Figure 4-12. S-IVC Scale Model Spilling Tests

GAUGE PRESSURE (PSIG)	STEADY STATE FLOW RATE (FT <sup>3</sup> /SEC)
5	.0225
13	.0400
35	.0655

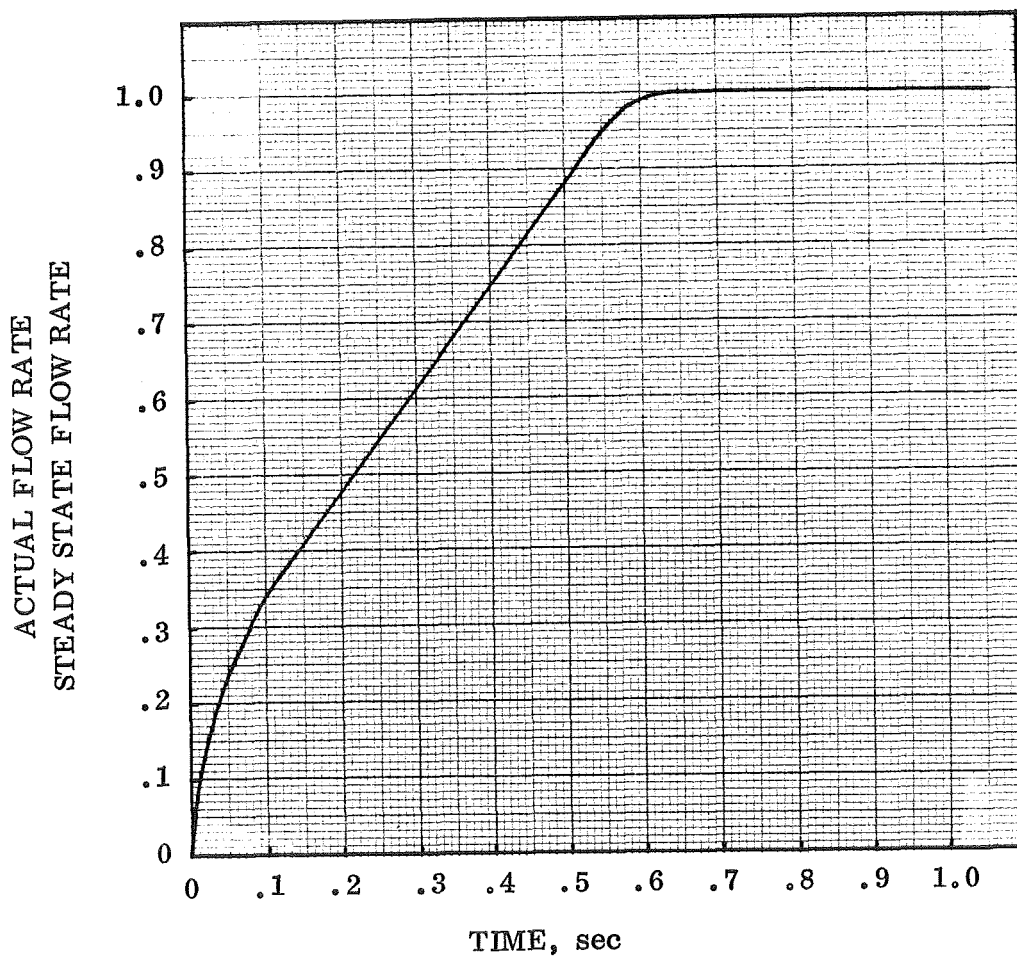


Figure 4-13. Transient Flow Rates — Pentane Spilling and Vapor Ingestion Tests

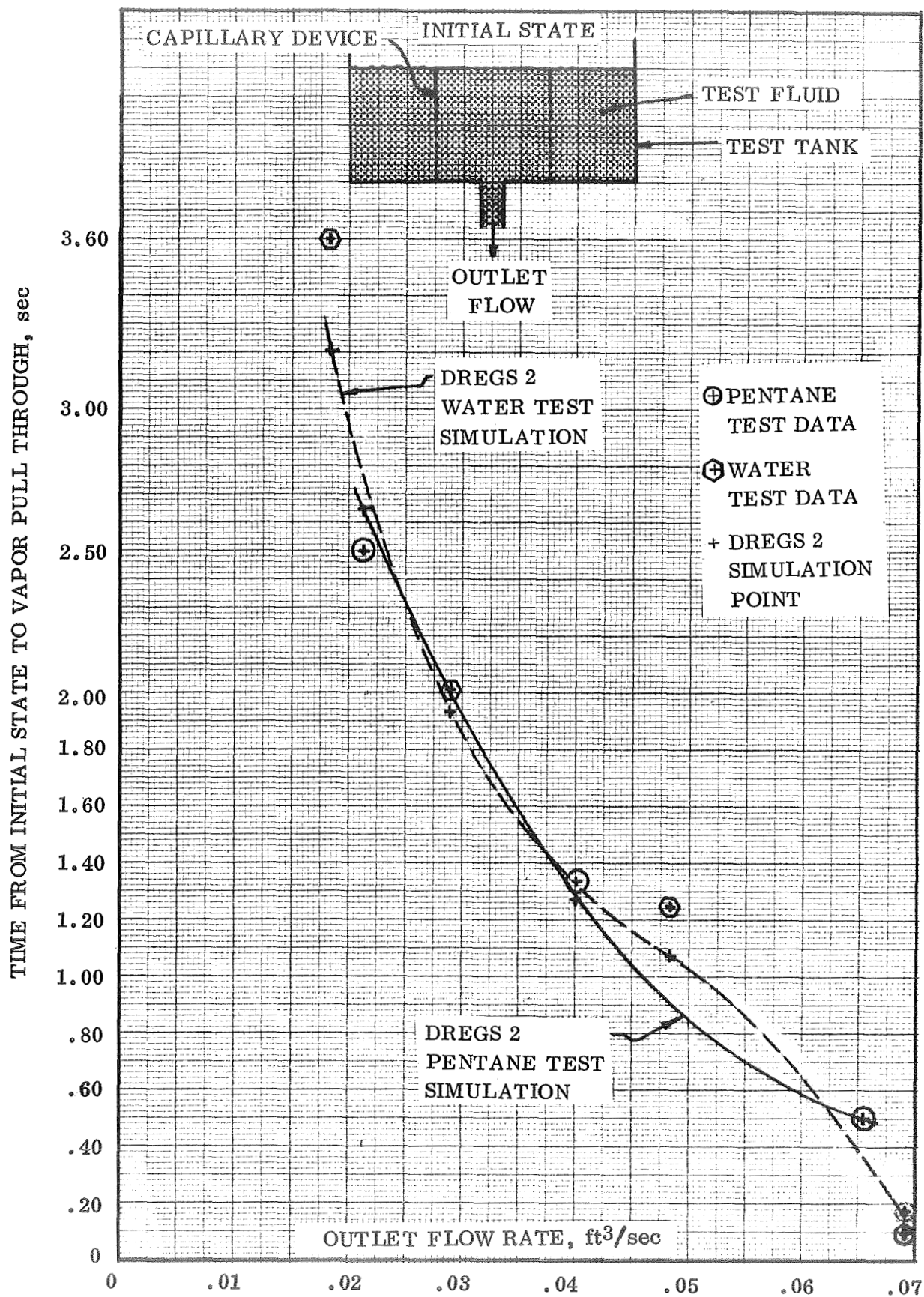


Figure 4-14. S-IVC Scale Model Residual Test Correlation

## Pullthrough Suppression Tests

A simple series of tests were designed to assess the feasibility of using screens to suppress pullthrough in a draining tank. The tests were performed using water and freon and dutch twill and square weave screens in a cylindrical tank with a centered outlet. Tests illustrated that screens can reduce pullthrough height by greater than 60%.

### Theory

The surface tension retention pressure of a screen may be used to resist vapor pullthrough as explained in Section 2.2. This retentive capability coupled with the straightening of the flow due to the presence of the screen should reduce pullthrough height substantially.

4.1.6 EXPERIMENT DESIGN. Tests were designed to examine several combinations of fluids and screens for evaluating pullthrough suppression. The plexiglass test tank shown in Figure 4-15 was designed so that screens could be stretched across the

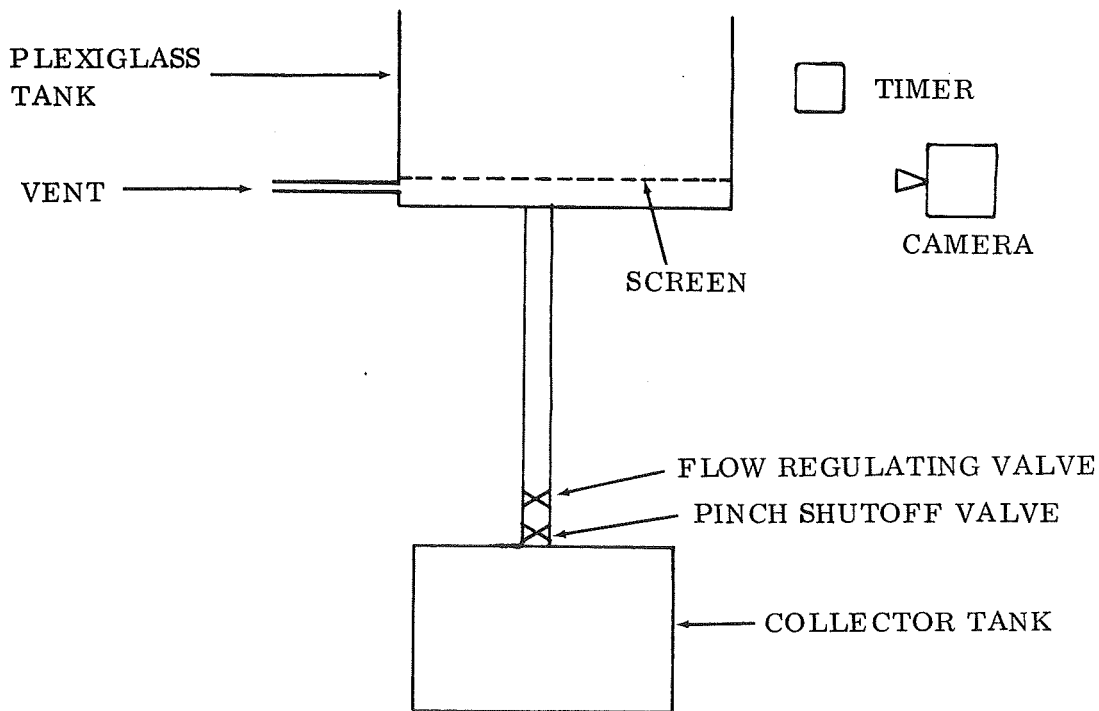


Figure 4-15. Cylindrical Outflow Test Schematic

bottom of the tank and sealed with gaskets. The gasket thickness was adjusted to vary the height of the screen above the outlet. Flow rates were varied from run to run by adjusting a valve at the collector tank, shown schematically in Figure 4-15. Flow rates and heights at pullthrough were measured from high speed motion pictures of the tests.

4.1.7 TEST PROCEDURE. The test tank was filled from the top using a stainless steel bucket containing distilled water or Freon TF. The vent was used to remove vapor which was trapped underneath the screen, however, some vapor remained at the start of a run. This vapor did not affect test results since it was expelled through the outlet well before the free surface approached the screen. The liquid in the tank was allowed to set until the rotational vortex induced by filling the tank had subsided. The regulating valve was then set and the shutoff valve opened with the motion picture camera and timer turned on. The camera was shut off after vapor entered the outlet from the free surface.

Runs were made initially with  $400 \times 400$  mesh screen to check out the apparatus. Runs were then made with water with no screen,  $165 \times 1400$  screen, and  $200 \times 1400$  screen. Subsequent freon runs were also made with no screen,  $165 \times 1400$  screen and  $200 \times 1400$  screen. The  $200 \times 1400$  screen height was then adjusted to lower positions including the lowest point, with no gasket, and runs were made with water and Freon.

#### Test Evaluation

Cylindrical outflow tests were evaluated, with and without screens for both water and Freon. Pullthrough was experienced at  $h_c$  as high as .60 inches with both water and Freon TF. Several screens, including  $165 \times 1400$  and  $200 \times 1400$  were placed at heights varying from .23 to .30 inches above the outlet. At flowrates similar to those run without a screen, no pullthrough was visually observable above the screen with either screen in place using either fluid. This is consistent with calculations made using screen pressure drop correlations and interface shape during draining based on equation 4-2.

4.1.8 CONCLUSIONS AND RECOMMENDATIONS. It appears that the analysis suggested in Section 2.2 can be used to size screen baffles for resisting pullthrough. Since screens serve as flow baffles in retarding vapor motion in a manner similar to an unperforated baffle, it is suggested that the additional attribute of reducing velocity gradients in the flow will allow capillary barriers to reduce pullthrough more than solid baffles. It is recommended that additional testing be accomplished to compare the performance of baffles of screens in obtaining minimum pullthrough heights.

## 4.2 WICKING TESTS

4.2.1 INTRODUCTION. Fluid wicking along a screen is an important phenomenon in maintaining liquid at a screen when the screen is subjected to heating and consequent evaporation. Evaporation may eventually dry out the screen, causing a loss of retention capability and hydrodynamic failure of a capillary device. Wicking from a pool of liquid outside the capillary device, as in a channel collector configuration, is useful in replenishing liquid evaporated from the surface of the capillary device without causing vapor to form within the capillary device.

4.2.2 SUMMARY. Wicking tests to simulate zero gravity wicking were designed to provide wicking rates for screens subjected to heating. The experimental method was dependent upon a thermal analysis of the wicking apparatus to determine the portion of heat applied from calibrated heaters which went into evaporating the test fluid. The evaporation rate was used to compute wicking velocities which were compared with the results of equations 2-1, 2-2, and 2-3 and the results of screen flow pressure drop testing carried out in the transverse direction. Wicking data was also obtained by visual inspection of the advancing liquid front in the screen as a function of time.

Wicking in horizontal dutch twill screens can be characterized by the equation

$$\Delta P_{\sigma} = \frac{A_{\omega} \mu V_w L}{D_a^2 g_c} = \frac{4 \sigma}{D_{BP}} \quad (4-3)$$

$$V_W = \frac{4 (D_a^2 g_c \sigma)}{A_{\omega} \mu L D_{BP}}$$

where  $A_{\omega}$  is a dimensionless constant determined by the test data. The value of  $A_{\omega}$  is dependent upon the wicking direction with respect to the orientation of the warp and shute wires. Wicking was not evidenced in the square weave screens tested.

4.2.3 EXPERIMENTAL METHOD. The wicking models which appeared promising were discussed in Section 2.4. The wicking apparatus is shown schematically in Figures 4-16, 4-17, 4-18, and 4-19. A photograph of the apparatus is shown in Figure 4-20.

The screen was kept in a horizontal position by means of the screws and clamps located on top of the fluid reservoir. The horizontal attitude of the screen was verified with a transit periodically during the running of each screen specimen.

Liquid was maintained at the top of the reservoir by a burette which dripped fluid into the reservoir. The atmosphere within the test enclosure was maintained saturated with pentane by wetting a blotter covering the bottom of the enclosure prior to testing and by using nitrogen gas saturated with pentane in a bubble chamber to maintain a slight positive pressure within the enclosure. This saturated nitrogen was allowed to exit through a small hole in the top of the enclosure. The nitrogen atmosphere was used to reduce any possible fire hazards presented by the evaporation of the pentane test fluid.

For the wicking runs with the heater in operation, the liquid was allowed to wick up the screen and under the plexiglass plate which minimized convection heat transfer to the heaters. A guard heater was employed at a similar temperature to the main heater to minimize side heat losses at the screen. The screen was soft soldered to the copper heaters using a special fixture to minimize wicking of the solder along the

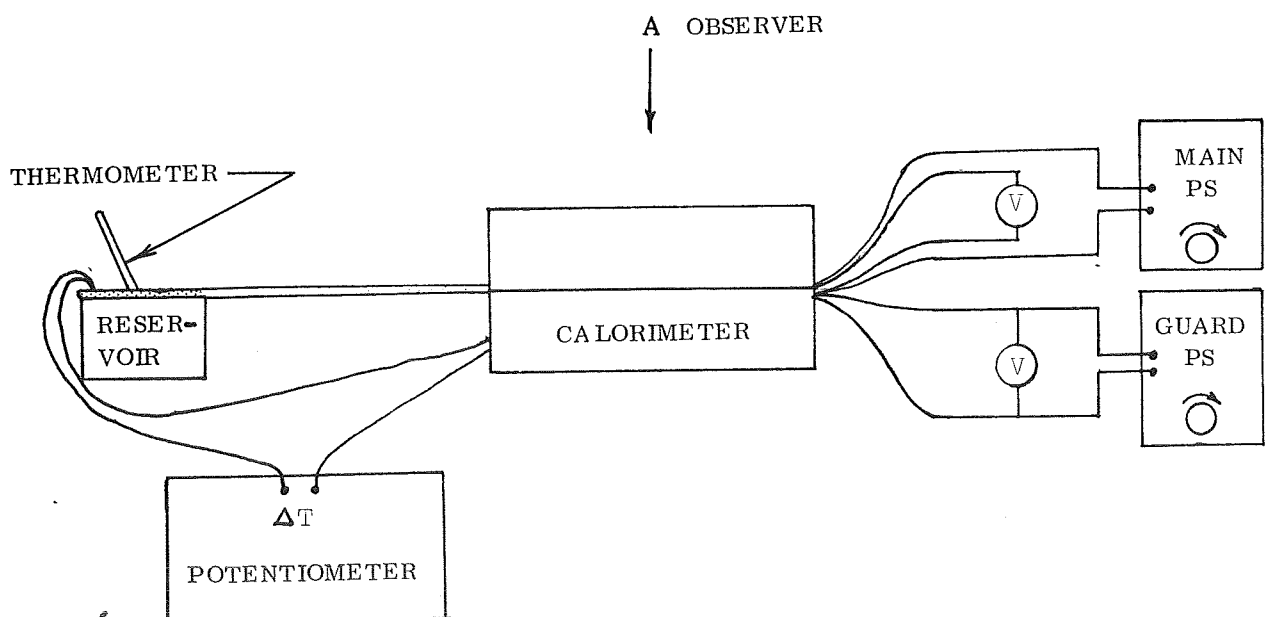
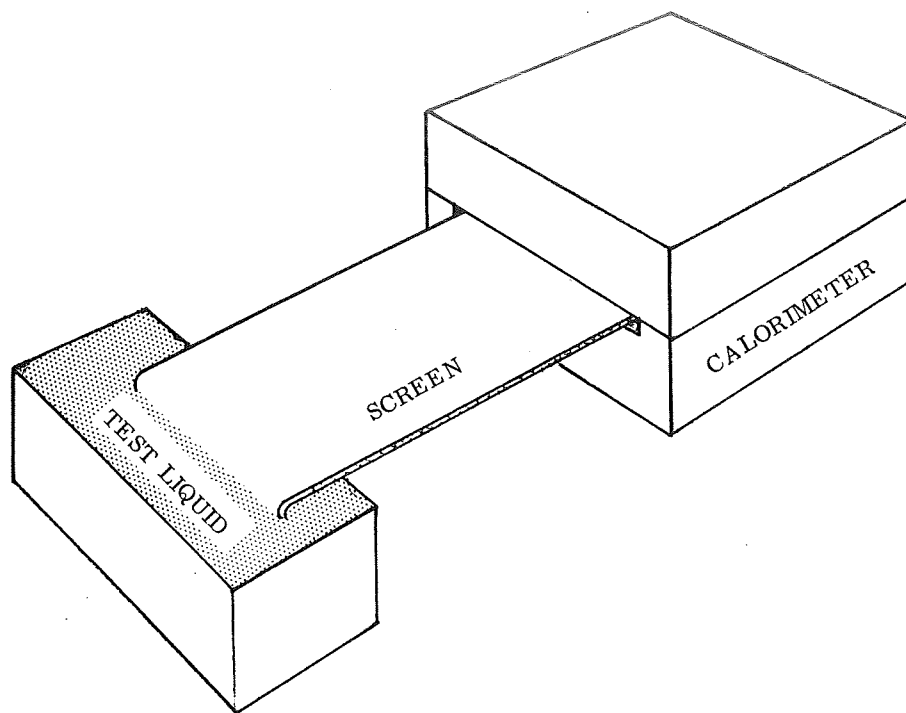


Figure 4-16. Wicking Test Set-up

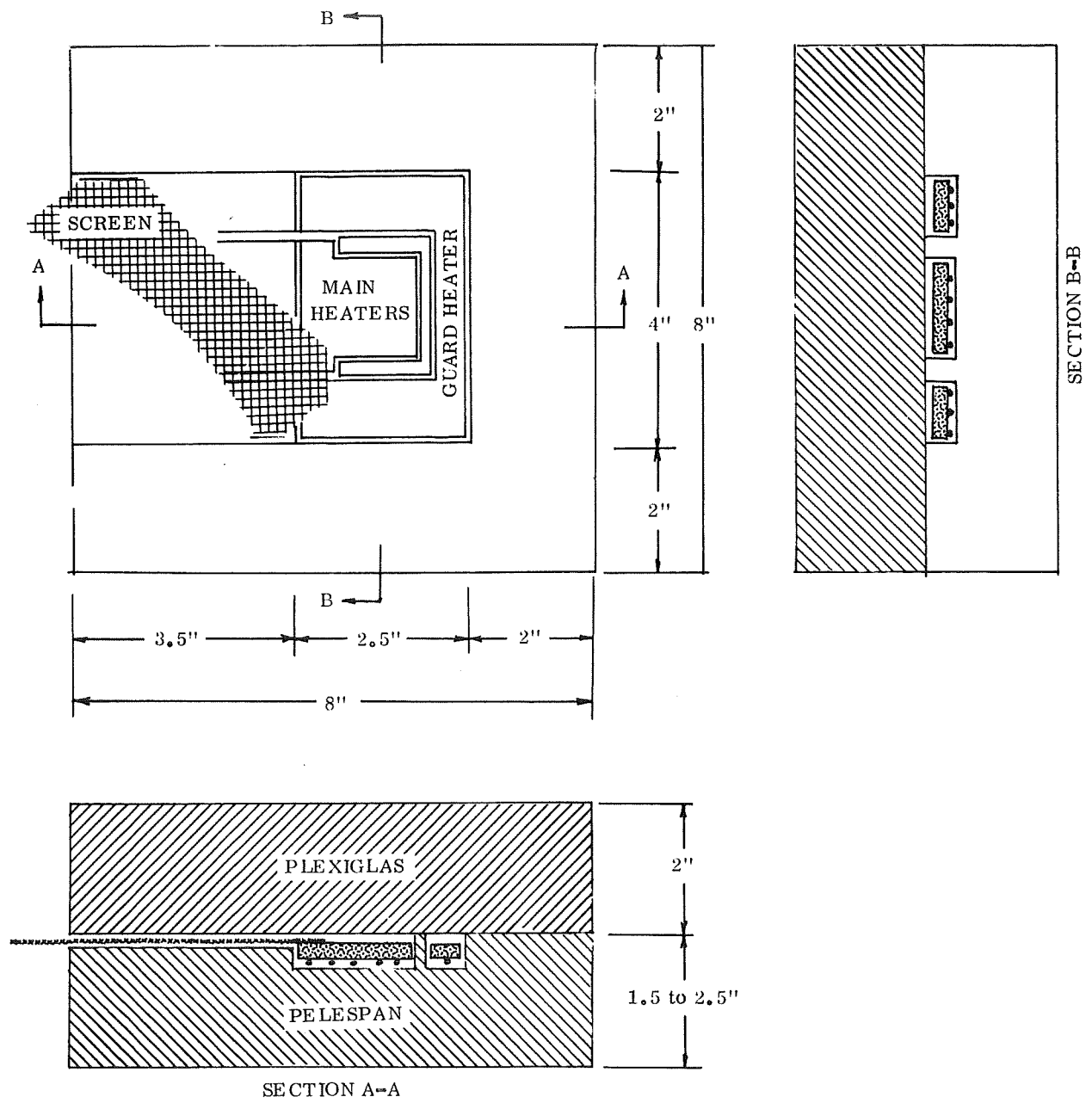
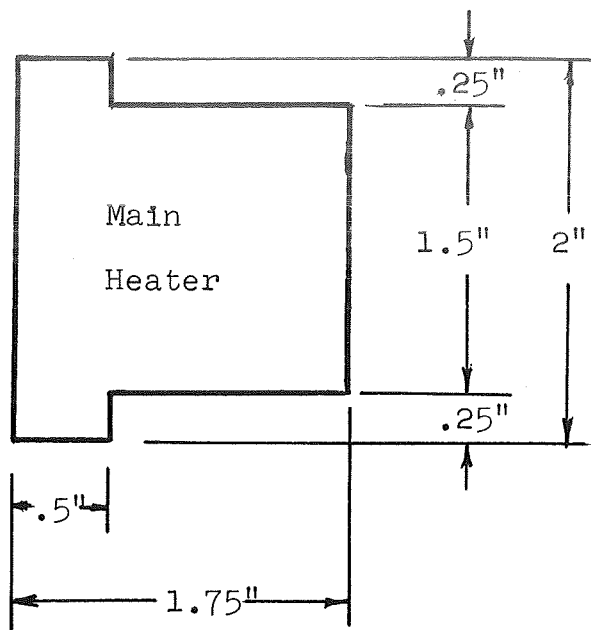
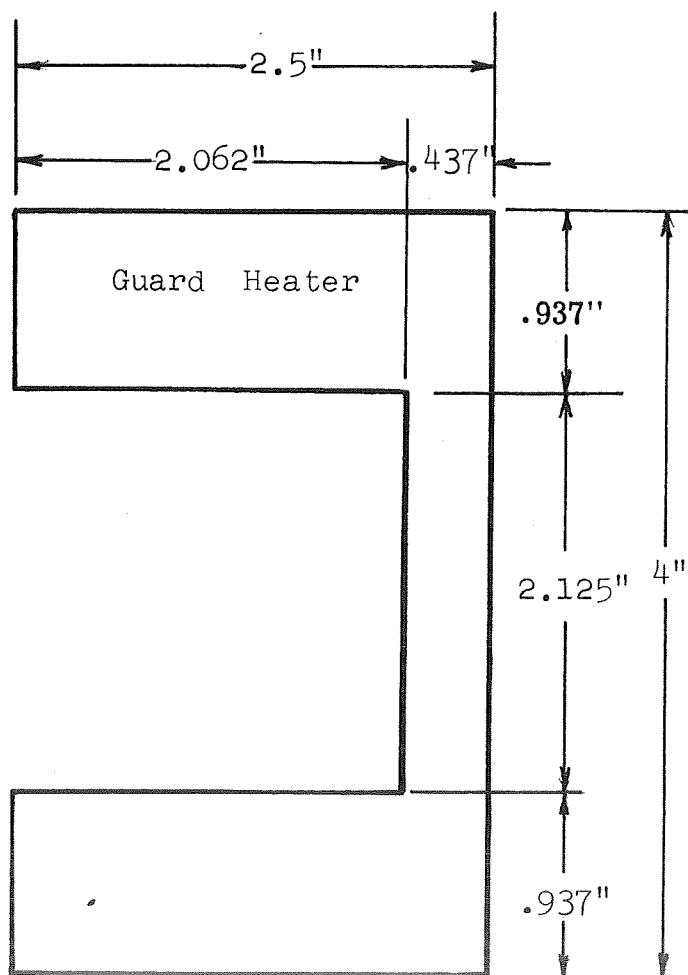


Figure 4-17. Wicking Test Calorimeter Assembly



Material: 0.25" copper



(full scale)

Figure 4-18. Wicking Test Heater Detail

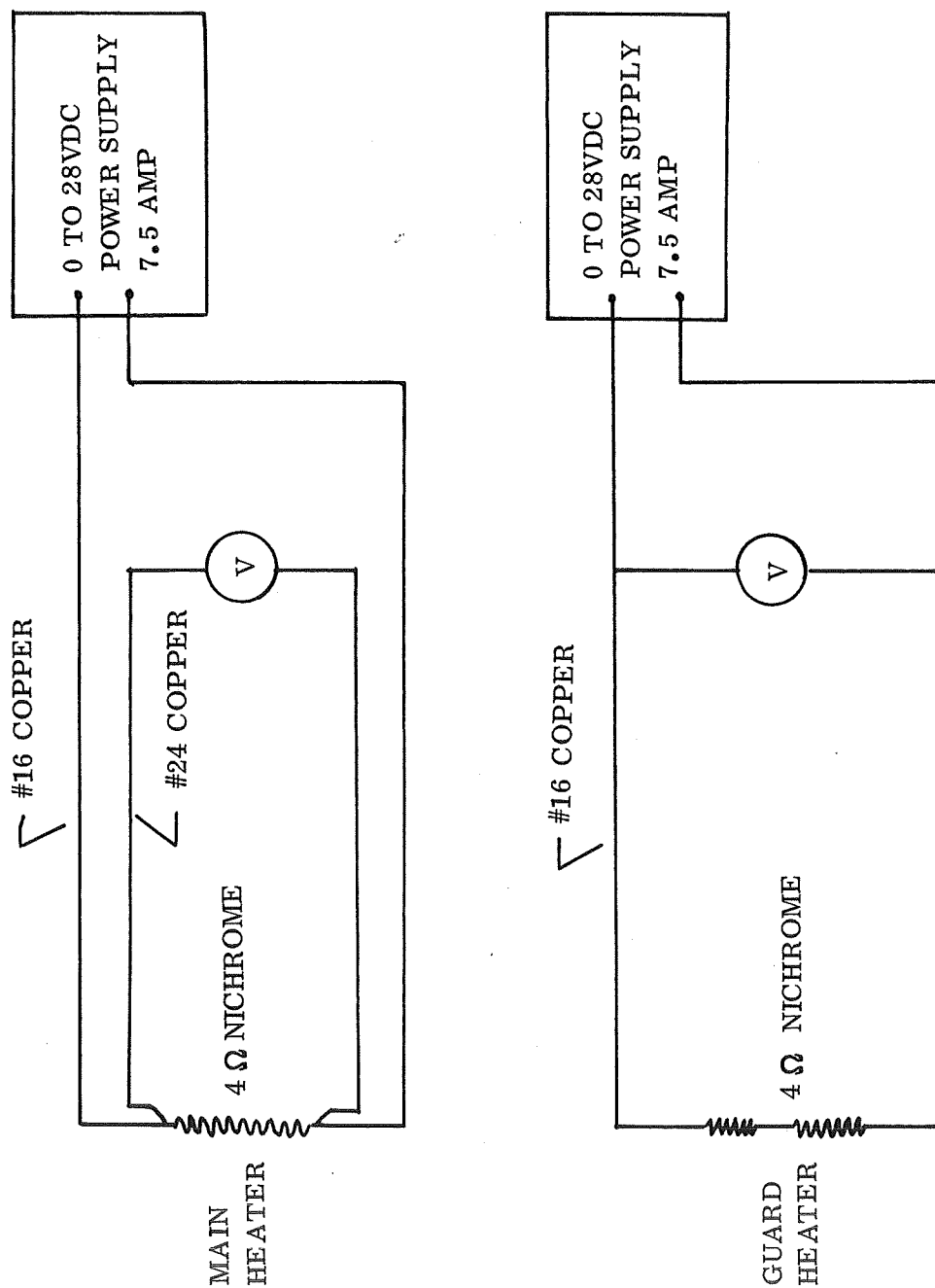


Figure 4-19. Electrical Schematic - Wicking Test

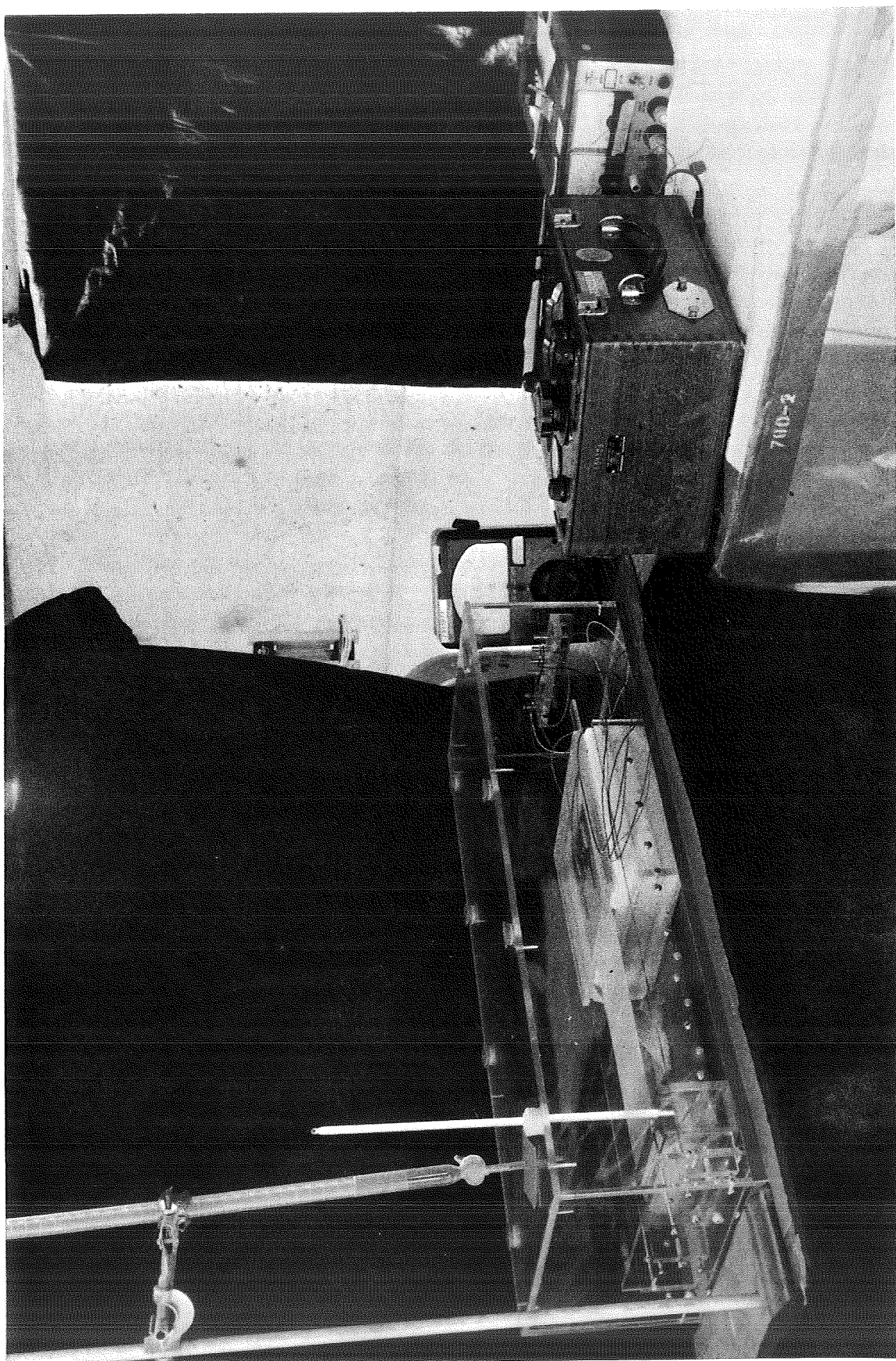


Figure 4-20. Wicking Test Apparatus

screen. The nonporous base of the calorimeter was a carved sandwich of pelespan foam which had thermocouple wires transmitted between the bond layers. The power to each heater was delivered across a nichrome wire of calibrated fixed resistance. The main heater voltage was monitored with separate potential leads to determine power delivered to the apparatus.

With the liquid at the screen-heater interface the power to the heater was slowly increased in steps allowing steady state conditions to occur between increments. When the liquid receded slightly from the screen heater interface and then remained as a stationary front, the evaporation rate was just balancing the wicking rate. This procedure was repeated to higher heater powers, however, heat losses became excessive when the liquid vapor interface moved more than a few tenths of an inch away from the heater.

Several runs were made by observing liquid flow, without heating, and recording distance travelled vs. time. These results were plotted and then graphically differentiated to obtain wicking velocity as a function of distance traveled from the reservoir.

The screen meshes used for testing with flow parallel to the warp wires were  $400 \times 400$ ,  $40 \times 40$ ,  $200 \times 600$ ,  $165 \times 1400$ ,  $80 \times 700$ , and  $30 \times 250$ . Pentane flow was perpendicular to the warp wires using silicone oil and  $30 \times 250$  screen. Visual tests were run with the  $30 \times 250$  screen samples because heater power was insufficient to evaporate wicking flow for these runs.

4.2.4 EVALUATION OF DATA. For the tests using the heater to evaporate the wicking fluid, wicking rates were determined in the following manner:

$$V_W = \frac{\dot{Q}_S}{(\Delta h + h_{fg})(\rho LA)} \quad (4-4)$$

where

$A = \phi \omega t$

$\omega$  = the width of the screen

$t$  = the thickness

$\phi$  = the porosity

$L = 2$  inches

$\Delta h$  = enthalpy difference between test fluid at ambient and screen-heater interface temperatures, BTU/lb<sub>m</sub>

$h_{fg}$  = heat of vaporization of test fluid at screen-heater interface temperature, BTU/lb<sub>m</sub>

$\phi$  and  $t$  are given in Table 2-5, Ref. 4-1

$\dot{Q}_S$ , the heat input to the screen must be determined by evaluating radiation, conduction and convection losses from the heater and screen.

The temperature of the pentane nitrogen environment,  $T_i$ , is the lowest temperature of the screen and is the temperature of the surrounding environment. Assuming that the average temperature of the screen is  $\frac{T_h + T_i}{2}$

$$\dot{Q}_R = \sigma \epsilon_s A_s \left[ \left( \frac{T_h + T_i}{2} \right)^4 - T_i^4 \right] + \sigma \epsilon_h A_h (T_h^4 - T_i^4)$$

is the radiant heat loss from the screen where s and h are subscripts denoting screen and heat respectively.

Conduction losses were considered between the heaters, through the phenolic strip, between the heaters through the foam, between the heater and the bottom of the foam, between the heater and the top of the plexiglass, and through the instrumentation wires.

These conduction effects are summoned  $Q_C = KA \Delta T$ . Convection between the screen and plexiglass is assumed to be negligible.

$$\dot{Q}_S = \dot{Q}_h - \dot{Q}_R - \dot{Q}_C$$

where  $\dot{Q}_h$  = the heat input to the heater = EI.

$V_W$  was then computed for each test point run.

**4.2.5 INTERPRETATION OF RESULTS.** Data was plotted in the form of velocity,  $V_W$ , vs. distance for each screen as shown typical for a  $30 \times 250$  screen in Figure 4-21. As can be seen, the analytical models and the screen flow test data vary widely from the test results. The difference in analytical models and data is expected when considering the similar deviation between the models and the screen flow data as explained in Reference 4-2, Section 2.1. Screen flow test data does not agree with wicking data because the screen flow data is for flow normal to the screen. The flow parallel to the screen is more restrictive than the flow normal to the screen. The equation which best represents the viscous nature of the flow is equation 4-3. For wicking parallel to the shute wires, values of  $A_w$  are presented below.

<u>Screen Mesh</u>	<u><math>A_w</math></u>
200 × 600	368
165 × 1400	580
80 × 700	6230
30 × 250	1120

For wicking parallel to the warp wires  $A_w$  was found to be 755 for the  $30 \times 250$  screen tested with Dow Corning 200 Silicone Oil. Tests indicated that, in the meshes commercially available (including  $400 \times 400$  mesh), square weave screens do not wick.

**4.2.6 CONCLUSIONS.** Wicking is a relatively low flow rate phenomena even in zero gravity, however, for relatively low heat flux conditions wicking flow can effectively be utilized to prevent screen drying and vapor formation. Replacement of evaporated fluid can be calculated by inverting equation 4-4 to solve for  $\dot{Q}_s$ .

- 1 —————  $f = \alpha/Re + \beta$ ,  $\alpha = 2.49$ ,  $\beta = .3$
- 2 - - - - - Armour and Cannon  $D_B$ ,  $\alpha = 8.61$ ,  $\beta = .52$
- 3 - - - - - Simplified Capillary Model
- 4 - - - - - Armour and Cannon,  $D_A$ ,  $\alpha = 8.61$ ,  $\beta = .52$
- 5 —○— Wicking Data
- 6 - - - - - Capillary Model Including Drag Terms
- 7 - - - - - Based on  $A_1 = 130$ ,  $A_2 = 12$  From Screen Flow Data

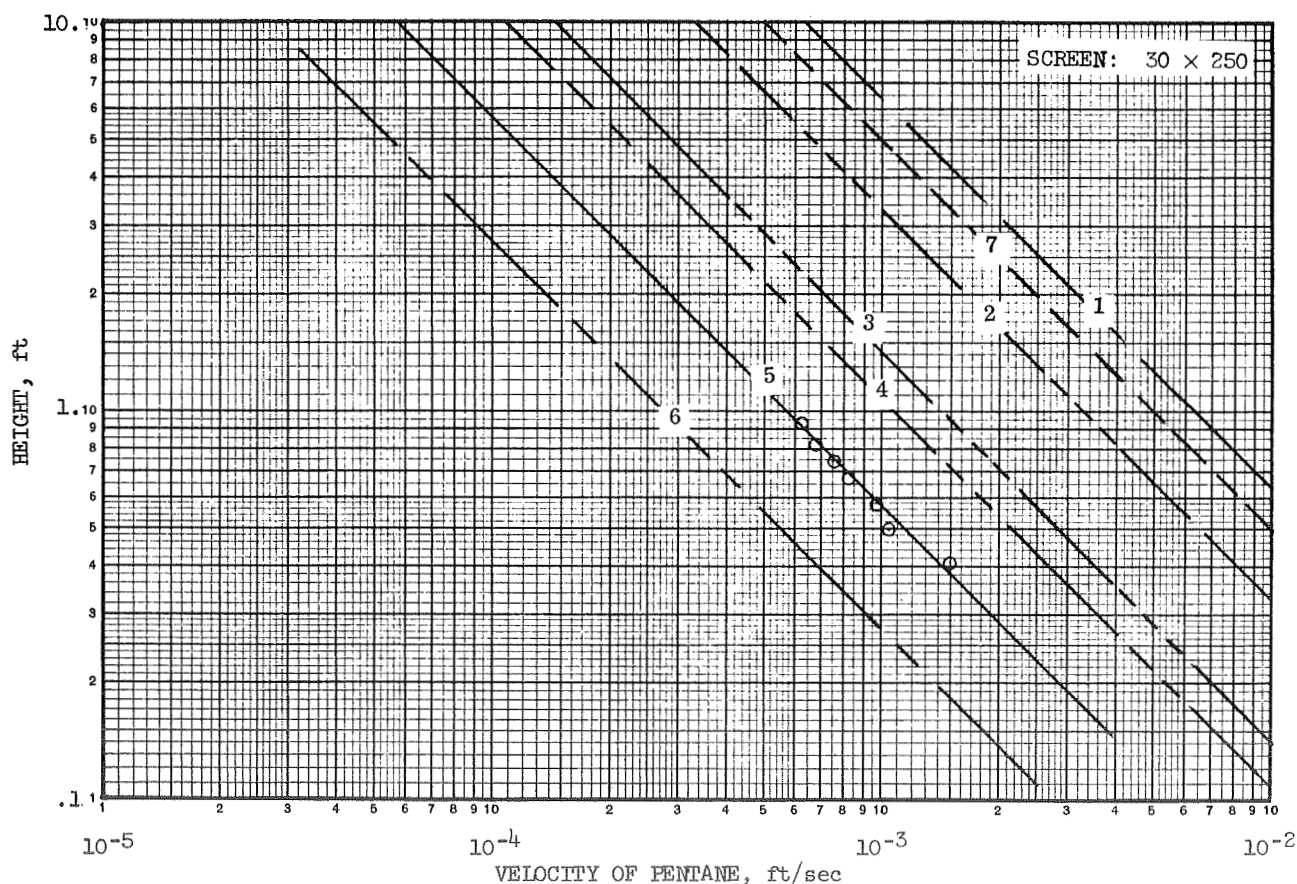


Figure 4-21. Typical Wicking Data With Predictive Models

# 5

## DETAILED DESIGNS

### 5.1 S-IVC FUEL START SYSTEM DESIGN

1. Start Reservoir
2. Collector System
3. Outlet duct accessories.

The basic parameters, ground rules and overall arrangement for the reservoir are shown in Figure 5-1 . The heat exchanger systems for the above area (including interconnections) are shown on the Figure 5-2 schematic. Figure 5-3 and 5-3A schematics are extensions of Figure 5-2 which shows the detail circuitry for the reservoir heat exchanger elements using series and parallel arrangements.

The fuel start basket is a 200 ft<sup>3</sup> annulus type reservoir which is profiled to fit within the envelope generated by the SIVB fuel tank wall and intermediate bulkhead. The complete assembly is a 120° annulus section and includes provisions for interconnecting with the 11-inch fuel tank outlet, an access opening at the outlet area, external capillary screens, heat exchanger coils attached to the exterior surfaces, and a removable internal gas deflector screen.

The reservoir is supported from the SIVB fuel tank wall and is subject to an external pressure on all surfaces; an external loading on the forward surface due to fluid impingement; and forces due to acceleration and vibration. The flat surfaces and the profiles which have large radii are sensitive to pressure gradients and therefore must incorporate a stiffener system. A series of perforated bulkheads (shear panels) interconnected with skins and stiffeners was selected as the basic structural arrangement. Other structural methods are discussed in the oxidizer tanker section. The system is similar to the skin stringer frame designs used in aircraft. A basic stress analysis was conducted for primary members, detailed design drawings created, and a weight breakdown generated. A complete structural investigation is outside the scope of this effort, therefore assumptions were made which would simplify the calculations and give results which are reasonably close to what may be expected from a comprehensive effort.

The heat exchanger coils on the basket surfaces are supplied with fuel from a collector system mounted on the inside wall of the fuel tank. A schematic for the overall system is shown in Figure 5-2 . Additional drawings describing physical plumbing interconnections and relative locations are included.

24.0 DIA ACCESS  
OPENING  
EQUIPPED WITH  
0.70 FT<sup>2</sup> OF  
SCREEN

PERFORATED  
SHEAR PANELS  
SPA. @ 24°

STIFFENER @  
F.S. LOCATED  
BETWEEN  
SHEAR PANELS

SURFACES  
EQUIPPED WITH  
HEAT EXCHANGER  
TUBES

MATERIAL & ALLOWABLES

2219 T62

F<sub>TU</sub> = 54,000

F<sub>TY</sub> = 36,000

1.5 PSI ULT.  
DESIGN PRESSURE  
ON FWD FACE OF  
BASKET  
.125 PSI ULT. FOR  
REMAINING  
SURFACES

STIFFENER  
RINGS

200 FT<sup>3</sup> VOL.  
275 FT<sup>2</sup> SURFACE  
AREA START  
BASKET

S-IVB PROPEL-  
LANT TANK  
MODIFIED WITH  
6" INTERNAL  
INSULATION

VIEW AA

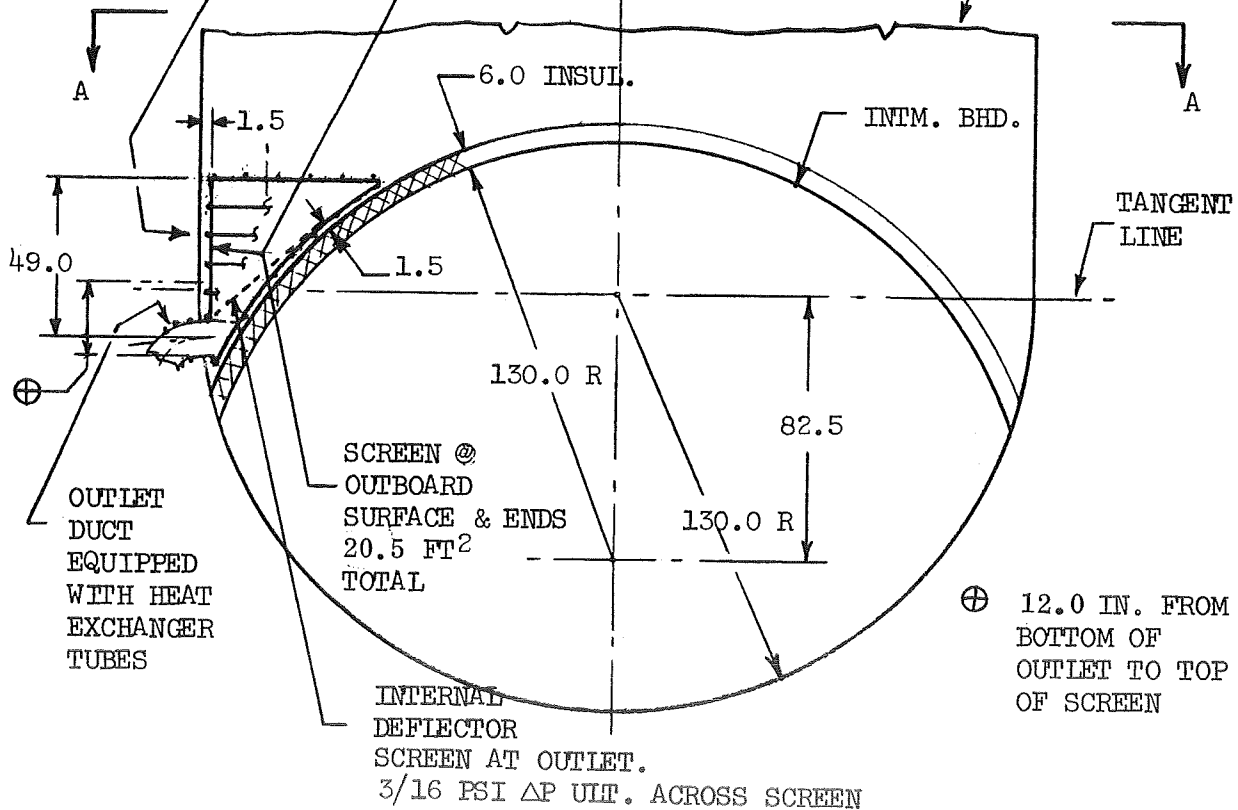


Figure 5-1. Fuel Start Basket General Assembly and Design Ground Rules

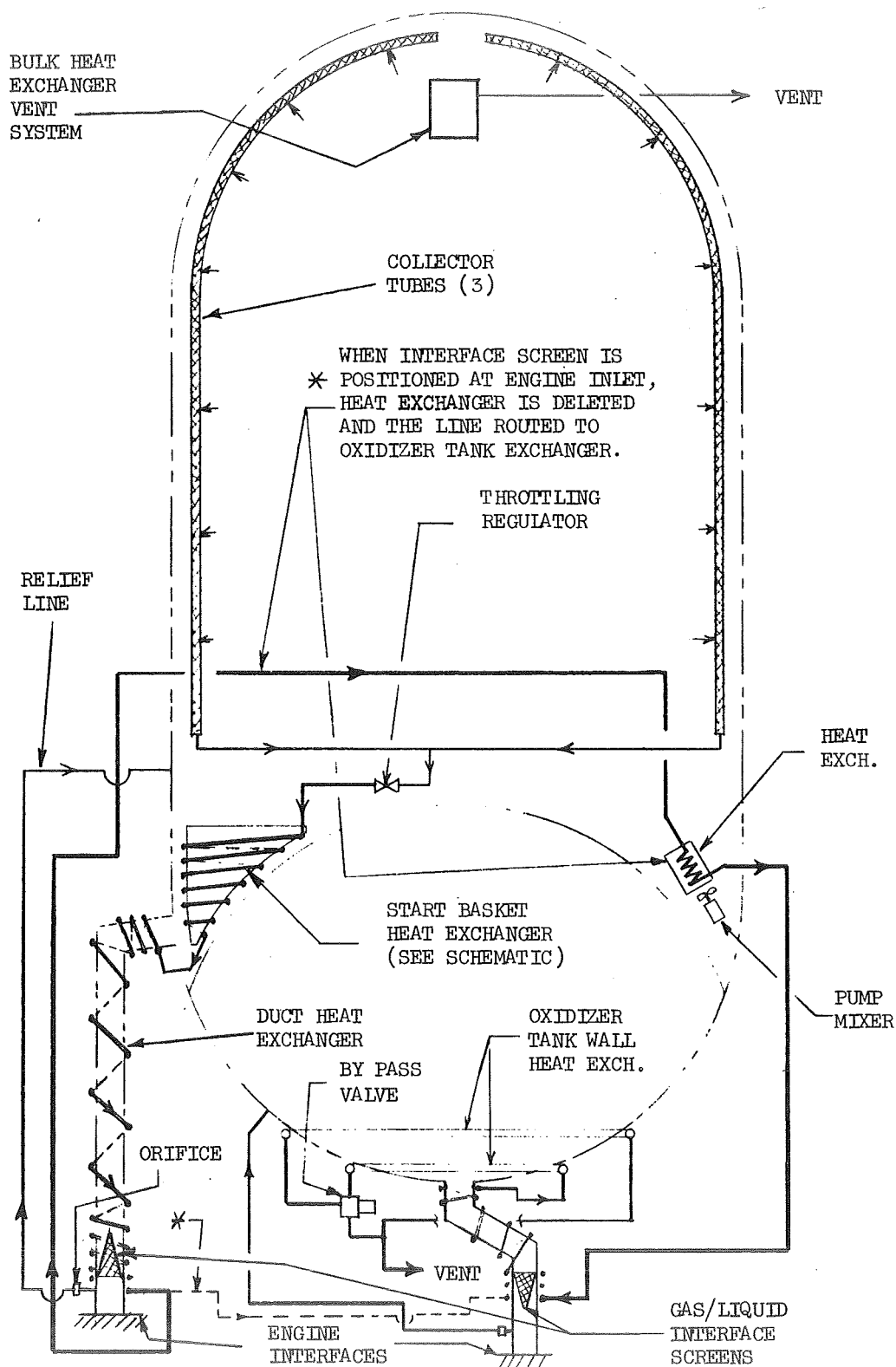


Figure 5-2. Heat Exchanger System Schematic

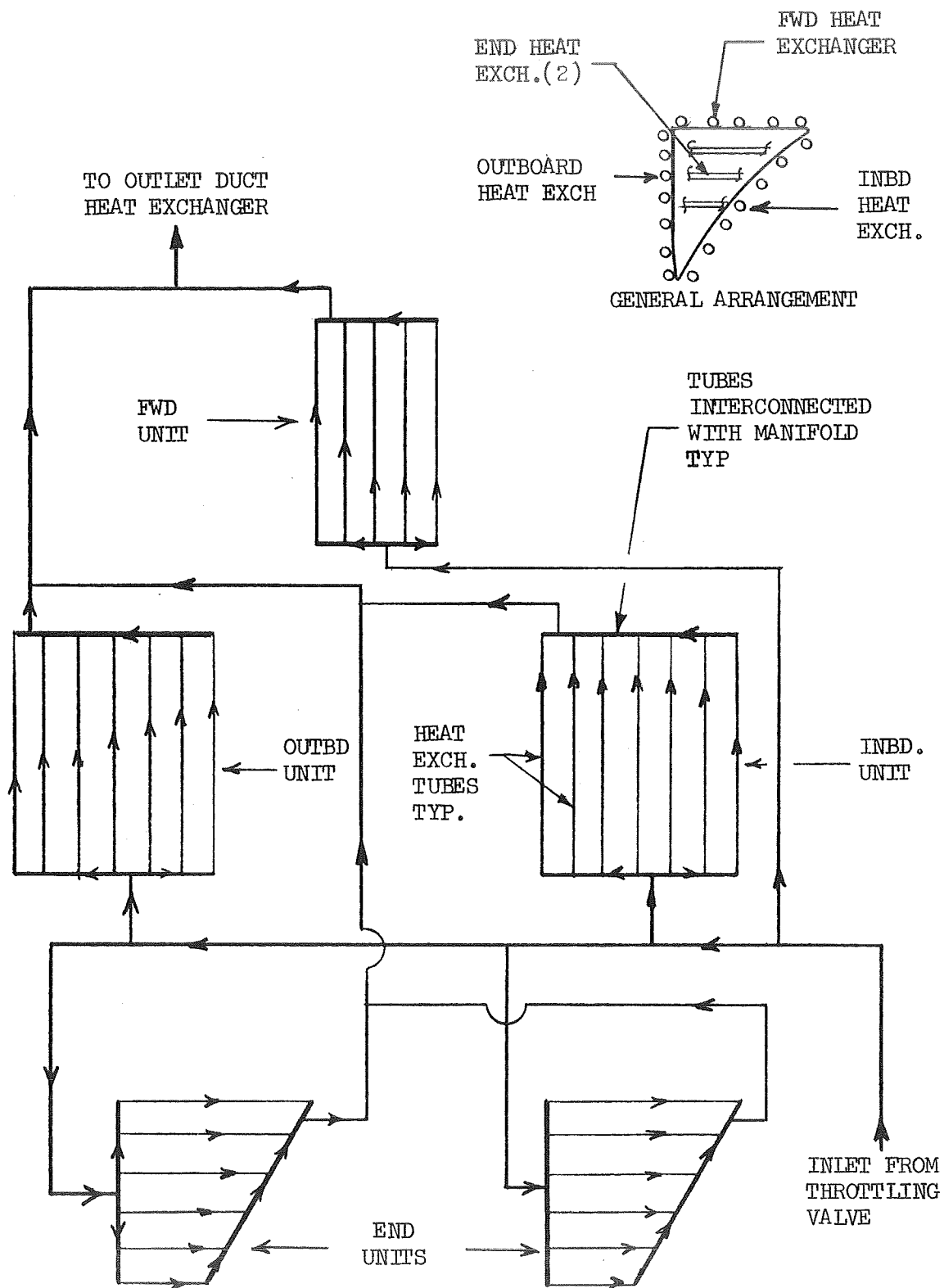


Figure 5-3. Start Reservoir Exchanger System Schematic (Parallel Arrangement).

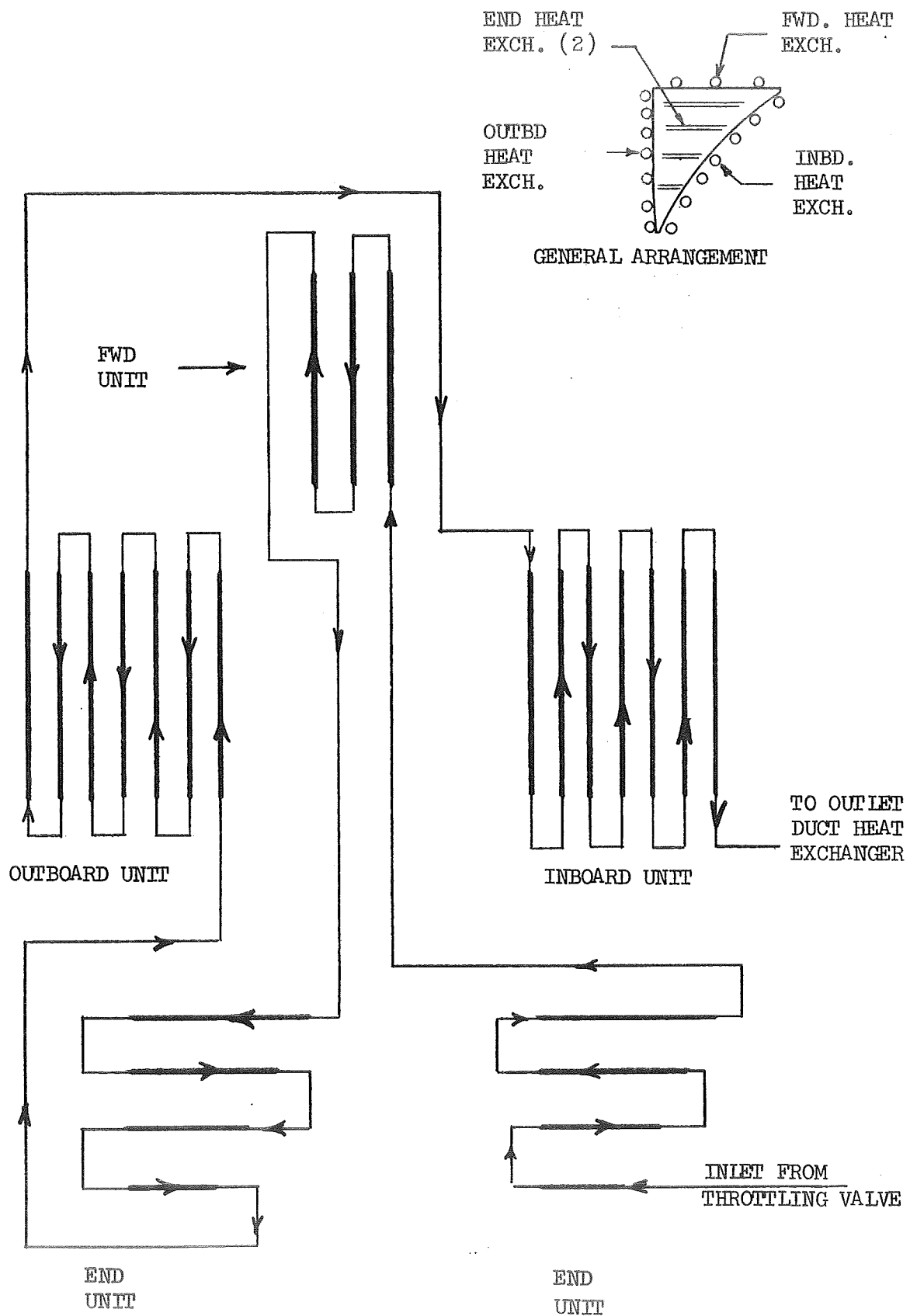


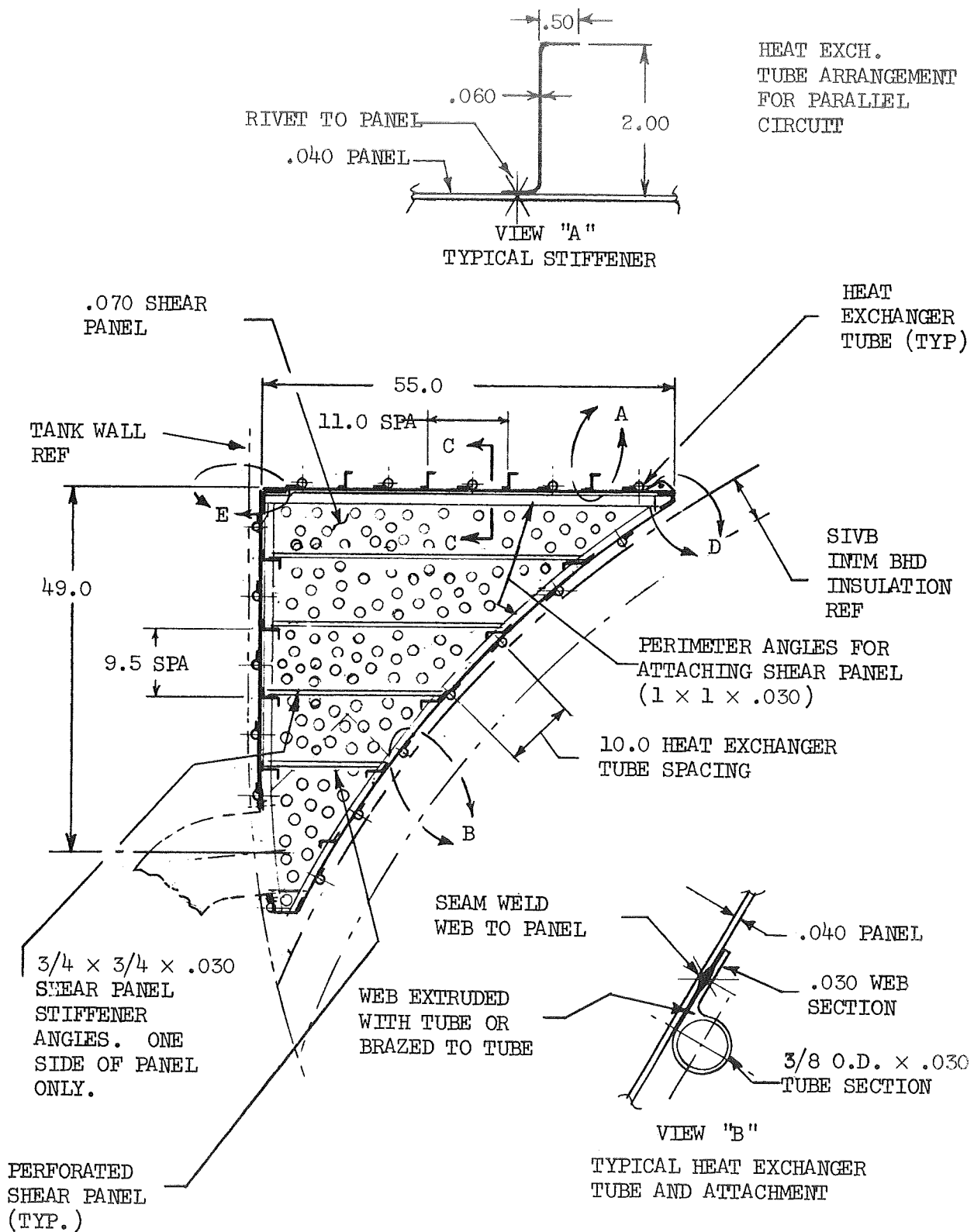
Figure 5-3A. Start Reservoir Heat Exchanger System Schematic (Series Arrangement)

The outlet duct accessories are those items associated with the heat exchangers, gas/liquid interface screen, fittings for assembling the system and a relief circuit for the downstream side of the screen (see Figure 5-1 for schematic). Detail drawings were generated for two gas/liquid interface locations and the advantages and disadvantages of each outlined. A detailed weight analysis for the accessories is included.

**5.1.1 RESERVOIR STRUCTURE** — A typical cross section showing the primary structural components and heat exchanger tubes are outlined in Figure 5-4. Figure 5-4A shows the tube locations for the Figure 5-3A series circuit. The fuel tank outlet elbow is included for identifying the interface problems. The reservoir is subject to external pressures, accelerations, and vibrations and therefore must reflect a framework for resisting the loads separately or in combination. Basically the assembly consists of six flat panel type bulkheads (shear panels) interconnected with stiffener rings and skin sections. "Z" shaped stiffeners are used on all faces. The forward wall of the reservoir is flat and equipped with four 120° circumferential ring sections which are welded or riveted to the panel. Additional radial type stiffeners (one per compartment) are located on the opposite face of the panel for reducing the span of the rings (see Figure 5-1. The forward panel is therefore divided into ten rectangular areas per compartment (50 total). Heat exchanger tubes equipped with webs are located between each "Z" ring which provides additional panel stiffness. The tubes are attached by seam welding the flat strips to the mating surfaces. The design shown in Figure 5-4 assumes that the tube and web are extruded as one unit. An alternate method uses standard tubing which is dip brazed to the strips (see Figure 5-4A).

The compartment formed by the two shear panels at the outlet requires an access opening to permit attaching the reservoir to the SIVB interface and for installing the internal deflector screen. The access hole intersects two stiffeners which must be discontinued at this area and a system of re-enforcement rings and doublers added at the opening. The heat exchanger tubes are locally routed around this zone.

The outboard cylindrical section of the reservoir requires five rings (frame sections) which are located on the inboard side of the skin to prevent interference with the fuel tank wall. Heat exchanger tubes are located on the opposite face (outboard side) and positioned between the stiffeners. Similar to the access area, the frames are discontinued at the outlet opening and interconnected with the local re-enforcement network. The outlet interface also includes provisions for mating and sealing with the fuel tank elbow which in turn would be reworked to include a flange equipped with self-locking nut plates. A portion of the cylindrical surface requires an open area covered with capillary screen (wire cloth). The panel is perforated at these areas and the cloth applied over the surface (see Figure 5-5). The screen is sealed at the perimeter by seam welding (using a backup strip to the mating surface). The heat exchanger tubes required on the capillary surface are seam welded to the screen and the panel (see Figure 5-5). The webs on the tubes act as backup strips. In some cases the backup strip shown for the perimeter welds may be replaced with the tube assembly providing the heat transfer distribution requirements are met.



SEE FOLLOWING DRAWING FOR VIEWS "CC," "D," AND "E"

Figure 5-4. Structural Arrangement

4 TUBES AT EACH  
END OF PANEL

3 TUBES AT  
FORWARD  
PANEL

BRAZE WEB  
TO TUBE

1/2 O.D. x .030  
TUBE WEB  
EXTRUSION

.030 WEB

SEAM WELD

TYP. HEAT EXCHANGER TUBE  
ATTACHMENT

ALTERNATE HEAT  
EXCHANGER TUBE

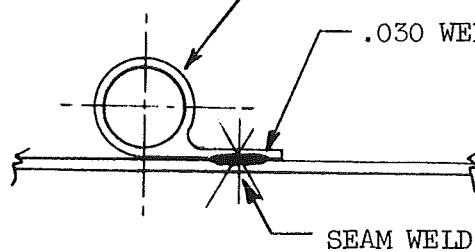
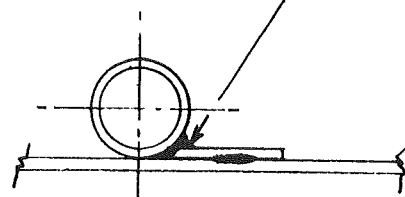


Figure 5-4A. Heat Exchanger Tube Arrangement for Series Circuit.

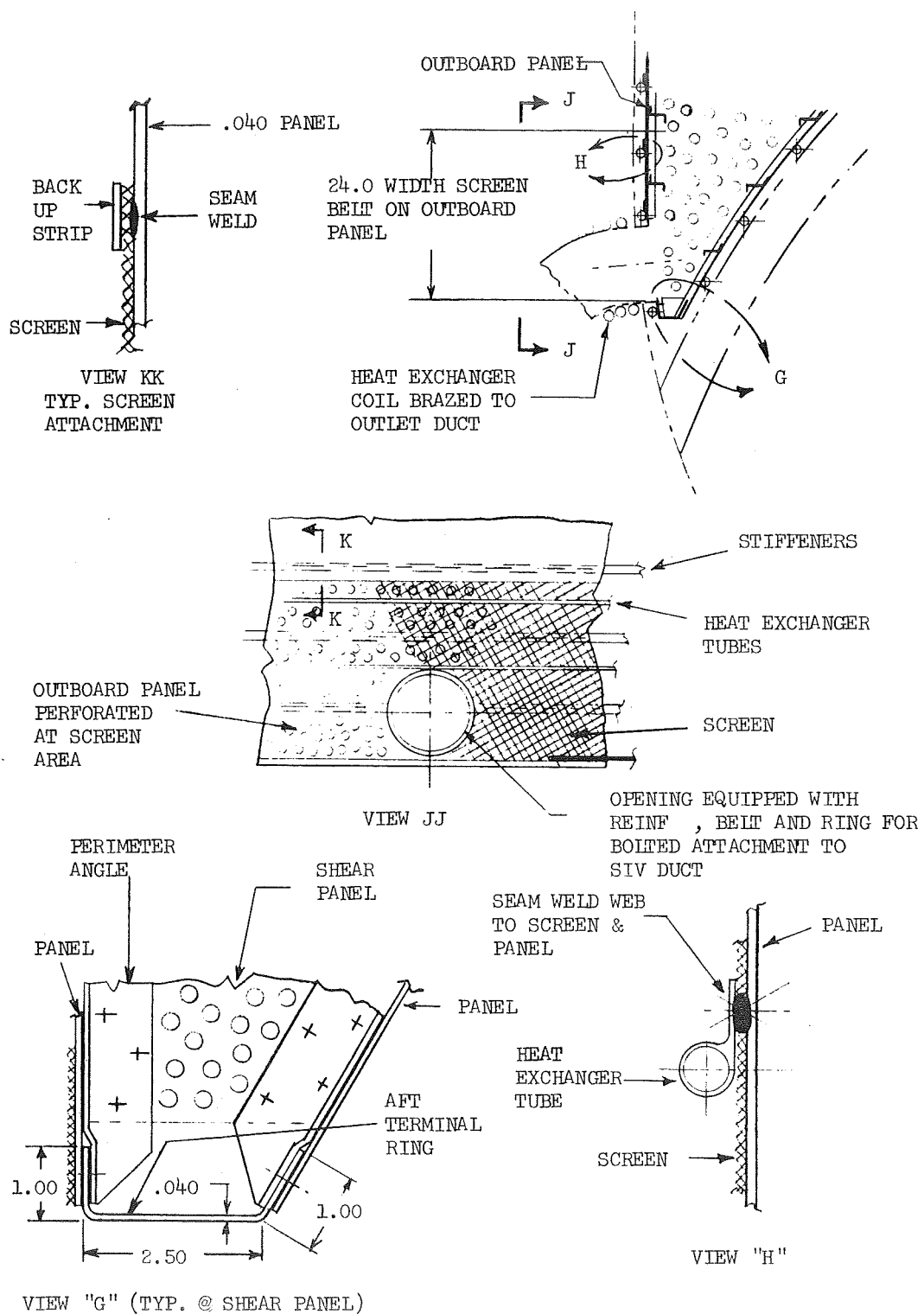


Figure 5-5. Outboard Panel and Outlet Zone Details

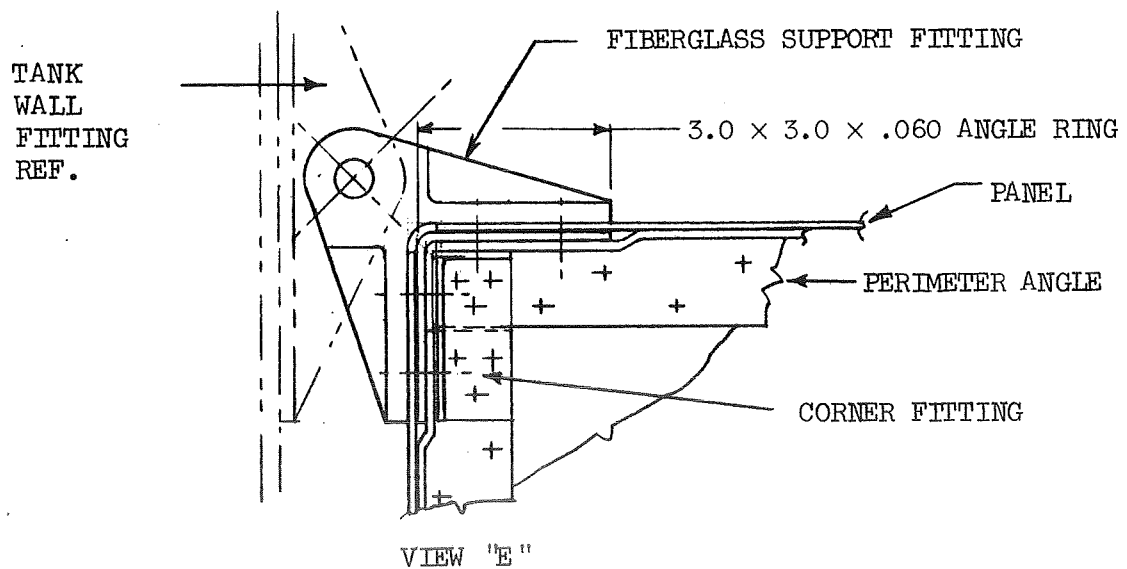
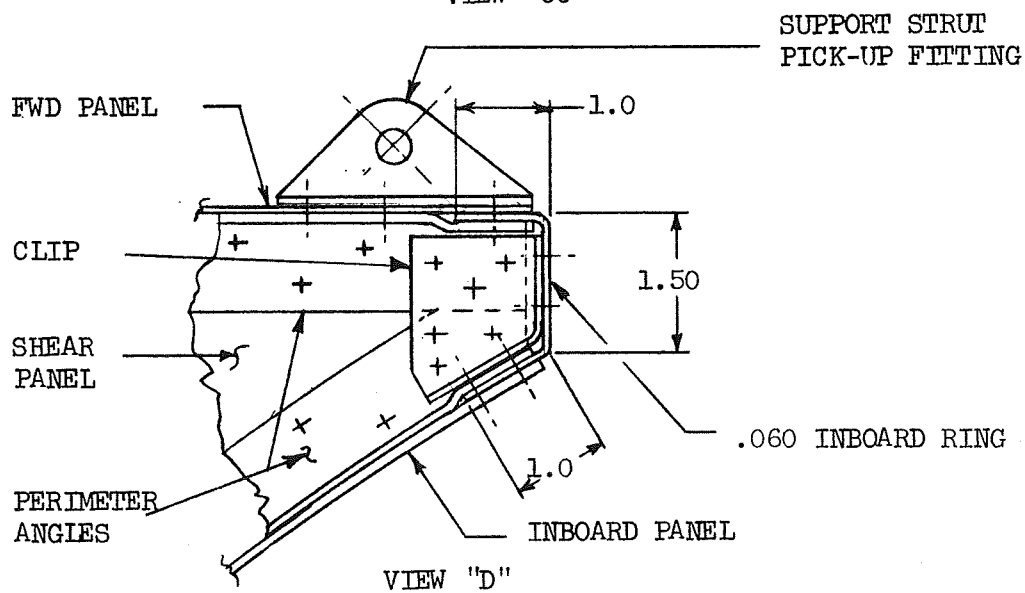
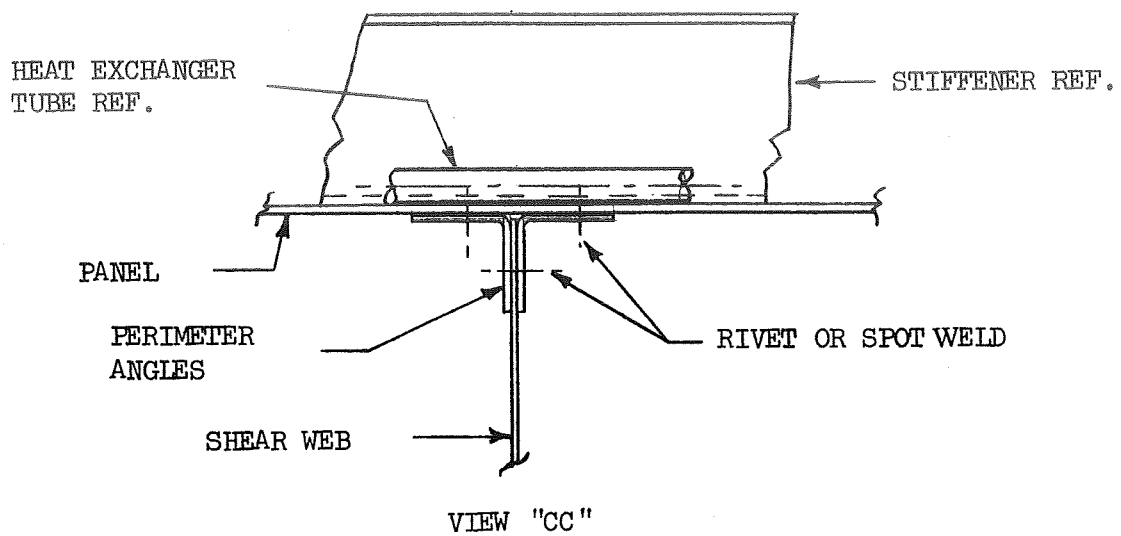


Figure 5-6. Detail for Structural Arrangement

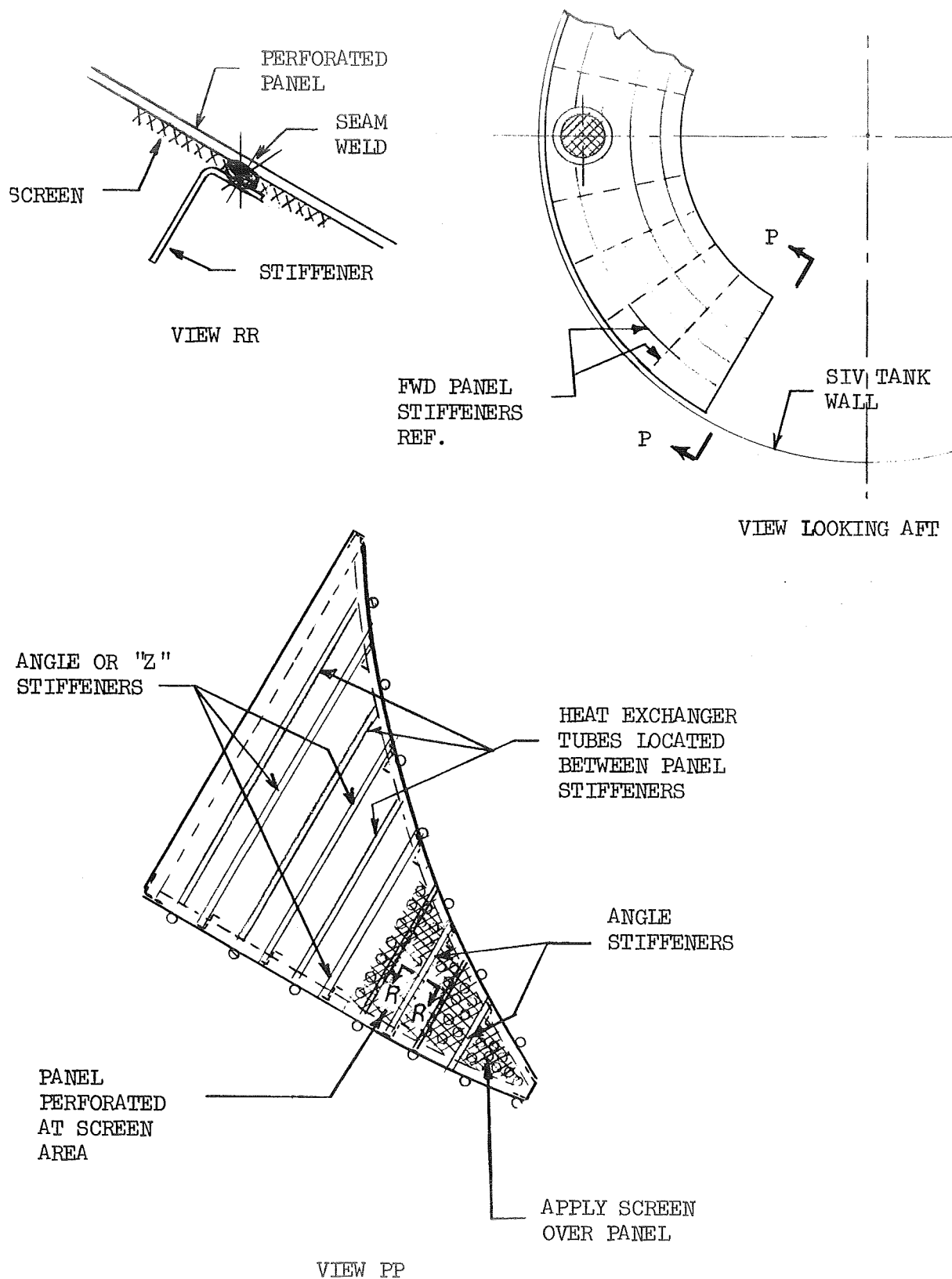


Figure 5-7. End Panel Details

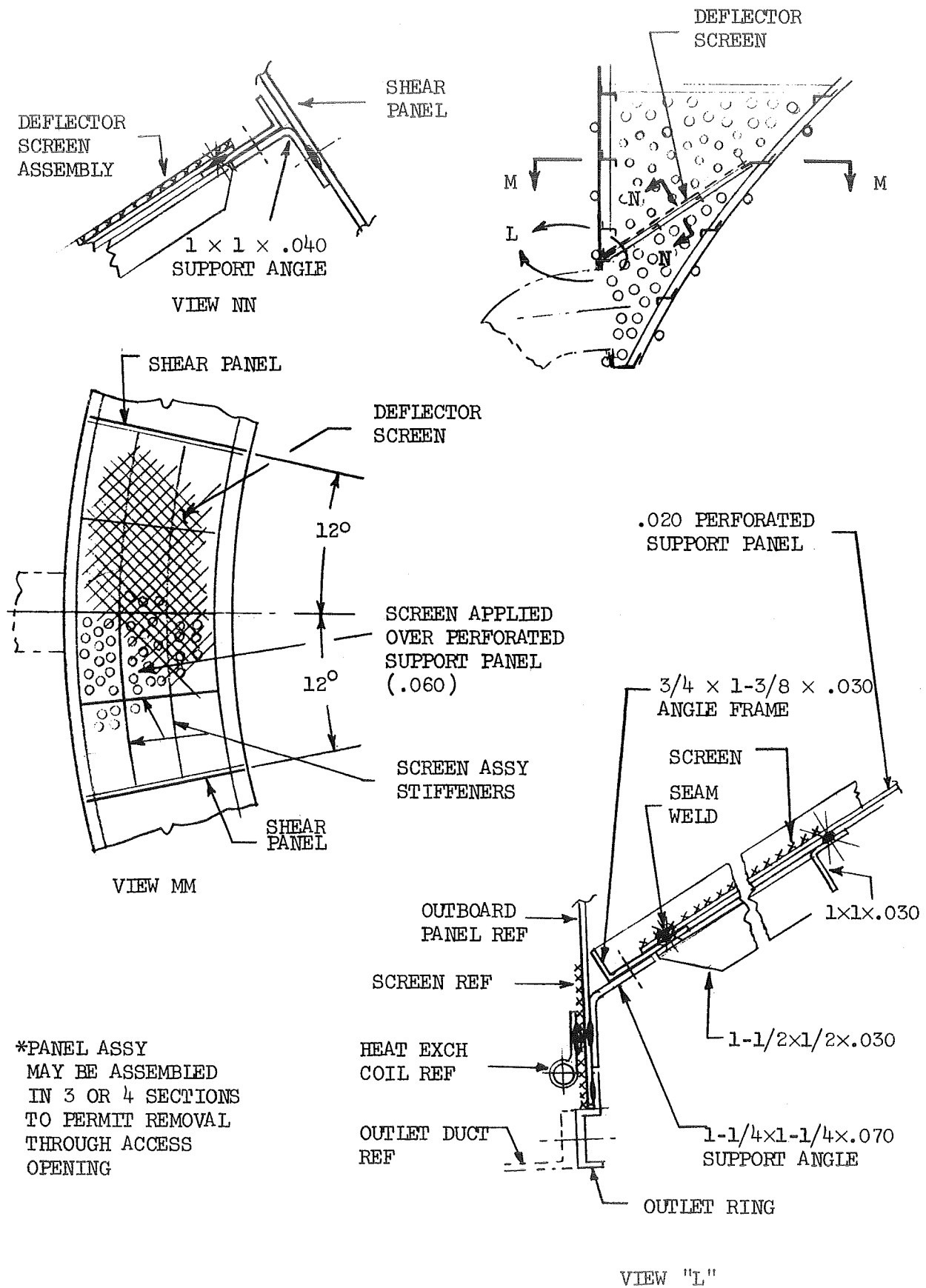


Figure 5-8. Deflector Screen Details

The inboard surface of the assembly is profiled to follow the contour of the SIVC intermediate bulkhead. Similar to the outboard cylindrical section, the stiffeners and heat exchanger tubes are placed on opposite sides of the panel. Most of the tubes are positioned between the frames to provide additional stability to the sheet metal areas.

The four shear panels inboard of the end faces are perforated to allow flow between compartments. The two additional bulkheads which form the end closures contain open areas equipped with screen which will be discussed later. Each panel is attached at the perimeter to the mating skins and rings using angles and rivets (see Figures 5-5 and 5-6). An intersection between stiffeners and panels is formed which can be accommodated by slotting the bulkhead (using perimeter angle sections) or discontinuing the rings at each panel. Either case would require the use of intersection clips which interlock the mating parts. The large area of the bulkheads coupled with perforations dictates the need for angle stiffeners oriented parallel to the forward face and positioned in line with the surface rings (see Figure 5-4). The angles are riveted to the panels and interconnected at the ends to the perimeter members.

Three primary corner rings are required as shown in Figures 5-4 and 5-5. The aft and inboard rings are channel shaped members connected to each shear panel assembly using corner fittings, offset flanges, etc. The outboard unit is an angle (equal legs) attached in a similar manner. Support fittings are required at each bulkhead (see Figure 5-6). The inboard fitting is a tee cross section member bolted to the shear panel perimeter angles and the corner ring. The outboard support fitting has two legs for attachment to the ring and the bulkhead angles. The boss section of this latter fitting is configured to mate with a clevis type pick-up from the fuel tank wall.

The end surfaces of the assembly are formed with two flat shear panels partially perforated, and equipped with wire cloth, heat exchanger tubes and stiffeners (see Figure 5-7). The angle or "Z" stiffeners are spaced over the entire surface including the areas equipped with screens. Attachments between screen, stiffeners and panel are accomplished with seam welding. Rivets can be used in those regions outside the screened surfaces. "Z" section members for the forward region of the panels are recommended due to the long spans. At the short span aft regions, the cross sections can be reduced to simple angles.

A deflector screen is required over the outlet area (see Figure 5-8). The assembly is a flat rectangular perforated panel containing a perimeter frame, interior stiffeners and wire cloth which covers the entire surface. Shelf angles attached to the outboard reservoir wall, and to the two bulkheads, provide the support and fasteners for the unit. The fourth side is attached to an inboard panel ring. A one piece unit can be detached from the supports and moved within the compartment to allow access to the outlet interface. A second approach uses a four piece deflector which can be removed through the access opening. The latter method is recommended. Attachments between screen, frames, and stiffeners are similar to that described earlier.

5.1.2 RESERVOIR SUPPORT SYSTEM — The reservoir assembly is subject to a uniform pressure over the forward panel area plus loading due to the weight of the unit. Figures 5-9 and 5-10 outline the methods, quantity of support points, and the force relations. The loads are reacted from the fuel tank wall only using adjustable tubular struts and fittings located at each shear panel. The pressure load on the forward panel is absent when the acceleration value is at a maximum, therefore the mass of the unit is the prime factor at this mode. When the uniform load is acting, the acceleration load is minor. This latter condition appears to control the design. Additional loads due to vibration, slosh, and lateral accelerations are present but are considered to play a minor role relative to overall external loading. The attachment at the fuel outlet projects additional redundancy into the system which requires special attention.

5.1.3 COLLECTOR SYSTEM — The primary components of the collector system are three tubes attached to the fuel tank wall and extending from a station near the forward face of the reservoir to the forward end of the tank bulkhead. The tubes are spaced 120°. Construction, quantity of supports, and type of fittings are shown in Figures 5-11 and 5-12. A typical assembly is a perforated tube covered with a capillary screen. The wire cloth section is fabricated separately as a tube, slipped over the perforated member and seal-welded at the ends. Screens and perforations are discontinued at the support points. The perforated tube therefore acts as a beam supporting the wire mesh.

The sections between supports are basically simply supported beams subject to vibrational modes, acceleration and slosh modes. A trade-off exists therefore between quantity of supports and tube diameter. For this effort, a two-inch diameter with a three foot span was selected. One support method shown on Figure 5-11 uses tee fittings welded to the tank wall. The tubing in turn is attached to the fittings with standard clamps. This method is simple, allows for misalignments, but lacks stiffness at planes 90° to the attaching surfaces. This latter feature may or may not be a disadvantage depending upon final loads analysis. A second support method offered in Figure 5-12 reduces the tank wall to centerline distance and provides an increased load capability. The arrangement consists of a webbed yoke mating with a cap section. The web section of the yoke is attached at two points to a fitting welded at the tank wall. The diameter formed by the yoke and cap would be sized to prevent a clamping action on the tube, therefore providing restraint in all radial directions while allowing axial motion. The "yoke/cap" method is more complex than using the standard clamps but may be required for certain loading conditions.

5.1.4 HEAT EXCHANGER PLUMBING — The external surfaces of the reservoir are equipped with heat exchanger tubes which must be interconnected to form circuits which are compatible with the overall system. Figure 5-13 shows a plumbing arrangement which uses three manifolds at each end panel for serving the forward, outboard and inboard panel tubes. The configuration is for the parallel set up shown in the Figure 5-3 schematic.

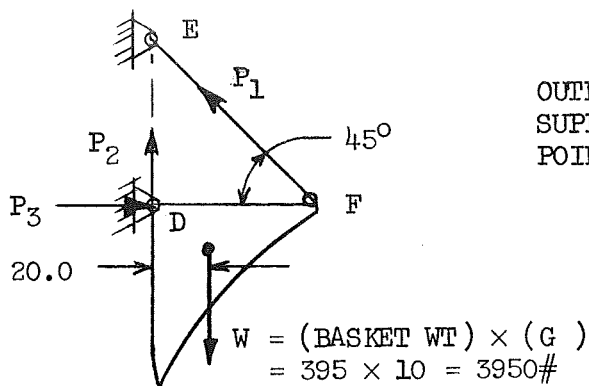


FIGURE B  
BASIC LOAD CONDITION  
DURING BOOST MODE

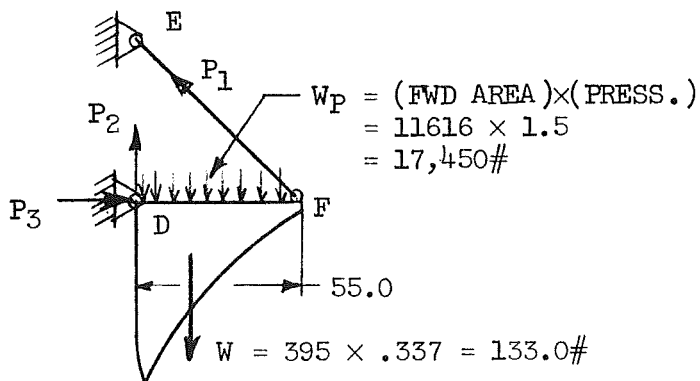
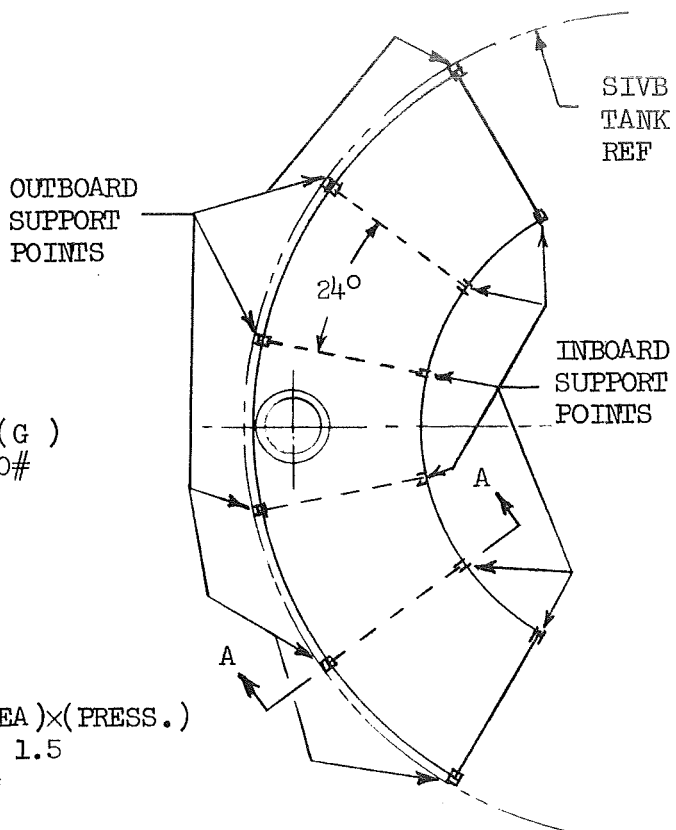
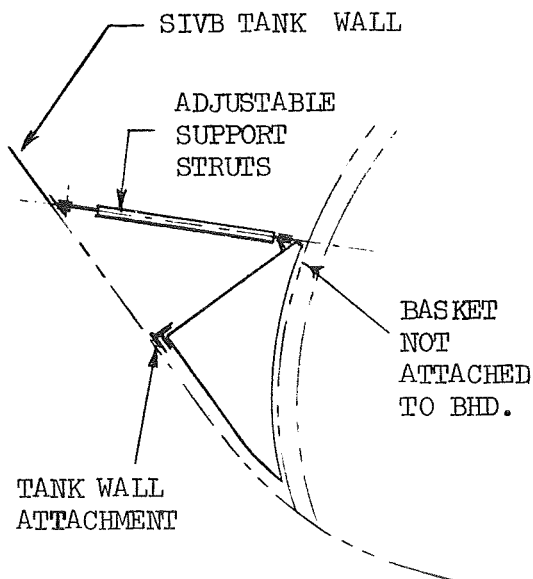


FIGURE C  
BASIC LOAD CONDITION DURING  
RE-START MODE



VIEW LOOKING AFT



VIEW AA

Figure 5-9. Reservoir Support System.

Using a typical 24° section, the conditions of Figure C, and moments about point "D,"

$$\frac{W}{5} \times 20 + \frac{W_P}{5} \times \frac{55}{2} = P_1 \times 55 \times \sin 45^\circ$$

$$4W + 5.5 W_P = 389 P_1$$

$$4 \times 133 + 5.5 \times 17,450 = 389 P_1$$

$$P_1 = \frac{96532}{389} = 2480\#$$

Summarizing the vertical loads;

$$P_2 + P_1 \sin 45^\circ = \frac{W_P}{5} + \frac{W}{5}$$

$$P_2 + 2480 \times .707 = 3480 + 26.6$$

$$P_2 = 1754.6\#$$

For the horizontal loads,

$$\begin{aligned} P_3 &= P_1 \cos 45^\circ \\ &= 2480 \times .707 \\ &= 1752 \end{aligned}$$

The strut lengths are approximately 72.0 inches which may present vibration problems when considering small diameters. A 1.50 inch O.D. × .040 wall is selected which provides .188 in<sup>2</sup> area. The tension stress = 2480/.188 = 13200 PSI. Steel can be used to increase the stiffness if required.

Additional load conditions may expose the struts to column actions which should be included in a final analysis. Strut designs should include features for length adjustments to ensure proper load distribution.

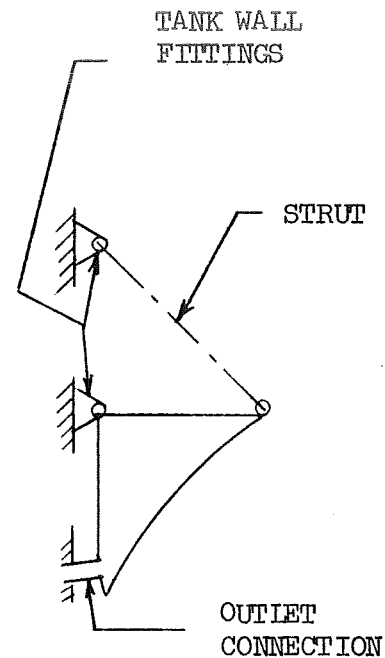


FIGURE D

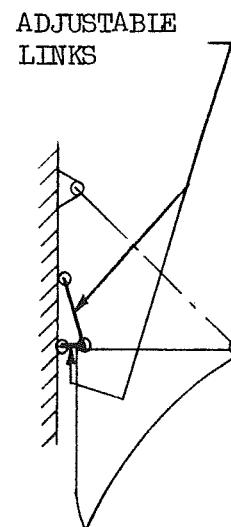


FIGURE E

ALT. ARRANGEMENT

Figure 5-10. Reservoir Support System

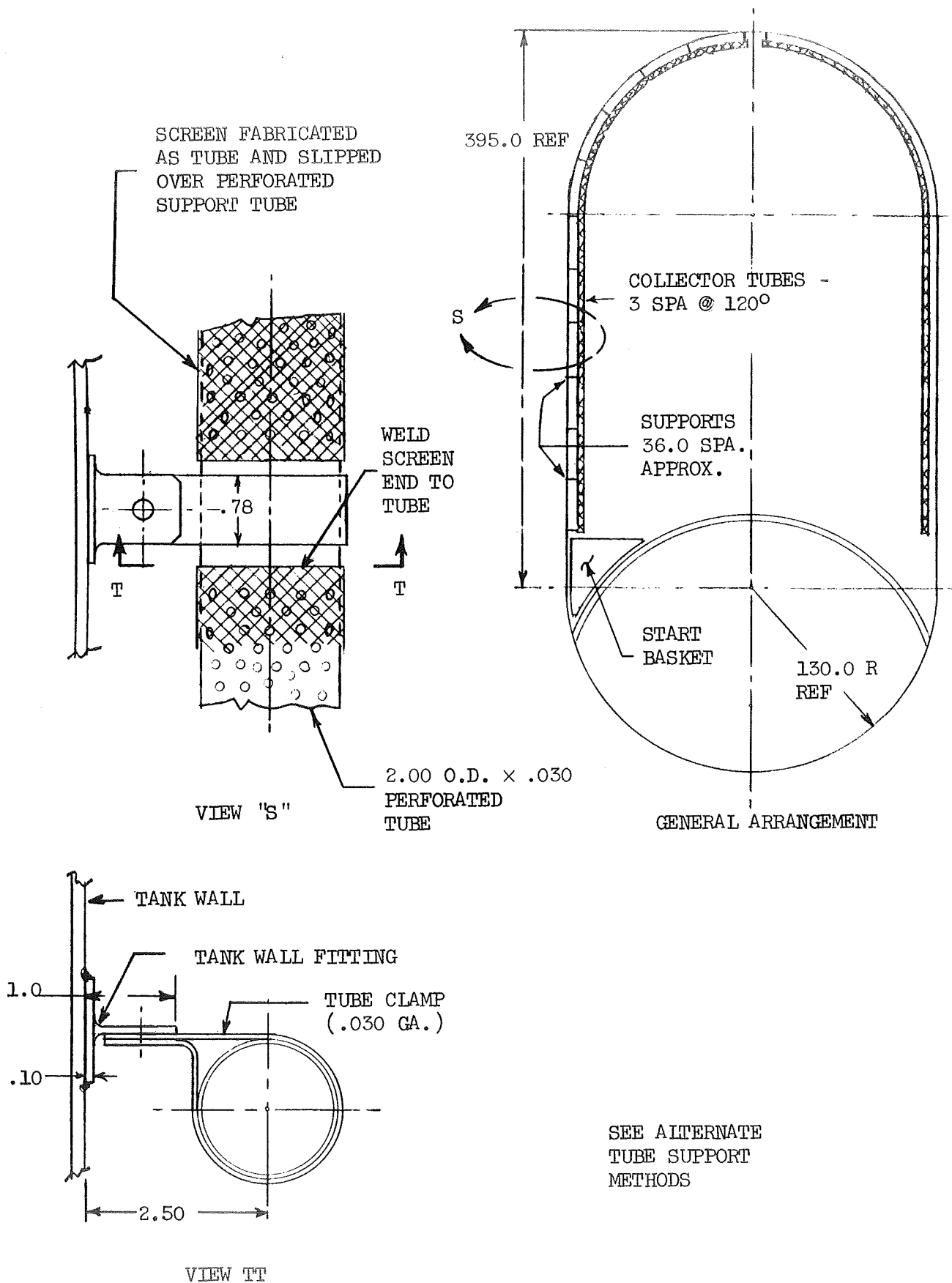


Figure 5-11. Collector Tube Details

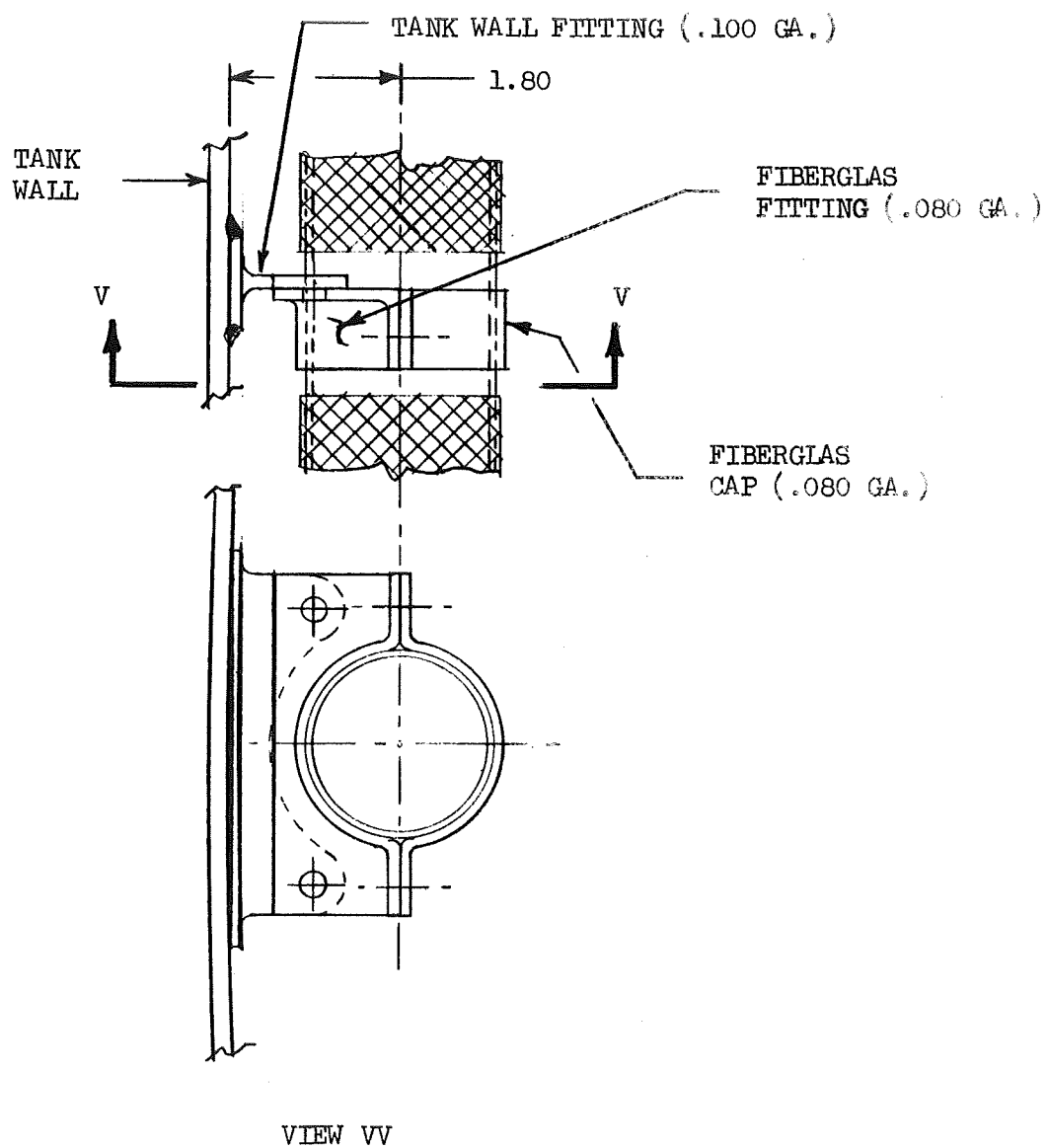


Figure 5-12. Alternate Collector Tube Support.

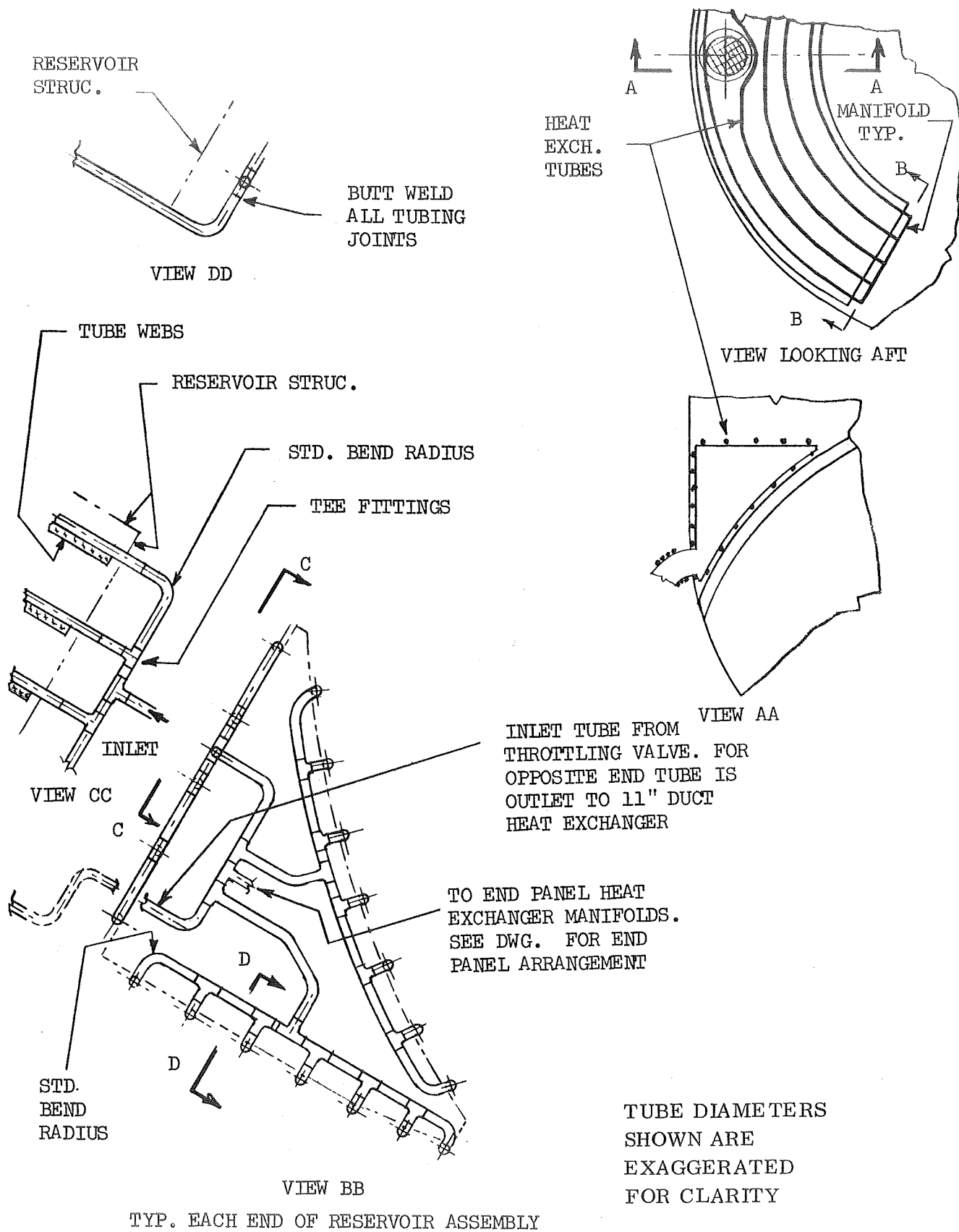


Figure 5-13. Plumbing Arrangement for Forward Outboard and Inboard Heat Exchanger Parallel Circuits

Each manifold is an assembly of elbows, tees and short straight sections which in turn are welded to the tube ends. The manifolds are interconnected to common inlet and outlet lines which interface with other system components. The plumbing network is spaced from the end panel surfaces to allow use of the portable orbit arc welding process and for inspection. Supports can be provided from the end panel stiffener members using angles, tees and standard clamps. The Figure 5-13 approach can also be applied to other circuit arrangements such as all series or a combination of parallel and series. For example, those tube sections requiring a series "hook-up" would reflect 180° bend fittings.

The end panel surfaces are also equipped with heat exchanger tubes which must interface with the system. Figure 5-14 shows an arrangement using two manifolds and the location of the components relative to the preceding assembly. The tubes are spaced from the panel surfaces and adjacent members to allow access for welding, inspection, and assembly.

The inlet and outlet interfaces of the reservoir heat exchanger system are attached to a throttling device and to the outlet duct exchanger. A plumbing arrangement is shown in Figure 5-15 which mounts the throttling assembly on a forward panel stiffener and routes the outlet tube from the exchanger circuit through a tank wall penetration fitting which is equipped with mechanical connectors. The upstream and downstream sides of the throttling package are equipped with tube runs which connect to three terminals on the collectors and two on the reservoir manifolds.

**5.1.5 OUTLET DUCT ACCESSORIES** — Heat exchanger tubes, a gas liquid interface screen, relief line, and a return line are required for the outlet duct which supplies fuel to the engines. A design is shown in Figure 5-16 which locates the gas/liquid interface upstream of the engine inlet area. The elbow section at the tank is aluminum alloy which in turn is connected to the steel section of the duct with a mechanical joint. Each section is equipped with heat exchanger tubes attached to the walls. A spiral pattern is shown with the pitch dimensions decreased at the elbow and interface areas. Figure 5-2 schematic shows an alternate circuit when the fuel tank heat exchanger/pump package is deleted. This would increase the number of coils on the duct. The tubes are brazed to the walls. An alternate approach would be the use of webbed tubes (similar to that used on reservoir walls) installed as rings and interconnected with jumper sections. The interface screen assembly consists of a tubular section which is welded to the base of a wire cloth cone. The coupling ends are in turn butt welded to the duct sections. An outlet boss (provided downstream of the screen) is plumbed forward through an orifice to a tank wall penetration fitting for relieving the pressure in the compartment aft of the screen. This outlet boss can be part of the coupling or installed separately in a duct section. Both the heat exchanger return and the relief tubes are supported from the duct using local clips welded to the wall and standard clamps.

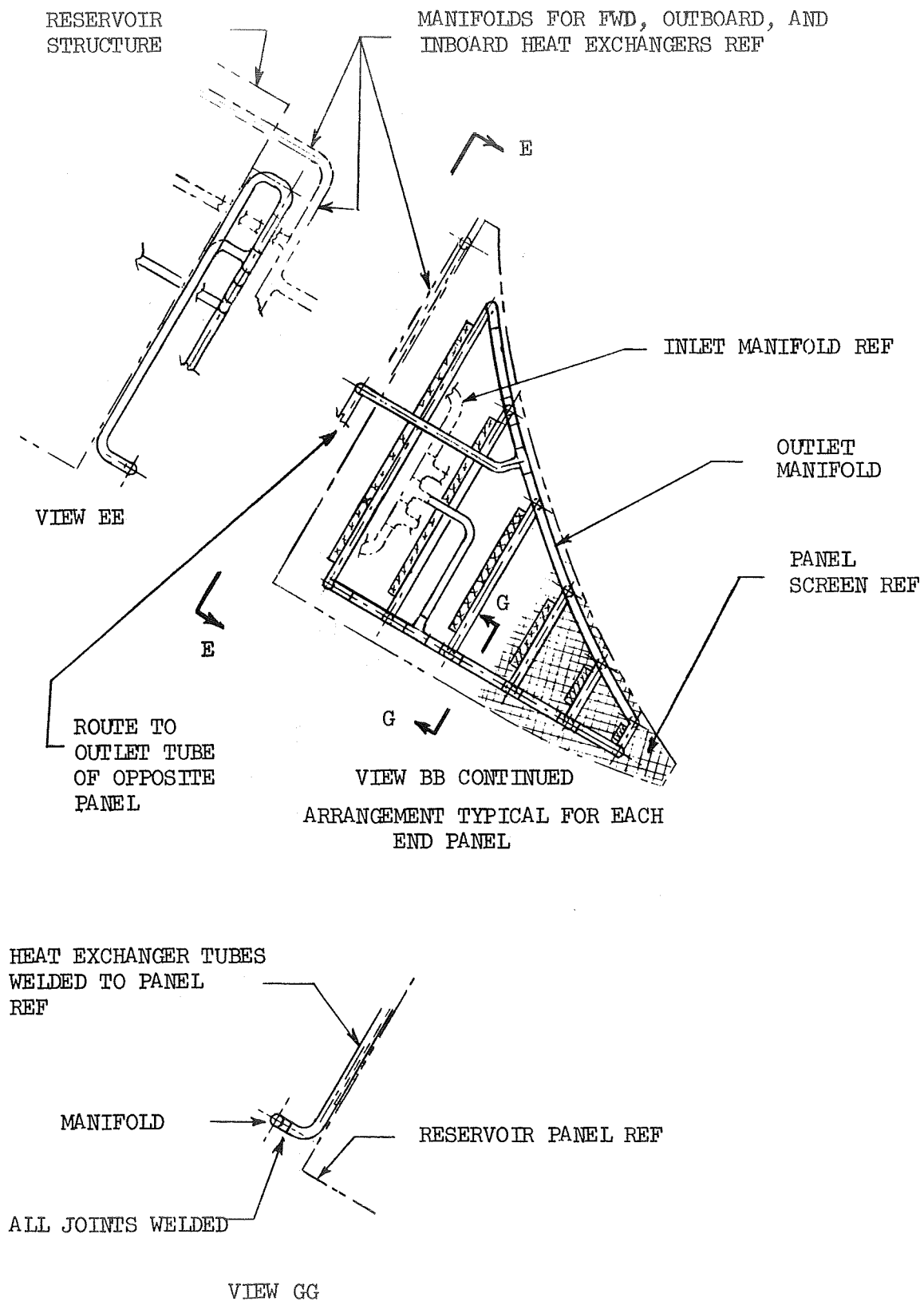


Figure 5-14. Plumbing Arrangement for End Panel Heat Exchangers

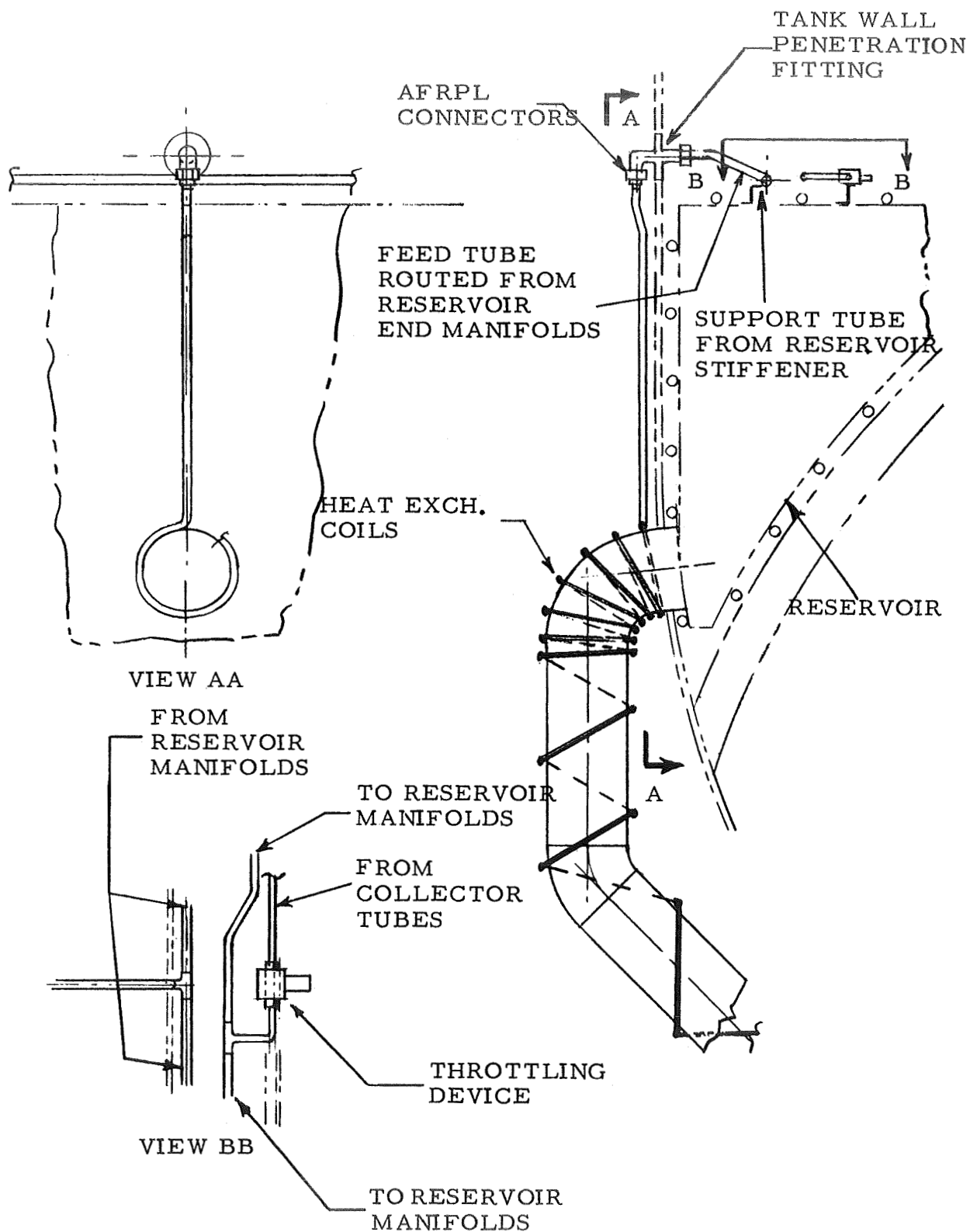


Figure 5-15. Plumbing Arrangement From Reservoir to Outlet Duct Heat Exchangers

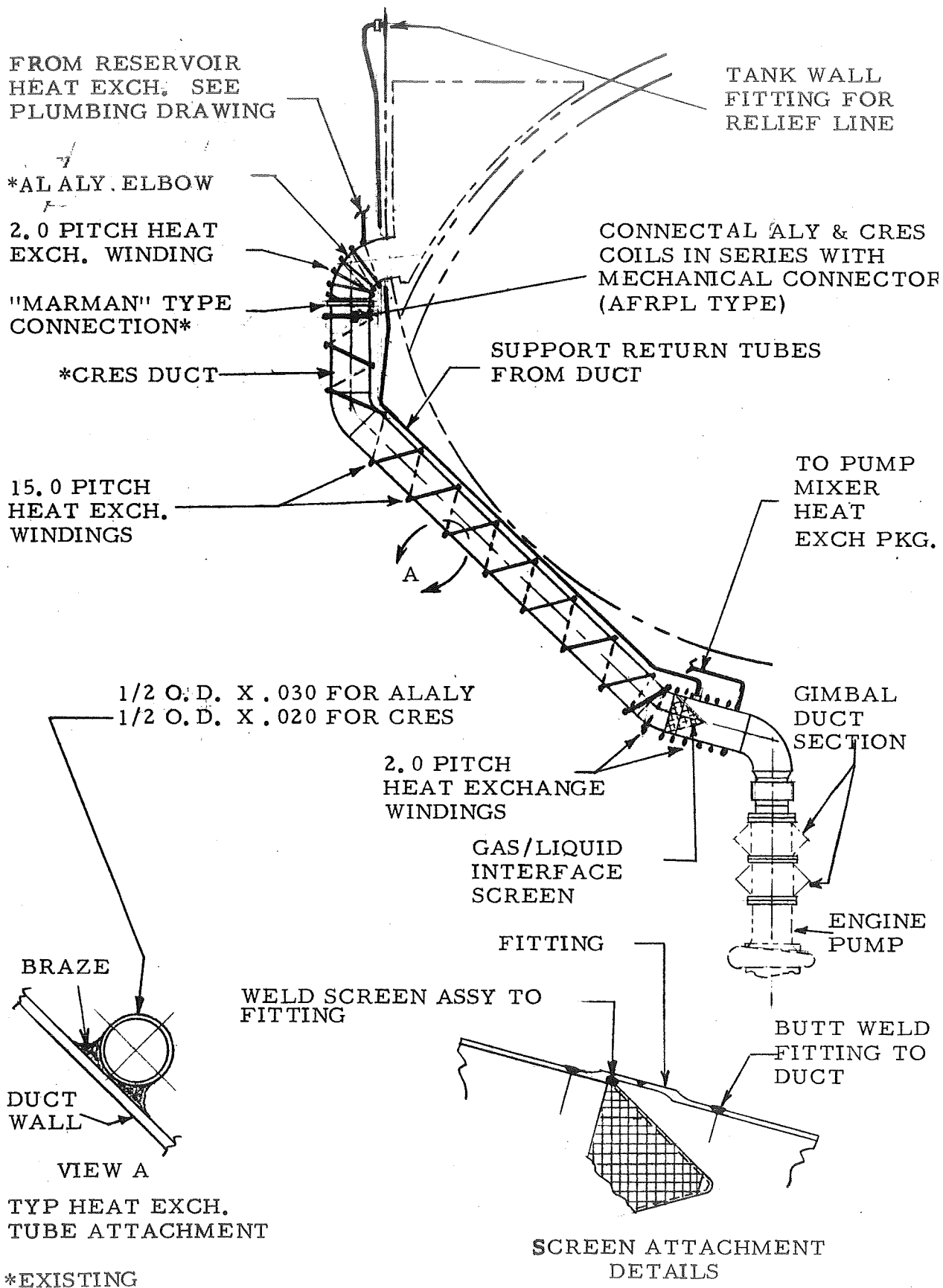


Figure 5-16. Feed Duct Accessories

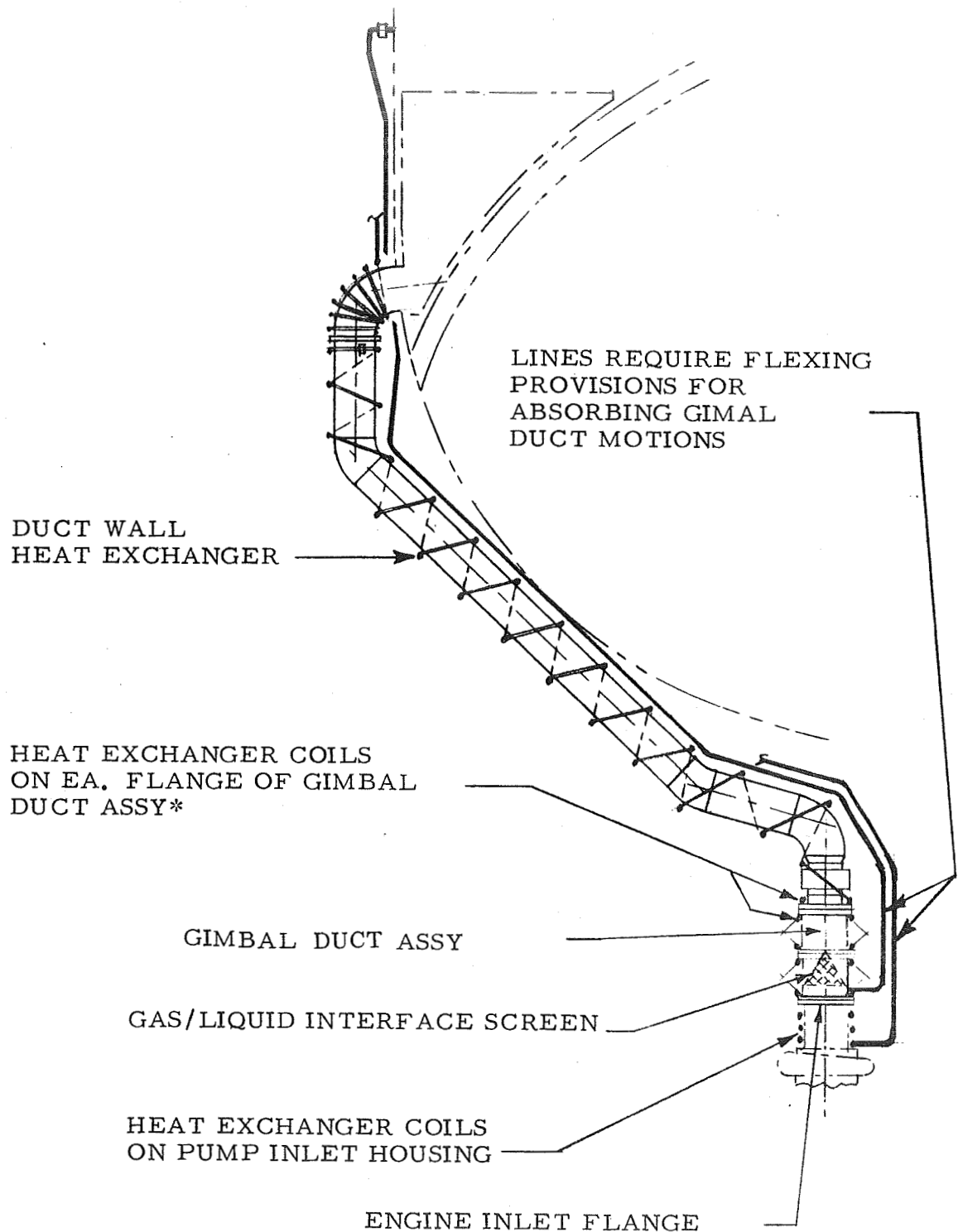
The Figure 5-16 arrangement minimized the amount of feed duct rework and overall complexity since the system does not span the gimbal duct section. Cases may develop however which require a gas liquid interface location at or near the engine inlet which is shown in Figure 5-17. The existing gimbal duct section is an assembly of flanges, bellows and external yoke type devices for stabilizing the bellows column. A heat exchanger is required at this dynamic section since the interface screen is located within the envelope. The simplest approach is shown which applies heat exchanger coils at the flanges only. Flexible connections between the coils would be required in the form of flex loops or hoses to accommodate the bellows motions. A second method is to jacket the bellows sections using the volume between jackets as the heat exchanger. This latter method would require redesign of the gimbal duct assembly. The Figure 5-17 arrangement also assumes heat exchanger provisions on the pump inlet housing in the form of coils or integral passages. Routing of the return and relief lines is similar to the Figure 5-16 design except flexing provisions must be included for the engine gimbal motions.

Considerable duct rework and general complexity can be expected for the Figure 5-17 configuration. If jacketed bellows are used, the envelope for the gimbal duct changes which in turn may interfere with adjacent equipment, increase the bellows spring load on the engine inlet and possibly move the station location of the engine. If heat exchange is applied at the flange areas only, flexing of the interconnecting jumpers plus increased complexity of the flanges must be considered. Propellant flow problems may be encountered when using screens for gas liquid interfaces. If valves are substituted for the screens, weight penalties and additional subsystems can be expected.

**5.1.6 WEIGHT ANALYSIS** — A detailed weight breakdown for the reservoir is shown in Figures 5-18 and 5-19, -20 and -21. A summary includes all structural members, support fittings, struts, manifolds, heat exchangers, re-enforcements, screens, and miscellaneous fasteners and clips. Basic dimensions are shown for most components. Weight comparisons are noted for the heat exchanger tubes involving series and parallel circuits. Due to the depth of the analysis, a 5% contingency factor was used instead of the previous 10%.

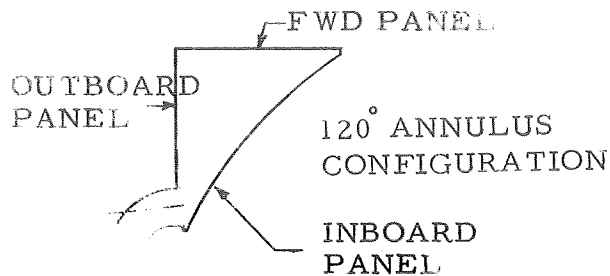
The weight summary for the collector system is Shown in Figure 5-22 and includes supports and fasteners for the tube assemblies. The tube manifold allowance is that section of the circuit which interconnects the collectors and routes to the throttling device located on the forward panel of the reservoir.

The feed duct manifold accessory weight is shown in Figure 5-23 which includes all heat exchanger coils, interface screen fittings, and attachments. An additional allowance is indicated when considering an interface location near the engine inlet.



\*ALTERNATE - USE JACKETS ON GIMBAL DUCT BELLOWS AND CONVEY GAS THROUGH THE ANNULUS. WOULD REQUIRE REDESIGN OF GIMBAL DUCT.

Figure 5-17. Feed Duct Accessories/Alternate Screen Location



200 FT<sup>3</sup> VOL.

MAT'L: AL ALY

\* 4.24# FOR SERIES CIRCUIT USING  
1/2 O.D. X .030 TUBES

ITEM	WT. LBS	REMARKS
<p>FWD PANEL STIFFENER RINGS</p>	14.94	4-120° RING SECTIONS 830" LGT. TOTAL
<p>FWD. PANEL</p>	46.00	
<p>FWD PANEL ACCESS OPENING</p>	2.00	RING REINF. PANEL DOUBLERS & COVER RING
<p>FWD PANEL RADIAL STIFFENERS</p>	17.30	5 @ 55" LGT EA.
<p>SUPPORT FITTINGS @ FWD PANEL</p>	1.20	6 EA. REQUIRED
<p>FWD PANEL HEAT EXCHANGER</p>	4.18*	830" LGT TOTAL
<p>FWD CORNER RING</p> <p>LOCATED @ OUTBD. CORNER</p>	9.78	272" LGT 1 REQ'D
<p>FWD CORNER RING</p> <p>LOCATED @ INBOARD CORNER</p>	3.30	157" LGT. 1 REQUIRED
<p>OUTBOARD PANEL</p>	51.00	272" LGT. 1 REQUIRED
<p>OUTBOARD PANEL SCREEN</p>	2.40	.053 #/FT <sup>2</sup>

CONTINUED ON NEXT PAGE

Figure 5-18. Weight Estimate/Fuel Start Basket

FWD PANEL

OUTBOARD  
PANEL

SHEAR PANELS

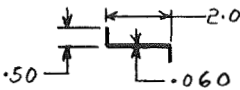
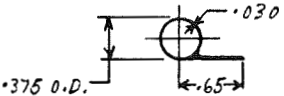
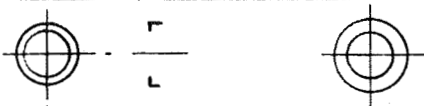
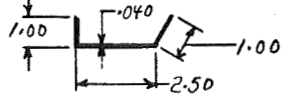
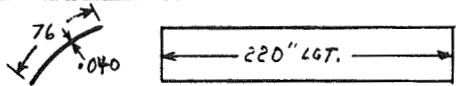
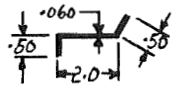
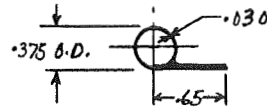
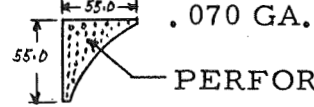
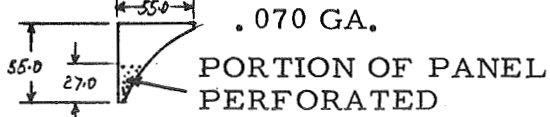

INBOARD  
PANEL

\* 11.0#

\*\* 6.12#

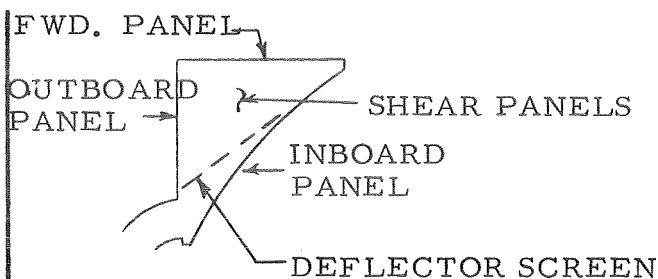
CIRCUIT

FOR SERIES USING  
1/2 O.D. X .030  
TUBING

ITEM	WT. LBS	REMARKS
 OUTBD. PANEL STIFFENER RINGS	24.50	5 REQUIRED 272" LGT EA.
 OUTBD. PANEL HEAT EXCHANGER	8.23*	6 REQUIRED @ 272" LGT. EA.
 OUTLET REINF. & INTERFACE RING	2.00	SIZED FOR 11" DIA. OUTLET
 AFT CORNER RING	4.90	272" LGT.
 INBOARD PANEL	67.00	
 INBOARD PANEL STIFFENER RINGS	19.90	5 REQD. @ 351, 239 222, 209 & 184 " LGT. RESPECTIVELY.
 INBD. PANEL HEAT EXCHANGER	4.60**	7 REQD. 1534" TOTAL LGT.
 INTERIOR SHEAR PANELS	24.16	4 REQD. .040 EQUIV. GA.
 END SHEAR PANELS	17.66	2 REQD.
 SCREEN FOR END PANELS	0.22	.053#/FT <sup>2</sup> 4.12 FT <sup>2</sup> REQD.

CONTINUED ON NEXT PAGE

Figure 5-19. Fuel Start Basket Weight Estimate (Continued)



ITEM	WT. LBS.	REMARKS
 END PANEL STIFFENERS	1.58	2 REQD. 44
 END PANEL STIFFENERS	1.06	2 REQ'D 32" LGT. EA.
 END PANEL STIFFENERS	.60	2 REQ'D. 24" LGT. EA.
 END PANEL STIFFENERS	.50	2 @ 17" LGT. 2 @ 10" LGT.
 SHEAR PANEL PERIMETER ANGLES	11.15	1860" LG'G TOTAL
 MSC. CLIPS FOR CORNER AREAS INTERSECTIONS, ETC.	2.00	
 SHEAR PANEL STIFFENERS	2.16	480" LGT TOTAL
 DEFLECTOR SCREEN	.42	8 FT <sup>2</sup> REQ'D .053#/FT <sup>2</sup>
 DEFLECTOR SCREEN FRAME	.92	12 FT REQ'D.
 DEFLECTOR SCREEN STIFFENERS	.65	6 FT. REQ'D.

CONTINUED ON NEXT PAGE

Figure 5-20. Fuel Start Basket Weight Estimate (Continued)

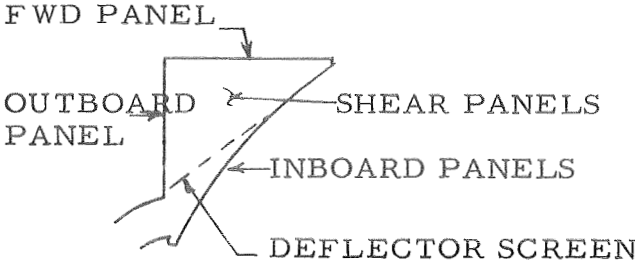
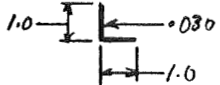

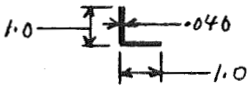
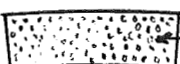

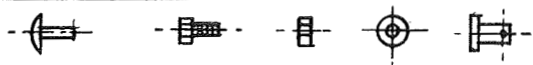
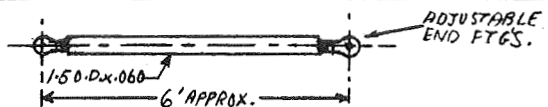
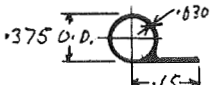
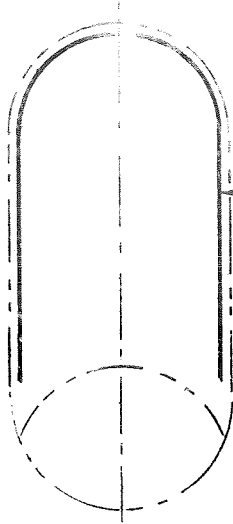
<div style="display: flex; justify-content: space-between; align-items: flex-start;"> <div style="width: 45%;">  </div> <div style="width: 50%;"> <p>*1.30# FOR SERIES CIRCUIT USING 1/2 O. D. X .030 TUBING</p> </div> </div>		
ITEM	WT. LBS	REMARKS
 DEFLECTOR SCREEN STIFFENERS	.60	8 FT. REQD.
 DEFLECTOR SCREEN SUPPORT	.48	4 FT. REQD.
 DEFLECTOR SCREEN SUPPORT PANEL	.77	8 FT. REQD.
 PERFORATED (.060 GA.)	3.46	8 FT <sup>2</sup> REQD. .030 EQUIV. GA.
 MSC. JUMPER TUBE & MANIFOLDS FOR HEAT EXCHANGERS	3.50	INCLS. END FTG'S. AND SUPPORTS
 MISC. FASTENERS	1.50	
 1/50 D x .060 6' APPROX.	18.0	6 REQ'D. 3.0 # EAC. INCL. FTGS.
 END PANELS HEAT EXCHANGERS	1.60*	300" LG'T.
TOTAL (ALL FIGURES)	376.22	
5% CONTINGENCIES	18.80	
GRAND TOTAL	395.02	

Figure 5-21. Fuel Start Basket Weight Estimate (Continued)

\*4.23# FOR SERIES  
CIRCUITS USING  
1/2 O.D. X .030 TUBES



COLLECTOR  
TUBES (3)

BASIC MAT'L.: AL. ALY.

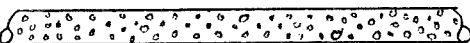

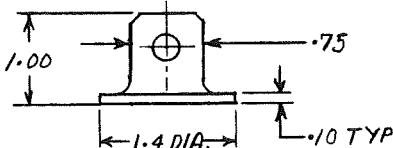
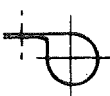
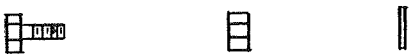

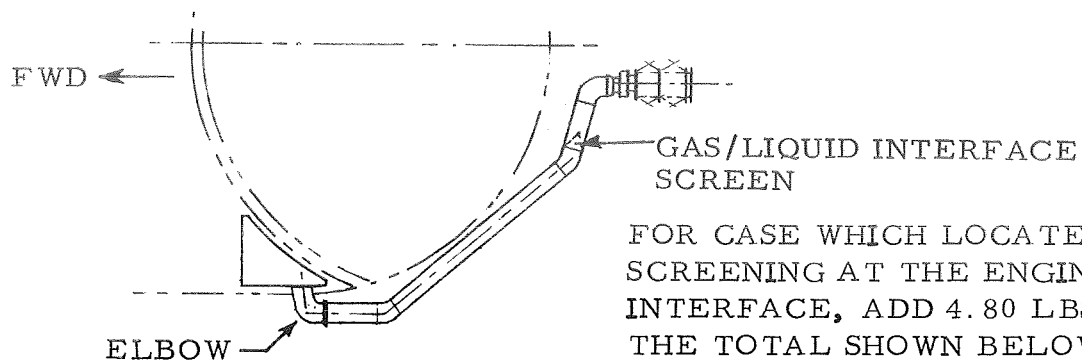
ITEM	WT. LBS	REMARKS
 PERFORATED SUPPORT TUBES	20.00	2.00 O.D. X .030 X 36 FT. 3 PIECES
 SCREEN TUBES	3.00	2.00 I.D. X 36 FT. 3 PIECES .053 #/FT <sup>2</sup>
 TANK WALL FITTINGS	0.83	36 REQ'D.
 CLAMPS	0.75	36 REQ'D.
 FASTENERS	1.00	
 MANIFOLD TUBING	3.18*	SIZE 3/8 X .030 X 900" AL. ALY.
TOTAL		28.76
10% CONTINGENCIES		2.87
GRAND TOTAL		31.63

Figure 5-22. Weight Estimate Fuel Collector Tubes.



FOR CASE WHICH LOCATES THE SCREENING AT THE ENGINE INTERFACE, ADD 4.80 LBS TO THE TOTAL SHOWN BELOW






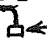
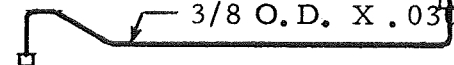

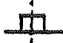





ITEM	WT. LBS	REMARKS
 1/2 O.D. X .030 AL. ALY ELBOW HEAT EXCH. COIL	1.20	6 TURNS 2 PITCH
 1/2 O.D. X .020 CRES DUCT SECTION HEAT EXCH.	4.52	10 TURNS 15" PITCH
 1/2 O.D. X .020 CRES SCREEN ZONE HEAT EXCH.	1.60	8 TURNS 2" PITCH
 BRAZE MATERIAL	2.00	
 1/2 O.D. X .030 AL. ALY HEAT EXCH. RETURN LINE  END FTGS.	1.75	280" LG'T.
 3/8 O.D. X .030 AL. ALY RELIEF LINE	2.10	250" LGT.
 CRES SCREEN ASSY. INCL. FITTING	2.60	
  DUCT & TANK WALL BOSS FTGS.	.85	
    MSC. FTGS. CLAMPS, NUTS, SCREWS	1.35	
TOTAL  10% CONTINGENCY  GRAND TOTAL	17.97	
	1.80	
	19.77	

Figure 5-23. Fuel Duct Accessories Wt. Estimate.

5.1.7 STRUCTURAL ANALYSIS — A complete structural analysis of the reservoir is relatively complex due to the interactions between circumferential and radial stiffeners, panels, bulkheads, external attachments and the type of loading, therefore simplified approaches were used for this study. For example, the circumferential stiffener ring sections on the forward panel are actually continuous curved beams with rigid supports at the shear panel locations, elastic type supports at the radial stiffeners, and elastically restrained connections. A typical section of the beam between supports was isolated and treated as a simple supported member uniformly loaded (see Figure 5-24). This approach is conservative but is partially compensated for when considering details such as additional secondary panel stiffeners for vibrational modes, any special end connections, etc. which may become apparent under a detailed analysis. Due to the capillary screens, heat exchanger tubes and the general redundancy of the system, most structural member sizing was controlled by limiting the deflections.

The forward stiffener system divides the panel into rectangular sections which are subject to a uniform load. These sections were treated as rectangular plates with large deflections and held edges (not fixed). Figure 5-25 outlines the analysis. Similar to the beam problem, the deflection at the center of the plate was limited. Any benefit derived from the heat exchanger tubes was neglected since in a final design all panel sections may not be equipped with tubes.

The ring sections for the outboard panel were treated similar to that shown for the forward panel stiffeners. The load and span for this case is changed from the previous item. Figure 5-26 outlines the approach and estimates the cross section required.

The primary bulkhead members (shear panels) are subject to the external loading system shown in Figure 5-27. The problem therefore is primarily one of instability. Since the panels are perforated, an equivalent gage was used in the calculations. Figure 5-27 indicates that the buckling stress is less than the applied stress, therefore a system of stiffeners is shown on Figure 5-28. The areas framed by the stiffeners are estimated in Figure 5-29 as rectangular flat panels loaded at all four simply supported edges.

Figure 5-30 outlines the approach used for the radial stiffeners on the forward panel. These are treated as uniformly loaded beam sections spanning between the outboard and inboard corner rings. A similar analysis is shown in Figure 5-31 for the primary stiffener members used on the deflector screen assembly.

The forward stiffeners are assumed as beams per the load conditions of Figure A.

The deflection

$$y = - \frac{5 W L^3}{384 EI}$$

where

$$W = 16.5 \times 25 = 412\#$$

$$E = \text{Modulus of Elasticity} = 10 \times 10^6$$

$$I = \text{Cross Sectional Moment of Inertia}$$

If the deflection is limited to .10 inch

$$\begin{aligned} .100 &= \frac{5 \times 412 \times (25)^3}{384 \times 10^7 \times I} \\ &= \frac{3.21}{384 I} \end{aligned}$$

$$I = \frac{3.21}{.100 \times 384} = .0835 \text{ in}^4$$

An approximate stiffener for the above I value is shown in Figure B.

Bending moment

$$\begin{aligned} M &= \frac{WL}{8} = \frac{412 \times 25}{8} \\ &= 1284 \text{ in.} \end{aligned}$$

Bending Stress

$$S = \frac{MC}{I} = \frac{1284 \times 1.0}{.0824} = 15600 \text{ psi}$$

Near the inboard area of the panel, the span L decreases which in turn would decrease I. For this estimate, the Figure B cross section is used for all stiffeners on the top panel.

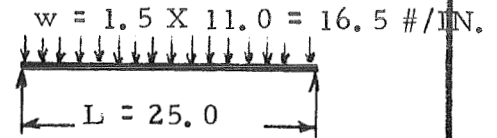


Figure A

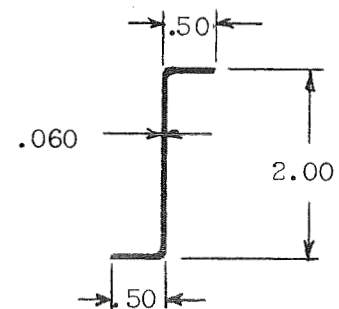


Figure B

Figure 5-24. Forward Panel Circumferential Stiffener Estimate.

The forward side is equipped with stiffeners which divide the surface into panels. Using the maximum size area as shown in Figure A, the

$$\frac{a}{b} = \frac{25}{11.0} = 2.27$$

assuming a thickness  $t = .060$

$$* \frac{wb^4}{Et^4} = \frac{1.5 (11.0)^4}{10^7 (.060)^4}$$

$$= \frac{21900}{129.5}$$

$$= 169.8$$

$E$  = Modulus of Elasticity

$$= 10 \times 10^6$$

From table,

$$\frac{Sb^2}{Et^2} = 19.00 *$$

where

$S$  = total stress (bending + diaphragm)

Therefore

$$S = \frac{19.00 \times 10^7 \times (.060)^2}{(11.00)^2}$$

$$= \frac{684000}{121.0}$$

$$= 5650 \text{ psi}$$

Deflection  $y = t \times 1.90 *$

$$= .060 \times 1.90$$

$$= .1140 \text{ inch}$$

$y$  should not exceed the value shown.

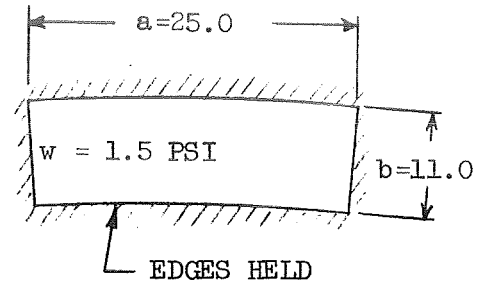


Figure A

\* Roark, 3rd Edition, p. 221 and 222

Figure 5-25. Forward Panel Estimate.

The outboard curved panel is stiffened with rings which span the areas between the shear panels. Using the load condition of Figure A and assuming the stiffener shown in Figure B, the deflection

$$y = - \frac{5 WL^3}{384 EI}$$

where

$$W = w \times L = 1.25 \times 50 = 62.5\#$$

$$E = \text{Modulus of Elasticity} = 10 \times 10^6$$

$$I = \text{Cross Sectional Moment of Inertia of Stiffener} = .10 \text{ in}^4$$

$$y = - \frac{5 \times 62.5 (50)^3}{384 \times 10^7 \times .10}$$

$$= \frac{3.90}{38.4} = .1015 \text{ inch}$$

Bending moment

$$M = \frac{WL}{8} = \frac{62.5 \times 50}{8} = 391 \text{ in}\#$$

Bending stress

$$S = \frac{M_c}{I} = \frac{391 \times 1.0}{.10} = 3910 \text{ psi}$$

The deflection should control the stiffener cross section due to the presence of heat exchanger coils and screen on the cylindrical surface.

$$w = .125 \times 10 = 1.25\#/\text{in}$$

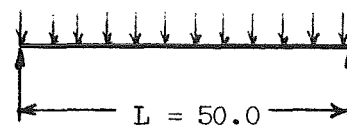


Figure A

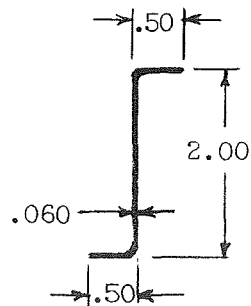


Figure B

Figure 5-26. Outboard Cylindrical Section Stiffeners.

The 1/8 psi external loading on the surfaces causes an approximate shear panel loading condition shown in Figure A. The expression for elastic instability of flat sheets in comparison is

$$*S_c = \frac{\pi^2 K_c E}{12 (1-\nu^2)} \left( \frac{t}{b} \right)^2$$

where

$S_c$  = compression buckling stress

$K_c$  = buckling coefficient.

For  $a/b = 36/72 = .5$

$K_c = 10$  (from curve p.C5.3)

$\nu$  = Poisson's ratio = .3

$t = .040$  effective gauge

therefore

$$\begin{aligned} S_c &= \frac{\pi^2 \times 10 \times 10^7}{12 [1-(.3)^2]} \left( \frac{.040}{72} \right)^2 \\ &= \frac{\pi^2 \times 30.9}{12 \times .91} \\ &= 27.9 \text{ psi} \end{aligned}$$

$$w = .125 \times 48.0 = 6\#/\text{inch}$$

where

48.0 = average length between shear panels, and

.125 = the external pressure

The applied compressive stress

$$S'_c = \frac{w}{t} = \frac{6}{.04} = 150 \text{ psi}$$

Since  $S_c < S'_c$ , stiffeners, increasing "t," or a combination of these is required.

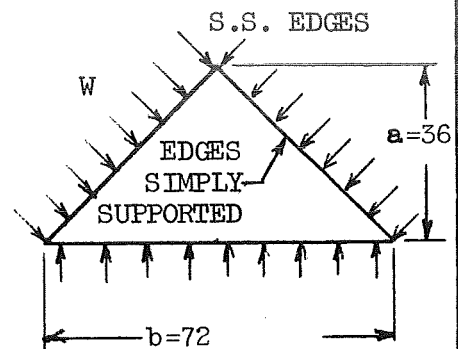


Figure A

\* Bruhn, 1965, p. C6.1

Figure 5-27. Shear Panel Estimate.

If two stiffeners are used which divide the panel into one triangular and two rectangular areas (per Figure B), the dimensions a and b for the triangular section reduce to 20 and 40 respectively.

$$S_c = \frac{\pi^2 \times 10 \times 10^7}{12 [1 - (.3)^2]} \left( \frac{.040}{40} \right)^2$$

= 90.5 psi which is less than the applied stress

It is recommended that stiffeners be applied to the panel as shown in Figure C. The location of these stiffeners match the panel ring locations. For the triangular section, a and b then become 10 and 20 respectively.

$$S_c = \frac{\pi^2 \times 10 \times 10^7}{12 [1 - (.3)^2]} \left( \frac{.040}{20} \right)^2 = 362 \text{ psi}$$

If the gauge is reduced to .030

$$S_c = 204 \text{ psi}$$

compared to the applied stress of 200 psi for  $t = .030$ .

Affective  $t = .040$  is recommended due to additional loads from vibration, acceleration and the 1.50 psi acting on the forward panel.

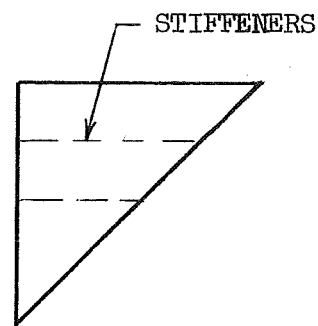


FIGURE B

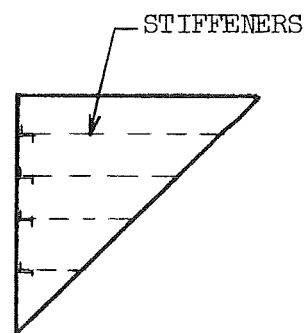


FIGURE C

Figure 5-28. Shear Panel Estimate (Continued).

When three stiffeners are used, rectangular panel sections are created with an approximate load condition per the Figure D. The a and b dimensions are for the forward section of the shear panel assembly.

When  $S_x = S_y$ , then the critical compressive buckling stress

$$S = S_e \left[ m^2 + n^2 \frac{a^2}{b^2} \right]$$

where

$$S_e = \frac{\pi^2 D}{a^2 t}$$

$$D = \text{flexure rigidity} = \frac{Et^3}{12(1-\nu^2)}$$

t = thickness = .040

E = Modulus of Elasticity =  $10 \times 10^6$

$\nu$  = Poisson's Ratio = .3

therefore

$$D = \frac{10^7 (.040)^3}{12(1-.09)} = \frac{640}{10.91} = 58.6$$

and

$$S_e = \frac{\pi^2 \times 58.6}{(50)^2 (.040)} = 5.77$$

M and n = number of half waves in the buckled plate in the x and y directions. For our case assume  $m = n = 1$ .

Therefore

$$S = S_e \left[ 1 + \frac{a^2}{b^2} \right] = 5.77 \times 40 = 231 \text{ psi}$$

The applied stress due to the 1/8 psi external pressure = 150 psi.

\* Theory of Elastic Stability, 2nd Edition by Timosheijko, p 358

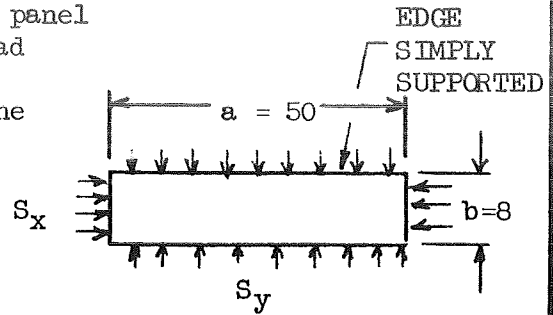


FIGURE D

Figure 5-29. Shear Panel Estimate (Continued).

The forward panel radial stiffeners reduce the span of the circumferential members by attaching to the outboard and inboard corner rings. These radial members are subject to end reactions from the circumferential beams. The magnitude of the load varies due to the tapered configuration of the panel. For estimating purposes, the load condition of Figure A is assumed.

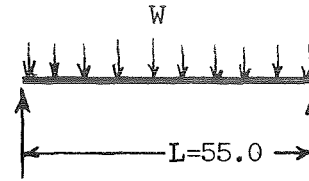


FIGURE A

The total load  $W = 412 \times 4 = 1648\#$  where the 412 is the total load for one 25 inch length circumferential beam and 4 is the number of beams.

The deflection

$$y = - \frac{5 W L^3}{384 EI}$$

where

$E$  = Modulus of Elasticity =  $10 \times 10^6$

$I$  = Moment of inertia of the beam cross section

If  $y$  is limited to .20 inches

$$I = \frac{5 \times 1648 \times (55)^3}{(.2) \times 384 \times 10^7} = 1.79 \text{ in}^4$$

The cross section shown in Figure B is used.

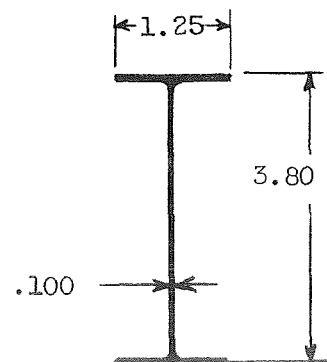


FIGURE B

Figure 5-30. Forward Panel Radial Stiffener Estimate.

The deflector screen assembly is exposed to 3/16 psi pressure differential. The stiffener system includes radial members subject to the load conditions of Figure A.

The deflection

$$y = - \frac{5WL^3}{384 EI}$$

where

$$W = 2.25 \times 24 = 54\#$$

$$E = \text{Modulus of Elasticity} = 10 \times 10^6$$

I = Cross sectional moment of inertia

If y is limited to .10

$$\begin{aligned} .100 &= \frac{5 \times 54 (24)^3}{384 \times 10^7 \times I} \\ &= \frac{.373}{384 I} \end{aligned}$$

therefore

$$I = \frac{.373}{38.4} = .00972 \text{ in}^4$$

$$M = \frac{WL}{8} = \frac{54 \times 24}{8} = 162 \text{ in } \#$$

$$S = \frac{M_c}{I} = \frac{162 \times .50}{.01} = 162 \times 50 = 8100 \text{ psi}$$

Use Z or angle members equivalent to Figure B.

$$w = \frac{\text{PANEL}}{\text{WIDTH}} \times \text{PRESSURE}$$

$$w = 12 \times 3/16 = 2.25\#/\text{in}$$

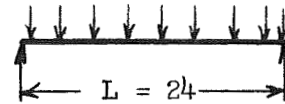


FIGURE A

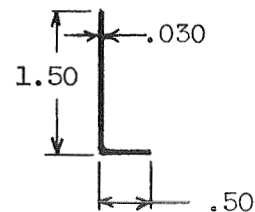


FIGURE B

Figure 5-31. Screen Deflector Stiffener Estimate.

## 5.2 S-IVC OXIDIZER START SYSTEM DESIGN

The following analysis was conducted for the oxidizer start reservoir (including an outlet screen and tank wall heat exchangers) and the outlet duct accessories. The basic parameters, ground rules, and general arrangement are shown in Figure 5-32. The external loading shown is considered an ultimate value which includes allowances for impact and margins of safety. The effort includes a basic structural analysis; detailed weight breakdowns for both the reservoir and the feed duct accessories; and a set of design drawings describing the structural arrangement, attachments, heat exchangers, and screened surfaces.

The reservoir is a conical shaped member equipped with a cylindrical skirt which in turn is attached to a land section provided on the tank wall. The forward end of the conical section and the aft skirt are equipped with capillary screens which in turn are supported by perforated sheet metal skins. Since the assembly is subject to external loading, vibration and acceleration, a stiffener system using rings and stringers are required.

The outlet screen located aft of the reservoir assembly is a circular member supported by a perforated diaphragm. The unit is attached to a land section integral with the oxidizer tank wall.

Two heat exchanger coils (one located forward of the reservoir support area and one positioned near the support area) are required. These coils are webbed tubular members welded to the outside surface of the tank.

The outlet duct accessories consist of heat exchanger coils, a gas/liquid interface screen, and interface tubes. A design drawing is included which outlines the hardware arrangements and relations to existing equipment.

**5.2.1 RESERVOIR STRUCTURE** — The basic structural arrangement is shown in Figure 5-33. Four rings at the inboard side and 24 stringers on the outboard face provide the stiffener system for the sheet metal conical skin. "Z" sections are used for both the rings and the radial members. A ring located at the forward end and one at the base interconnect the stringers and the conical panel for resisting radial loads. A skirt section consisting of a perforated cylinder (one end flanged) is attached to the base ring and to the tank wall land. The perforated area is covered with a capillary screen.

Figure 5-34 shows the basic geometry at the apex area and the attachments between the screen, ring, conical skin and radial stiffeners. The screen is a separate assembly consisting of a perforated support diaphragm seam welded to the screen using one back up strip. The assembly is riveted or bolted to the ring. The diameters of the above units could be increased for accessibility purposes if required. The radial stringers, conical skin and an inboard collar piece are riveted to the ring. The collar provides additional cross sectional area for resisting the compressive loads.

# MAT'L & ALLOWABLES

2219 - T62

F<sub>TU</sub> = 54,000

F<sub>TY</sub> = 36,000

\*FWD COIL CONTINUOUSLY  
ATTACHED TO TANK WALL.  
AFT COIL ATTACHED @  
17 POINTS (1.0" LG'T WELD PATCHES)

HEAT EXCHANGER TUBES  
MOUNTED ON OUTSIDE FACE  
OF TANK WALL - 2 TURNS  
1/2 O.D. X .030 WALL.\*

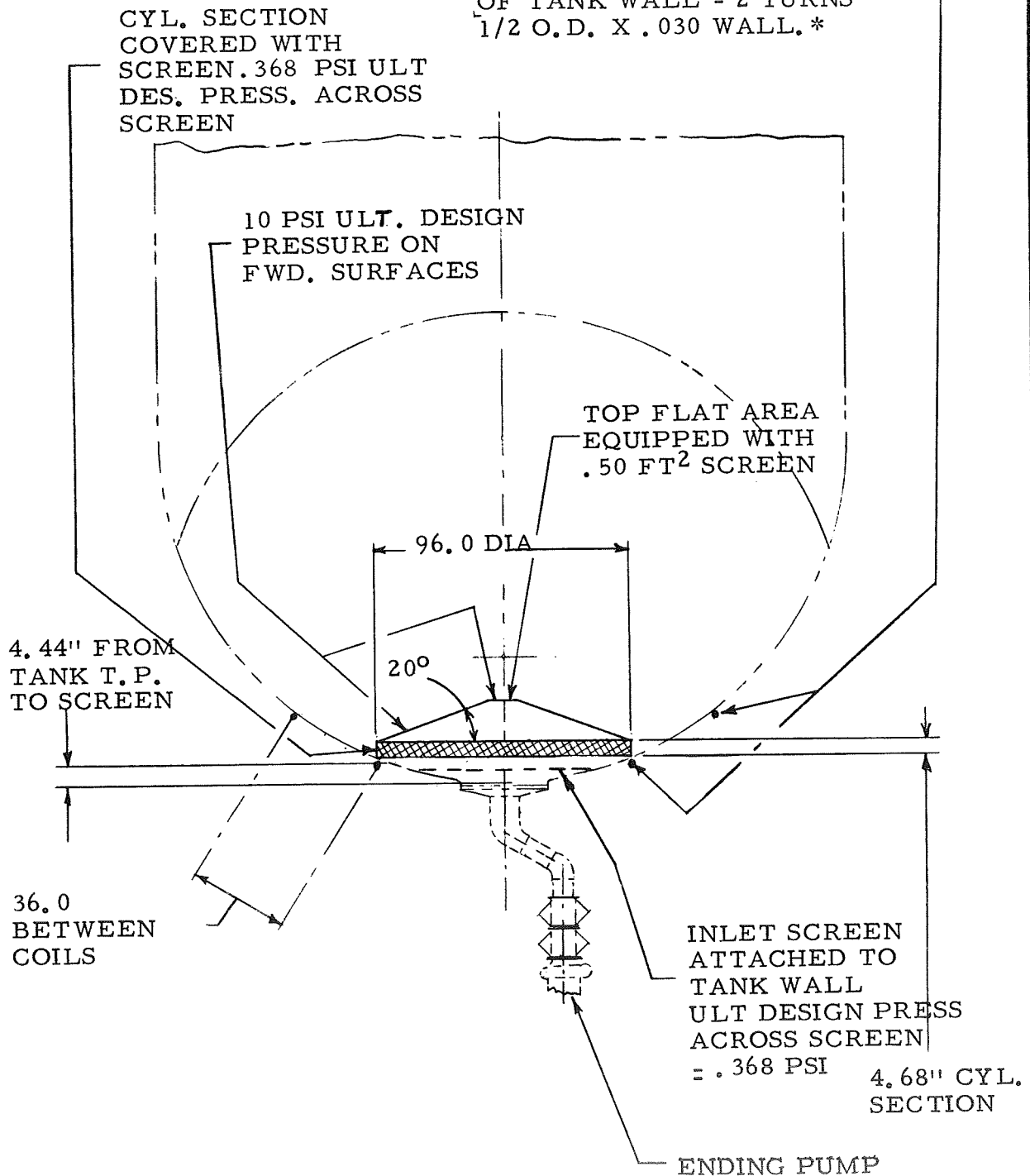
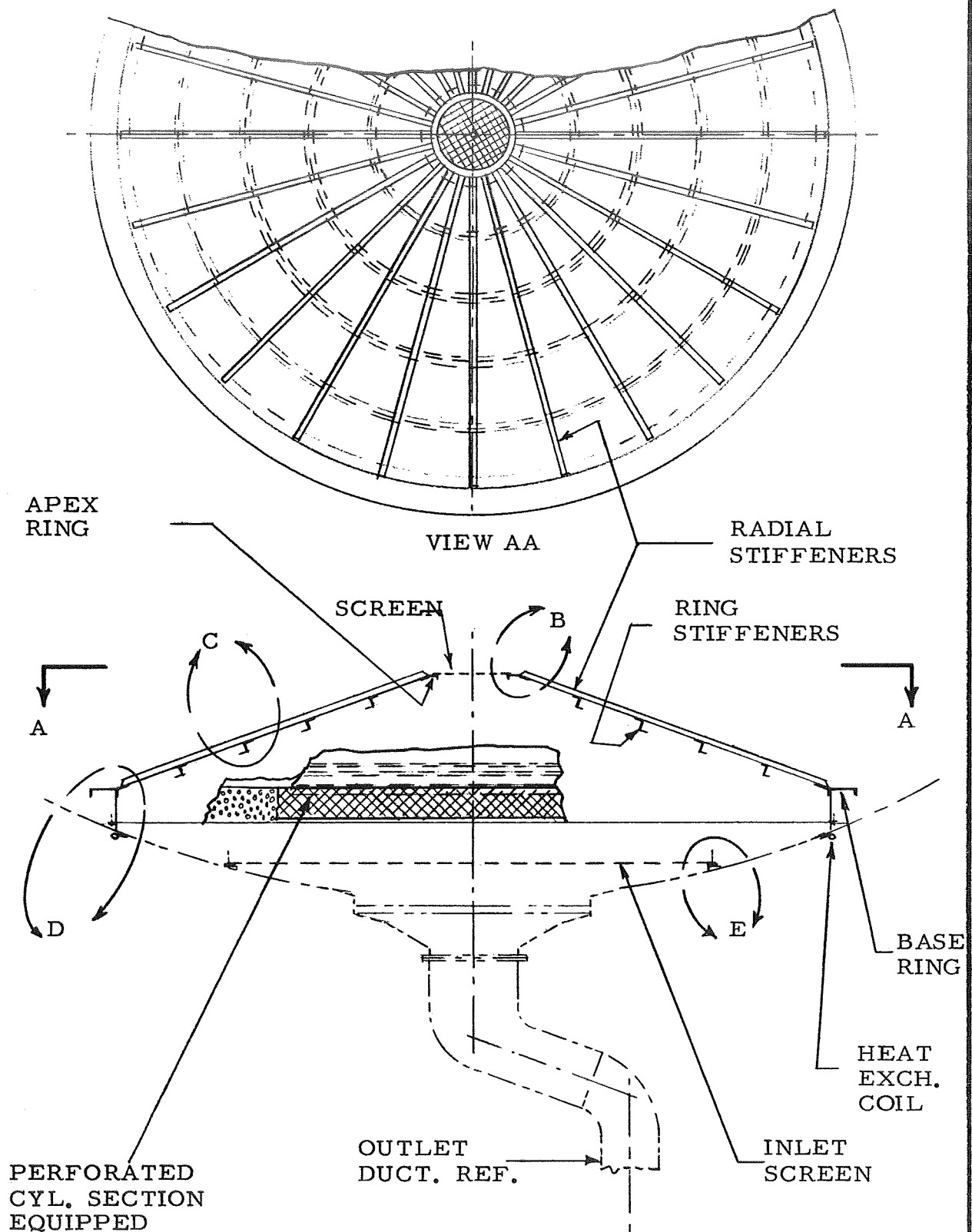
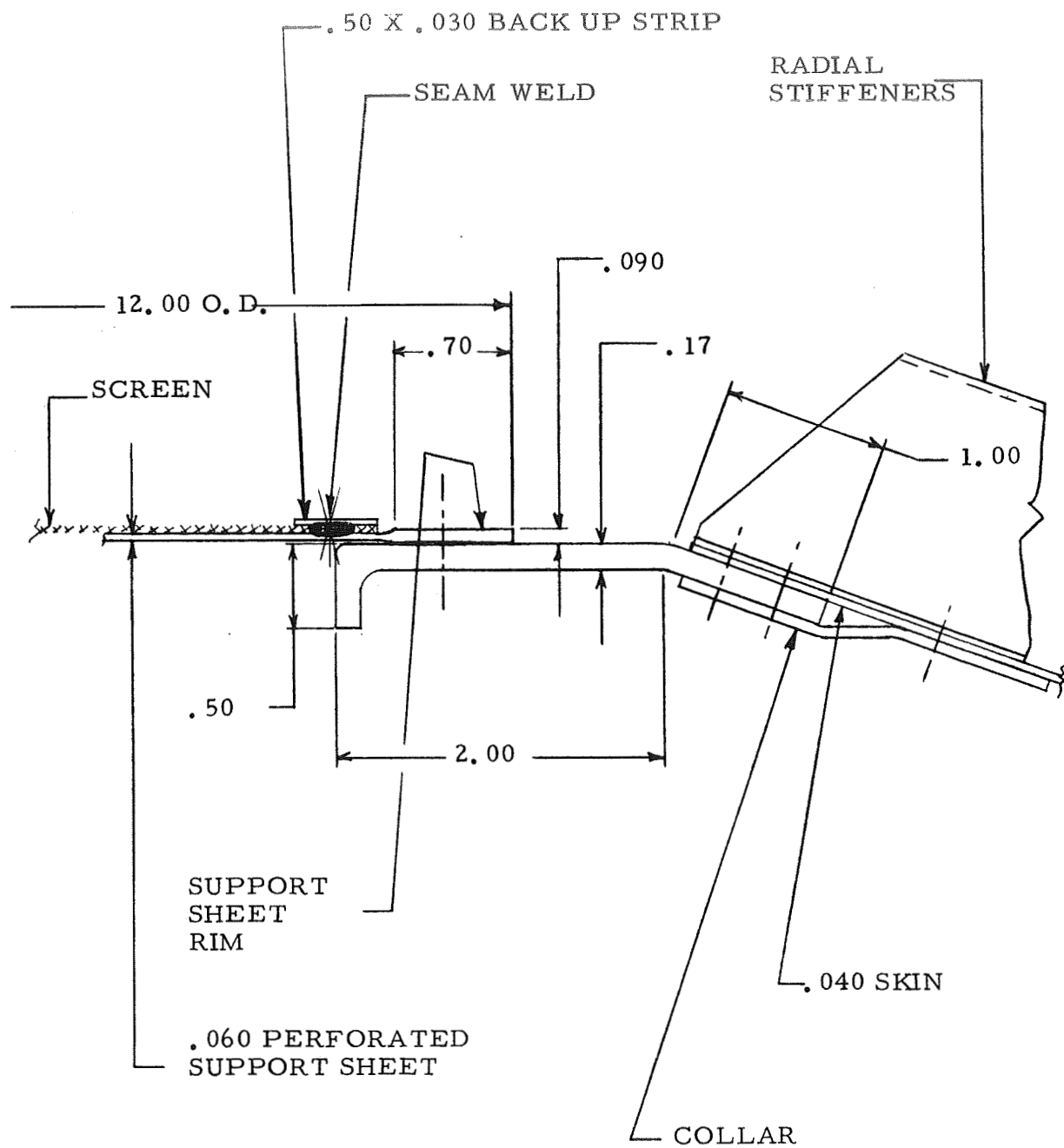


Figure 5-32. Oxidizer Tank Reservoir General Arrangement and Design Ground Rules.



THE DESIGN ASSUMES ONE ADDITIONAL ACCESS OPENING IN THE OXIDIZER TANK. RESERVOIR IS PLACE IN TANK PRIOR TO FINAL WELD. RESERVOIR CAN INCORPORATE ACCESS OPENING IF REQUIRED.

Figure 5-33. Oxidizer Reservoir Structural Arrangement.



VIEW "B"  
(SEE STRUCTURAL ARRANGEMENT DRAWING)

Figure 5-34. Oxidizer Reservoir Structural Details.

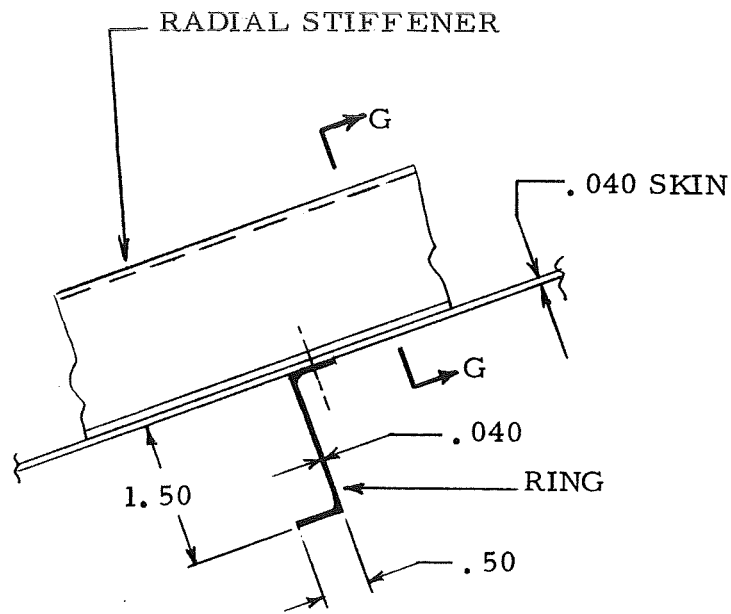
The attachments between stiffeners, and the basic profiles are shown in Figure 5-35. "Z" type sections are used for both members with riveted connections at junctions formed by the flanges and the skin.

Figure 5-36 outlines the ring, cylinder, screen and heat exchanger coil at the aft end. The base ring is a channel shaped member equipped with a web for attachment to the conical skin and to the stiffeners. One leg of the ring is attached to the skirt section. The cylindrical portion of the assembly is a perforated sheet metal band equipped with a flange at the aft end and a capillary screen which covers the outboard surface of the perforated area. The screen is attached by seam welding to the forward and aft ends of the cylinder using back-up strips. A local ring type land equipped with tapped holes is provided in the tank wall for attaching the reservoir assembly. The outboard face of this attachment zone is a series of local bosses for the tapped holes. The heat exchanger coil required near the support zone is a single turn unit consisting of a tube equipped with 17 local web sections or tabs which in turn are seam welded to the tank wall. A second single turn coil located forward of this area (see Figure 5-32 ) has identical attachment methods except a continuous web and seam weld replaces the local tabs. Jumper tubes are used to interconnect the coils through a by-pass valve (see fuel system schematic).

The outlet screen located aft of the reservoir assembly is shown in Figure 5-37. The unit consists of a perforated diaphragm equipped with a corrugated shaped screen seam welded at the perimeter using a back-up strip. The assembly is bolted to a local land area in the tank wall which contains tapped holes. Similar to the reservoir support area, the outboard side opposite the tapped holes contains a series of local bosses for accommodating the thread depths.

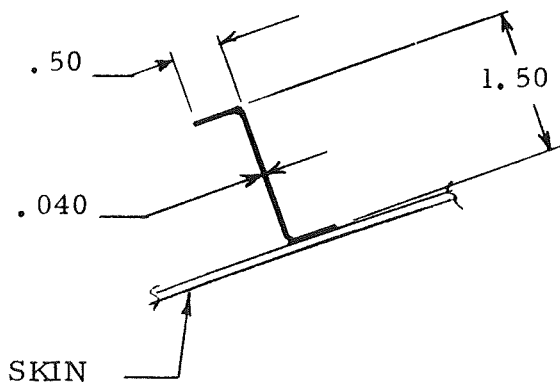
**5.2.2 OUTLET DUCT ACCESSORIES** — The outlet duct is an assembly of elbows, flex joints and a special gimbal section for absorbing the engine interface motions during thrust vector control. It is required to equip the duct with an internal gas/liquid interface screen, external heat exchanger coils, and a downstream relief line. Figure 5-38 shows the general arrangement and relations to the existing equipment. The heat exchanger section forward of the gimbal duct assembly is a helical coil brazed to the duct wall. For the gimbal portion, a single turn is used at three flanges and interconnected with jumper tubes which in turn incorporate flexing provisions for absorbing the length changes between flanges. An alternate design would use flanges containing flow passages and terminal bosses for interconnecting the paths.

The gas/liquid interface screen is a conical assembly containing a fitting at the base which in turn is welded to the duct components (see the arrangement for the fuel system). A relief line routing from the downstream side of the screen to a tank wall penetration boss is included. Both the heat exchanger supply and the relief tubes are supported from the duct walls using clips and standard clamps. Considerable



VIEW "C"

(SEE STRUCTURAL ARRANGEMENT DRAWING)



VIEW "GG"

Figure 5-35. Oxidizer Reservoir Structural Details.

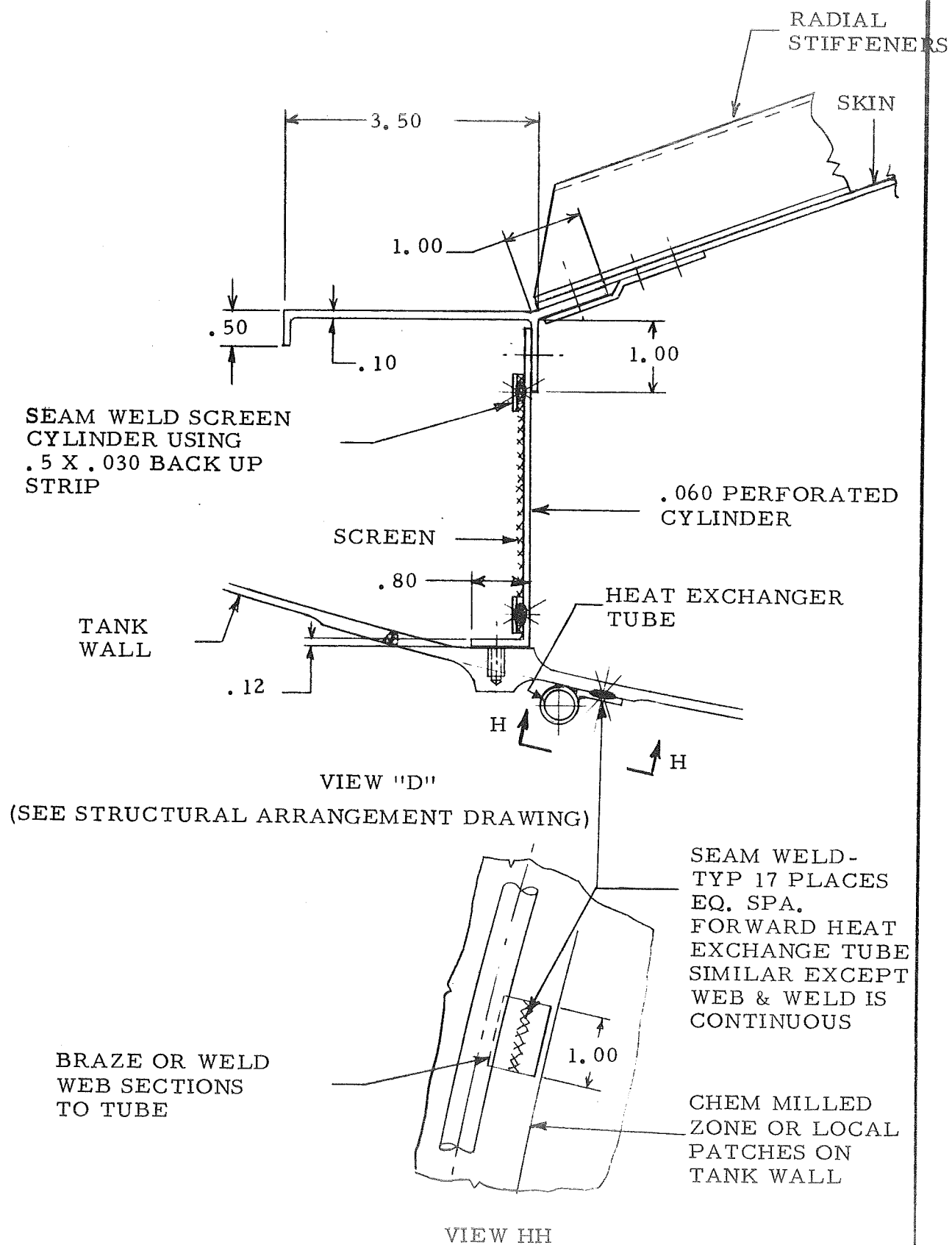


Figure 5-36. Oxidizer Tank Reservoir Structural Details.

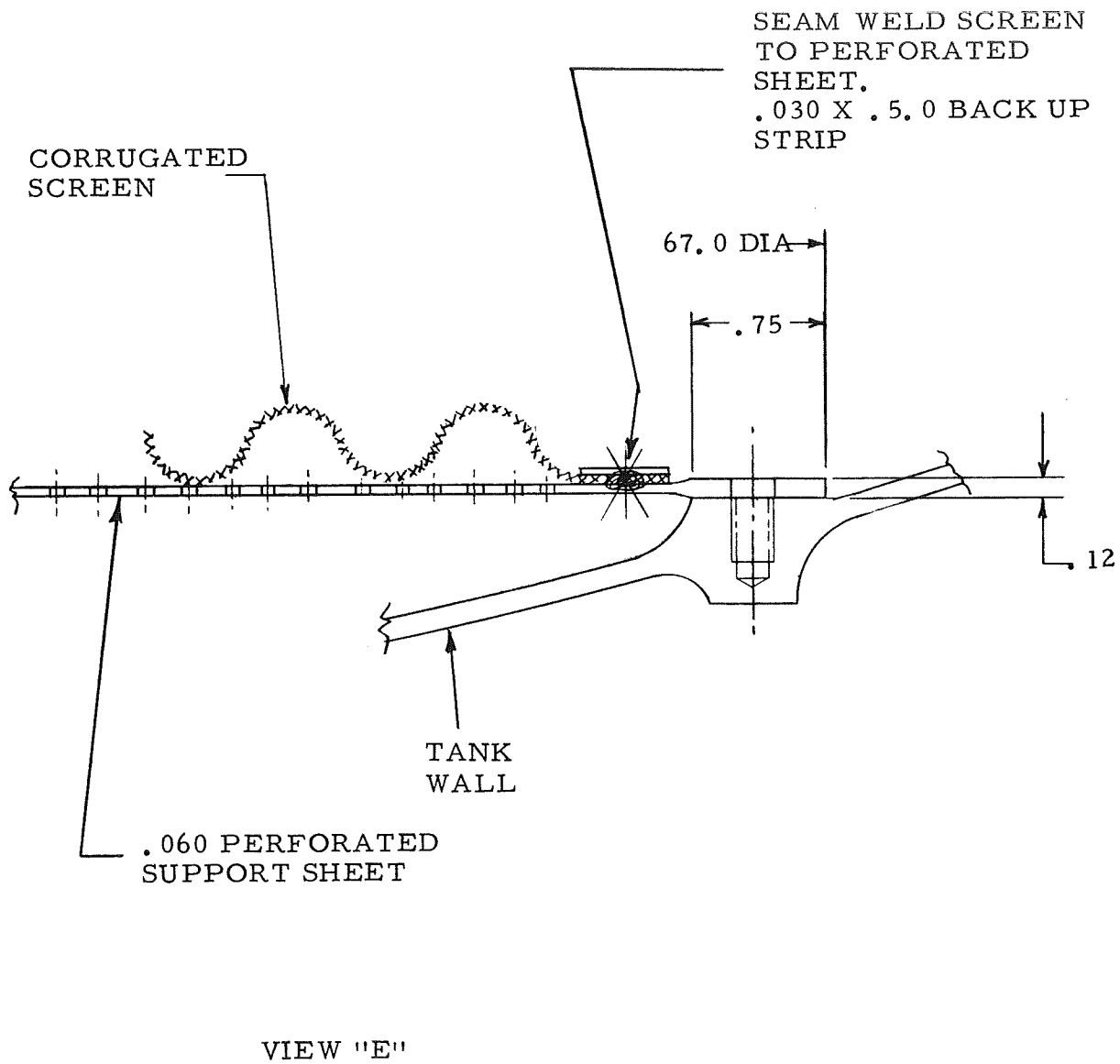


Figure 5-37. Oxidizer Tank Inlet Screen Details.

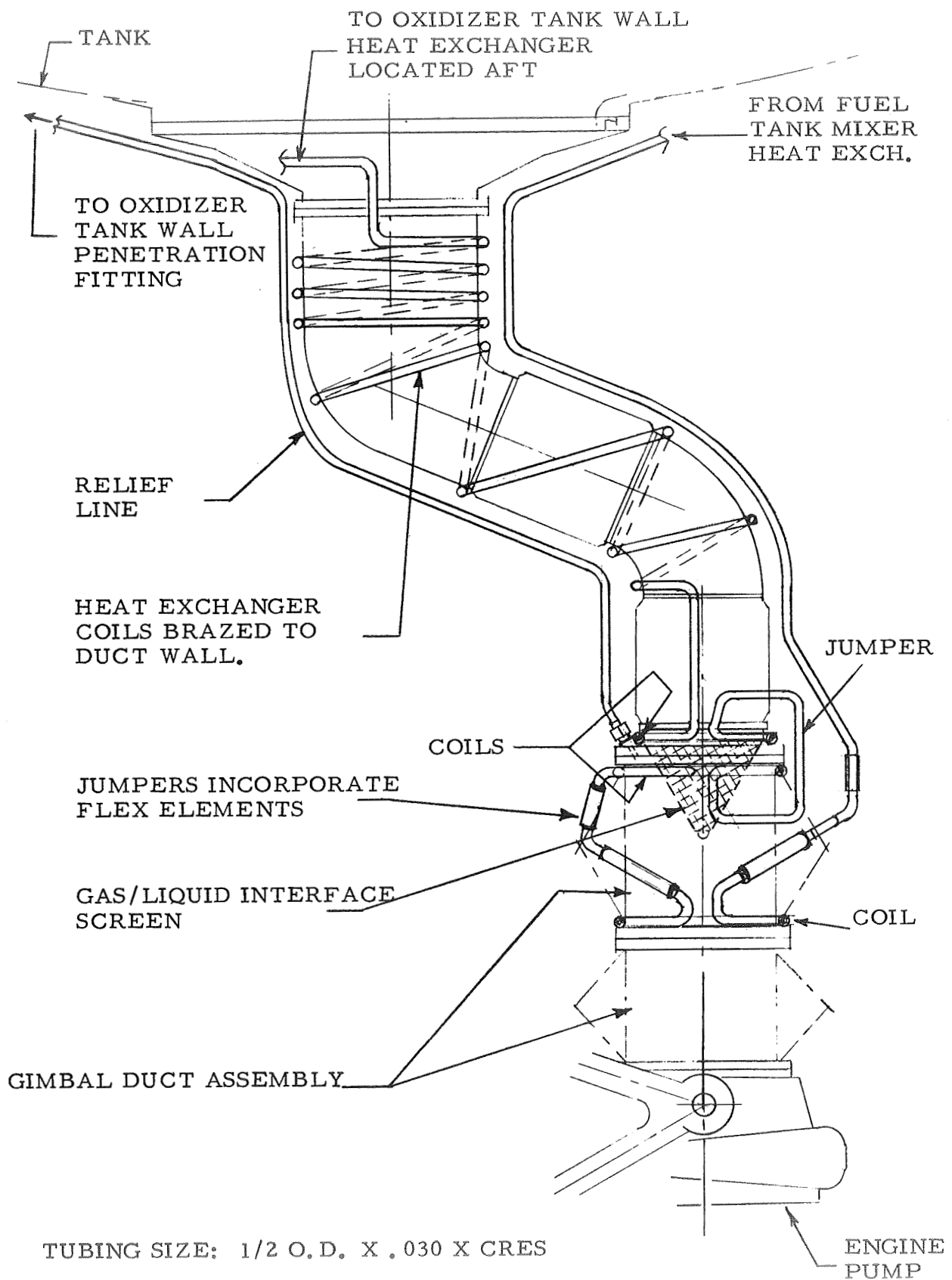


Figure 5-38. Oxidizer Feed Duct Accessories.

rework of the oxidizer duct assembly is expected. The screen location shown will require redesign of the flanges and the interface between flanges and bellows. The revision is further complicated when considering jumpers which must have a fatigue life equal to or greater than the bellows.

5.2.3 WEIGHT ESTIMATES — Figures 5-39 and -40 summarize a detailed weight breakdown for the oxidizer reservoir, inlet screen and tank wall heat exchangers. The list includes all major structural members, screens, welding backup strips, material added to the tank wall for attachments, and an allowance for miscellaneous fasteners. Equivalent gages were used for those areas having perforations. The parts list includes the basic geometry for each component as a reference.

A similar weight analysis is shown in Figure 5-41 for the oxidizer feed duct access-ories.

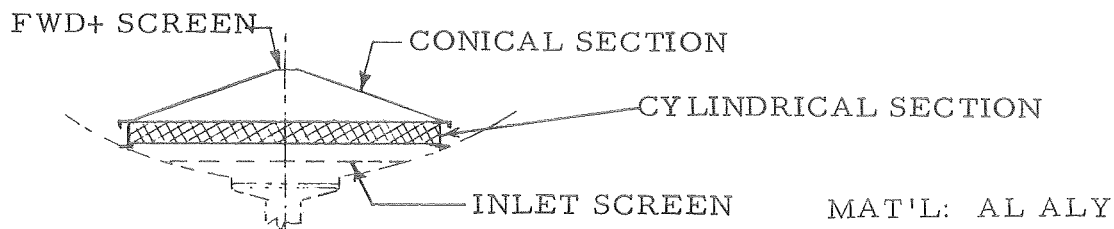
5.2.4 STRUCTURAL ANALYSIS — Simplified approaches were used in sizing all structural members. The overall load condition is shown in Figure 5-42 for the base ring of the conical section. The uniform pressure acting on the forward surface creates a kick load at the base which is reacted by hoop tension in the ring.

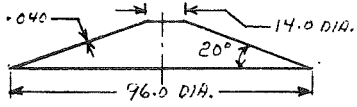
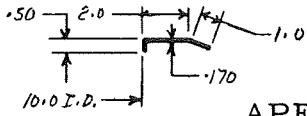
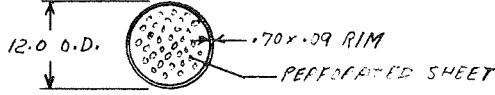
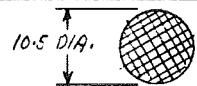


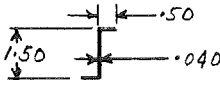
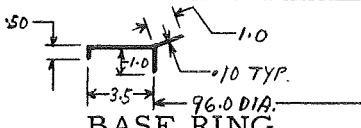
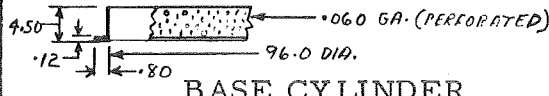
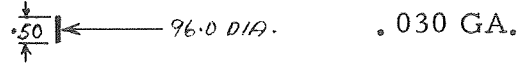
Figure 5-43 outlines the approach used for estimating the radial stiffener or stringer cross sections. The members in effect are continuous beam columns on elastic supports. A section of the beam between stiffener rings is isolated and treated as a uniformly loaded beam column with an end fixity equal to one. The member is also checked for critical buckling stress. A section of skin attached to the flange (which contributes to overall strength of the beam) is neglected in this analysis. For compressive modes, it is assumed that a portion of the skin and the stringers share the loads. The uniform load "w" was determined by the pressure acting on the maximum panel size located at the base. The above is conservative but is assumed to compensate for additional requirements that may arise from a detailed investigation.

The stringers for the conical section have intermediate elastic supports which are the rings located at the inboard side. An equivalent radius was assumed and the cross section of the rings estimated using the relation shown in Figure 5-44 which is for cylindrical shells.

The ring at the forward end of the cone is exposed to external loading per the conditions shown in Figure 5-45. The member is checked for critical buckling load, for compressive stress, and the cross sectional area estimate.

The forward screen is supported by a perforated sheet metal member which is attached at the perimeter to the apex ring. The unit acts as a uniformly loaded diaphragm with



DESCRIPTION	WT. LBS	REMARKS
 <p>CONICAL SECTION SKIN</p>	31.00	
 <p>APEX RING</p>	2.43	
 <p>FWD. SCREEN SUPPORT</p>	.50	.030 AFFECTIVE GA.
 <p>FORWARD SCREEN</p>	.04	.053 #/FT <sup>2</sup>
 <p>FWD SCREEN BACK UP STRIP</p>	.05	
 <p>STIFFENER RINGS</p> <div style="display: flex; justify-content: space-between;"> <div></div> <div> <p>*DIA'S.</p> <p>80.0</p> <p>62.0</p> <p>45.0</p> <p>28.0</p> </div> </div>	6.75	4 REQ'D. 675" LG'T TOTAL
 <p>RADIAL STIFFENERS</p> <div style="display: flex; justify-content: space-between;"> <div></div> <div> <p>44.0</p> <p>LENGTH</p> </div> </div>	10.55	24 REQ'D.
 <p>BASE RING</p>	18.85	
 <p>BASE CYLINDER</p>	8.35	
 <p>BACK UP STRIPS</p>	.45	2 REQ'D.

CONTINUED ON NEXT PAGE

Figure 5-39. Oxidizer Reservoir Weight Estimate.

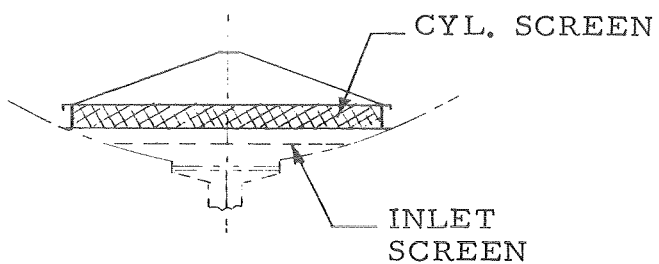

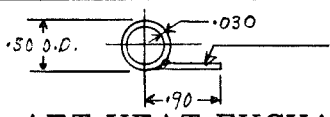

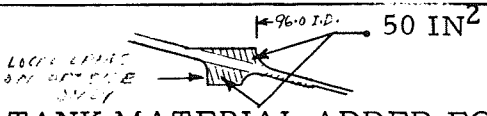
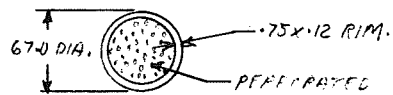
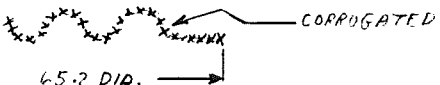
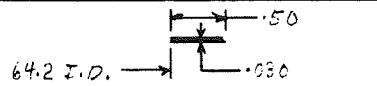
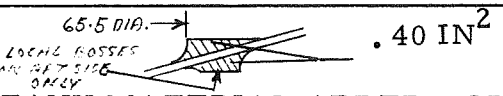
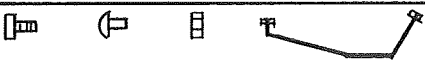
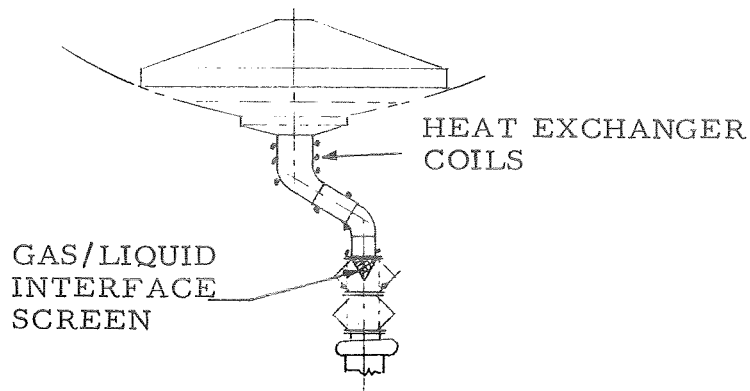
		
DESCRIPTION	WT. LBS	REMARKS
 CYLINDER SCREEN	.41	.053 #/FT <sup>2</sup>
 LOCAL LABS (17) AFT HEAT EXCHANGER COIL	1.41	300" LG'T. 1 TURN @ 96.0 DIA.
 SAME AS ABOVE EXCEPT WEB IS CONTINUOUS AFT HEAT EXCHANGE COIL	3.71	500 " LG'T. 1 TURN AT 160.0 DIA.
 TANK MATERIAL ADDED FOR RESERVOIR ATTACHMENT	11.25	INCLUDES ALLOW FOR HEAT EXCH. COIL WELD LANDS
 OUTLET SCREENS SUPPORT	11.97	.030 AFFECTIVE GA.
 OUTLET SCREEN	1.84	.075 #/FT <sup>2</sup>
 BACK UP STRIP	.31	
 TANK MATERIAL ADDED FOR OUTLET SCREEN	6.28	
 MSC. FASTENERS & JUMPER TUBES	5.00	
TOTAL	121.12	
5% CONTINGENCIES	66.05	
GRAND TOTAL	127.17	

Figure 5-40. Oxidizer Reservoir Weight Estimate (Continued).










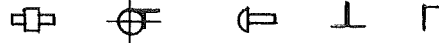
ITEM	WT. LBS	REMARKS
 1/0 O. D. X HEAT EXCH. COIL .030 CRES	5.65	10 TURNS TOTAL 400" TOTAL INCL. ENDS
 BRAZE MATERIAL	2.00	
 FLEX JUMPERS	4.00	
 SCREEN ASSY INCL. ENDS	5.00	
 1/2 X .030 INLET LINE AL. ALY.	1.50	240" LG'T. HAS END FTG'S.
 OUTLET LINE	.75	100" LG'T.
 TANK WALL FITTINGS	.85	
 MSC. FTG'S, CLAMPS, NUTS, BOLTS	1.40	
TOTAL  10% CONTINGENCIES  GRAND TOTAL		
	19.15	
	1.92	
	21.07	

Figure 5-41. Oxidizer Accessories Weight Estimate.

The conical portion of the reservoir is subject to a uniform load due to propellant impingement. This loading causes a radial reaction at the base of the core which is reacted with a ring (see Figure A).

The total load

$$\begin{aligned} P &= w \times .785 (96.0)^2 \\ &= 10 \times 7230 \\ &= 72300\# \end{aligned}$$

The reaction per inch in the y-y direction

$$\begin{aligned} N_y &= \frac{72300}{\pi \times 96} \\ &= 240\#/\text{in.} \end{aligned}$$

$$N_R = \frac{P \cot 20^\circ}{\pi \times 96} = \frac{72300 \times 2.75}{302} = 658\#/\text{in}$$

The base ring is in hoop tension as shown in Figure B. The magnitude of this tension load =  $N_R 2R = 658 \times 96 = 63200\#$ .

The ultimate room temperature tensile strength for 2219-762 aluminum alloy  $F_{t_u} = 54000$  psi, therefore the cross sectional area of the ring

$$A = \frac{63200}{2 \times 54000} = .585 \text{ in}^2$$

The section shown in Figure C is used.

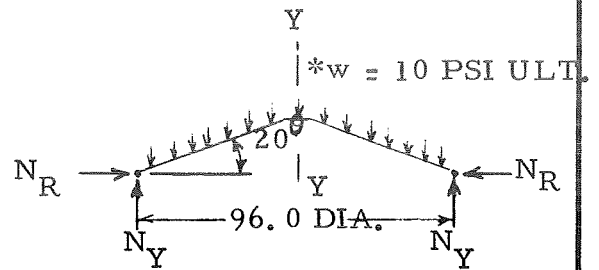


Figure A.

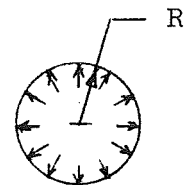


Figure B

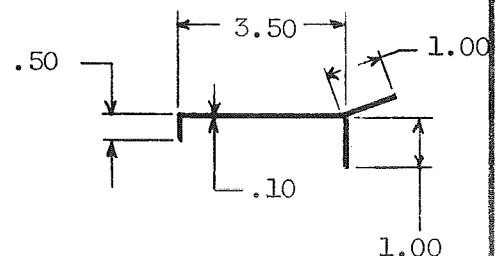


Figure C

Figure 5-42. Oxidizer Reservoir Base Ring Estimate for Conical Section.

If the stiffeners are treated as beam columns,

$$N_L = \frac{P}{24 \sin 20^\circ} = \frac{72300}{24 \times .342} = 8800 \#$$

24 is the number of stringers.

The maximum bending moment

$$M = \frac{w \ell^2}{8} \lambda(\mu) *$$

where

$$\lambda(\mu) \text{ is a function of } \mu = \frac{\ell}{2} \sqrt{\frac{P}{EI}}$$

$$E = \text{Modulus of Elasticity} = 10 \times 10^6$$

$$I = \text{Cross Section Moment of Inertia} = .03375 \text{ in}^4$$

$$\mu = \frac{9}{2} \sqrt{\frac{8800}{10^7 \times .03375}} = 4.5 \sqrt{\frac{8.80}{337}} = 4.5 \times .1615 = .726$$

$$2\mu = 1.452$$

$$\text{From Table A-2 p. 529 } * \lambda(\mu) = 1.28$$

$$M = \frac{93.9 \times (9)^2}{8} \times 1.28 = 1218 \text{ in}\#$$

$$\text{Bending Stress} = \frac{1218 \times .75}{.03375} = 27000 \text{ psi}$$

The stringers are subject to local buckling.  
The critical buckling compressive stress

$$S = \frac{K_w \pi^2 E}{12(1-\nu^2)} \left(\frac{t_w}{b_w}\right)^2 **$$

where

$K_w$  = buckling coefficient

$$\frac{b_F}{b_w} = \frac{.46}{1.46} = .315 \text{ and } \frac{t_w}{t_F} = 1.0$$

From Figure C6-4 \*\*

$$K_w = 4.30$$

\* Theory of Elastic Stability by Timoshenko, Second Edition, p 10

\*\* Bruhn, 1965, p. C6-2 and C6.3

$$w = \left(\frac{\text{UNIT}}{\text{PRESS.}}\right) \times \cos 20^\circ \times \left(\frac{\text{MAX. PANEL}}{\text{WIDTH}}\right)$$

$$= 10 \times .939 \times 10 = 93.9 \#/\text{in.}$$

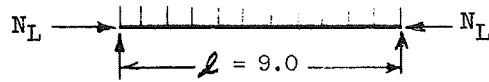


Figure A

$$b_F = .50 - .04 = .46$$

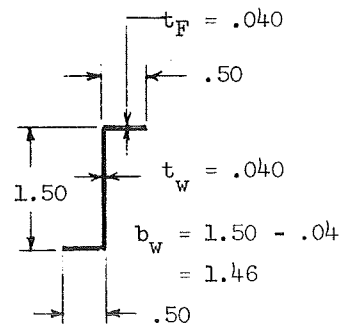


Figure B

Figure 5-43. Oxidizer Reservoir Stiffener Estimate for Conical Section

$$V = \text{Poisson's Ratio} = .30$$

$$(1 - V^2) = .91$$

$$\left(\frac{t_w}{b_w}\right) = \frac{.040}{1.46} = .0274$$

$$S = \frac{4.30 \times \pi^2 \times 10^7}{12 \times .91} (.0274)^2$$

$$= \frac{42.4 \times 7500}{10.91} = 29100 \text{ psi}$$

Figure B section is used. It is assumed that the compressive stress is distributed to the stiffeners and the skin (no skin buckling). A local doubler near the apex may be required.

Figure 5-43. Oxidizer Reservoir Stiffener Estimate  
for Conical Section (Continued).

The radial stiffeners located on the forward side of the cone are subject to the column loads due to  $N_L$ . These members are continuous beams on elastic supports (see Figure A). The supports in this case are the rings located at the inboard side.

For estimating purposes, an equivalent cylinder is used and the moment of inertia section "I" for these rings expressed as follows:

$$I = \frac{C_F \times M \times D^2}{EL} *$$

where

$$C_F = \text{coefficient} = 6.84 \times 10^{-4}$$

$$M = \text{Equivalent Moment} = \pi R_1^2 N_L'$$

using an equivalent cylinder radius  $R_1 = 40.0$

$$N_L' \text{ for Equiv. Cyl.} = 698 \times \frac{48}{40} = 838 \#/\text{in.}$$

Therefore

$$M = \pi (40)^2 \times 838 = 4.22 \times 10^6$$

$$E = \text{Modulus of Elasticity} = 10 \times 10^6$$

$$L = \text{Ring Spacing} = 9.0 \text{ inches}$$

$$I = \frac{(6.84 \times 10^{-5}) (4.22 \times 10^6) (80)^2}{10 \times 10^6 \times 9} = .0205 \text{ in}^4$$

Use the section shown in Figure B

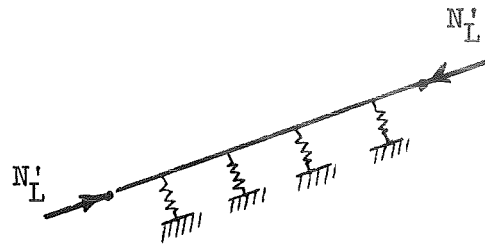


Figure A

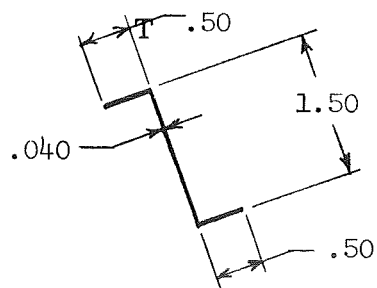


Figure B

\* Tech. Paper "Simplified Analysis of General Instability of Stiffened Shells in Pure Bending," By F. R. Shanley, 1949.

The radial load  $N_R$  for the base member is reacted at the apex region by a ring subject to the loading conditions of Figures A and B. The critical radial load

$$N_{CR} = \frac{3EI}{R^3} *$$

where

$E$  = Modulus of Elasticity

$$= 10 \times 10^6$$

$I$  = Cross Section Moment of Inertia

For  $N_{CR} = N'_R$

$$I = \frac{5264 (6)^3}{3 \times 10^7} = \frac{1138}{3} = .0379 \text{ in}^4$$

The compressive stress may control the ring cross section rather than the above relation, therefore using the configuration shown in Figure C, the cross sectional area  $A = 3.5 \times .17 = .595 \text{ in}^2$

Compressive stress

$$S = \frac{5264 \times 6}{.595} = 53000 \text{ PSI}$$

$F_{tu}$  for 2219-T62 Al Aly = 54000 PSI (R.T.)

Use Figure C cross section or equivalent.

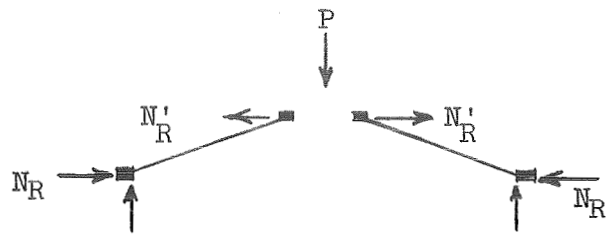


Figure A

$$N'_R = 658 \times \frac{48}{6} = 5264 \text{ \#/in}$$

$$= 5264 \text{ \#/in}$$

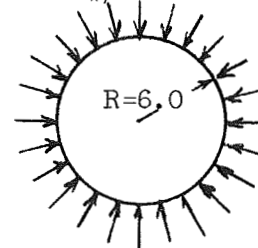


Figure B

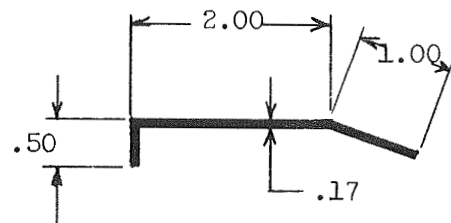


Figure C

\* Theory of Elastic Stability, by Timoshenko, 2nd Edition, Page 291.

Figure 5-45. Oxidizer Reservoir Apex Ring Estimate for Conical Section.

the edges held. An affective gage is used and the maximum stress and deflection estimated, per Figure 5-46 . To avoid stressing the screen, which may alter the absolute micron rating, it is recommended that the wire cloth member include flexing provisions. This latter feature would permit the screen load to be transferred to the diaphragm. A similar condition is shown in Figure 5-47 for the outlet screen located aft of the reservoir. A pleated type cross section is required for the outlet screen to satisfy the affective flow area. This configuration should include features for transferring the load from the wire cloth to the perforated support member.

The screen at the apex region of the conical section is supported with a perforated sheet which is subject to a uniform load (see Figure A). The load condition causes diaphragm stresses "S<sub>D</sub>" in the perforated member.

$$* S_D = 0.423 \sqrt[3]{\frac{E w^2 R^2}{t^2}} \text{ at the center.}$$

where

E = modulus of elasticity =  $10 \times 10^6$

t = .030 (minimum affectize gage).

$$S_D = 0.423 \sqrt[3]{\frac{10^7 \times (10)^2 \times 5^2}{(.030)^2}}$$

$$= .423 \sqrt[3]{2.78 \times 10^{13}}$$

$$= .423 \times 30300$$

$$= 12820 \text{ psi}$$

The maximum deflection at the center of

$$y = 0.662 R \sqrt[3]{\frac{wR}{Et}} *$$

$$= .182 \text{ in.}$$

It may be required to form the perimeter of the screen per Figure B to compensate for the deflection or add stiffeners to the perforated sheet.

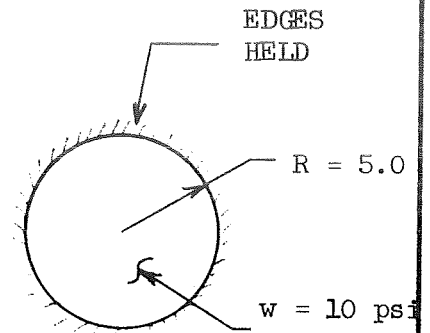


Figure A

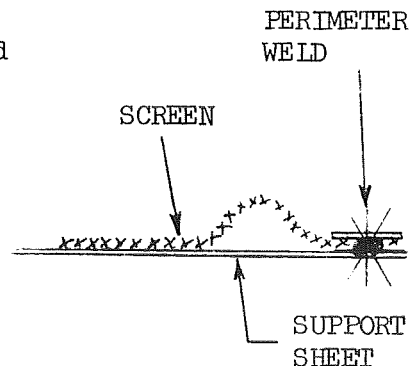


Figure B

\* Roark, 3rd Edition p. 223

Figure 5-46. Oxidizer Reservoir Support Skin Estimate for Forward Screen at Cone Apex.

The outlet screen located aft of the reservoir is supported by a perforated diaphragm which is subject to a uniform load.

The stress at the center

$$S_D = .423 \times \sqrt[3]{\frac{E w^2 R^2}{t^2}} *$$

where

$$E = 10 \times 10^6$$

Using an effective  $t = .030$

$$S_D = .423 \sqrt[3]{\frac{10^7 (.368)^2 (32)^2}{(.030)^2}}$$

$$= 11580$$

The deflection at the center

$$y = .662 R \sqrt[3]{\frac{w R}{E t}} = .720 \text{ in.}$$

The screen design includes convolute type pleats for increasing the effective area. This configuration should have sufficient flexibility to follow the above deflection without permanent deformation of the screen.

\*Roark, 3rd Edition. P, 223

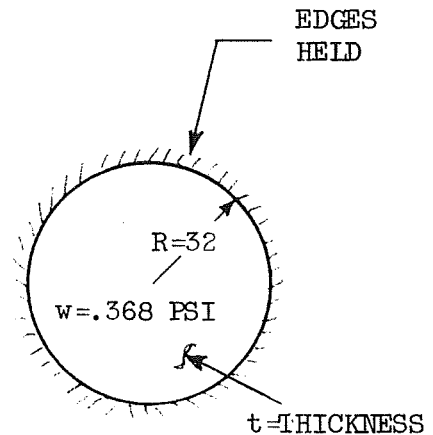


Figure A

Figure 5-47. Oxidizer Outlet Screen Support.

### 5.3 OXIDIZER TANKER COLLECTOR SYSTEM DESIGN

The collector system for the oxidizer tanker consists of eight channels interconnected at the equator with additional sections. The system includes a cylindrical reservoir located at the tank outlet which is attached to the eight collectors. Figure 5-48 outlines the general arrangement of the major components, and lists the design ground rules including loads, cooling coils and screened surfaces. A heat exchanger circuit schematic for the support areas and the outlet zone is shown in Figure 5-49. The study was conducted in two parts covering the collectors and the reservoir. A simplified structural check was made for major components and a detailed weight breakdown generated for each area.

Several structural approaches can be employed using honeycomb panels, truss core, waffle, monocoque and skin stringer frame. Each approach presents advantages and disadvantages relative to weight, manufacturing complexity, quality control, check-out, design complexity, cost and repairability. A comprehensive study would include design cuts for each of the candidates with a final selection based on tradeoffs. For this effort the "skin stringer frame" method was used due to relative simplicity and adaptability to ordinary manufacturing methods. The above was also considered for the fuel and oxidizer systems on the SIVB tanks.

**5.3.1 COLLECTOR STRUCTURAL DESIGN** — The collectors are rectangular box members extending from the reservoir to the forward area and are contoured to follow the spherical wall of the tank. A typical cross section consists of four "ZEE" shaped stiffeners (or stringers) interconnected with two flat perforated panels (see Figure 5-50). The web sections of each stringer contain holes. Both the panels and the two outboard members are covered with screens which are seam welded at the perimeters (using back up strips) which also serve as structural attachments.

An alternate approach is shown in Figure 5-51 which replaces the "Z" sections with channels. This latter method separates the screen attachment from the structural connections which may provide a manufacturing advantage. For example the panel can be equipped with capillary screens, checked out and cleaned prior to the final assembly. Furthermore the independent structural connection may be accomplished by welding or riveting. If rivets are used, the spacing may become critical because the interfaces must form a seal equivalent to a wetted screen. Seam welding is a reliable seal but presents disadvantages when considering re-work and maintaining a cleanliness level.

The Figure 5-51 design may also provide advantages during the assembly sequence. The two inboard channels for example are first attached to the face sheets using the 1-1/2-inch space between the panels for back up tool access. The second phase consists of positioning the two outboard members and attaching at the open flanged area. When using the "Z" sections of Figure 5-50, one face sheet only is attached

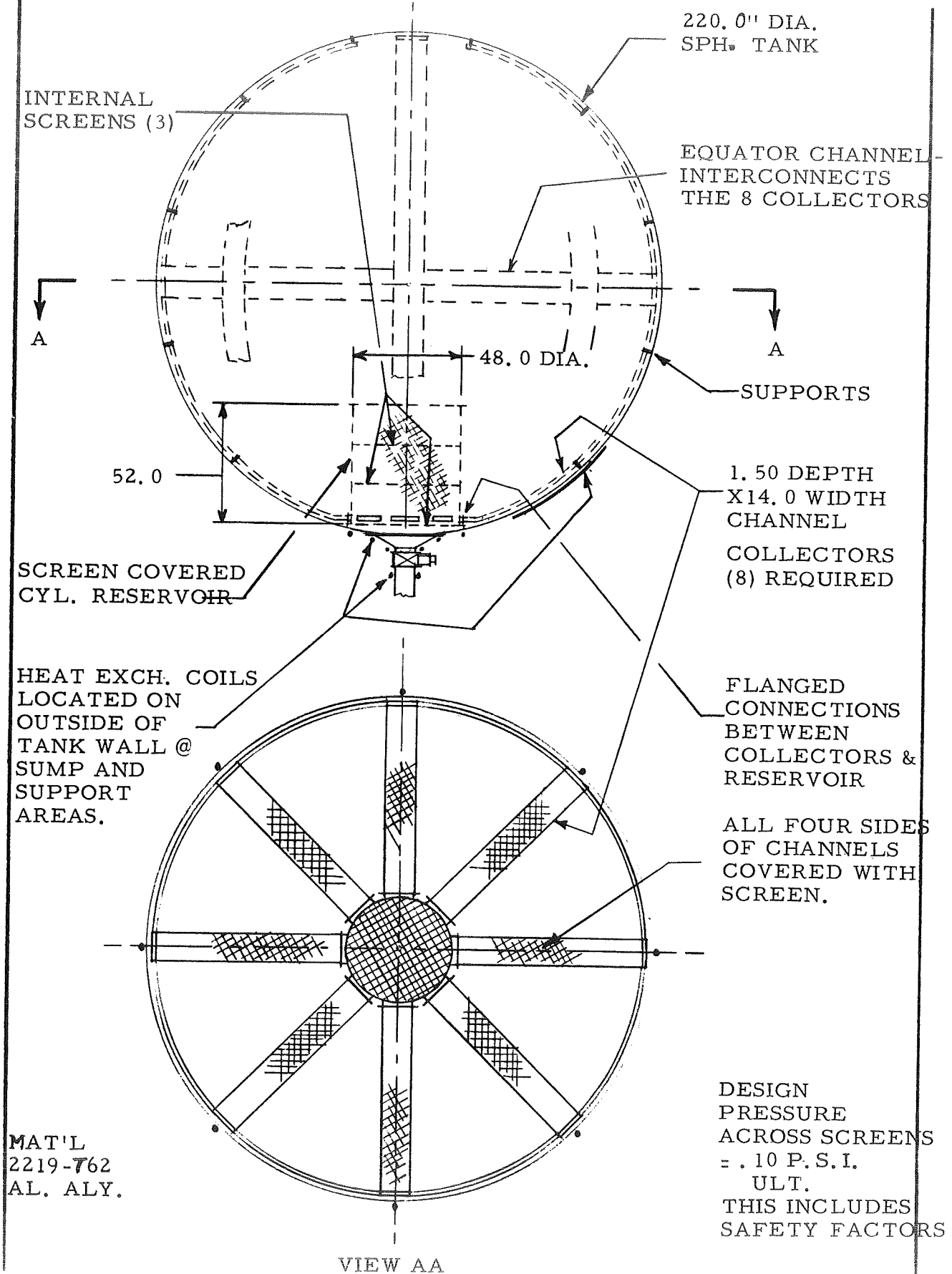


Figure 5-48. Oxidizer Tanker General Arrangement and Design Ground Rules.

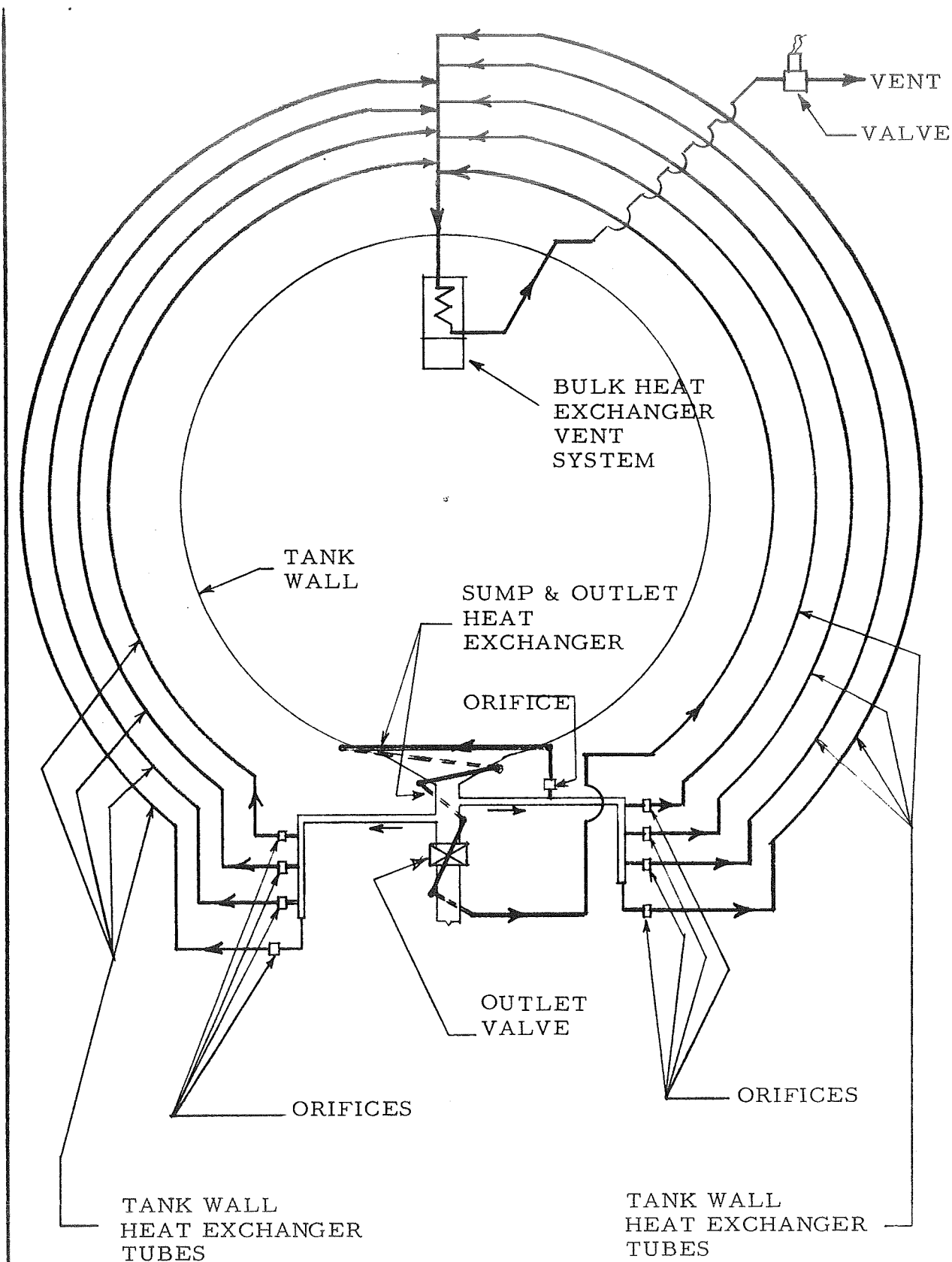


Figure 5-49. Oxidizer Tanker Heat Exchanger Schematic.

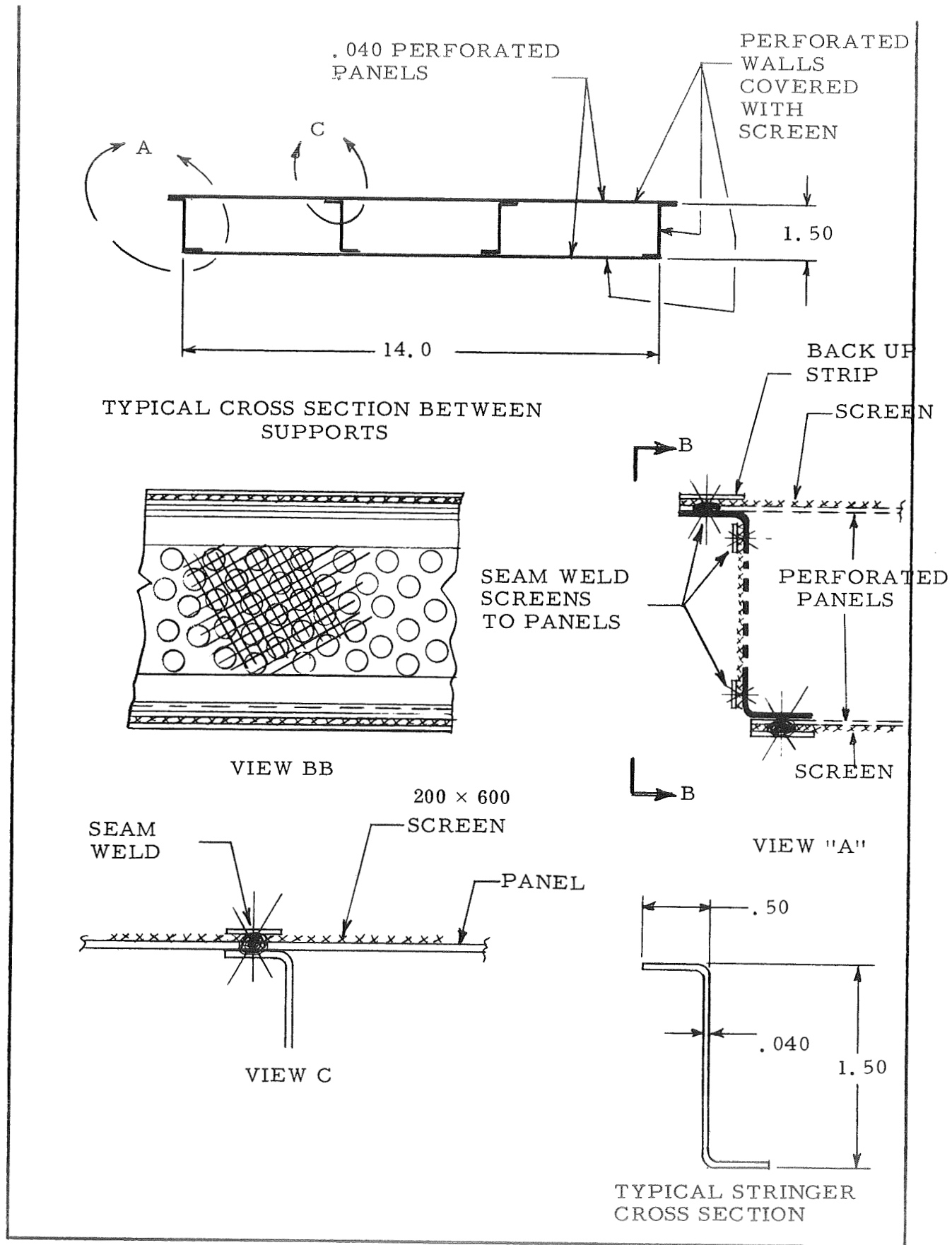


Figure 5-50. Oxidizer Tanker Collector Structural Arrangement (see Alternate- next page).

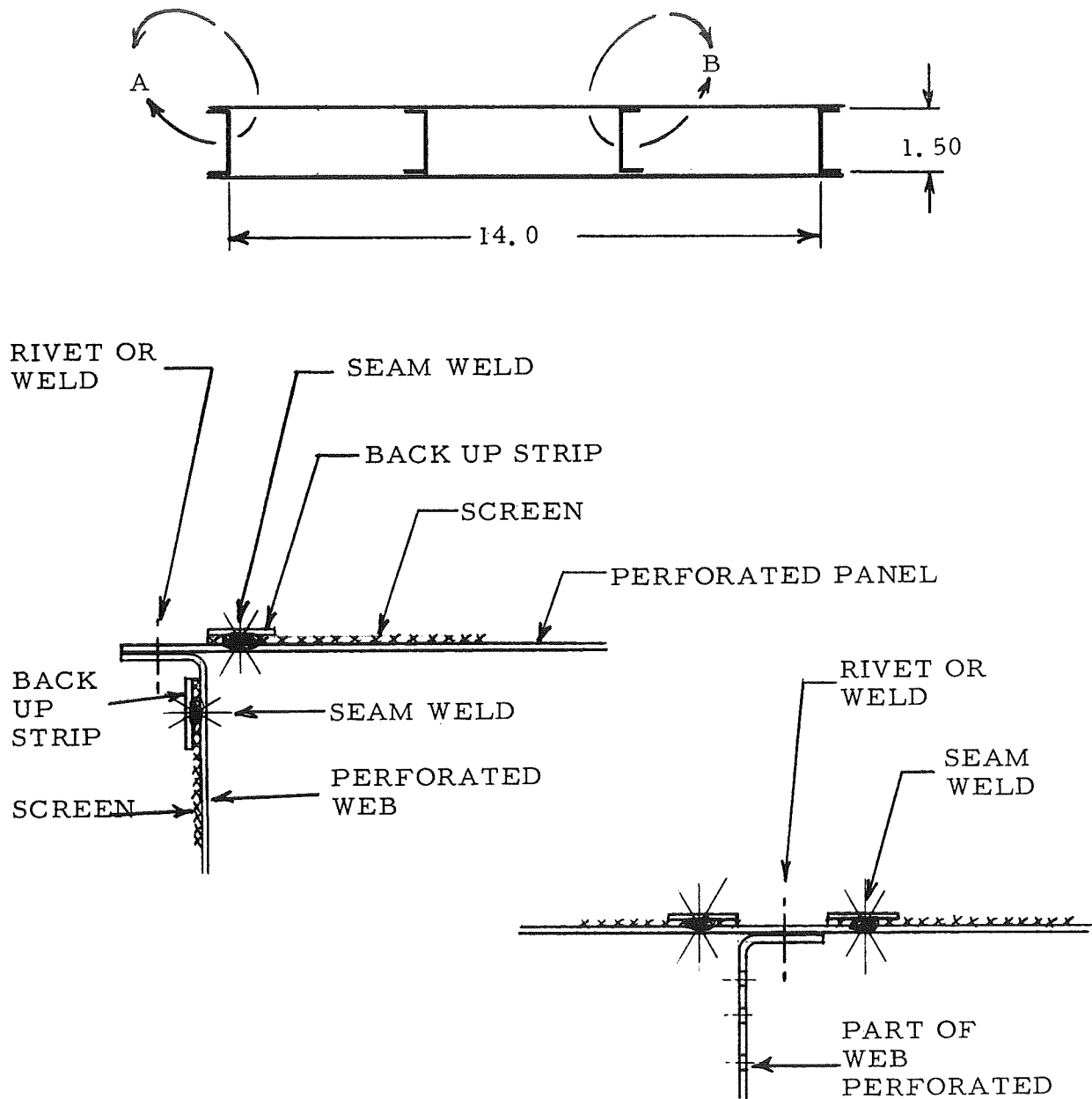


Figure 5-51. Oxidizer Tanker Collector Alternate Structural Arrangement.

to the stiffener flanges to permit tool access. When installing the second sheet of Figure 5-50 the panel would have to be flexed to permit tool access for the inboard stringers. Flexing could cause damage to the screen assembly.

Reduction of overall flow area due to the separate seam weld zones is a disadvantage of the Figure 5-51 design. This area reduction however can be overcome by increasing the overall dimensions of the channel which in turn increases the weight. Assuming that the change in area has negligible overall effects, the Figure 5-51 approach is recommended due to manufacturing and quality control advantages.

Each collector is supported from the tank wall at 5 planes (see Figure 5-48 ). A sixth attachment occurs at the reservoir flanges. Two low conductive links and one drag strut provide the radial and tangential restraints at each of the 5 zones. Support in a direction parallel to the collector run is provided by the reservoir. A typical design is shown in Figure 5-52.

A perforated bulkhead or shear panel member is used to carry the loads from the stringers to the tank wall. Each side of the collector is equipped with a clevis type fitting which is interconnected to the stringers and the bulkhead using angle chips and rivets. One end of the support links and struts are pinned to the fitting and the opposite ends are attached to clevis type members which are welded to the tank wall. Figure 5-52 shows Zee type stringers but the arrangement is adaptable to the Figure 5-51 design by revising the end fittings as shown in Figure 5-51A and 5-60B.

A force applied at the pin (see Figure 5-52 ) is transferred through the support fitting to the angle clips which in turn pass the load to the bulkhead web. This path can be reduced by extending the cross beam through the outboard channel members and attaching fittings directly to the web (see Figure 5-52A). An "I" section is used for the cross members. A section of flange on each channel is removed and the intersections between webs and flanges are butt welded to ensure a seal. Two angle type fittings; incorporating raised land sections for controlling the clevis width and the pin bearing area; are riveted to the "I" and channel member webs. The primary load route is through the fitting to the web by the shear action on those rivets which penetrate the web of the "I" member.

The disadvantage of the Figure 5-52A method is the requirement for seal welds at the splice area since the outboard members are discontinued. When considering Figure 5-52 method (using "ZEE" or channel components) the load paths are relatively indirect, however, the magnitude of these forces are small and the overall weight penalties would be negligible. The Figure 5-52 approach is recommended.

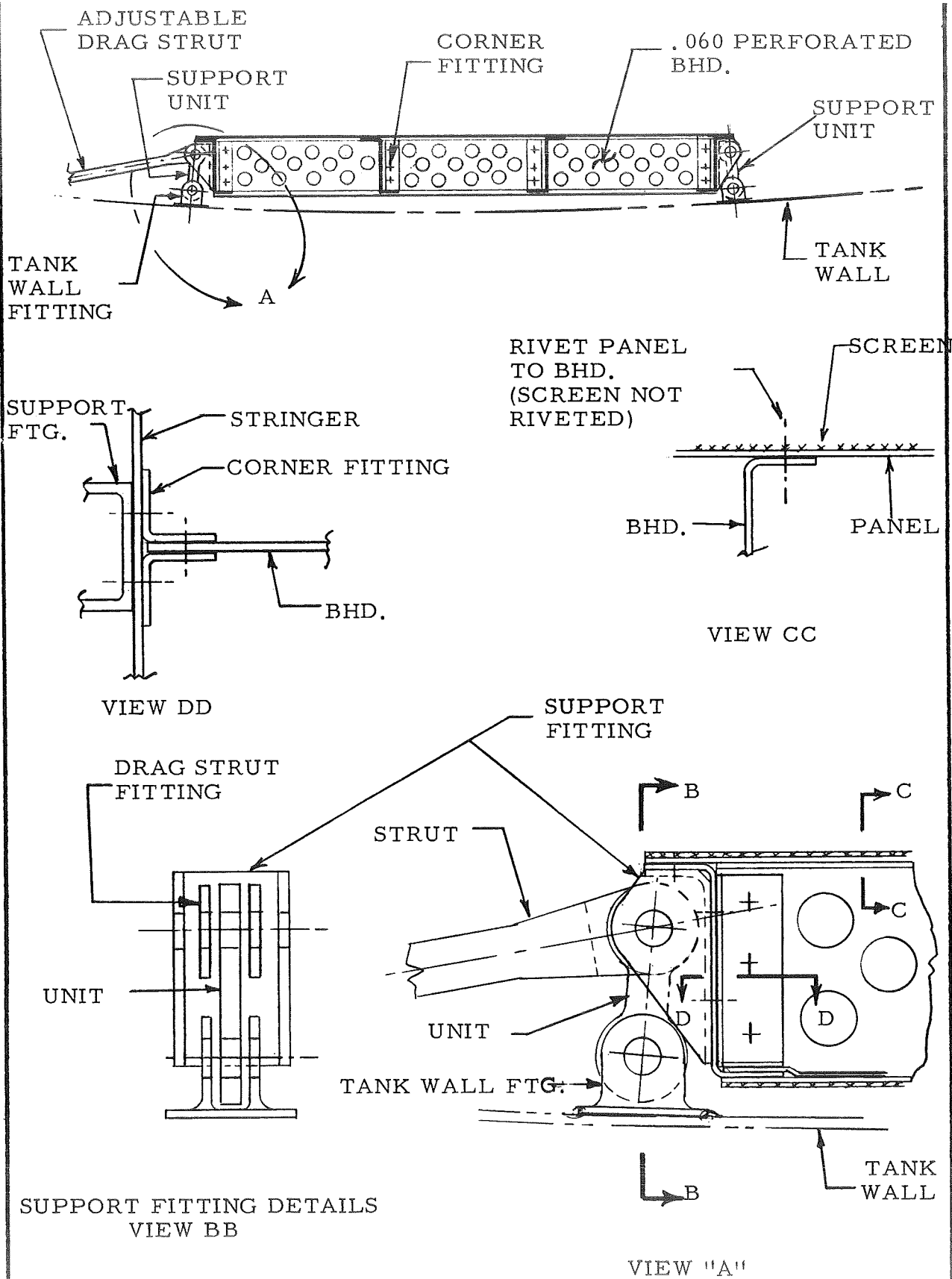


Figure 5-52. Oxidizer Tanker Collector Support Fitting Arrangement

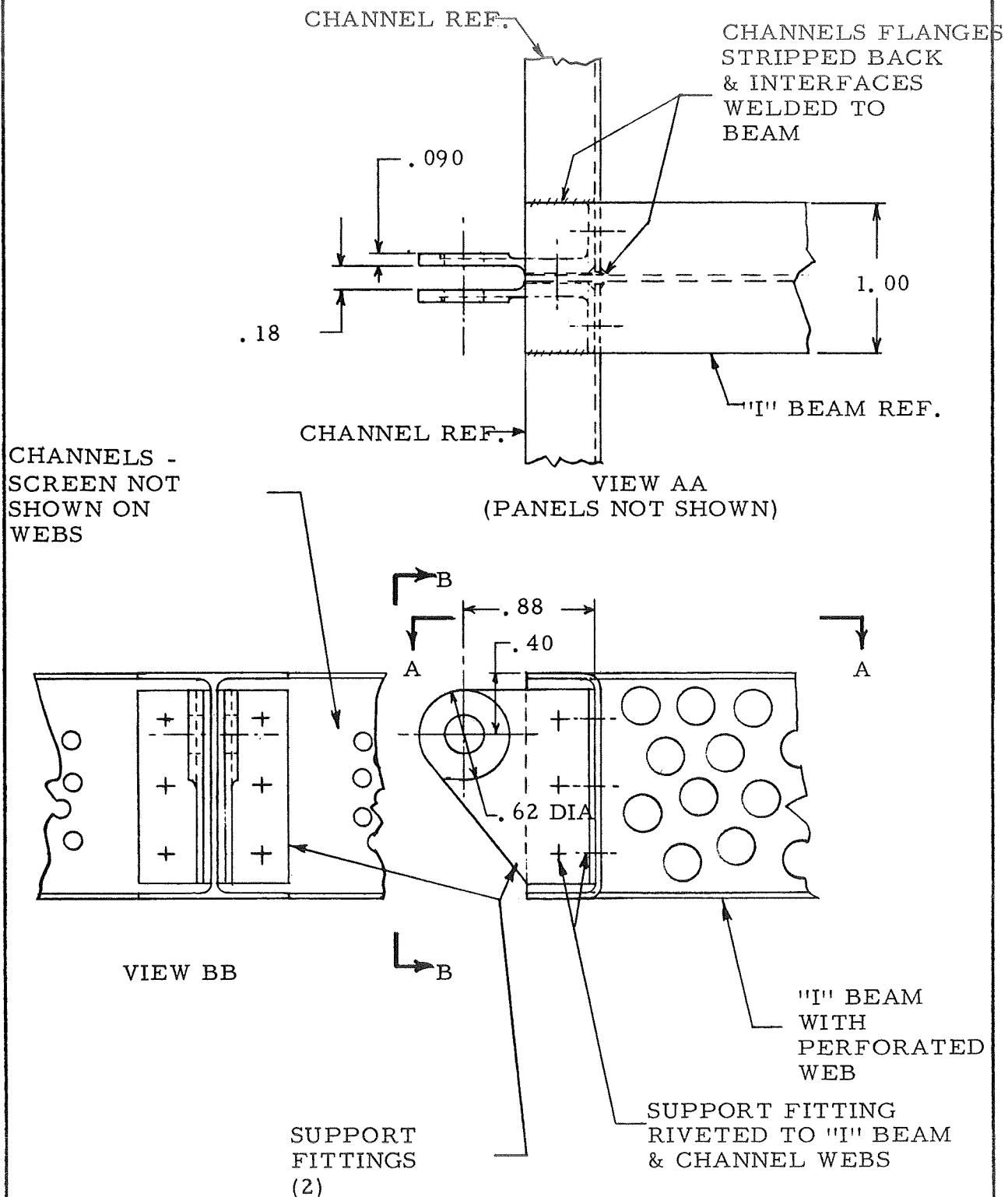


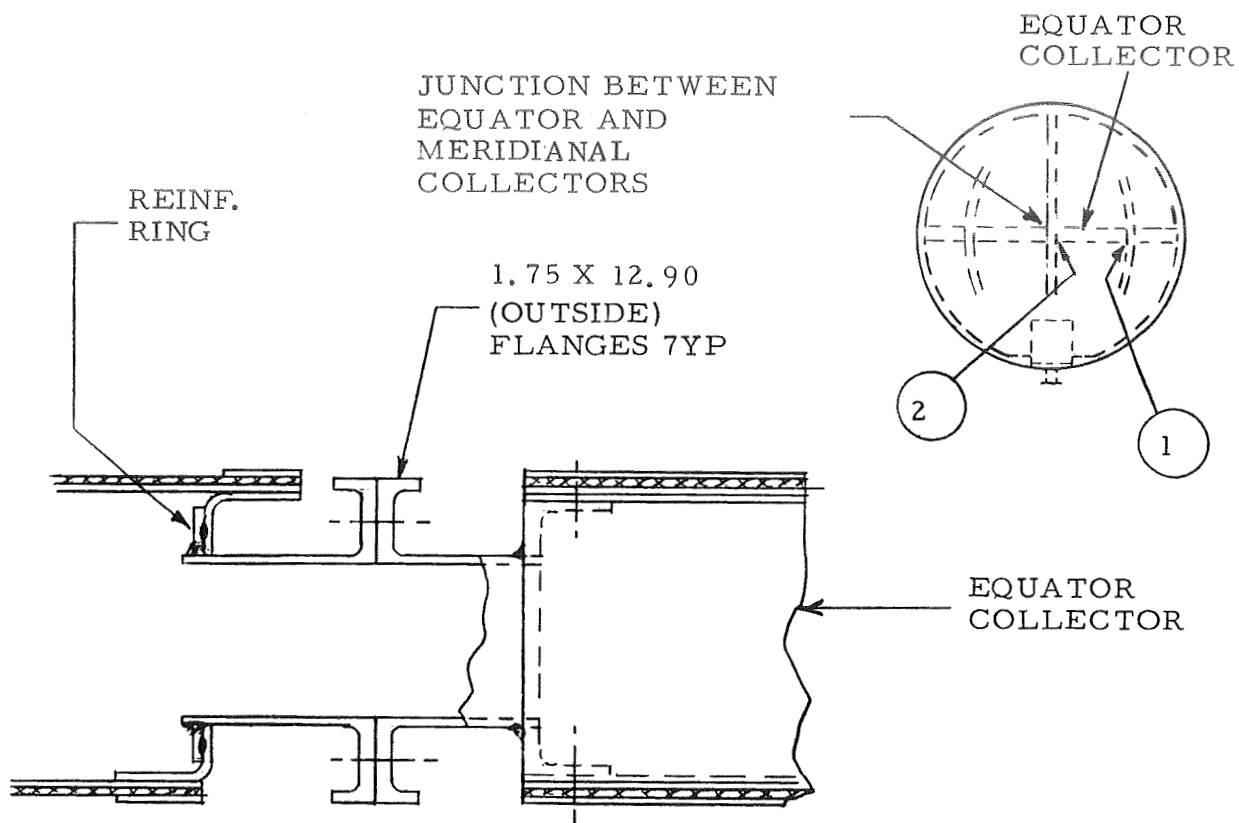
Figure 5-52A. Oxidizer Tanker Collector Support Fitting Arrangement (Alternate).

The collectors are interconnected at the equator by eight channel sections equipped with end fittings which serve as supports, flow passage connectors; and allow for length changes due to tolerances and tank wall deflections. A typical design is shown in Figure 5-53. One end of the assembly provides radial restraint only by using a sliding interface equipped with a boot seal. The opposite end is a flanged connection which supports the assembly in all planes. The rectangular shaped flanges are equipped with short neck sections which in turn are welded to the end adapter in the collectors. The arrangement shown is also adaptable to the Figure 5-51 design which replaces the "ZEE" stringers with channel type members.

**5.3.2 RESERVOIR STRUCTURAL DESIGN** — The collectors are interconnected at the outlet area of the tank with a reservoir equipped with flanged interfaces. The reservoir is a cylindrical member consisting of a screen covered perforated shell stiffened with rings (see Figure 5-54). The forward, aft, and the intermediate rings are also equipped with screens which are supported by the perforated sheets. The screens, support sheets and the rings are seam welded at the perimeter (see Figure 5-55). Stiffeners are used on each of the flat panel sections. The aft ring contains the interface flanges including provisions for mounting onto the storage tank wall (see Figure 5-56).

An alternate layout is shown in Figure 5-57 which separates the screen and structural connections, and allows access to the intermediate compartments without severing components. These features may be an advantage when considering cleaning, inspection, or repair. Each screen and the support diaphragm is fabricated as a sub-assembly which is cleaned and checked out prior to riveting or bolting to the support rings. The diameters of the intermediate sections are decreased to allow assembly after completion of the cylindrical shell section. The disadvantage of the Figure 5-57 design is a decrease in screen area and a weight penalty due to the skirt selections on the rings. The Figure 5-57 configuration is recommended and is used for the weight estimate.

**5.3.3 HEAT EXCHANGER TUBES** — The outboard surface of the spherical storage tank is equipped with heat exchanger tubes for conducting heat locally at each collector support area. A typical layout showing relations between attachments is outlined in Figure 5-58. The routing shown can be varied using additional bends or runs designed to exchange energy at two or more points at each support zone. Details of the attachments are given in Figure 5-59. The conductive points are formed by brazing or welding the tubes to web sections which in turn are welded to the tank wall. The tube is prevented from contacting the tank at the mid-span areas by attaching low conductive washers to web pieces. For cases involving lengths which require intermediate supports, Figure 5-60 provides tank wall fittings which are riveted or bolted to the tube webs using fiberglass angle clips. Tube bends can be used as shown or the support clips may be reversed which would place the tube at the support points near the tank wall surface, therefore minimizing the amount of off set.



CONNECTION AT 2

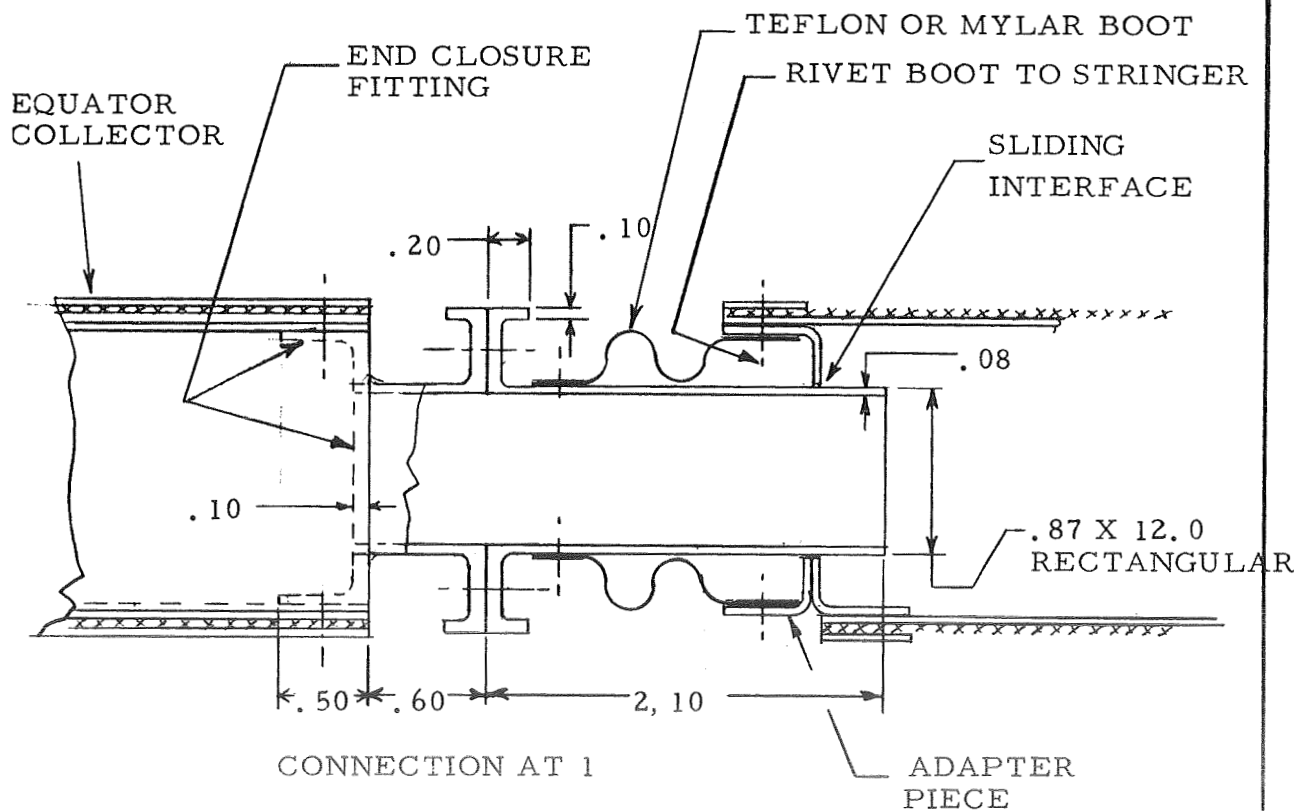


Figure 5-53. Oxidizer Tanker Collector Arrangement at Equator Junction.

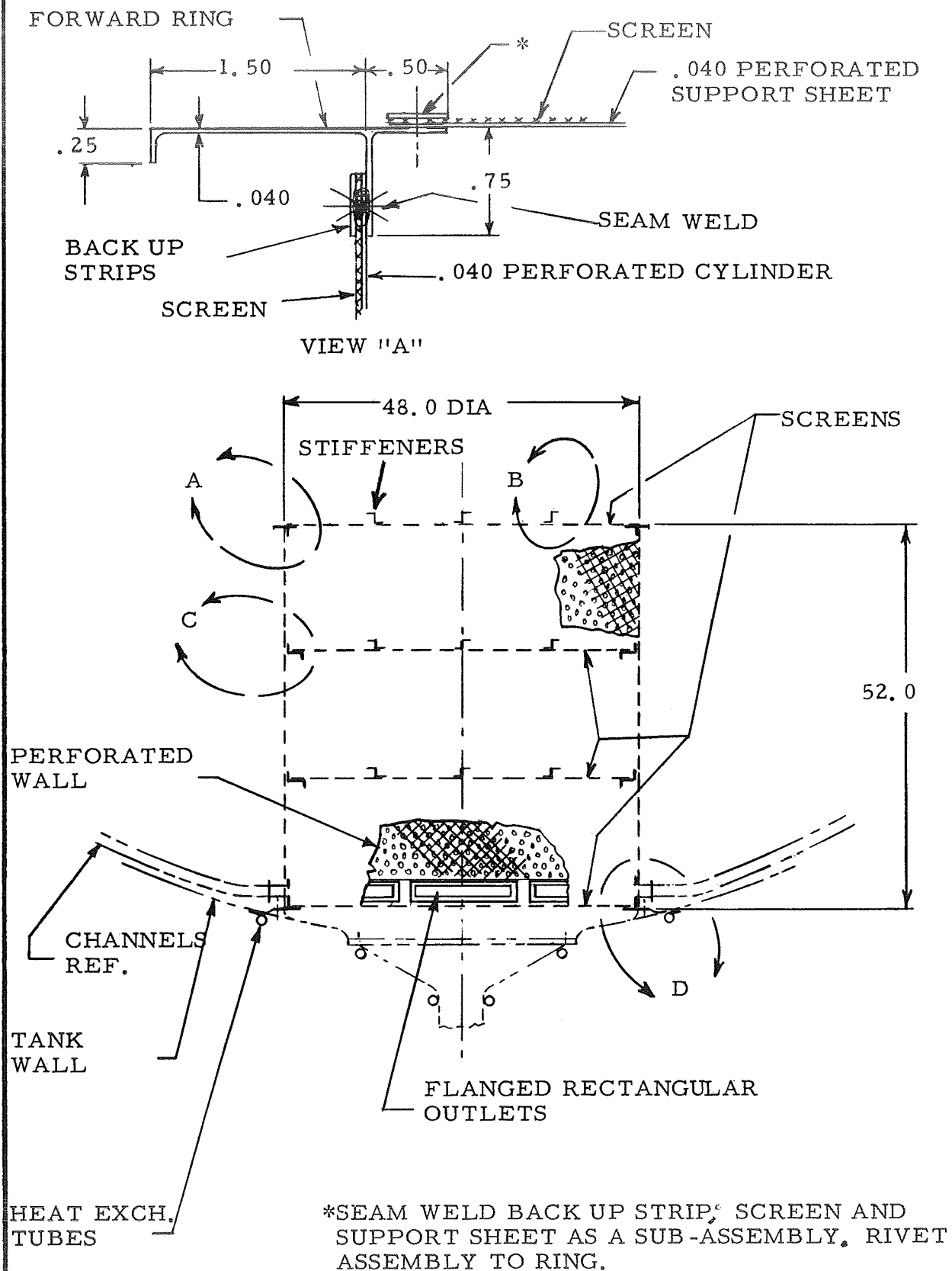
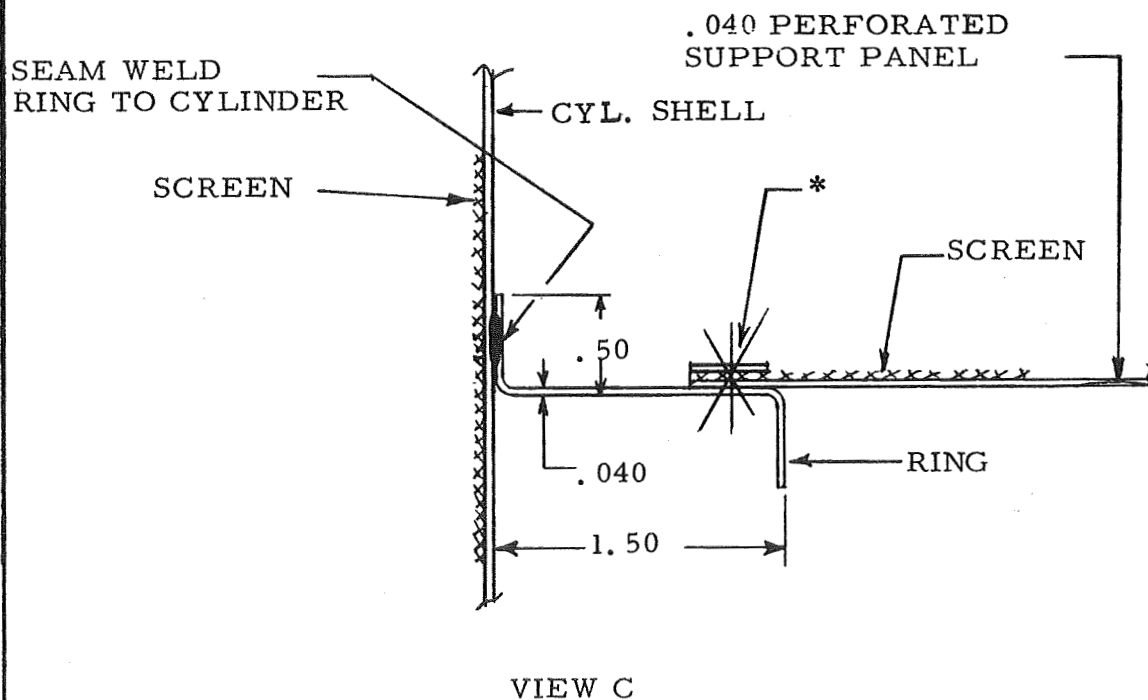
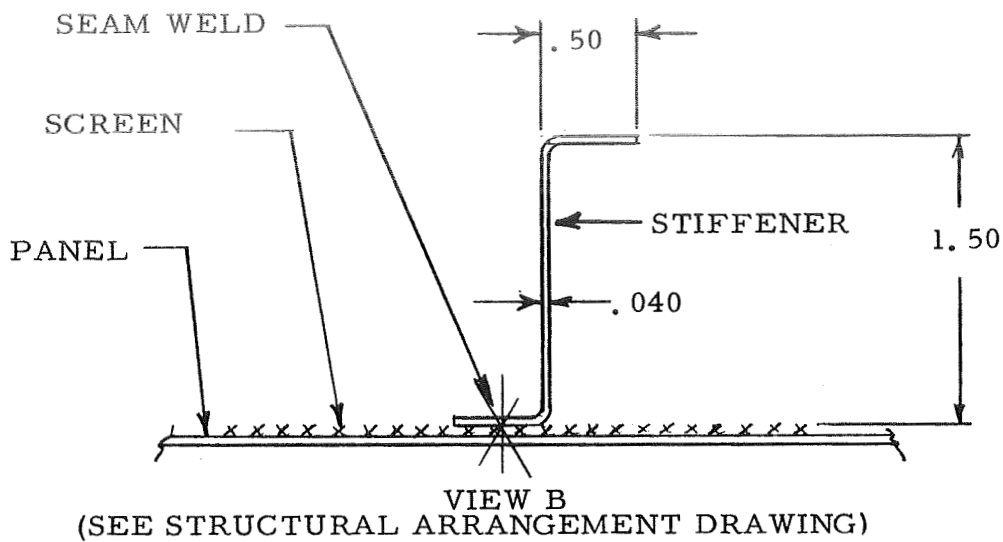


Figure 5-54. Oxidizer Tanker Reservoir Structural Arrangement.



\*SEAM WELD BACK-UP STRIP, SCREEN AND PANEL AS A SUB-ASSEMBLY. RIVET ASSEMBLY TO RING.

Figure 5-55. Oxidizer Tanker Reservoir Structural Details.

\* SEE DETAIL DRAWING FOR TYPICAL  
HEAT EXCHANGER ATTACHMENT.

\*\*THIS AREA OF BASE RING MAY BE  
PERFORATED AND EQUIPPED WITH  
SCREEN IF REQUIRED.

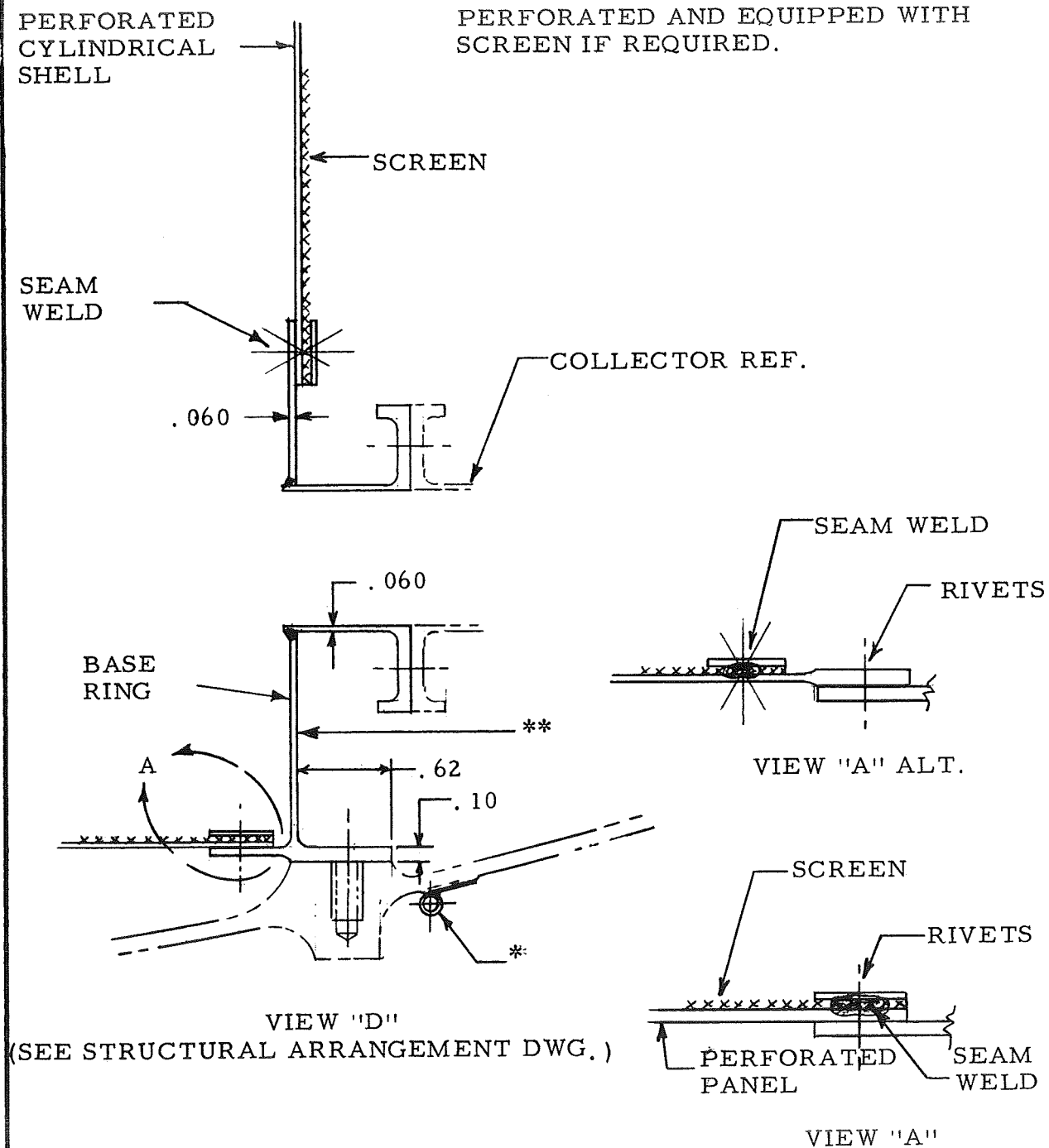


Figure 5-56. Oxidizer Tanker Reservoir Structural  
Details.

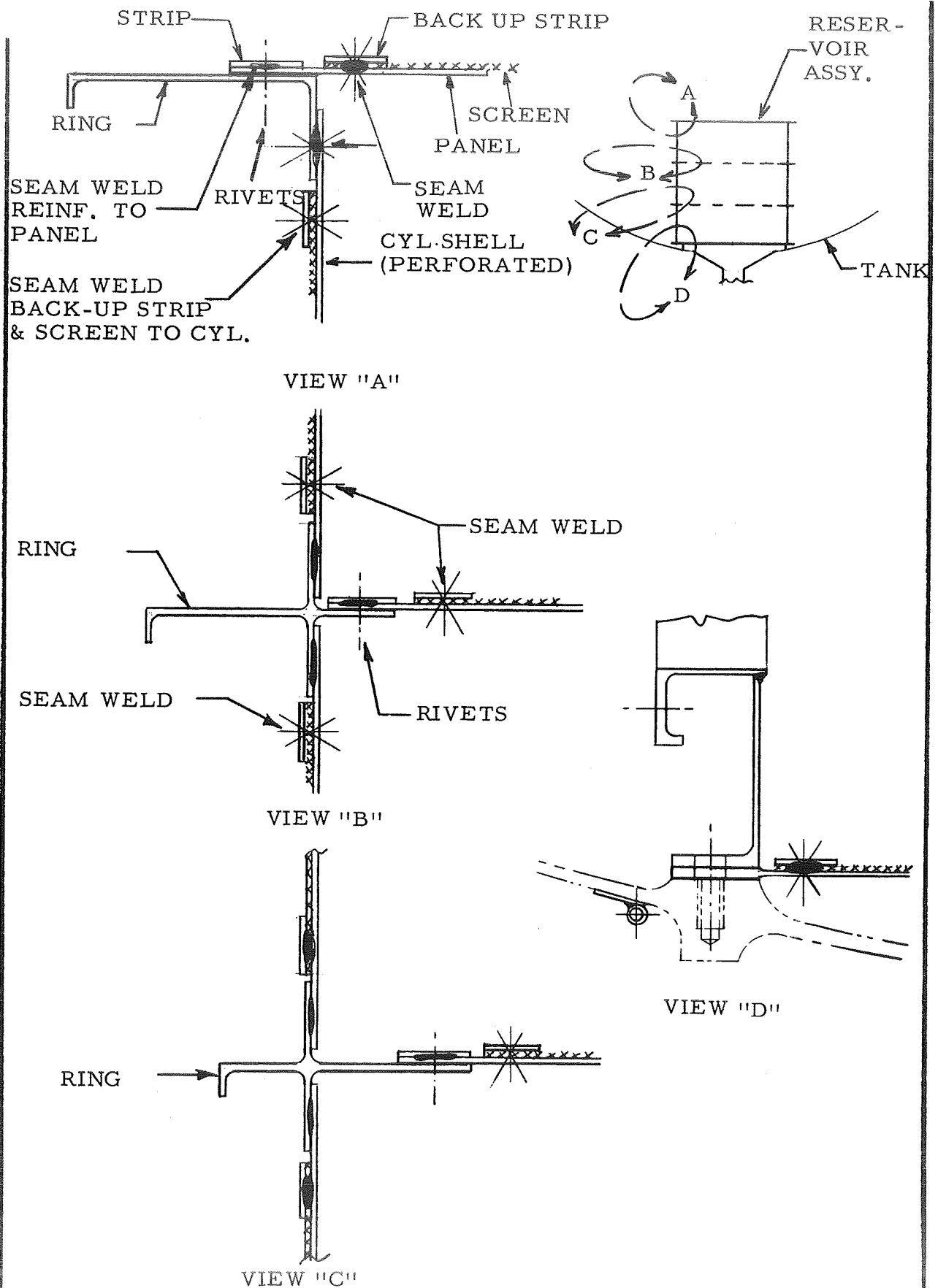


Figure 5-57. Oxidizer Tanker Reservoir Structure (Alternate Ring Details).

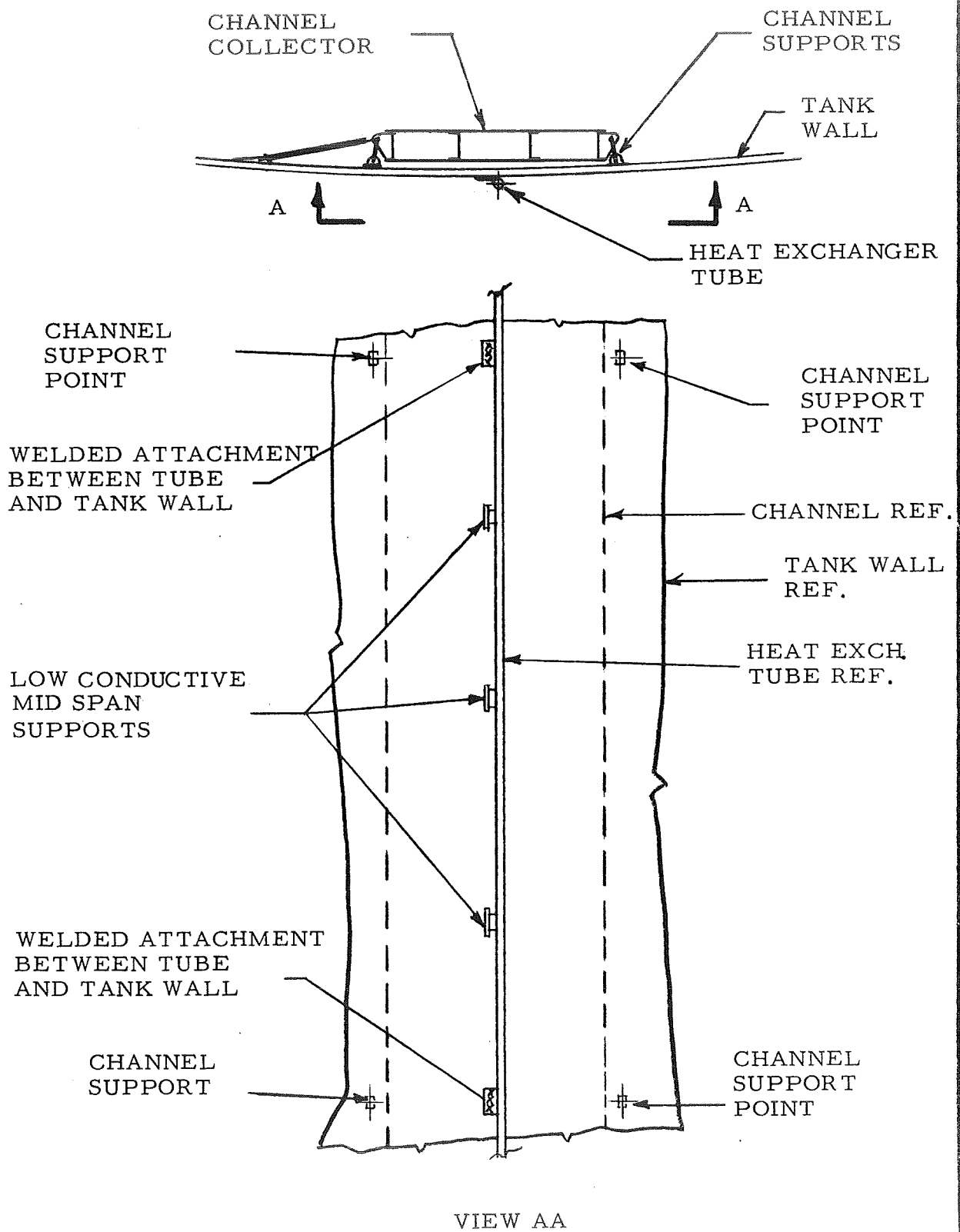


Figure 5-58. Location of Heat Exchanger Coils Relative to Collector Supports (External Systems).

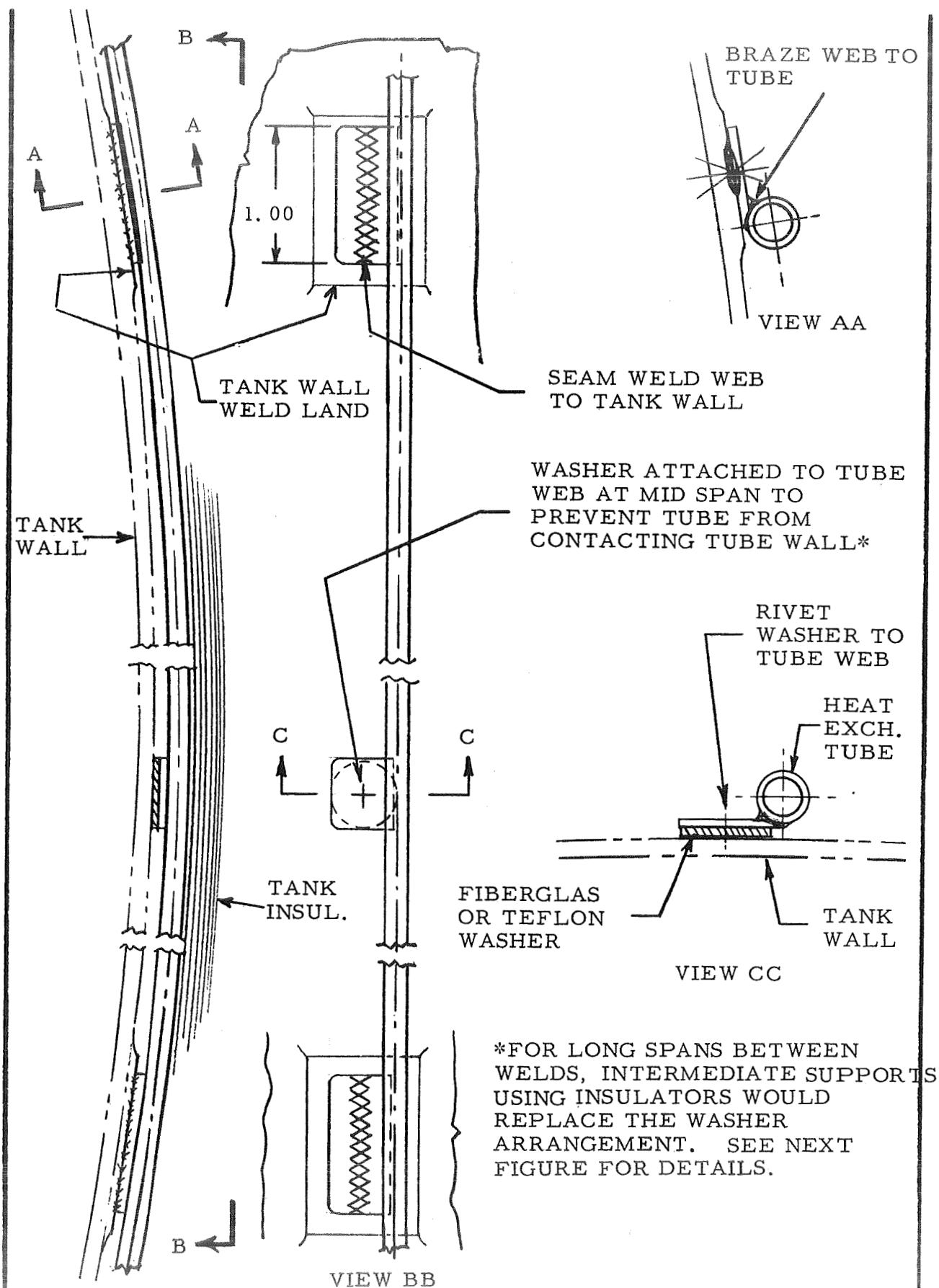


Figure 5-59. Oxidizer Tanker Heat Exchanger Coils  
(Typical Attachment Methods).

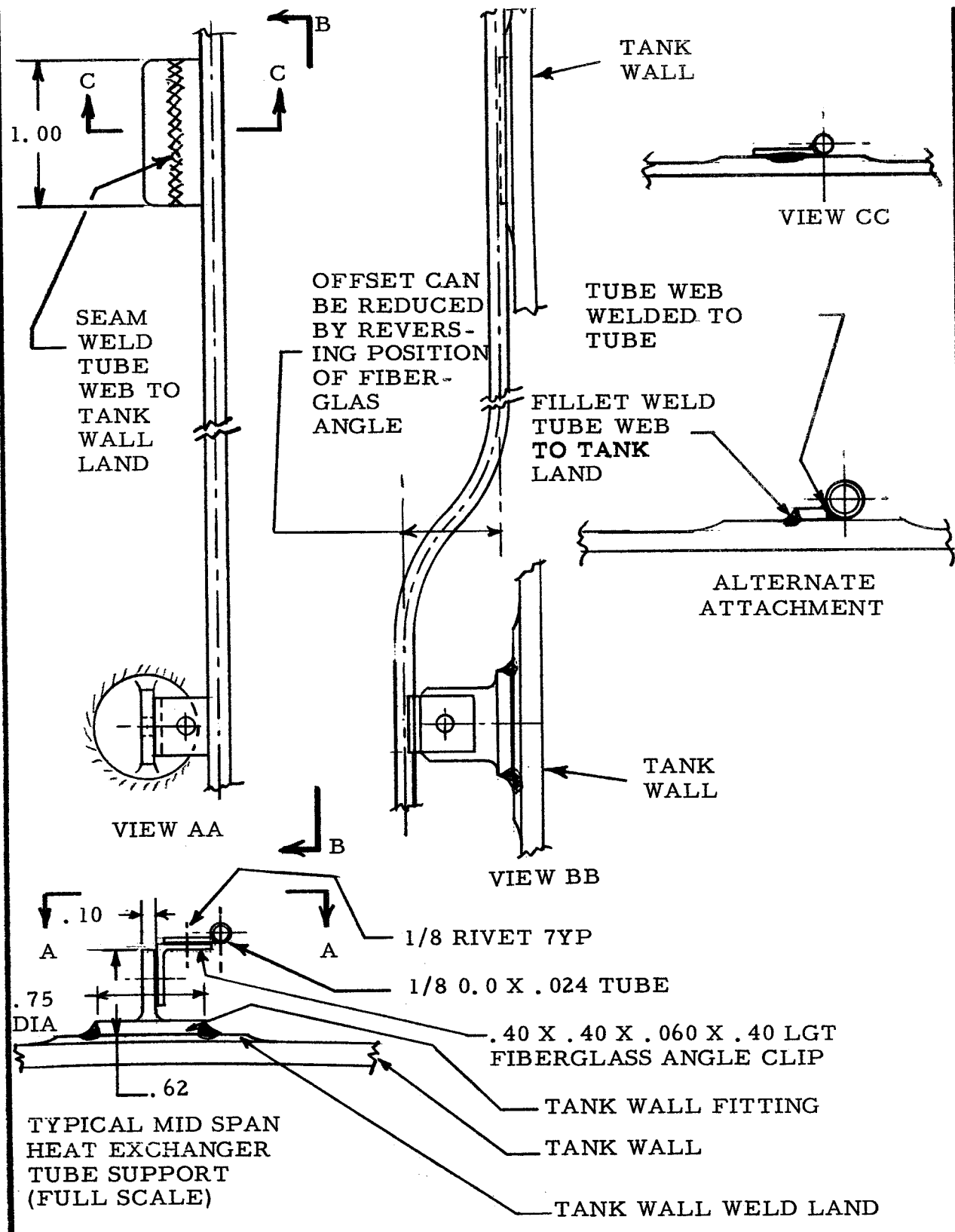


Figure 5-60. Oxidizer Tanker Heat Exchanger Coils (Alternate Support Method).

An alternate heat exchanger system is shown in Figure 5-60A which places the tubes inside the channels. The flow starts at a bleed point located on the forward end of a channel and is routed through the collector support pins. The circuits can be arranged in parallel or series depending upon the distribution requirements. The tubes are supported from the channel frame work using standard clamps. A typical pin fastener used for interconnecting the support components and for conveying cooling fluid is shown in Figure 5-60B . The pin incorporates a shoulder, a lock ring and two ends machined to permit butt welding to the heat exchanger tubes. The tubes which attach to each end of the pin are routed through the channel to the opposite side.

The relations between bleed port, support pin, and the collector structure at the forward end is shown in Figure 5-60C . The bleed terminal consists of a flanged boss (welded to the channel wall) containing internal threads and a seal land for receiving the orifice fitting. The orifice and pins are interconnected in series with external jumper tubes which are welded to the terminals.

**5.3.4 WEIGHT ANALYSIS** — A detailed weight analysis is shown in Figures 5-61, -62, -63 and -64 for the collectors and the reservoirs. The summaries include all structural members, fittings, screen, heat exchanger tubes, fasteners and a contingency allowance. Basic dimensions for most components are listed for reference.

**5.3.5 STRUCTURAL ANALYSIS** — A simplified structural check for major components only was conducted. Figure 5-65 shows an estimate for the collectors which are treated as simply supported uniformly loaded beams. A critical buckling check for the flat panel sections is included. It is assumed that no structural strength is derived from the screens. The flat panel sections are also subject to the uniform loading condition shown in Figure 5-66. The deflections are low which is desirable for a screened covered surface.

The flat diaphragms for the reservoir are exposed to a pressure differential which subjects the perimeter rings to the external loading condition shown in Figure 5-67. A ring cross section was estimated and a stiffener allowance for the flat sheets included.

The reservoir perforated cylindrical shell is exposed to an external pressure which may cause buckling. Figure 5-68 shows an estimate which assumes a section between rings, simply supported edges, an equivalent thickness, and no contributions from the screen.

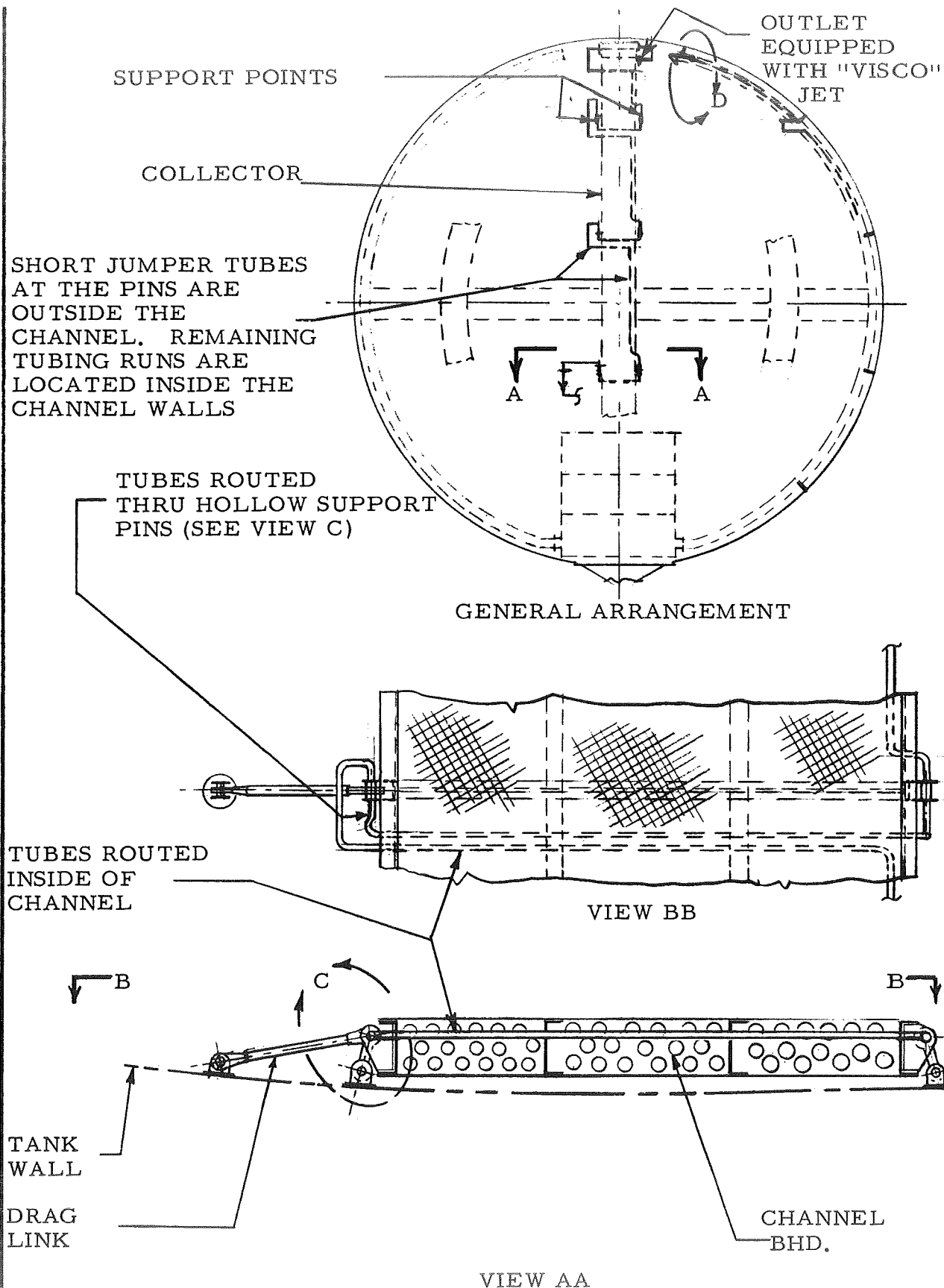


Figure 5-60A. Heat Exchanger System Located Inside of Tank.

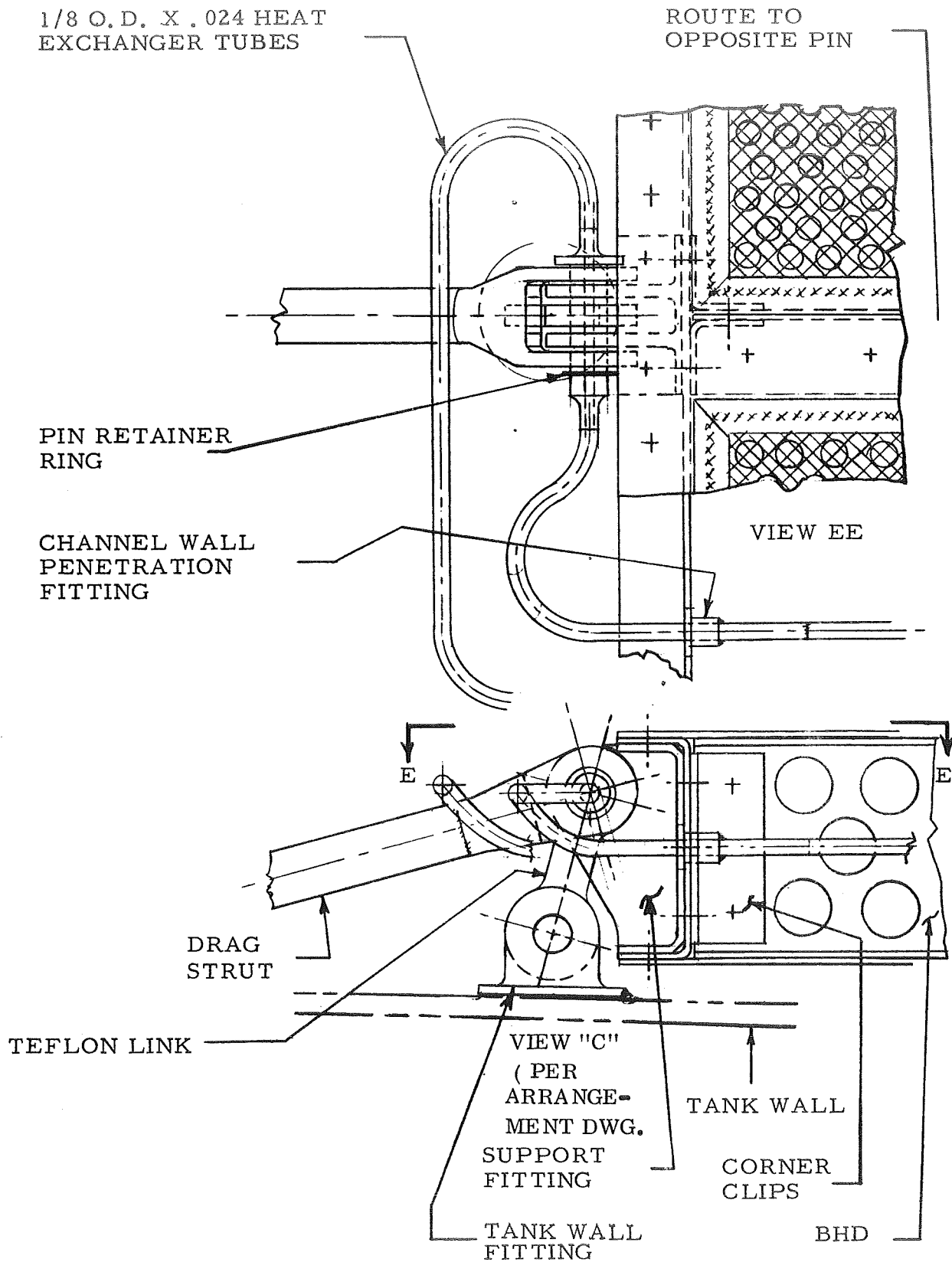


Figure 60B. Collector Support Heat Exchanger Details.

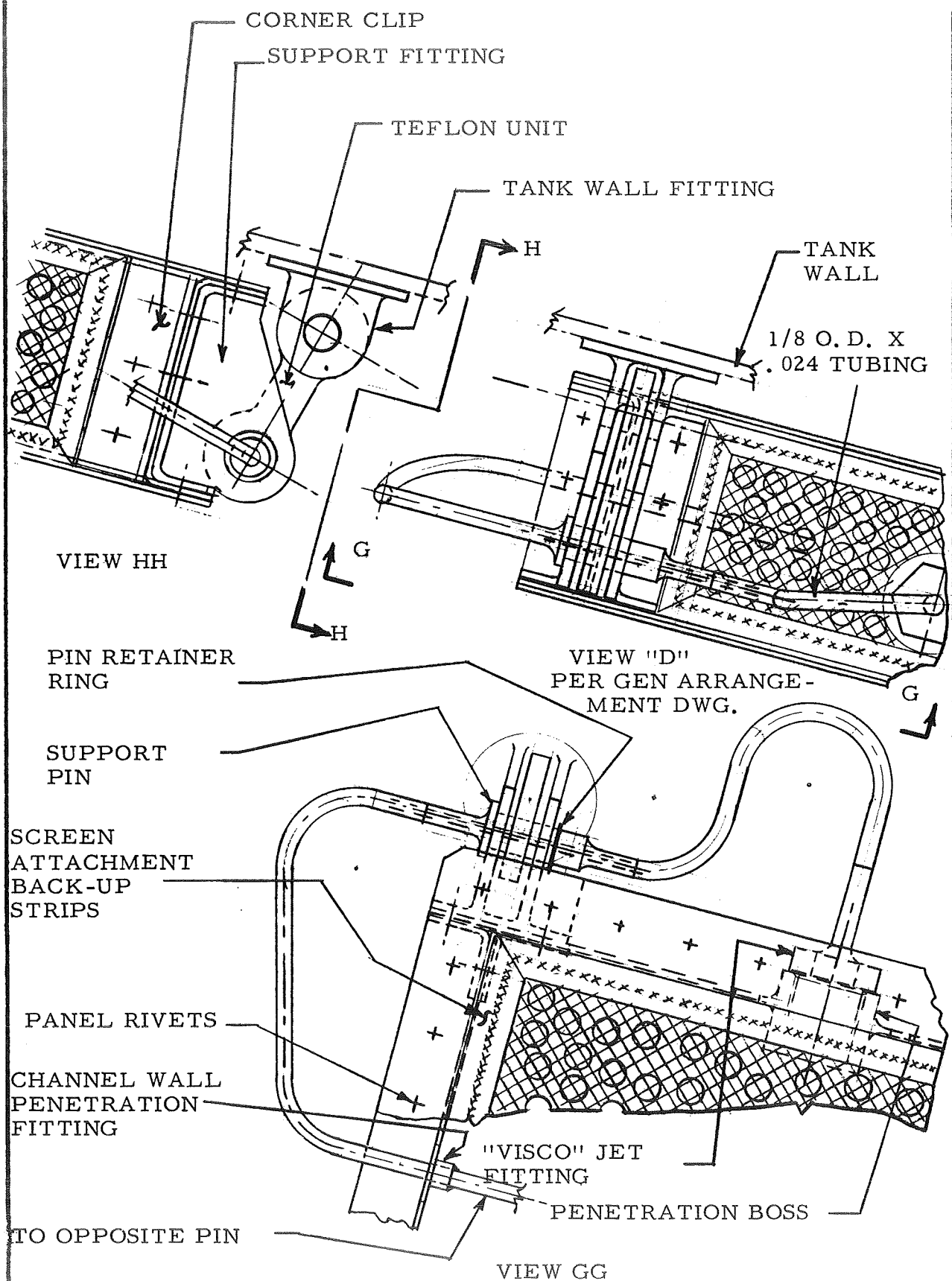


Figure 5-60C. Collector Support Heat Exchanger Details.

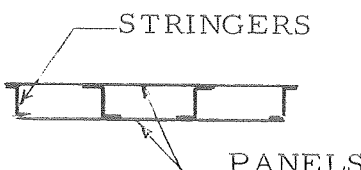
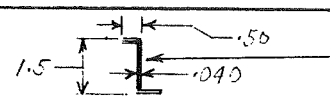


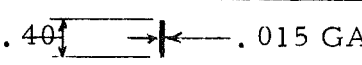
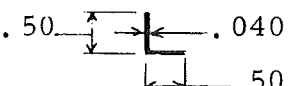
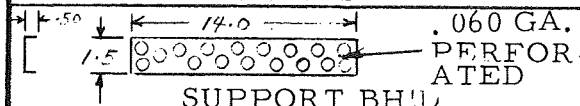
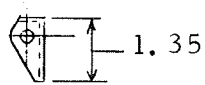
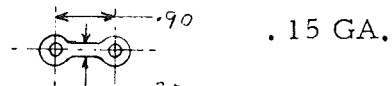
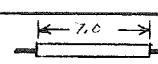
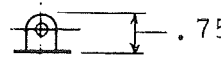
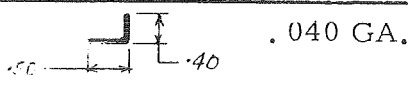
		
ITEM	WT. LBS	REMARKS
 PORTION OF WEB PERFORATED STRINGERS	96.30	32 @ 298" LG'T 32 @ 68 1/2" LG'T
 .040 PERFORATED PANELS	179.00	.021 EQUIV. GA.
 SCREEN	34.60	.053 #/FT <sup>2</sup> 652 FT RQ'D.
 .40 x .015 GA BACK-UP STRIPS	26.40	12 @ 29.38" LG'T
 .50 x .040 CORNER CLIPS	2.80	464 @ 1.5" LG'T
 .060 GA. PERFORATED SUPPORT BH'LD.	6.00	.040 EQUIV. GA. 40 REQ'D
 1.35 SUPPORT FITTINGS	.40	40 REQ'D
 .90 .15 GA. .30 SUPPORT LINES	.40	TEFLON 40 REQ'D
 7.0 3/8 O.D. X .020 CRES DRAG STRUTS	4.00	40 REQ'D ADJUSTABLE TYPE
 .75 TANK WALL FITTINGS	3.40	120 REQ'D INCL. ALLOW FOR WELD LAND
 .040 GA. .50 .40	.50	17.0" LGT 8 REQ'D

Figure 5-61. Oxidizer Tanker Collector Channels Weight Estimate.

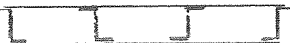
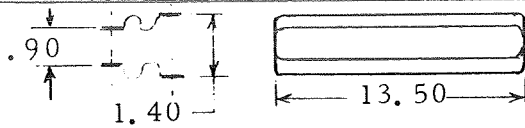
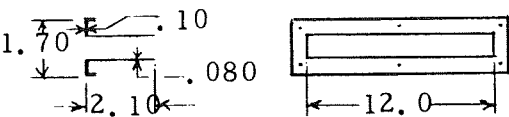
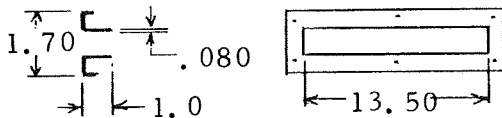
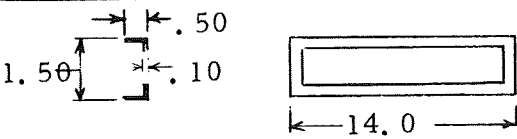
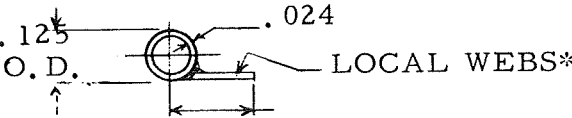
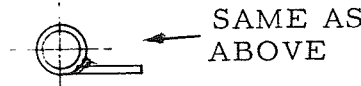
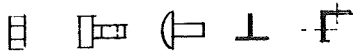
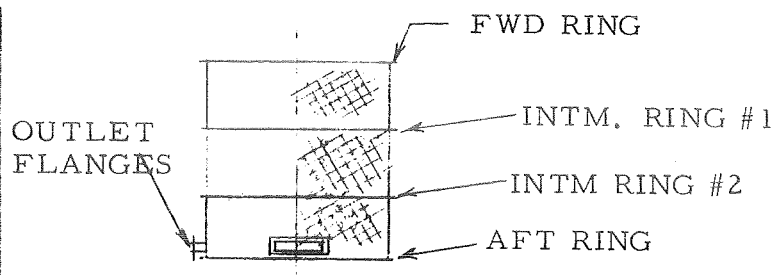
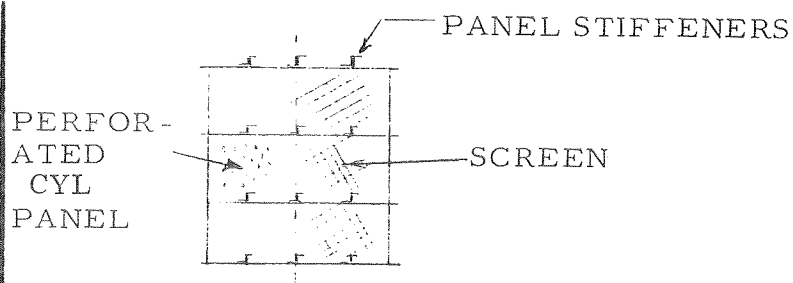
		
ITEM	WT. LBS.	REMARKS
 BOOT SEAL	2.75	8 REQ'D TEFLON .060 AVG. GA
 FLANGED ADAPTER	4.80	8 REQ'D
 FLANGES	13.00	32 REQ'D
 CLOSURE FITTINGS	5.52	24 REQ'D
 HEAT EXCH. COILS FOR CHANNEL	3.50	230 FT. REQD. *AT EACH SUPPORT AREA
 HEAT EXCH. COILS FOR SHIP AREA	1.00	30 FT. REQ'D INCLUDES WELD LANDS
 MSC. FASTENERS & SUPPORT CLIPS	4.00	
TOTAL 5% CONTINGENCIES GRAND TOTAL	388.87	
	19.45	
	408.32	

Figure 5-62. Oxidizer Tanker Collector Channels Weight Estimate  
(Continued).



ITEM	WT. LBS	REMARKS
<p>FORWARD RING</p>	1.72	
<p>HOLES</p> <p>FORWARD SUPPORT PANEL</p>	4.66	.024 EQUIV. GA. .50 WIDTH RIM @ .040 GA.
<p>REINF &amp; BACK-UP STRIPS/ FWD PANEL</p>	.30	320" LG'T
<p>FORWARD SCREEN</p>	.67	12.6 FT <sup>2</sup> .053 #/FT <sup>2</sup>
<p>INTM RING #1</p>	2.00	
<p>INTM RING #2</p>	1.90	
<p>AFT RING</p>	4.00	CUT OUTS FOR THE OUTLETS NOT INCLUDED
<p>OUTLET FLANGES</p>	2.64	8 REQ'D
<p>SUPPORT PANEL, SCREEN AND BACK-UP STRIPS AT INTM AND AFT RINGS</p>	16.89	*USE SAME AS CALC FOR ABOVE ITEMS. 3 ASSEMBLIES REQ'D

Figure 5-63. Oxidizer Tanker Reservoir Weight Estimate.



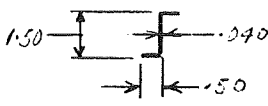
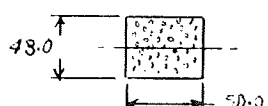
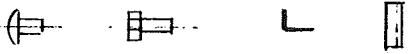
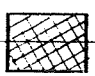
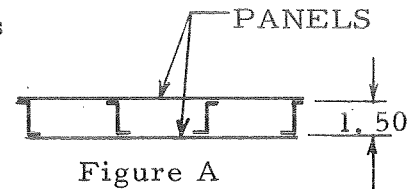
ITEM	WT. LBS	REMARKS
 PANEL STIFFENERS	4.80	4 @ 48" LG'T EA. 8 @ 36" LG'T EA.
 CYLINDER PANEL	22.60	
 MSC. RIVETS, BOLTS, CLIPS ETC.	7.85	
 CYL PNAEL SCREEN	2.78	.053 #/FT <sup>2</sup>
<div>TOTAL</div> <div>5% CONTINGENCIES</div> <div>GRAND TOTAL</div>		
	66.89	
	3.34	
	30.23	

Figure 5-64. Oxidizer Tanker Reservoir Weight Estimate  
(Continued).

A typical channel cross section consists of four stringers welded to two panels which forms the box section shown in Figure A. The channels are supported at six points inside the oxidizer tank. A section spanning two supports is treated as shown in Figure B.

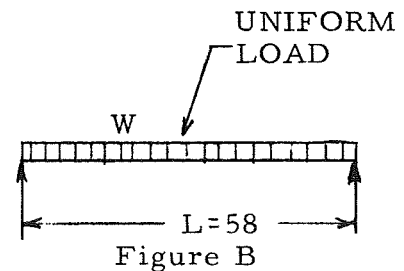


The approximate weight per inch for the beam is .132. Assuming 10 gs,  $W = .132 \times 58 \times 10 = 76.5\#$ . The maximum bending moment

$$M = \frac{WL}{8}$$

$$= \frac{76.5 \times 58}{8} = 555.0 \text{ in } \#$$

The deflection at mid-span  $Y = \frac{5WL^3}{384EI}$



Where

$$E = 10 \times 10^6$$

$$I = \text{moment of inertia of total cross section}$$

$$= .56 \text{ approx.}$$

$$Y = \frac{5 \times 76.5 \times (58)^3}{384 \times 10^6 \times .56} = \frac{7.45}{215} = .0347''$$

The bending moment subjects the flat panel sections to a compressive stress  $Sc = \frac{Mc}{I}$

where

$$c = \frac{1.5}{2} = .75$$

$$Sc = \frac{555 \times .75}{.56} = 743 \text{ psi}$$

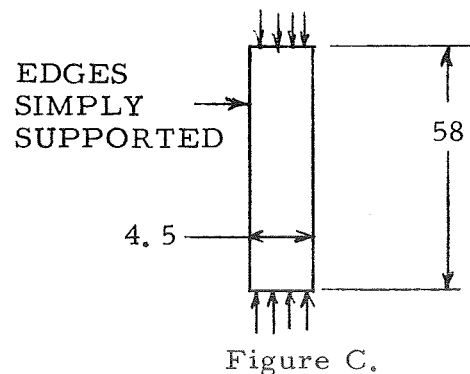


Figure 6-65. Oxidizer Tanker Collector Channel Panel Estimate.

The critical buckling stress under the Figure C load conditions

$$S_{cR} = \frac{\pi^2 K_c E}{12 (1-\nu^2)} \left( \frac{t}{b} \right)^2$$

where

- $K_c$  = buckling coefficient  
From curves (PAGE C5.2\*),  
 $K_c = 4.0$
- $E$  =  $10 \times 10^6$  = Modulus of elasticity
- $\nu$  = Poisson's ratio = .30
- $t$  = Equivalent panel gage = .021

$$\begin{aligned} S_{cR} &= \frac{\pi^2 \times 4.00 \times 10^7}{12 \times [1 - (.3)^2]} \left( \frac{.024}{4.5} \right)^2 \\ &= \frac{39.4 \times 218}{12 \times .91} \\ &= \frac{8550}{10.9} = 790 \text{ psi} \end{aligned}$$

Buckling will not occur since  $S_{cR} > S_c$ .

\*"Bruhn" 1965 P. C5.11.

Figure 5-65. Oxidizer Tanker Collector Channel Panel  
Estimate (Continued).

The flat panel sections of the channels are exposed to .10 psi external pressure. The coefficient

$$C = \frac{wb^4}{Et^4} *$$

where

$$t = .021 \text{ equiv.}$$

$$E = 10^7$$

Therefore

$$C = \frac{.10(4.5)^4}{10^7 \times (.021)^4} = 21.10$$

From table

$$\frac{Sb^2}{Et^2} = 7.00$$

S = total stress. (diaphragm plus bending).

$$S = \frac{7.00 \times E \times t^2}{b^2}$$

$$= \frac{7.00 \times 10^7 \times (.021)^2}{(4.5)^2} = \frac{30,900}{20.2} = 1,530 \text{ psi}$$

From table \*,  $\frac{Y}{t} = .90$

where

y = deflection

y = t X .90

= .021 X .90

= .0189 inches

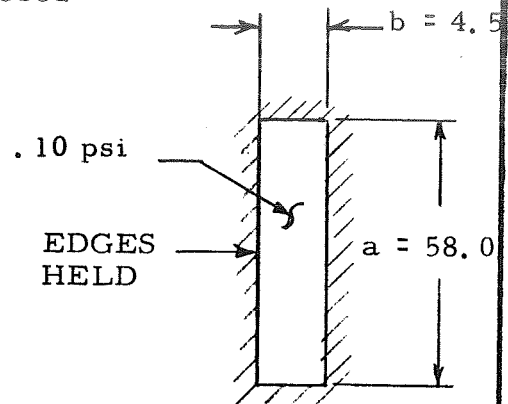


Figure A

\*"ROARK" 3rd edition P. 222

Figure 5-66. Oxidizer Tank Collector Channel Panel Estimate.

A perforated flat panel is assumed at the forward end which is exposed to a .10 psi uniform load (See Figure A). The diaphragm stress

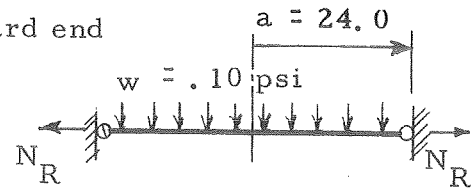


Figure A.

$$S_D = 0.328 \sqrt[3]{\frac{E w^2 a^2}{t^2}} *$$

where

E = Modulus of elasticity =  $10 \times 10^6$

t = .020 equivalent gage

$$S_D = 0.328 \sqrt[3]{\frac{10^7 \times (.1)^2 (24)^2}{(.020)^2}} =$$

$$0.328 \times \sqrt[3]{144 \times 10^9} = 1720 \text{ psi}$$

$$N_R = 1720 \times t = 1720 \times .020 = 34.4 \text{ \#/in}$$

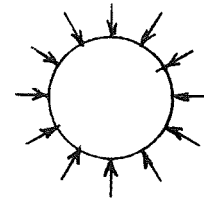


Figure B.

$N_R$  externally loads the forward ring as shown in Figure B. The initial unit load  $p'$  is expressed by

$$p' = \frac{3EI}{R^3} **$$

For  $p' = N_R$  the cross sectional moment of inertia for the ring

$$I = \frac{N_R R^3}{3E}$$

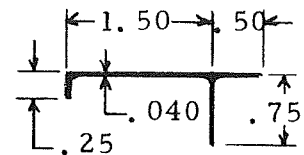


Figure C.

where

$$R \approx a + 1.5 = 25.5$$

$$I = \frac{34.4 (25.5)^3}{3 \times 10^7} = .019 \text{ in}^4$$



Figure D.

use the ring per Figure "C" or equivalent. Three stiffeners for the diaphragm are included in the weight analysis to compensate for vibrational modes (see Figure D).

Figure 5-67. Oxidizer Tanker Cylindrical Reservoir Forward Panel and Ring Estimate.

The maximum deflection Y for the diaphragm (excluding stiffeners)

$$* Y = .662 a \sqrt[3]{\frac{w a}{E t}} = .364 \text{ inches.}$$

\*\*"Theory of elastic stability" by Timoshenko, 2nd edition, P. 291

\*"ROARK" 3rd edition, P. 223

The reservoir is subject to an external pressure which may cause buckling of the cylindrical shell. If a section between two rings is isolated and the edges assumed simply supported (see Figure A) then:

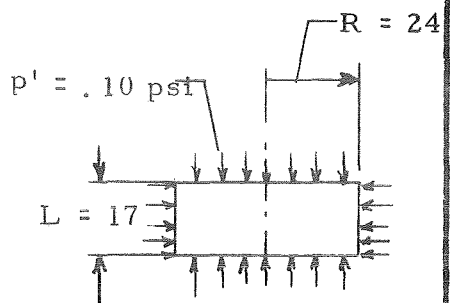


Figure A.

$$\frac{F_c R}{\eta} = K_p \frac{\pi^2 E}{12 (1 - \mu^2)} \left( \frac{t}{L} \right)^2 *$$

where

$F_c R$  = Allowable buckling stress

$\eta$  = Plasticity correction term

= 1.0 for our case

$E$  = Modulus of elasticity =  $10 \times 10^6$

$\mu$  = Poisson's ratio = .30

$t$  = Wall gage. For our case an equivalent thickness of .020 is used since the shell is perforated. The screen is neglected.

$K_p$  = Buckling coefficient which is related to  $Z = \frac{(L)^2}{R} (1 - \mu^2)^{1/2}$

$$= \frac{(17)^2}{24 \times .020} \left[ 1 - (.3)^2 \right]^{1/2}$$

$$= 575$$

from curve on P. 14-7-4-4\*  $K_p = 18$

Substituting the above,

$$\frac{F_c R}{1} = 18 \frac{\pi^2 \times 10^7}{12 [1 - (.3)^2]} \left( \frac{.020}{17} \right)^2 = 225 \text{ psi}$$

The critical buckling pressure  $P_{cR} = \frac{F_c R t}{R} = \frac{225 \times .020}{24} = .187 \text{ psi}$

The applied pressure = .10 psi ultimate. An .040 perforated shell appears reasonable.

\*Aerospace fluid component designers' handbook, Vol. II, Rev. C. Air Force Rocket Propulsion Laboratory Research & Technology Div. RPL-TOR-64-25 Project 3058.

Figure 5-68. Oxidizer Tanker Reservoir Cylindrical Shell Estimate.

# 6

## CONCLUSIONS AND RECOMMENDATIONS

### CONCLUSIONS

Based on the system comparison of Phase I capillary devices are effective means of cryogenic propellant control for large scale vehicles. This assessment was made on overall consideration of weight, reliability, cost and manufacturing feasibility.

The design handbook developed as part of this contract contains fluid, thermal and structural design information which should be used as a foundation for capillary device design. This handbook contains a description of state of the art techniques developed during the current contract including computer programs, parametric data, empirical correlations and design techniques.

Current knowledge is adequate to successfully design a cryogenic capillary device for restart or propellant transfer however, in order to minimize design conservatism and improve system performance additional research and development effort is required in the following areas.

### RECOMMENDATIONS

To refine the capillary device cooling configuration prototype testing should be conducted with small scale models in cryogenic fluids to analyze effect of mixing in capillary device cooling and to verify the coupling of a thermodynamic vent system and capillary device. Thermal testing on a component level should be conducted to evaluate the thermal conductivity of representative screen materials and to verify the use of a thermodynamic vent system and propellant control screen to maintain a feedline free of vapor.

In the fluid analysis area work is required to successfully predict liquid settling and reorientation under high Weber number conditions. Coupled with this study, refilling of capillary devices by reoriented collected fluid should be considered. Low gravity draining of a capillary device should be handled by coupling a technique similar to that embodied in the DREGS2 program with low gravity interface shape and pullthrough analysis as it becomes available. Prediction of low gravity mixing must be made and successfully correlated with low gravity data. Some of this data is obtainable through drop tower testing.

Fabrication of a large capillary device such as that required for the LOX tanker should be undertaken in order to verify subassembly fabrication procedures, and in-

tank checkout and repair procedures. Procedures need to be established for capillary device in-tank checkout prior to launch by measuring capillary device bubble point and pressure drops.



## REFERENCES

- 2-1 Blatt, M. H. , et. al. , "Low Gravity Propellant Control Using Capillary Devices in Large Scale Cryogenic Vehicles, " GDC-DDE70-007, Contract NAS8-21465, August 1970.
- 2-2 Blatt, M. H. , Merino, F. , Perkins, C. R. , and Stark, J. A. , "Low Gravity Devices in Large Scale Cryogenic Vehicles, " Interim Progress Report 584-4-437, Contract NAS8-21465, December 1969.
- 2-3 Blatt, M. H. , Siden, L. E. , and Stark, J. A. , "Low Gravity Propellant Control Using Capillary Devices in Large Scale Cryogenic Vehicles, " Design Handbook, GDC-DDB70-006, Contract NAS8-21465, August 1970.
- 2-4 Abramson, N. H. , "The Dynamic Behavior of Liquids in Moving Containers, " NASA-SP-106, NASr-94(07), 1966.
- 2-5 Kolmogorov, A. N. , "On the Disintegration of Drops in Turbulent Flow, " (in Russian), Doklady Akad. , Nank, S.S.S.R. , 66, p 825 (1949).
- 2-6 Hinze , J. E. , Turbulence, McGraw-Hill, New York, 1959.
- 2-7 Armour, J. C. and Cannon, J. N. , "Fluid Flow Through Woven Screens, " AIChE Journal, Volume 14, Number 3, May 1968.
- 2-8 Katzoff, S. , "Heat Pipes and Vapor Chambers for Thermal Control of Spacecraft, " AIAA Paper No. 67-310, presented at Thermophysics Specialist Conference, April 1967.
- 3-1 Tuck, G. , "Zero-G Report LH<sub>2</sub> Boiling Threshold, " Report No. 55-D 859-3, Convair/Astronautics, May 1962.
- 3-2 Mitchell, R. C. , Stark, J. A. , et. al. , "Study of Zero-Gravity, Vapor/Liquid Separators, " GDC-DDB65-009, NAS8-20146, January 1966.
- 3-3 Poth, L. J. , Van Hook, J. R. , et. al. , "A Study of Cryogenic Propellant Stratification Reduction Techniques, " GD/FW FZA-419-1, NAS8-20330, September 15, 1967.
- 3-4 Eckert, E. R. G. , and Drake, R. M. , Heat and Mass Transfer, McGraw-Hill, 1959.
- 3-5 Schneider, P. J. , Conduction Heat Transfer, Addison-Wesley, 1957.
- 3-6 Cows, R. S. , "Feasibility of Modifying the S-IVB Stage as an Injection Stage for Manned Planetary Flyby Missions, " Douglas DAC-57997, May 1967.

- 3-7 Blatt, M. H. , "Empirical Correlations for Pressure Rise in Closed Cryogenic Containers, " AIAA Journal of Spacecraft & Rockets, June 1968.
- 3-8 O'Neill, R. F. , et. al. , "Convair Thermal Analyzer, " Computer Program No. P4560, GDC-BTD69-005, 29 May 1969.
- 3-9 Shapiro, A. H. , The Dynamics and Thermodynamics of Compressible Fluid Flow, Ronald Press, 1953.
- 3-10 Brentari, E. G. , et. al. , "Boiling Heat Transfer for O<sub>2</sub>, N<sub>2</sub>, H<sub>2</sub> and He, " NBS TN317, TN NASA CR-68814, 20 September 1965.
- 3-11 Lee Viscojet Catalogue, The Lee Co. , Westbrook Connecticut, Rev. A 5M 2-66L439.
- 4-1 Blatt, M. H. , Siden, L. E. , and Stark, J. A. , "Low Gravity Propellant Control Using Capillary Devices in Large Scale Cryogenic Vehicles, " Design Handbook, GDC-DDB70-006, Contract NAS8-21465, August 1970.
- 4-2 Blatt, M. H. , Burton, K. R. and Evans, E. A. , "Low Gravity Propellant Control Using Capillary Devices in Large Scale Cryogenic Vehicles, " Related IRAD Studies, GDC-DDB70-009, August 1970.